KU LEUVEN

ARENBERG DOCTORAL SCHOOL
Faculty of Engineering Science

Grey-Box Based Optimal Control for Thermal Systems in Buildings

Unlocking Energy Eff ciency and Flexibility

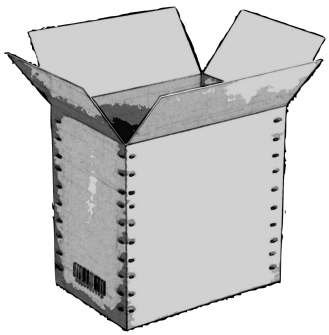

Roel De Coninck

Supervisor:
Prof. dr. ir. L. Helsen

Dissertation presented in partial
ful llment of the requirements for the
degree of Doctor in Engineering Science:
Mechanical Engineering

June 2015

Grey-Box Based Optimal Control for Thermal Systems in Buildings

Unlocking Energy Efficiency and Flexibility

Roel DE CONINCK

Examination committee:
Prof. dr. ir. H. Hens, chair
Prof. dr. ir. L. Helsen, supervisor
Prof. dr. ir. J. Driesen
Prof. dr. ir. D. Saelens
Prof. dr. ir. G. Henze
(University of Colorado)
dr. ir. M. Wetter
(Lawrence Berkeley National Lab)
dr. ir. A. Woyte
(3E)

Dissertation presented in partial fulfillment of the requirements for the degree of Doctor in Engineering Science: Mechanical Engineering

June 2015

Preface

De kiemen voor dit doctoraat zijn gelegd in 2006, op een conferentie in Luik waar ik Lieve, mijn latere promotor, en Clara ontmoette. Ik had het geluk vanuit 3E regelmatig workshops en conferenties te kunnen bijwonen, en het contact met wetenschappers en hun onderzoek deden het kriebelen om me zelf te verdiepen in een boeiend onderwerp, zonder de tijdsdruk van consultancy. Twee jaar later zat ik naast Lieve op een vlucht naar Japan. Japan is ver, maar de tijd vloog. Een lang, onbewust en wederzijds sollicitatiegesprek? Ik herinner me op die reis trouwens geanimeerde gesprekken met de voorzitter van mijn jury. De conclusie leek vaak: "alles is al onderzocht". Hugo, ik ging er blijkbaar niet mee akkoord.

Het is pas in 2010 dat de puzzelstukken in elkaar vielen, vooral dankzij de visionaire geesten van Lieve en Geert. Jullie geloof in dit project heeft ons door een aantal moeilijke fases geloodst en daar ben ik jullie enorm dankbaar voor.

We zijn nu meer dan vijf jaar later, en er is veel veranderd. Mijn kinderen zijn geen peuters meer. Mijn opa, die er vandaag als eerste ter wereld had willen bij zijn, kan dit niet meer meemaken. Op wereldschaal gaat het precies steeds sneller. Of ligt dat aan mijn leeftijd (die bijzonder hoog is volgens mijn piepjonge KU Leuven collega's, de sysi's).

En toch gaan er veel dingen niet snel genoeg. 2014 was het warmste jaar sinds de metingen, maar dat is al lang vergeten. De dreiging van klimaatverandering lijkt een fait divers geworden. Wie erover begint, die zaagt. Maar misschien ís dat ook wel zo? Misschien moeten we stoppen met erover te praten en eindelijk eens iets doen? Think global, act local. Dat gevoel is sterk gegroeid de voorbije jaren en heeft geboorte gegeven aan Opengrid. Ik dank iedereen die mee doet, in het bijzonder alle developers: bedankt voor al die boeiende avonden. We staan nog niet ver, maar je voelt dat we erin geloven en dat geeft energie. En binnenkort heb ik eindelijk wat meer tijd.

Het waren vijf boeiende jaren. Ik wil iedereen bedanken die de tijd heeft genomen

me iets bij te leren of me te helpen met een al dan niet praktisch probleem. Lieve, jouw geloof in positieve samenwerkingen heeft me vaak energie gegeven, soms ten koste van jezelf. Hopelijk wordt het ooit minder druk. Ruben, we hebben samen vele watertjes doorzwommen en ik was steeds onder de indruk van je inzicht en kennis. Mats, bedankt voor de intensieve samenwerking (en sorry voor de bugs). Dieter, jouw geloof in een betere wereld en je ondernemerszin werken zeer motiverend. Stefan, ik bewonder je attentie en aandacht voor anderen. Bedankt ook aan alle andere knappe koppen bij de sysi's voor de inspiratie en de vele toffe momenten: Jan, Maarten, Clara, Damien, Filip, Arnout, Brecht, Joachim, Bram, Ercan, Alessia: ik ben fier dat ik erbij mocht horen! Ook Bart en Juan wil ik bedanken voor de samenwerking rond Modelica en IDEAS. Ik had ook een geweldige werkplek met een koffiemaatje Wouter, een fietsheld Daniël de onverstoorbare Andreas en wat latin flavour en female touch van Juliana. Ik had te veel fantastische collega's op TME en BWK om op te noemen. Ik ben blij hen stuk voor stuk te leren kennen en me door hen te laten inspireren. Valérie, je hebt me goed geholpen met dingen waar ik een hekel aan heb: merci!

Ook op 3E ben ik geweldig omringd door warme en boeiende mensen. Geert, Werner, Achim: bedankt voor het vertrouwen, om er steeds in te blijven geloven en me de nodige ruimte te geven voor het onderzoek. Clara, jouw inzichten en snelle geest dagen me steeds weer uit. Ik hoop dat we nog vele eureka-momenten mogen beleven en dat we de uitdagingen op 3E samen aankunnen! Dirk, jouw analytisch vermogen kent geen grenzen, je energie evenmin. Hopelijk kunnen we nog veel samenwerken. Ik kreeg ook enorm veel steun van alle andere 3E collega's, zowel praktisch als moreel. Zelfs als het eens mis ging op een maandagmorgen... Sorry voor de kou!

I also spent a few weeks in Lund, Sweden. Johan and especially Fredrik: many thanks for the hospitality and the many great discussions. It was truly a fruitful collaboration and I hope to continue it.

Raf en Jan Willem, onze vanzelfsprekende vriendschap is goud waard. Aan de ballekes, burgies, kotgenoten, oude vrienden uit 't Gentse en nieuwe uit Boutersem: bedankt voor alle bezorgdheid, aanmoedigingen en steun.

Papa en mama, jullie hebben me altijd heel veel kansen gegeven en me gevormd tot wie ik ben. Ik toon het niet altijd, maar ik ben jullie daar enorm dankbaar voor. Ook van de levenswijsheid van Rita en Laurent heb ik al veel geleerd. Riet en Kobe, bedankt voor de steun en om de broer en zus te zijn waar ik zo van houd. Roger en Marja, jullie nemen al jaren een grote last van onze schouders. Bedankt voor alles, ook voor de rabarbertaart. Ik heb ook het geluk een grote en warme familie te hebben: bedankt liefste oma, grootva alle nonkels en tantes, neven en nichten.

Bavo en Ada, kinderen van mijn dromen, mogen jullie opgroeien tot gelukkige, geëngageerde en ondernemende mensen. Ik hoop echt dat jullie ook nog van het leven kunnen genieten zoals het hoort.

Lies, zelfs als ik op honderd manieren verwoord wat jij voor mij betekent en wat je voor mij gedaan hebt doe ik je tekort. Ik heb mezelf altijd voorgehouden dat ik dit doctoraat evenwichtig wou afronden, maar ik heb gefaald. Zonder jou was het nooit gelukt. Ik wens dat we, gezond en gelukkig, samen oud mogen worden.

Roel

Abstract

Improving the energy efficiency of building energy systems is a key challenge for the mitigation of climate change. In particular, bad control and operation often causes large energy efficiency losses, both in new and old buildings. The implementation of model predictive control (MPC) in buildings could enable an improved thermal comfort, lower operational costs and lower CO_2 emissions. Moreover, such a controller can offer services to the energy market by using the flexibility of the building energy system to shift its loads. Unfortunately, MPC has not yet been applied to many buildings. The main reason is the large implementation effort, in particular for developing the control model.

The objective of this work is to *develop and demonstrate a tool chain for automated deployment of MPC in buildings based on data-driven, grey-box building models.* The tool chain serves two purposes in order to facilitate the transition to a low-carbon society:

1. energy efficient building operation and
2. optimal use of building flexibility.

In the first part of this work, the multi-disciplinary Modelica library *IDEAS* has been developed in collaboration with researchers of different departments at KU Leuven. The aim of IDEAS is to investigate buildings, thermal and electrical systems at district level. With IDEAS we have quantified photovoltaic curtailing losses in dwellings and proposed simple rule-based controllers to reduce these losses. However, these rule-based controllers have their limits, specifically when larger thermal energy storage capacities are available.

A model predictive controller can predict and anticipate and is expected to outperform rule-based control when the time constants or the degrees of freedom of the system increase. One of the main bottlenecks for the implementation of MPC in buildings is the development of an appropriate system model.

In a second part of this work, a *grey-box buildings toolbox* is developed with the aim of facilitating and even automating this process. The choice for grey-box models, as opposed to black-box models, results in physical models with interpretable parameters. This is a major advantage with regard to both model development and validation.

In a third part of this work, a methodology is proposed to quantify the flexibility of a building. The methodology makes use of a grey-box model and returns both the amount of electricity that can be shifted and the associated costs for the building operator. The method is applied to the office building of 3E in Brussels, the *KK building*. This building has a hybrid heating system composed of a condensing gas boiler and two air/water heat pumps. The results reveal a high variability of both the amount of flexibility and the associated costs. While most of the day, the KK building can deliver flexibility at a lower cost than the imbalance price in the Belgian power system, there are several hours where the flexibility is more expensive.

Finally, an MPC has been implemented in the KK building. To this end, a tool chain is developed that covers all required functionality for applying MPC to real buildings. The grey-box buildings toolbox is at the core of this tool chain. Other elements are the forecasting of disturbances, a state estimation, the configuration of the optimal control problem with an appropriate objective function and constraints and the handling of monitoring data and control signals. While many of these elements can still be substantially improved, this tool chain sets the field for a cost-effective roll-out of MPC in buildings.

The MPC for the KK building controls the thermal power of the gas boiler and both heat pumps. In comparison with the conventional control system, the MPC reduces the operational costs for heating by 30 % to 40 %. The savings are realised by a combination of a much earlier start-up (pre-heating of the building), use of the heat pumps instead of the gas boiler and a drastic reduction of the supply water temperature once the building has reached its temperature set point.

While some of these savings can possibly be realised by adapting the conventional control, others can not. The anticipation of MPC on the building dynamics and expected disturbances makes this concept hard to beat. With the developed tool chain, this work hopes to bring the implementation of MPC in buildings a significant step closer to reality.

Beknopte samenvatting

Het verbeteren van de energieprestatie van gebouwen is een cruciale uitdaging om de klimaatverandering tegen te gaan. Vooral een slechte regeling in zowel nieuwe als oude gebouwen is verantwoordelijk voor inefficiënt energiegebruik. De toepassing van modelgebaseerde voorspellende regelaars (MPC[1]) kan zorgen voor een beter thermisch comfort, lagere operationele kosten en een lagere CO_2-uitstoot. Daarenboven kan een dergelijke regelaar bijkomende diensten aanbieden aan de energiemarkten door de flexibiliteit van het gebouwenergiesysteem te gebruiken om het verbruik te verschuiven. MPC is echter nog nauwelijks toegepast in gebouwen. De hoofdreden is de grote inspanning die nodig is om de regelaar te implementeren, in het bijzonder voor de ontwikkeling van het nodige gebouwmodel.

De doelstelling van dit werk is *het ontwikkelen en demonstreren van een methodiek voor automatische implementatie van MPC in gebouwen op basis van data-gedreven grey-box gebouwmodellen.* De methodiek kan op twee manieren bijdragen aan de transitie naar een koolstof-arme maatschappij:

1. door een energetisch efficiënte gebouwregeling en
2. door de flexibiliteit van het gebouw optimaal te benutten.

In het eerste deel van dit werk is, samen met onderzoekers van verschillende departementen aan de KU Leuven, de multidisciplinaire Modelica bibliotheek IDEAS ontwikkeld. IDEAS stelt ons in staat onderzoek te doen naar wijken bestaande uit gebouwen, thermische en elektrische systemen. Met IDEAS hebben we de elektriciteitsproductieverliezen van fotovoltaïsche systemen in woningen gekwantificeerd en eenvoudige regelgebaseerde oplossingen voorgesteld om deze verliezen te verminderen. Deze regelgebaseerde controle heeft echter

[1] Engels: Model Predictive Control

haar limieten, met name wanneer er meer thermische opslagcapaciteit ter beschikking staat.

Een modelgebaseerde voorspellende regeling kan echter vooruitkijken en anticiperen. Daardoor zal ze beduidend beter presteren dan een regelgebaseerde controle als de tijdsconstanten en het aantal vrijheidsgraden in het systeem toenemen. Eén van de grootste belemmeringen om MPC in gebouwen toe te passen is de ontwikkeling van het aangepaste systeemmodel.

Om dit process te vereenvoudigen en zelfs te automatiseren is in een tweede deel van dit werk een *grey-box toolbox voor gebouwen* ontwikkeld. Door te kiezen voor grey-box modellen, in tegenstelling tot black-box, hebben de verkregen modellen een fysisch logische structuur met interpreteerbare parameters. Dit is een enorm voordeel voor zowel de modelontwikkeling op zich als de modelvalidatie.

In een derde deel van dit werk wordt een methode voorgesteld om de flexibiliteit van gebouwen te kwantificeren. De methode maakt gebruik van een grey-box model en resulteert enerzijds in de hoeveelheid elektriciteit die verschoven kan worden en anderzijds in de bijhorende kost voor de gebouwbeheerder. Deze methode is toegepast op het kantoorgebouw van 3E te Brussel, het *KK gebouw*. Dit gebouw heeft een hybride verwarmingssysteem bestaande uit een condenserende gasketel en twee lucht/water warmtepompen. De resultaten tonen een sterke spreiding in zowel de hoeveelheid flexibiliteit als de bijhorende kosten. Gedurende het grootste deel van de dag kan het KK gebouw flexibiliteit aanleveren aan een lagere kost dan de op dat ogenblik geldende Belgische onevenwichtsprijs maar tijdens verscheidene uren is de flexibiliteit duurder.

Tot slot is de MPC toegepast op het KK gebouw. Hiervoor is een methodiek ontwikkeld die alle functionaliteit bevat die nodig is om MPC in reële gebouwen te implementeren. De grey-box toolbox voor gebouwen vormt de kern van deze methodiek. Andere elementen zijn het voorspellen van de verstoringen, het schatten van de toestanden van het regelmodel, de configuratie van het optimalisatieprobleem met een aangepast objectief en beperkingen en de behandeling van meetgegevens en regelsignalen. Hoewel vele van deze elementen nog substantiëel verbeterd kunnen worden zet deze methodiek de lijnen uit voor een kostenefficiënte toepassing van MPC in gebouwen.

De MPC voor het KK gebouw regelt het thermisch vermogen van de gasketel en beide warmtepompen. In vergelijking met de conventionele regeling slaagt de MPC erin de dagelijkse energiekosten voor verwarming met 30 % tot 40 % te reduceren. Deze besparing wordt bereikt door een combinatie van een veel vroegere opstart (voorverwarming van het gebouw), het overwegend gebruik van de warmtepompen in plaats van de ketel en een drastische verlaging van de toevoerwatertemperatuur zodra het gebouw de gewenste temperatuur bereikt

heeft.

Hoewel een deel van deze besparing mogelijk ook behaald kan worden door de conventionele regeling aan te passen geldt dit zeker niet voor het geheel. De anticipatie van de MPC op de gebouwdynamica en de verwachte verstoringen maken dit een moeilijk te verslaan concept. Met de ontwikkelde methodiek hoopt dit doctoraat de toepassing van MPC in gebouwen een significante stap dichterbij te brengen.

Abbreviations

4SID	Subspace State Space System Identification
BAU	Business As Usual
BPS	Building Physics and Systems
DAE	Differential and Algebraic Equations
DHW	Domestic Hot Water
DR	Demand Response
DSM	Demand Side Management
EE	Energy Efficiency
EES	Electrical Energy Systems
FCC	Flexibility Cost Curve
HP	Heat Pump
HVAC	Heating Ventilation and Air-Conditioning
LTI	Linear Time-Invariant system
MPC	Model Predictive Control
OCP	Optimal Control Problem
PV	Photovoltaic
RBC	Rule-Based Control
SE	State Estimation

TES Thermal Energy Storage

Contents

Chapter 1

Introduction

1.1 Problem statement

Reducing the energy use in buildings is a major challenge for mitigation of global warming. This can be achieved by renovation of the building stock and sustainable design of new buildings. However, this is not sufficient. Bad control is responsible for large energy efficiency losses. Even in new and modern buildings, inefficient control and operation often increase the primary energy consumption for heating, cooling and air-conditioning (HVAC) by 20 % or more [1, 2].

Simultaneously, buildings are often put forward as potential suppliers of flexibility services to the electricity market. Through demand-side management (DSM) or distributed energy storage, partly as thermal energy, building loads can be shifted from times where electricity is scarce to times where it is abundant. This would support the continued integration of power plants with variable and stochastic production profiles, like wind and solar electricity generation plants. For this purpose, it is required to assess the *interaction* between different buildings and their joint flexibility potential. Again, this requires efficient control algorithms, both for individual buildings and for clusters of buildings.

Every building is different in its construction and operation. The design, implementation and commissioning of efficient control systems requires a lot of case-specific manual work. The field of building control would benefit from a generic, model-based tool chain that could take care of a large part of the building-specific manual tuning. In such a tool chain, the mentioned HVAC control challenges can be met by Model Predictive Control (MPC) [3–7]. By

specifying high-level objectives and using the power of numerical optimization, a model-based predictive controller can automatically adapt to new operating conditions and take into account expected future building dynamics. The controller can also incorporate the delivery of additional services like reserves [8] or peak load reduction [9]. Moreover, if the tool chain is self-learning, it can cope with changes in building use or replacement of equipment.

One of the main bottlenecks for this generic model-based control tool chain in buildings is the required model [10, 11]. Each building needs its own model. As long as the development of these models requires a lot of manual work and expert knowledge, MPC will never find its way to the building market.

A solution can be found in data-driven modelling techniques. These techniques do not require much meta-information about the building like its geometry, envelope properties, equipment characteristics etc. Instead, a model is derived from building monitoring data, which can be considered as a track, a footprint of a specific building. Currently, technological developments are eliminating all practical and economical barriers to (remote) sensing, allowing building monitoring data to be widely available.

When the structure of the data-driven building model has no link with the physical phenomena encountered, it is a black-box model. Models that are based on those physical principles are grey-box models. The inclusion of physical laws in a grey-box model has two main advantages. First, an interpretation of the obtained model parameters can support the model validation. Second, these models are better suited for extrapolation to operating conditions outside of those encountered in the training dataset. More information about this white-grey-black modelling paradigm can be found in Section 2.2 and Chapter 4.

Besides model identification and MPC, the envisaged tool chain has to contain functionalities to forecast disturbances (like weather and user behaviour), perform state estimation and communicate with the building to send control signals and obtain monitoring data. An overview of the complete tool chain is given in Section 2.2.

1.2 Concepts and terminology

Some concepts on which this work relies are explained below.

Demand side management (DSM)

Gellings [12] defines DSM from a utility perspective as *"the planning and implementation of those electric utility activities designed to influence customer uses of electricity in ways that will produce desired changes in the utility's load shape"*. In other words, all measures and actions that influence the demand fall under the umbrella of DSM.

By simplifying the categories of DSM proposed by Palensky and Dietrich [13] we can say that DSM is composed of energy efficiency (EE) and demand response (DR). Energy efficiency groups all measures that *reduce* the energy use. Demand response groups all measures that modify the load profile. It's important to realise that DR can contradict the ambitions of EE and *increase* the energy use.

Optimal control problem (OCP)

In words, an optimal control problem is a mathematical problem to find the control trajectories that will drive a system *optimally*. The OCP specifies the system, what *optimally* means, which constraints apply, which disturbances apply and from which state the system starts.

Mathematically, this is expressed as follows (in continuous time):

$$\underset{u}{\text{minimize}} \quad J(t, \dot{x}, x, w, y, u) \tag{1.1a}$$

$$\text{subject to} \quad F(t, \dot{x}, x, w, y, u) = 0, \tag{1.1b}$$

$$g(t, \dot{x}, x, y, u) = 0, \tag{1.1c}$$

$$h(t, \dot{x}, x, y, u) \geq 0, \tag{1.1d}$$

$$x(0) = x_0. \tag{1.1e}$$

In this formulation, $t \in [0, t_h]$ is time with t_h the prediction horizon, $u \in \mathbb{R}^n$ is the control signal, J the objective, $F(\cdot)$ is the system model with states x, algebraic variables y and disturbances w. $g(\cdot)$ and $h(\cdot)$ are additional equality and inequality constraints. $x, \dot{x}, w, y$ and u are all time-dependent but for readability we have omitted the time dependency notation.

Model predictive control (MPC)

Model predictive control is a control concept in which an OCP is solved at every control step. The OCP is initialised from an estimated state of the system based on measurements (= feedback) and takes into account forecasted disturbances and dynamic system behaviour (= feedforward) [14].

The implementation of MPC requires a system model, forecasts of all disturbances, state estimation (see below) and a framework to solve the OCP. A general overview of MPC is given in Section 2.2.

State estimation (SE)

State estimation is a required step in a model predictive control scheme. The state estimation problem boils down to to examining the past monitoring data and reconciling these measurements with the model to determine the most likely value of the state at the current time [15]. The theory of state estimation is linked to the concept of observability of the model. More information can be found in Appendix A.

1.3 Objective

The objective of this work is to *develop and demonstrate a tool chain for automated deployment of MPC in buildings based on data-driven, grey-box building models.* The tool chain serves two purposes in order to facilitate the transition to a low-carbon society:

1. energy efficient building operation and
2. optimal use of building flexibility.

1.4 Guide to the reader

This work is structured as follows. I have defined four main problems that have to be solved in order to reach the objective. Figure 1.1 gives a schematic overview of these problems, the approach taken to solve them, and the related chapters. Most chapters are based on articles that are published or submitted for publication in internationally peer reviewed journals or conferences.

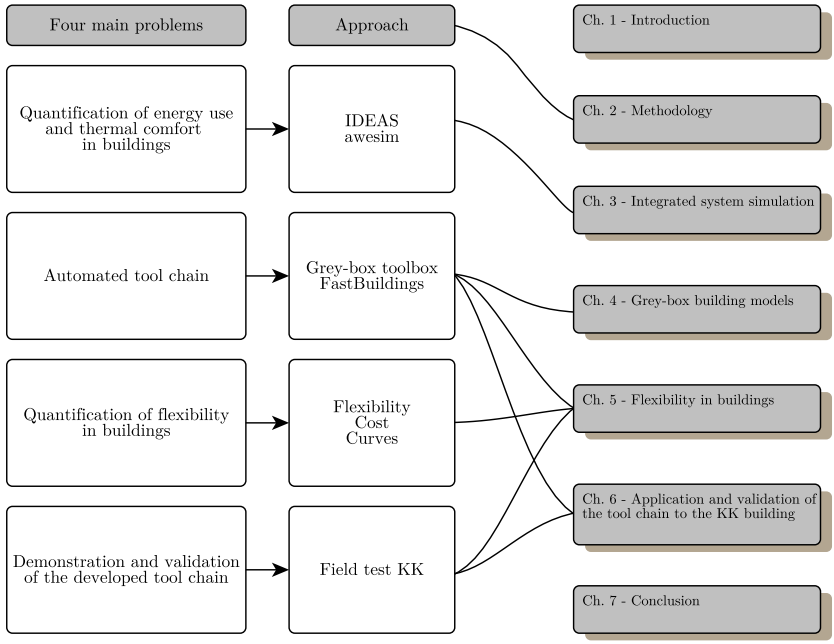

Figure 1.1: Schematic overview of the main problems, the approaches followed to find solutions and the related chapters.

Chapter 2 - Methodology details each problem presented in Figure 1.1 and the approach taken to find the solution. This chapter elaborates on the tools, model libraries and frameworks that have been developed in this thesis.

Chapter 3 - Integrated system simulation compiles three publications.

1. The article *Modelling and simulation of a grid connected photovoltaic heat pump system with thermal energy storage using Modelica* [16] presents detailed simulations for a single dwelling in order to estimate the grid load of a photovoltaic (PV) system in combination with an air-to-water heat pump (HP).

2. The article *Assessing electrical bottlenecks at feeder level for residential net zero-energy buildings by integrated system simulation* [17] shows the need for a different simulation framework in order to assess neighbourhoods. This article quantifies local overvoltage in a residential neighbourhood by

means of detailed simulation with the multidisciplinary Modelica library *IDEAS* (see Chapter 2 for more information about IDEAS).

3. The article *Rule-based demand side management of domestic hot water production with heat pumps in zero energy neighbourhoods* [18] builds further on the previous article. In this publication, a thermal energy storage (TES) model is developed and different rule-based control strategies are proposed to mitigate the PV generation losses by demand shifting.

The aim of this chapter is to illustrate the challenges in analysing energy use and thermal comfort in buildings and neighbourhoods and to introduce the interdisciplinary solutions that were developed in this work, in particular IDEAS.

Chapter 4 - Grey-box building models presents the development and validation of a toolbox for largely automated system identification of grey-box building models. The chapter describes the methodology, numerical solution and application of the toolbox on a monitored single-family dwelling in Munich, Germany.

Chapter 5 - Flexibility in buildings proposes a general methodology to quantify the amount of flexibility a building can offer and the associated costs. The methodology requires a low-order model of the building, typically a grey-box model like those developed in Chapter 4. A case study is performed on the office building of 3E in Brussels, resulting in different cost curves depending on weather, building operation and HVAC design.

Chapter 6 - Application and validation of the tool chain to the KK building reports on the application of the total model-based tool chain to the field test, the office building of 3E in Brussels. The building is situated at Kalkkaai 6 and referred to as *KK*. This chapter gives an overview of the building, the monitoring, the grey-box model development, the forecasting of disturbances and the implementation of the MPC. Finally, the benefits of MPC in comparison to the conventional rule-based control (RBC) are assessed based on monitored performance of the KK building.

Chapter 7 - Conclusion summarizes this work, highlights the specific contributions and gives an outlook to future research and development.

1.5 Bibliography

[1] M. Ardehali and T. F. Smith, "Literature review to identify existing case studies of controls-related energy-inefficiency in buildings for national building controls information program", University of Iowa, Department of Mechanical Engineering, Iowa City, Iowa, Tech. Rep., 2001, p. 159.

[2] D. Gyalistras, M. Gwerder, F. Oldewurtel, C. N. Jones, M. Morari, B. Lehmann, K. Wirth, and V. Stauch, "Analysis of energy savings potentials for integrated room automation", in *10th RHEVA World Congress CLIMA*, Antalya, Turkey: REHVA, May 2010.

[3] J. Široký, F. Oldewurtel, J. Cigler, and S. Prívara, "Experimental analysis of model predictive control for an energy efficient building heating system", *Applied Energy*, vol. 88, pp. 3079–3087, 2011, ISSN: 03062619. DOI: 10.1016/j.apenergy.2011.03.009.

[4] M. Gwerder, D. Gyalistras, C. Sagerschnig, R. S. Smith, and D. Sturzenegger, "Final report : use of weather and occupancy forecasts for optimal building climate control – part ii : demonstration (opticontrol-ii)", Automatic Control Laboratory, ETH, Zurich, Zwitzerland, Tech. Rep. September, 2013, p. 156.

[5] P. Li, D. Li, D. Vrabie, S. Bengea, and S. Mijanovic, "Experimental demonstration of model predictive control in a medium-sized commercial building", in *3rd International High Performance Buildings Conference*, Purdue, Jul. 2014.

[6] G. Henze, D. Kalz, S. Liu, and C. Felsmann, "Experimental analysis of model-based predictive optimal control for active and passive building thermal storage inventory", *HVAC&R Research*, vol. 11, no. 2, pp. 189–213, 2005, ISSN: 1078-9669. DOI: 10.1080/10789669.2005.10391134.

[7] S. C. Bengea, A. D. Kelman, F. Borrelli, R. Taylor, and S. Narayanan, "Implementation of model predictive control for an hvac system in a mid-size commercial building", *HVAC&R Research*, vol. 20, pp. 121–135, 2014, ISSN: 1078-9669. DOI: 10.1080/10789669.2013.834781.

[8] G. S. Pavlak, G. P. Henze, and V. J. Cushing, "Optimizing commercial building participation in energy and ancillary service markets", *Energy and Buildings*, vol. 81, pp. 115–126, Oct. 2014, ISSN: 03787788. DOI: 10.1016/j.enbuild.2014.05.048.

[9] J. E. Braun, "Reducing energy costs and peak electrical demand through optimal control of building thermal storage", *ASHRAE transactions*, vol. 96, no. 2, pp. 876–888, 1990.

[10] S. Prívara, "Building modeling and identification for predictive control", PhD thesis, Czech Technical University in Prague, 2013.

[11] G. P. Henze, "Model predictive control for buildings: a quantum leap?", *Journal of Building Performance Simulation*, vol. 6, no. 3, pp. 157–158, May 2013, ISSN: 1940-1493. DOI: 10.1080/19401493.2013.778519.

[12] C. Gellings, "The concept of demand-side management for electric utilities", *Proceedings of the IEEE*, vol. 73, no. 10, pp. 1468–1470, 1985.

[13] P. Palensky and D. Dietrich, "Demand side management: demand response, intelligent energy systems, and smart loads", *Industrial Informatics, IEEE Transactions on*, vol. 7, no. 3, pp. 381–388, 2011, ISSN: 1551-3203. DOI: 10.1109/TII.2011.2158841.

[14] C. Verhelst, "Model predictive control of ground coupled heat pump systems for office buildings", PhD thesis, KU Leuven, 2012, ISBN: 9789460184970.

[15] J. Rawlings and D. Mayne, *Model Predictive Control - Theory and Design*. Mar. 2013, pp. 31–39, ISBN: 9781119963981. DOI: 10.1002/9781119941446.ch3.

[16] R. De Coninck, R. Baetens, B. Verbruggen, J. Driesen, D. Saelens, and L. Helsen, "Modelling and simulation of a grid connected photovoltaic heat pump system with thermal energy storage using modelica", in *8th International Conference on System Simulation in Buildings (SSB2010)*, P. Andre, S. Bertagnolio, and V. Lemort, Eds., Liège, 2010, P177.

[17] R. Baetens, R. De Coninck, J. Van Roy, B. Verbruggen, J. Driesen, L. Helsen, and D. Saelens, "Assessing electrical bottlenecks at feeder level for residential net zero-energy buildings by integrated system simulation", *Applied Energy*, vol. 96, no. Special issue on Smart Grids, Renewable Energy Integration, and Climate Change Mitigation - Future Electric Energy Systems, pp. 74–83, 2012, ISSN: 03062619. DOI: 10.1016/j.apenergy.2011.12.098.

[18] R. De Coninck, R. Baetens, D. Saelens, A. Woyte, and L. Helsen, "Rule-based demand side management of domestic hot water production with heat pumps in zero energy neighbourhoods", *Journal of Building Performance Simulation*, vol. 4, no. 7, pp. 271–288, 2014. DOI: 10.1080/19401493.2013.801518.

Chapter 2

Methodology

This chapter elaborates the four main problems of Figure 1.1 and the approach used to find their solutions.

2.1 Quantification of energy use and thermal comfort in buildings

2.1.1 Problem description

In this work, different control strategies will be developed. They can be applied to a single building or a cluster of buildings, like a neighbourhood. Their performance has to be compared to a conventional, *business as usual* (BAU) control. How can we quantify the impact of a specific control strategy on energy use and thermal comfort in buildings?

There are two approaches to this problem: experiments and simulation. Simulation offers several advantages compared to experiments. Simulations are more flexible, faster, cheaper and more repeatable than experiments. To quantify energy use and thermal comfort in buildings under different assumptions and operating conditions, a simulation framework is created.

However, simulations cannot take into account many of the practical issues and uncertainties that affect real-life buildings. Therefore, a field test is set-up to apply the developed tool chain to a real building. We consider the field test

as a validation experiment. It is discussed in Section 2.4 and Chapter 6. The remainder of the current Section describes the simulation framework.

2.1.2 Approach

There are different requirements for the simulation framework.

Firstly, the framework has to be able to simulate the thermal processes in buildings with a level of detail allowing to obtain *sufficiently accurate* results for energy use and thermal comfort. In this context, *sufficiently accurate* means that a multi-zone building model is required, taking into account the effects of solar radiation, infiltration and ventilation, building envelope construction, occupant behaviour, heating and cooling systems.

Secondly, to simulate the effect of DSM and more specifically DR on neighbourhood or district level, the electricity distribution network has to be modelled. The network model should have active and reactive power at every node as input in order to calculate the node voltage (with absolute value and phase angle) and ohmic losses in the lines and transformer.

Thirdly, a representative set of stochastic occupant behaviour profiles is needed. The profiles need to contain information about presence, equipment use and domestic hot water (DHW) consumption.

As described in our paper *Assessing electrical bottlenecks at feeder level for residential net zero-energy buildings by integrated system simulation* [1] (included in Chapter 3), there are two main approaches for simulation at district level: (i) models using thermal Building Physics and Systems (BPS) as starting point, or (ii) models using Electrical Energy Systems (EES) as starting point.

BPS-based models at neighbourhood level combine a dynamic simulation of the heating and cooling demand with a stochastic approach on occupant behaviour. EES-based models at feeder level combine a physical calculation of the electricity generation and distribution with a stochastic approach on power loads. A more thorough description of the state of the art of neighbourhood simulation is presented in Chapter 3.

At the start of this research in January 2010, there was no simulation framework that united these requirements. With the authors of [1], we therefore developed our own simulation framework *IDEAS (Integrated District Energy Assessment by Simulation*). The need to facilitate the execution and post-processing of many different simulations led to a second development, *awesim*. Both developments are presented below.

IDEAS

IDEAS differs from existing BPS-based and EES-based models by integrating the dynamics of the hydronic, thermal as well as electrical energy systems and networks at both the building and aggregated level within a single model and solver. The transient thermal processes are modelled in detail based on the control volume method, whereas the electric models are developed with stationary nodal and line models.

Occupancy behaviour is not directly integrated in IDEAS. Pre-computed stochastic profiles for occupancy, use of appliances, lighting and DHW use are read from files during the simulation. The computation of these profiles is described in more detail by Baetens and Saelens [2].

IDEAS is a Modelica library. Modelica is an equation-based modelling language for cyber-physical systems [3]. The choice for Modelica for the development of IDEAS is based on several arguments. Firstly, Modelica allows for linear, non-linear and hybrid model formulations and therefore it does not limit the model structure as such. Secondly, Modelica can handle multi-domain and stiff models and is equation-based. Thirdly, Modelica has a *connector* concept to support component-based modelling. The object-oriented philosophy stimulates model reuse, and is well suited for library development.

In 2010, the Modelica library *Buildings* [4] was already available in an early version. This library was initially developed for detailed single building and HVAC simulation, analogous to the BPS type of models introduced above. Complementary, the focus of IDEAS was on simulation of districts. The upscaling to districts required simplifications, some of which are briefly mentioned here. All pressure drop calculations in hydronic components were omitted. Pumps were modelled as flow sources with a fixed pressure drop parameter to compute their power consumption. HVAC equipment models, though dynamic, were based on performance maps rather than modelling the heat and mass transfer processes in detail. In the thermal zone model, radiation exchange is calculated based on the surface only, view factors are not implemented.

Since the start of the IEA EBC [1] Annex 60 project in 2013, in which KU Leuven has a prominent role [5], the focus of both the Buildings library and IDEAS has widened. Moreover, both libraries are now extending from the same base classes (the *Annex60* library). Also the library of RWTH Aachen, *AixLib*, is currently being transformed to use the *Annex60* base classes [6]. This allows exchanging models, avoids duplication of development and is an important step

[1] International Energy Agency's Energy in Buildings and Communities Programme

towards unification of both developments. Since version 0.2, more detailed HVAC models can be developed or used within IDEAS thanks to the *Annex60* base classes.

IDEAS continues being actively developed by KU Leuven. Broadening of the scope leads to more overlap with the Buildings library and less incentives to maintain and develop IDEAS. Most researchers at KU Leuven use IDEAS, and models in general, as a tool. Developing a model or library is not a goal on itself. The availability of other open-source libraries like *Buildings* and *AixLib* can therefore be seen as an opportunity for researchers but a threat to the continuation of IDEAS. On the other hand, developing a model is often the best way for a researcher to understand his/her topic and learn Modelica, skills that are required also for using other libraries. This modelling-based path to expertise can be a driver for continued development of IDEAS or other libraries.

I am personally very satisfied with the common direction of development of IDEAS and the Buildings library. The collaboration within *Annex60* leads to better models in both libraries. Maybe it is important for the future of IDEAS to go back to the initial ambition and focus more on neighbourhoods and districts. This ensures differentiation while model exchange with more detailed building simulation libraries will always be possible thanks to the *Annex60* base classes. IDEAS is distributed with the *Modelica license 2* and can be found in the *openIDEAS* source code repository on Github [7].

awesim

The decision to use Modelica and develop IDEAS introduced another need: the automation of the simulation workflow, including pre- and post-processing of simulations. The built-in analysis in Modelica tools like openModelica and Dymola were not sufficient. In 2010, Matlab was the de-facto software for general scientific computing but the involvement of the company 3E in this research and expensive commercial Matlab licenses was a strong driver for using the free and open-source Python environment instead of Matlab.

Manually managing multiple simulation results quickly becomes time-intensive and error-prone. More specifically, we needed a solution for filtering hundreds of simulations based on their parameters and results. I therefore started to develop my own simulation management tools which led to the birth of *awesim*.

The main class of awesim is the `Simdex` class, a contraction of Simulation index. A `Simdex` object can contain meta-information of thousands of simulations. The class provides methods to query parameters, filter based on parameter existence or value and extract and plot results. An automatic post-processing can be

applied when a new simulation is added to a `Simdex`, for example to apply the formulas to calculate thermal comfort or do arithmetic operations on simulation trajectories. awesim also includes code to run parametric simulations in parallel by use of a precompiled `dymosim` binary from Dymola.

Almost a year after the development of awesim was started, Kevin Davies started the development of *ModelicaRes* [8], another Python module with similar ambitions. ModelicaRes has much more advanced post-processing features for single simulations, but lacked the concept of the `Simdex` class. In Annex 60, the decision was made to use ModelicaRes as a starting point for workflow automation. I actively supported this decision for the main reason that I and other KU Leuven or 3E colleagues could not free the time to continue development of awesim when a more active and well-written alternative exists. In the mean time, the `Simdex` concept has already been implemented in ModelicaRes in the framework of Annex 60. The results presented in this work have been post-processed with awesim.

2.2 Automated tool chain

2.2.1 Problem description

The objective of this work is to *develop and demonstrate a tool chain for automated deployment of MPC in buildings based on data-driven, grey-box building models.* This section introduces the skeleton of the tool chain and elaborates on the main developments that were needed: the *greybox* toolbox and *FastBuildings* library.

Figure 2.1 shows a functional overview of the tool chain. The figure is interpreted as follows. Dashed lines are offline work flows, solid lines are online work flows. The *building* to be controlled needs a *monitoring system* to provide data for the *Model Identification.* The model identification is an offline workflow by default and results in a *Grey-Box Controller Model.* Once this model has been identified, its initial state is updated at each control step with the results of a *State Estimation.* There are two work flows for forecasting of the *disturbances*: an endogenous procedure (based on the monitoring data) and an exogenous procedure, eg. for weather forecasts. An *objective function* and *constraints* are added to form an *Optimal Control Problem.* The solution of this problem is converted into a suitable *Control* signal which is sent to the building.

One of the main challenges of this tool chain is the model identification. This is also recognised by S. Prívara in his PhD thesis where he writes that *"modelling and system identification are the most difficult and time-consuming part of*

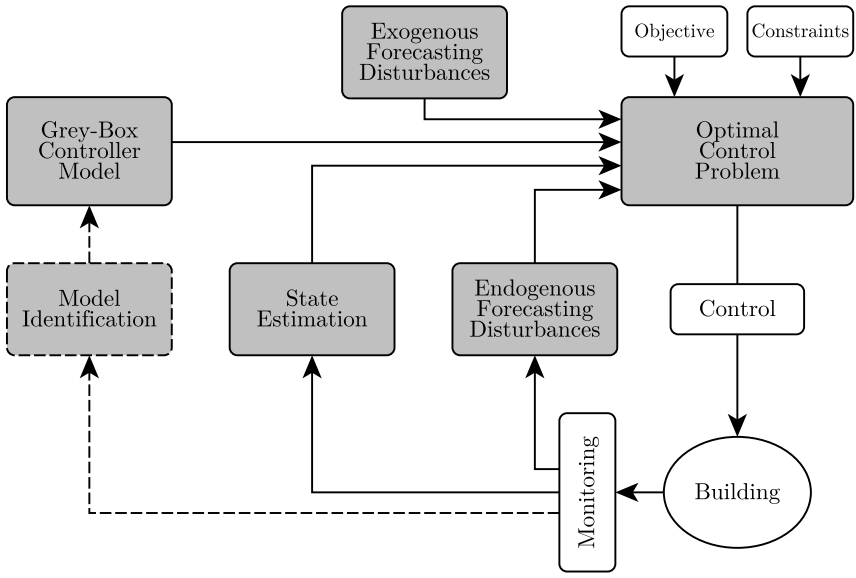

Figure 2.1: Functional overview of the tool chain

the automation process" [9]. According to G.P. Henze [10], the process of model identification accounts for 70 % of the effort for implementing an MPC controller. Reducing this effort is one of the main concerns of this thesis. If we want to apply the tool chain in practice for existing buildings, we can identify required and desired features for the model identification step. These are listed in Tables 2.1 and 2.2 respectively.

Table 2.1: Required features for model identification in the MPC tool chain.

Requirements
Automatic model identification with no or minimal manual intervention
Applicable to existing buildings
Good simulation performance
No or minimal need of meta-information
Applicable to a wide range of building types
Limited requirements for monitoring dataset

Table 2.2: Desired features for model identification in the MPC tool chain.

Desired features
Linear, non-linear and hybrid models
Physically interpretable models
Models can be implemented in IDEAS
Based on open-source software
Multi-zone models

2.2.2 Approach

Grey-box toolbox

The requirements and desired features of Tables 2.1 and 2.2 led to the development of a toolbox for model identification of grey-box models, the *grey-box toolbox*. Previous work on model identification for MPC in buildings did not cover the entire wish list. Some reported model identification approaches are excluded beforehand because they start from an existing detailed simulation model to apply model order reduction techniques to obtain a low-order model [11, 12] or to generate identification data with specific excitations [13, 14]. For the purpose of physical interpretation and good out-of-sample simulation performance, grey-box approaches are generally preferred above black-box models [15]. Correctly identified and validated models can be simple, yet showing a good performance [16, 17]. A very strong and detailed overview of system identification approaches for building control is given by Prívara et al. [14]. Their conclusion is that grey-box models are powerful for little complex buildings, but become difficult to estimate for large datasets (with multi-zone monitoring information). For buildings with hundreds of inputs/states, Prívara et al. put forward Subspace State Space System Identification (4SID). However, this methodology is also vulnerable to the quality of the dataset. That is why they either need prior information about the system to be modelled or a detailed model to generate better identification data. This again limits the use of 4SID to existing buildings.

I therefore developed a grey-box based toolbox with some features that are important for incorporation in the general tool chain. The rationale, methodology and validation of this toolbox are given in Chapter 4. Follow-up projects both at 3E and KU Leuven will continue to develop the grey-box toolbox. The toolbox is not a public open-source development but is freely available for research purposes under specific conditions.

FastBuildings library

The grey-box toolbox is developed for buildings. Prior knowledge of the modelled system is one of the cornerstones of the grey-box approach [18]. In the toolbox, most of this prior knowledge is translated into the Modelica library *FastBuildings*. This library contains low-order models for the physical and thermal processes in buildings. As such, these models specify the system of differential and algebraic equations (DAE) for which the toolbox estimates the unknown parameters.

In control theory, the concepts of observability, controllability, reachability and identifiability are often used. For linear state space models, observability and controllability are well defined and easy to verify if the state space model matrices are known. The developed toolbox does not use a state-space representation of the models. The models may be non-linear and time variant and for such models, observability and controllability are more difficult to verify. However, as these concepts are core concepts in modern control theory, an overview of the definitions and implications is given in Appendix A.

The library has sub-packages for thermal zone models (including windows), HVAC, user behaviour, inputs, buildings and examples. Single and multi-zone building models can be created easily by instantiating one of the predefined templates in the `Building` sub-package and redeclaring the desired submodels, like the thermal zone, HVAC or window model. This library is explained in more detail in Chapter 4. The *FastBuildings* library is distributed with the *Modelica license 2* and can be found in the *openIDEAS* source code repository on Github [7]. This library may be integrated in IDEAS in the near future.

2.3 Quantification of flexibility in buildings

2.3.1 Problem description

One of the common arguments for the introduction of smart grids is that they will unlock the flexibility potential of buildings [19, 20]. There are mainly three processes involved. Firstly, demand response on household appliances like dishwashers, washing machines and tumble driers allows shifting the electricity consumption of households according to the availability of (renewable) power. Secondly, buildings often accommodate active thermal energy storage (TES) capacity. This can be as hot water storage tanks for DHW and cold storage like ice storage in utility buildings. These systems are an evident target for DR. Finally, passive thermal storage capacity is present in every building, by the thermal capacity of the building envelope and internal mass. This capacity can

be used to shift the heating and/or cooling operation. This research does not consider demand side management of household appliances. Instead, I focus on the control of HVAC systems, including active and passive TES. It has been shown before that DR with thermal building systems is possible and effective to reduce utility costs [21, 22].

There are two challenges with regard to flexibility of buildings: (i) defining how much flexibility buildings can offer and (ii) calculating the costs of the associated DR actions.

2.3.2 Approach

Flexibility is easy to define, but difficult to quantify. Petersen et al. specify that *"[...] the flexibility of a given system is a unique, innate, state-and time dependent quality. In conversation it is therefore sometimes said that flexibility is the ability to deviate from the plan. That characterization of flexibility is very insightful, but it still leaves us with the problem of defining both the ability to deviate and the plan"* [23]. In my opinion, this is not sufficient: we also have the problem of defining the *cost to deviate from the plan.* When we are able to compute this cost for different systems, we can choose the most cost-effective ones to deliver the required flexibility for a given power system. Cochran et al. present a comprehensive overview of different techno-economical interventions to increase flexibility (see Figure 2.2) [24]. However, the authors mention that the relative costs are illustrative, confirming the need to quantify them in more detail.

For power systems, Cochran et al. give an overview of methods to quantify flexibility. However, a literature review (see Chapter 5) revealed that there is little work on quantifying the amount and cost of flexibility for buildings. One publication however, deserves explicit mentioning. Oldewurtel et al. developed a very similar idea as the one described below and presented their work on the 52nd Conference on Decision and Control in December 2013 [25]. This is only a few months after I presented my work on the 13th International Building Simulation Conference (August 2013). I compare both approaches below.

Flexibility cost curves

I propose a generic methodology to compute a *flexibility cost curve* (FCC) for a building. The cost curve is time dependent. It shows both how much flexibility a building can provide and the associated costs for a given point in time.

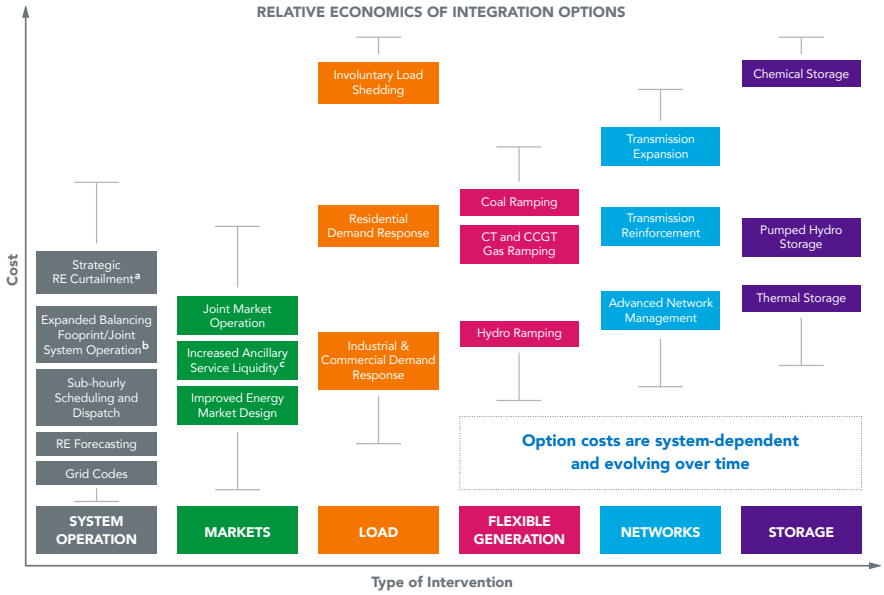

Figure 2.2: Costs of integrating flexibility according to Cochran et al. [24]. Note: Relative costs are illustrative, as actual costs are system dependent.
a) There is a tradeoff between costs of flexibility and benefits of reduced (or no) curtailment, hence a certain level of curtailment may be a sign that the system has an economically optimal amount of flexibility.
b) Joint system operation typically involves a level of reserve sharing and dispatch co-optimization but stops short of joint market operation or a formal system merger.
c) Wind power can increase the liquidity of ancillary services and provide generation-side flexibility. Curtailed energy is also used to provide frequency response in many systems, for example Xcel Energy, EirGrid, Energinet.dk.

Reprinted with permission of the National Renewable Energy Laboratory, from http://www.nrel.gov/docs/fy14osti/61721.pdf, Accessed May 6th, 2015.

The method is based on the solution of at least three optimal control problems (OCPs) with an appropriate system model. The first OCP solves the BAU operation of the building. This OCP typically has the objective to minimise the operational costs with constraints on thermal comfort and a prediction horizon of one or more days. This solution is *the plan* according to Petersen et al. [23].

To obtain the *deviation from the plan* for a given moment in time (both in positive and negative direction, respectively more and less consumption), two additional OCPs are solved. These OCPs have an additional term in the objective function expressing the desired effect, respectively maximising or minimising the load. Both solutions will have an increased cost compared to the BAU case. This means that together with the *amount of energy* that can be shifted, we have an indication of the *cost to deviate from the plan*. By smart construction of different objective functions, intermediate points can also be obtained in the cost curve.

This methodology is developed and applied to the KK building in Chapter 5. The cost curves can be used to assess how much load shifting really costs. This enables comparing DSM solutions with other technological solutions like electrical energy storage or peak power generation. The method can also be used in the design phase to incorporate possible flexibility services that the building could offer on the energy markets. For operational decision-making, the cost curves are not sufficient, but the underlying models and optimisation formulation could be integrated in a multi-agent smart grid framework.

As mentioned above, Oldewurtel et al. developed a similar approach in their paper entitled *Towards a standardized building assessment for demand response* [25]. The main similarity is the use of numerical optimization to compute deviations from a cost-optimal BAU operation, both in positive and negative direction. There are many small and large differences though. Firstly, their methodology is developed based on MPC, not OCPs. Secondly, the deviations are enforced by using price spikes, one for each hour of the day in each direction. These price spikes are not included in the predictions beforehand, but are only considered in the MPC problem at the hour when the spikes take place. The reason is that the authors want to test the response to sudden power shifting requests without preparing the building. Another difference is evident from the presentation of the results: Oldewurtel et al. do not compute cost curves. Instead, they compute a power shifting potential and power shifting efficiency and average each of these indicators for the same hour for different days. This allows them to see seasonal differences in the flexibility potential of a building.

A flexibility cost curve offers the advantage of visualising the total economical cost of a DR operation for a given building. This cost is a function of the

applied tariff(s) and supposes that this tariff is not influenced by the control of the building. Therefore, the cost curve can be used to decide whether a specific remuneration for the flexibility is lower or higher than the cost for the building. Another advantage is the possibility to compute intermediate points on the curve which is not possible with the approach of Oldewurtel et al. On the other hand, visualisation of the flexibility for different subsequent periods is a good idea to obtain more general results for a given building. This visualisation is applied to the KK building in Chapter 5.

2.4 Demonstration and validation of the developed tool chain

2.4.1 Problem description

Developing a library, toolbox or tool chain can be an interesting experience, but without application to the problem it is supposed to solve its merits are unknown. The best way to prove the added value of the developments is to apply it to an occupied building with the uncertainties and practical issues that occur in real-life. The proof of the pudding is in the eating.

2.4.2 Approach

Field test KK

In order to demonstrate, test and validate the tool chain, a field test has been developed. The building is the office building of 3E in Brussels (Belgium), it will be referred to as *KK*. It is a medium-sized office (960 m^2) composed of two floors. A monitoring system is present. The operation freedom is situated entirely at the heat production level in the technical room as the end-units in the building cannot be controlled remotely. In the technical room, two air-to-water heat pumps and a condensing boiler produce hot water for space heating and preheating of the ventilation supply air.

The developed tool chain is applied to the KK building, which is elaborated and reported in detail in Chapter 6. Application of the research results on a real and occupied building was time consuming. Nevertheless I think it was worth the effort. Several issues and problems had to be solved on the road to a reliable MPC. Each of the encountered problems resulted in an improved

tool chain and a growing awareness of the challenges involved when bringing research results to (commercial) application.

2.5 Bibliography

[1] R. Baetens, R. De Coninck, J. Van Roy, B. Verbruggen, J. Driesen, L. Helsen, and D. Saelens, "Assessing electrical bottlenecks at feeder level for residential net zero-energy buildings by integrated system simulation", *Applied Energy*, vol. 96, no. Special issue on Smart Grids, Renewable Energy Integration, and Climate Change Mitigation - Future Electric Energy Systems, pp. 74–83, 2012, ISSN: 03062619. DOI: 10.1016/j.apenergy.2011.12.098.

[2] R. Baetens and D. Saelens, "Integrating occupant behaviour in the simulation of coupled electric and thermal systems in buildings", in *8th International Modelica Conference*, Dresden, Germany: Linköping University Electronic Press, Linköpings universitet, Mar. 2011. DOI: DOI: 10.3384/ecp11063.

[3] H. Elmqvist, B. Bachmann, F. Boudaud, J. Broenink, and D. Brück, "Modelica - a unified object-oriented language for physical systems modeling", Lund, Sweden, Tech. Rep., 1999, pp. 1–49.

[4] M. Wetter, "A modelica-based model library for building energy and control systems", in *Building Simulation 2009 - Eleventh International IBPSA Conference*, Glasgow, Schotland: IBPSA, Jul. 2009, pp. 652–659.

[5] M. Wetter and C. Van Treeck, *Iea ebc annex 60 - new generation computational tools for building and community energy systems based on the modelica and functional mockup interface standards*, http://iea-annex60.org/about.html, Accessed: 2015-01-14.

[6] E.ON Energy Research Center, RWTH Aachen University, *Aixlib*, https://github.com/RWTH-EBC/AixLib, Accessed: 2015-03-18, 2015.

[7] KU Leuven and 3E, *Open-ideas source code repository*, https://github.com/open-ideas, Accessed: 2015-03-18.

[8] K. Davies, *Modelicares*, http://kdavies4.github.io/ModelicaRes/, Accessed: 2015-03-18.

[9] S. Prívara, "Building modeling and identification for predictive control", PhD thesis, Czech Technical University in Prague, 2013.

[10] G. P. Henze, "Model predictive control for buildings: a quantum leap?", *Journal of Building Performance Simulation*, vol. 6, no. 3, pp. 157–158, May 2013, ISSN: 1940-1493. DOI: 10.1080/19401493.2013.778519.

[11] S. Goyal and P. Barooah, "A method for model-reduction of non-linear thermal dynamics of multi-zone buildings", *Energy and Buildings*, vol. 47, pp. 332–340, Apr. 2012, ISSN: 03787788. DOI: 10.1016/j.enbuild.2011.12.005.

[12] D. Sturzenegger, D. Gyalistras, M. Morari, and R. S. Smith, "Semi-automated modular modeling of buildings for model predictive control", *Proceedings of the Fourth ACM Workshop on Embedded Sensing Systems for Energy-Efficiency in Buildings - BuildSys '12*, p. 99, 2012. DOI: 10.1145/2422531.2422550.

[13] S. Royer, S. Thil, T. Talbert, and M. Polit, "A procedure for modeling buildings and their thermal zones using co-simulation and system identification", *Energy and Buildings*, vol. 78, pp. 231–237, Aug. 2014, ISSN: 03787788. DOI: 10.1016/j.enbuild.2014.04.013.

[14] S. Prívara, J. Cigler, Z. Váňa, F. Oldewurtel, C. Sagerschnig, and E. Žáčeková, "Building modeling as a crucial part for building predictive control", *Energy and Buildings*, vol. 56, pp. 8–22, Jan. 2013, ISSN: 03787788. DOI: 10.1016/j.enbuild.2012.10.024.

[15] T. Bohlin, "Editorial - special issue on grey box modelling", *International journal of adaptive control and signal processing*, vol. 9, pp. 461–464, 1995.

[16] M. Gwerder, D. Gyalistras, C. Sagerschnig, R. S. Smith, and D. Sturzenegger, "Final report : use of weather and occupancy forecasts for optimal building climate control – part ii : demonstration (opticontrol-ii)", Automatic Control Laboratory, ETH, Zurich, Zwitzerland, Tech. Rep. September, 2013, p. 156.

[17] M. Sourbron and L. Helsen, "Sensitivity analysis of feedback control for concrete core activation and impact on installed thermal production power", *Journal of Building Performance Simulation*, vol. 00, pp. 1–17, Sep. 2013, ISSN: 1940-1493. DOI: 10.1080/19401493.2013.824028.

[18] T. Bohlin, *Practical Grey-box Process Identification*, Advances i, M. J. G. Johnson and M. A., Eds. London: Springer London, 2006, p. 351, ISBN: 9781846284021. DOI: 10.1007/1-84628-403-1.

[19] R. Sims, P. Mercado, W. Krewitt, G. Bhuyan, D. Flynn, H. Holttinen, G. Jannuzzi, S. Khennas, Y. Liu, L. J. Nilsson, J. Ogden, K. Ogimoto, M. O'Malley, H. Outhred, Ø. Ulleberg, and F. van Hulle, "Integration of renewable energy into present and future energy systems", in *IPCC Special Report on Renewable Energy Sources and Climate Change Mitigation*, O. Edenhofer, R. Pichs-Madruga, Y. Sokona, K. Seyboth, P. Matschoss, S. Kadner, T. Zwickel, P. Eickemeier, G. Hansen, S. Schlömer, and C. von Stechow, Eds., Cambridge, United Kingdom and New York, NY, USA: Cambridge University Press, 2011.

[20] G. Reynders, T. Nuytten, and D. Saelens, "Potential of structural thermal mass for demand-side management in dwellings", *Building and Environment*, vol. 64, pp. 187–199, Mar. 2013, ISSN: 03601323. DOI: 10.1016/j.buildenv.2013.03.010.

[21] G. P. Henze, C. Felsmann, and G. Knabe, "Evaluation of optimal control for active and passive building thermal storage", *International Journal of Thermal Sciences*, vol. 43, no. 2, pp. 173–183, 2004.

[22] G. P. Henze, "Energy and cost minimal control of active and passive building thermal storage inventory", *Journal of Solar Energy Engineering*, vol. 127, no. 3, p. 343, 2005, ISSN: 01996231. DOI: 10.1115/1.1877513.

[23] M. Petersen, K. Edlund, L. Hansen, J. Bendtsen, and J. Stoustrup, "A taxonomy for modeling flexibility and a computationally efficient algorithm for dispatch in smart grids", in *American Control Conference (ACC), 2013*, Washington, DC: IEEE, Jun. 2013, pp. 1150–1156, ISBN: 9781479901784.

[24] J. Cochran, M. Miller, O. Zinaman, M. Milligan, D. Arent, B. Palmintier, M. O'Malley, S. Mueller, E. Lannoye, A. Tuohy, *et al.*, "Flexibility in 21st century power systems", National Renewable Energy Laboratory (NREL), Golden, CO., Tech. Rep., 2014.

[25] F. Oldewurtel, D. Sturzenegger, G. Andersson, M. Morari, and R. S. Smith, "Towards a standardized building assessment for demand response", in *Proceedings of the IEEE Conference on Decision and Control*, Firenze, Italy: IEEE, Dec. 2013, pp. 7083–7088, ISBN: 9781467357173. DOI: 10.1109/CDC.2013.6761012.

Chapter 3

Integrated system simulation

This chapter compiles the following publications:

R. De Coninck, R. Baetens, B. Verbruggen, J. Driesen, D. Saelens, and L. Helsen, "Modelling and simulation of a grid connected photovoltaic heat pump system with thermal energy storage using modelica", in *8th International Conference on System Simulation in Buildings (SSB2010)*, P. Andre, S. Bertagnolio, and V. Lemort, Eds., Liège, 2010, P177
Personal contribution: 75 %

R. Baetens, R. De Coninck, J. Van Roy, B. Verbruggen, J. Driesen, L. Helsen, and D. Saelens, "Assessing electrical bottlenecks at feeder level for residential net zero-energy buildings by integrated system simulation", *Applied Energy*, vol. 96, no. Special issue on Smart Grids, Renewable Energy Integration, and Climate Change Mitigation - Future Electric Energy Systems, pp. 74–83, 2012, ISSN: 03062619. DOI: 10.1016/j.apenergy.2011.12.098
Personal contribution: 10 %

R. De Coninck, R. Baetens, D. Saelens, A. Woyte, and L. Helsen, "Rule-based demand side management of domestic hot water production with heat pumps in zero energy neighbourhoods", *Journal of Building Performance Simulation*, vol. 4, no. 7, pp. 271–288, 2014. DOI: 10.1080/19401493.2013.801518
Personal contribution: 80 %

3.1 Introduction

This chapter describes three different case studies treating roughly the same research question: what is the interaction between one or more buildings and the electricity distribution grid and to what extent can this interaction be influenced by rule-based controls?

In the first paper, a single-dwelling simulation study is carried out. The dwelling has a stochastic user profile, a PV system and a heat pump with a hot water storage tank. The interaction between the dwelling and the distribution grid is characterised by the one percent peak power and the percentage of time with a net grid exchange above 5000 W. Different control strategies and hot water storage sizes are combined in order to attempt to reduce both grid impact indicators.

This first paper has a clear drawback: without taking into account the other buildings connected to the same distribution network, it is impossible to judge on the impact of the dwelling on the grid. Therefore, the next step is to extend the model to the entire local distribution network. The second paper in this chapter models a neighbourhood consisting of 33 low-energy dwellings with PV and heat pumps. The aim of the paper is to develop and demonstrate the IDEAS library in order to assess the joint interaction of the buildings, PV inverters and distribution network. By modelling both the buildings, the thermal and electrical systems, the joint effect of the electrical loads in each building on the voltage at each connection can be studied. This allows to simulate curtailing of the PV inverters as a function of the design of the distribution network.

The last paper in this chapter builds on the previous results. From assessing the problem of PV curtailing we make the step to mitigating the resulting production losses by simulating several rule-based control strategies. The paper illustrates that it is important to assess and solve problems at the correct system level. In the case of the interaction between buildings and the grid, this means simulation of the buildings together with the distribution system in order to correctly capture the time-dependent interactions.

3.2 Modelling and simulation of a grid connected photovoltaic heat pump system with thermal energy storage using Modelica

Modelling and simulation of a grid connected photovoltaic heat pump system with thermal energy storage using Modelica

R. De Coninck[1,2]*, R. Baetens[3], B. Verbruggen[4], J. Driesen[4], D. Saelens[3], L. Helsen[1]

[(1)] Division of applied mechanics and energy conversion section, Department of mechanical engineering

[(2)] 3E, BE-1000 Brussels, Belgium

[(3)] Division of building physics, Department of civil engineering

[(4)] Electrical energy computer architectures, Department of Electrical engineering

[(1)(3)(4)] K.U.Leuven, BE-3000 Leuven, Belgium

ABSTRACT

When the penetration of renewable electricity production in the electricity infrastructure increases, an increased part of the production follows a stochastic behaviour. In order to reduce grid peak loads and to maintain the required balance between production and consumption at all times, two solutions can be envisaged: electricity storage and demand side management (DSM).

One typical DSM solution consists of using thermal energy storage (TES) to decouple electric loads from thermal demands. In order to study the dynamic interaction between thermal (incl. building) and electric systems, their integration in one single simulation environment is required.

This study develops a model in the object oriented language Modelica and uses the model to assess the impact of additional TES capacity. The model describes an energy concept consisting of a dwelling with a grid connected photovoltaic system, a compression heat pump, a hot water storage tank and a control strategy. The multi-disciplinary model, developed in this study, is a first step towards the simulation of complex systems in which thermal and electric components are combined in order to study for example the effects of DSM on grid stability.

The results of a simulation study, using the newly developed model, are presented. The benefits of adding thermal storage capacity with regard to the overall seasonal performance factor (SPF) and the impact of the system on the electrical grid are analysed for a standard control strategy and two variants: a control strategy focusing on operation during daytime and a control strategy focusing on limiting net power exchange peaks. The daytime strategy is able to increase the overall SPF for different storage tank sizes if the storage tank is sufficiently insulated. Both alternative control strategies are able to substantially reduce the number of net power exchange peaks, even with relatively small storage tanks.

Keywords: Photovoltaic, heat pump, thermal energy storage (TES), grid load, simulation, Modelica

1. INTRODUCTION

On May 18th 2010 the European parliament adopted a recast of the Directive on Energy Performance of Buildings (2002/91/EC - the Directive is expected to be published in the official journal in June 2010, the version adopted by the European Parliament on the 23rd of

April 2009 can be found in (The European Parliament, 2009)). Article 9 of this Directive obliges EU member states to build only 'near zero energy buildings' (near ZEB) from 2020 onwards.

Although the definition of a near ZEB in the EU Directive is not elaborated, many different definitions for ZEB can be found in the literature. Torcellini et al. (2006) discuss the impact of four different definitions and conclude that the choice of definition in the design phase influences the energy concept of the building. However, for each of the definitions, it is possible to reach the ZEB target by a combination of energy efficiency, heat pumps and sufficient photovoltaic (PV) systems. In such an all-electric building, the PV system has to cover the electricity consumption on a yearly basis in order to be a site, source or emission ZEB. Only a cost ZEB – for which the net yearly energy services bill has to be zero - might require more PV production than the yearly consumption, depending on the electricity tarification.

From this analysis it can be expected that buildings with a heat pump and a photovoltaic system will become standard practice in new constructions in the short to medium term. Already today we see a strong growth on the domestic heat pump and PV markets (European Heat Pump Association, 2010), (EurObserv'ER 2009).

The major flaw of each of the definitions investigated by Torcellini et al. (2006) is the yearly basis for the analysis. If a large share of the buildings would be ZEB with PV and heat pumps installed, the impact on the electricity grid could be substantial: all these buildings would inject electricity on the grid when the local production exceeds consumption and take electricity from the grid in the opposite cases. These time periods characterized by either peak injection or consumption would occur simultaneously for the majority of these buildings as the weather conditions (both solar radiation and temperature) dictate to a large extent both the electricity production (via PV) and consumption (via the heat pumps). This simultaneity can cause grid stability problems, as described in different contributions (Pepermans, Driesen, Haeseldonckx, Belmans, & D, 2005), (Vu Van, Woyte, Soens, Driesen, & Belmans, 2003), (Houseman, 2009). The specific case of grid coupled PV with a heat pump heating system has been simulated by Baetens et al. (2010).

In this paper, solutions to reduce the grid impact of a combined PV and heat pump concept for a single family dwelling are investigated, while keeping track of the heat pump system performance. The paper focuses on the influence of the size of the storage tank and the control strategy for the heat pump with the aim to increase the SPF of the whole system (and thus lowering total energy use) and reduce both the size and amount of net power exchange peaks.

2. MODEL DEVELOPMENT

A detailed model has been developed in Modelica (The Modelica Association, 1997). Modelica is an open source, object oriented and equation based modeling language. Modelica offers the advantage that the differential and algebraic equations (DAE) that describe the physical behaviour of the components are solved in one DAE system instead of solving all components sequentially. The object oriented approach also enables an easier integration of previous modelling work. Through the use of Optimica, Modelica offers extended functionality with regard to (dynamic) system optimisation (Åkesson, Årzén, Gäfvert, Bergdahl, & Tummescheit, 2009).

The model is schematically presented in Figure 1. It consists of a 2-zone building, an air-to-water heat pump, a stratified storage tank, a heat distribution system with two radiator circuits

and a grid connected PV system. The different components of the model are described in sections 2.1 to 2.4.

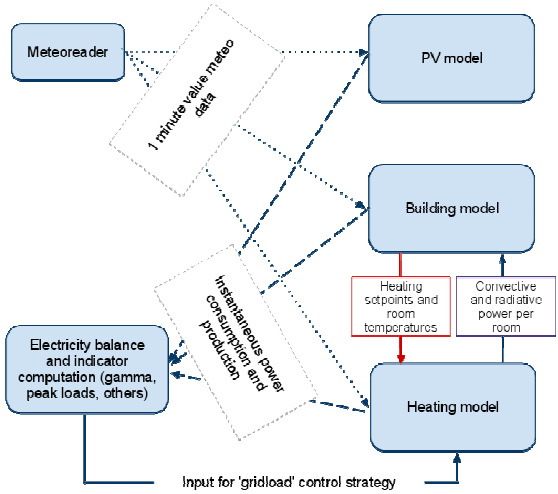

Figure 1 – General model scheme

2.1 Building

In this paper, a high-order lumped capacitance model (Clarke 2001, Underwood & Yik 2004) for predicting the unsteady building response is developed within Modelica. A first-order lumped capacitance approach is used for each of the different construction layers of the building, whereas a second-order model is used for all surface layers in order to cope with restrictions for low Biot-numbers (Incropera et al. 2007) and to allow a more accurate prediction of indoor surface temperatures. Similarly as in the TRNSYS type56, inter-surface longwave radiation is modeled by means of a zone star temperature (Davies 1993), reducing the complexity of the model compared to view factors and allowing a straight-forward implementation of internal convective and radiative gains.

The absorption, transmission and reflection of solar radiation through the array of air and glass layers in the windows is modeled with the embedded technique described by Edwards (1977, 1982). The transmitted diffuse short-wave solar radiation is distributed over all room surfaces weighted to their surface and absorption coefficient, whereas the direct short-wave solar gains are modeled to fall on the floor. Liesen & Pedersen (1997) show that only small differences would arise when making different assumptions on the distribution of the transmitted solar energy.

Within the developed building model, a stochastic generated occupancy profile from Richardson et al. (2008) and domestic load profile are included. The modeled domestic electricity consumption profile takes into account standby power (de Almeida et al. 2008) and domestic cooling appliances (Firth et al. 2008, Liu et al. 2004), lighting (Stokes et al. 2004, Richardson et al. 2009), fan operation, cooking (Glorieux & Vandeweyer 2002, Wood & Newborough 2003) and the use of media like television and computer (Glorieux &

Vandeweyer 2002, TPDCB 2010). For the purpose of detailed energy prediction and simulation, the original tool for lighting has been coupled to minute global irradiance data derived from Meteonorm 6.1 (Meteotest, 2008) for Uccle, Belgium. The use of the washing machine and tumble dryer are not modelled in detail as their current use is determined by the day and night regime of electricity resulting in a lack of relevant information on their usage and consumption profiles.

The modelled building is conceived as an energy regulation complying building with two rectangular thermal zones (day zone and night zone) with a floor surface of 80 m² each. The walls are massive cavity walls with 15 cm of mineral wool (λ=0.036 W/mK), The roof also contains 15 cm of mineral wool, the floor is insulated with 10 cm PUR. All windows have double glazing (U=1.1 W/m²K). An uncontrolled natural ventilation with fixed air change rate of 0.3 ACH is assumed. All internal gains as well as the occupation hours are based on the stochastic methods described above. The occupation determines the heating set point (21°C in the day zone, 16°C in the night zone), there is no heating outside the occupation hours.

2.2 Heating system

The hydraulic scheme of the heating system is presented in Figure 2. The model is based on the 'hydronic heating' example in the Modelica Building library v0.8, developed by Michael Wetter (2009). The heat production system is composed of an air-to-water heat pump (on-off control), a storage tank, supply and return ducts and a pump (P1). The heat distribution side consists of a pump (P2), a three-way valve to control the water temperature, supply and return ducts and two heat emission circuits, each composed of a radiator, a thermostatic valve and two ducts.

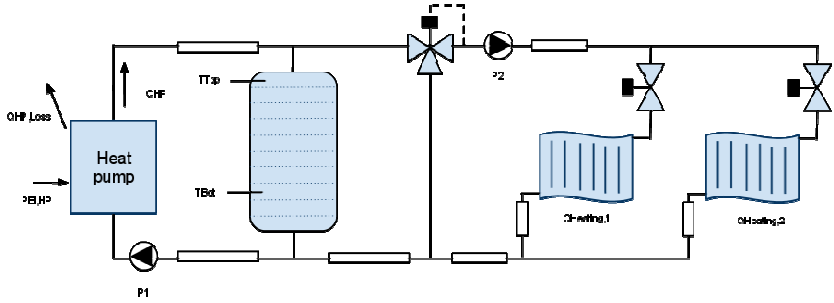

Figure 2 – Simplified hydraulic scheme of the heating system, with basic nomenclature

The heat pump characteristics are derived from catalogue data from the Viessmann Vitocal 350 heat pump (Viessmann, 2006). The thermal (Q_{HP}) and electric power ($P_{El,HP}$) are expressed as a function of ambient temperature and condenser temperature T_{HP}, as presented in equations (1) and (2).

$$P_{El,HP} = \frac{Q_{HP,nom}}{10000} \cdot \left(26.14 \cdot T_{Amb} + 84.62 \cdot T_{HP} + 138.3 \right) \quad (1)$$

$$Q_{HP} = \frac{Q_{HP,nom}}{10000} \cdot \left(1.48 \cdot T_{Amb}^{\ 2} + 241.75 \cdot T_{Amb} + 10989 \right) \quad (2)$$

In the model developed within this study, the heat pump has an internal water volume and internal dry mass which are coupled to assign an equal temperature. Thermal heat pump losses are modeled between on the one hand this internal volume and dry mass and on the other hand the surroundings (assumed to be constant at 15°C). The instantaneous coefficient of performance (COP) of the heat pump can be calculated as $Q_{HP}/P_{El,HP}$. Equations (3) and (4) define two different seasonal performance factors (SPF), based on the nomenclature of Figure 2.

$$SPF_{heat\ pump} = \frac{\int Q_{HP}}{\int P_{El,HP}} \tag{3}$$

$$SPF_{system} = \frac{\int Q_{heating,1} + \int Q_{heating,2}}{\int P_{El,HP} + \int P_{El,P1} + \int P_{El,P2}} \tag{4}$$

The storage tank has ten stratification layers with a uniform temperature each. Heat conduction is modeled between the layers through the fluid, and between the layers and the surroundings (at constant temperature of 15°C). Temperature inversion is detected and the concerned layers are ideally mixed (Wetter, 2009). Two temperature sensors are available in the tank, TTop in the upper layer and TBot, in the 8th layer (2nd but last).

A dynamic radiator model has been implemented. To allow for varying mass flow rates, the transferred heat is computed using a discretization along the water flow path (10 steps), and heat is exchanged between each compartment and a uniform room air and radiation temperature. For the transient response, heat storage is computed using a finite volume approach for the water and the metal mass, which are both assumed to be at the same temperature (Wetter, 2009).

The thermal behavior of the ducts is neglected. The ducts are simulated taking into account only their pressure drop (dp) with a fixed flow coefficient $k=m_{flow}/\sqrt{(dp)}$. Near the origin, the square root relation is linearized to ensure that the derivative is bounded. A linearized flow characteristic is assumed for all valves, the three-way valve has a leak flow rate of 1% of the nominal flow rate. The pumps have a (linear) flow characteristic that defines the relation between flow rate and pressure drop (Wetter, 2009).

Pump P2 (Figure 2) is pressure drop controlled: it keeps a predefined pressure drop between its inlet and outlet at all times. The thermostatic valves are temperature controlled. A temperature setpoint (operative temperature) is received from the building model, based on occupancy. A proportional controller converts the difference between the setpoint and actual operative temperature in a control signal between 0 and 1 that is passed to the thermostatic valve.

2.3 Photovoltaic system

The PV panels are modeled using the single-diode equivalent circuit. This consists of a current source, I_{ph}, a Diode with current I_o, a shunt resistor R_{sh} and a series resistor R_s. Here I_{ph} represents the light current and I_o the diode reverse saturation current. The equation of this equivalent circuit is given by (5), with i representing the current flowing out of the panel and v the voltage at the clamps.

$$i = I_{ph} - I_o \left(e^{\frac{v+iR_s}{n_s V_t}} \right) - \frac{v+iR_s}{R_{sh}} \tag{5}$$

The five parameters in this model, I_{ph}, I_o, R_{sh}, R_s and V_t are calculated following the method described by Sera, Teodorescu, and Rodriguez (2007). The parameters are calculated based on characteristics of the PV panel which are, in most cases, provided by the manufacturer. These specifications are the current I_{mpp} and voltage V_{mpp} at the maximum power point under standard testing conditions (STC), the short circuit current I_{sc} and open circuit voltage V_{oc} at STC, and the temperature coefficients k_i and k_v of the short circuit current and open circuit voltage. Given V_{mpp} and I_{mpp} should satisfy equation (5), the derivative of the power with respect to the voltage at maximum power point should be zero and the derivative of the current with respect to the voltage at short-circuit current should be the negative of the shunt conductance, R_s, R_{sh} and V_t can be calculated. I_o and I_{ph} at STC can be found from equation (5) for the short-circuit and open-circuit condition.

In this study, 30 panels, all considered to be identical, with 230 W_p each are modeled. The output per PV panel is calculated given perfect maximum power point tracking capability. This output is assumed to be dependent on the position of the sun, the radiation and the ambient temperature.

The position of the sun is given by minute values of the zenith angle from the meteoreader and the orientation is calculated using the time of the day. The sun's position together with the orientation and tilt of the PV panels, gives the incidence angle of direct beam radiation on the panel and allows to calculate the amount of beam radiation that gets reflected and passes the PV panel cover using incidence angles modifiers derived from De Soto, Klein, and Beckman (2006).

The absorbed solar radiation is calculated given the incidence angle modifiers and minute values for the diffuse and direct beam radiation supplied by the meteoreader, together with the ground reflected radiation (De Soto et al. 2006). The ambient temperature, together with the temperature rise caused by the absorbed radiation and the panel efficiency, enable to estimate the cell temperature. Cell temperature and absorbed radiation are used to calculate the parameters of the PV panel for non-reference working conditions (De Soto et al. 2006). Solving equation (5) for these new parameters and given the assumption of perfect maximum power point tracking capability and constant inverter efficiency yields the electrical energy output of the PV system.

2.4 Heat pump control

A heating curve is defined, through which the heating curve temperature (T_{hc}) is calculated as follows (Wetter, 2009):

$$T_{hc} = T_R + \left(\frac{T_{S,N} + T_{R,N}}{2} - T_R \right) \cdot Q_{Rel}^{\ m^{-1}} + \left(\frac{T_{S,N} - T_{R,N}}{2} - T_R \right) \cdot Q_{Rel} \tag{6}$$

In this equation, T_R is the room temperature, $T_{S,N}$ and $T_{R,N}$ are the nominal supply and return temperature and Q_{Rel} is the relative heat demand calculated as:

$$Q_{Rel} = \frac{T_R - T_{Ambient}}{T_R - T_{Design}} \tag{7}$$

with T_{Design} the minimum outdoor temperature for which the heating system is designed.

This heating curve incorporates the heat emission characteristics of the radiators by taking into account the heat transfer exponent m. In most heating systems, the heating water temperature set point (HWTS) is a running average of the heating curve temperature with a time lag typically between four and twelve hours. However, as shown in Figure 3, such a HWTS is still relatively sensitive to intra-day temperature variations.

Another approach would be to apply a first order filter to the heating curve in order to flatten out the intra-day oscillations. The effect of a first order filter with a time constant of twelve hours is presented in Figure 3, showing that a filtered HWTS is more dampened.

Optimization of the HWTS is not the subject of the present study. All simulations are made with a first order filter with a time constant of twelve hours on the set point.

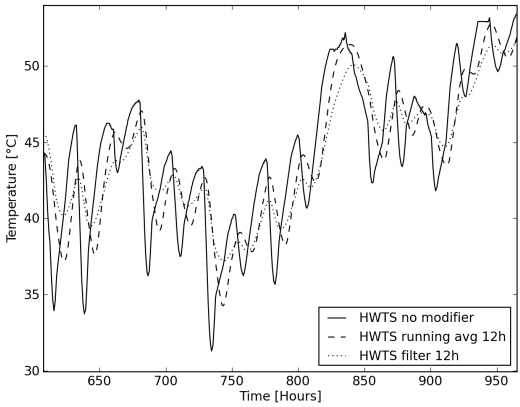

Figure 3 – HTWS without modifier (= T_{hc}), as running average with twelve hours time lag and filtered with twelve hours time constant for two weeks. T_{hc} is calculated based on T_R =20°C, $T_{S,N}$ =60°C, $T_{R,N}$ =50°C and T_{Design}=-8°C

The heat pump control strategy is based on comparing the top and bottom tank temperatures (TTop and TBot) with the current HWTS as shown in equations (8) and (9).

$$HP_{on} \ when \ TTop < HWTS + 3K \tag{8}$$

$$HP_{off} \ when \ TBot > HWTS + 4K \tag{9}$$

The HWTS has not only a large impact on the COP of the heat pump, it also influences to some extent the operation time of the heat pump when a storage tank is present. This is shown in equation (8): when the HWTS is rising, HP_{on} will become true and the heat pump has to start.

In systems with a small storage tank, the heat pump has to follow the heat demand closely. Therefore we can say that the heat pump operation is largely determined by the heat demand and the time derivative of the HWTS, whereas the heat pump's COP is mainly determined by the HWTS and the ambient temperature.

Three different control strategies have been analysed in this work:

1. Heating Curve – control of the heat pump solely based on the equations (8) and (9);

2. Daytime – satisfaction of equation (8) + additionally trying to charge the storage tank during a predefined daytime period;
3. Grid load - satisfaction of equation (8) + additionally starting AND shutting down the heat pump when the net power exchange exceeds predefined boundary values;

The details of these control strategies are explained in their respective sections in the next chapter.

3. SIMULATION RESULTS AND DISCUSSION

3.1 Modelica simulation

The simulations are all carried out over a period of 6 weeks, starting at the 1st of January, thereby focusing on heating during the winter season. The meteodata are minute values for solar radiation and ambient temperature computed by Meteonorm 6.1 (Meteotest, 2008) for Uccle, Belgium. The solar irradiation on the building and PV surfaces are computed with a radiation processor TRNSYS 16 and imported in Modelica.

All simulations are performed with Dymola 7.3. For information, the simulation duration for 6 weeks ranged from 1h to 2h (depending on the computer used) with 4th and 5th order stiff solvers esdirk34a and esdirk45a.

3.2 Reference situation

The reference situation has a storage tank with a volume of 300 l and a thermal resistance of the insulation of 2.5 m²K/W. The averaged (over six weeks) heat demand of the building as a function of the hour of the day is presented in Figure 4, which shows that the majority of the heat demand occurs in the morning with a second, much smaller peak towards the evening. However, similar to all user behavior, the heat demand is stochastically computed and therefore this average demand cannot be seen as a profile.

A sequence (time series) of temperatures for 4 days is presented in Figure 5. This figure shows the stochastic nature of the operative room temperatures, and consequently the heat demand, and the occurrence of short occupancy periods. In average over the six simulated weeks, there are two occupancy periods per day. To check the thermal comfort, all hours for which the operative temperature of one of the rooms is 1K below the setpoint are summed. For all simulations discussed in this paper, the number of thermal discomfort hours is in the range [57h – 63h].

Taking into account thermal losses from the heat pump to the surroundings, the heat pump SPF, as defined in equation (3) is 2.41 for the reference situation. The heating system SPF, defined in equation (4) reaches 2.29.

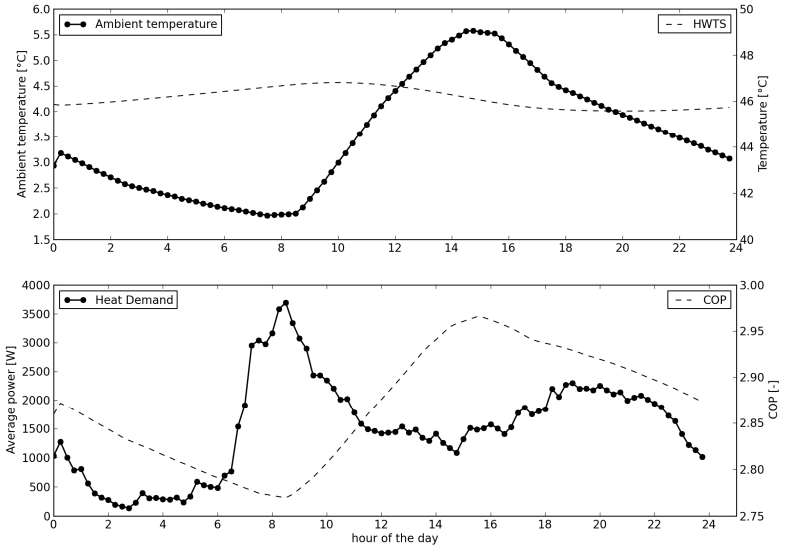

Figure 4 – Average ambient temperature (top) and heat demand (bottom) by hour of the day over six weeks. The figure also shows the averaged HWTS (top) and the averaged nominal COP of the heat pump (bottom)

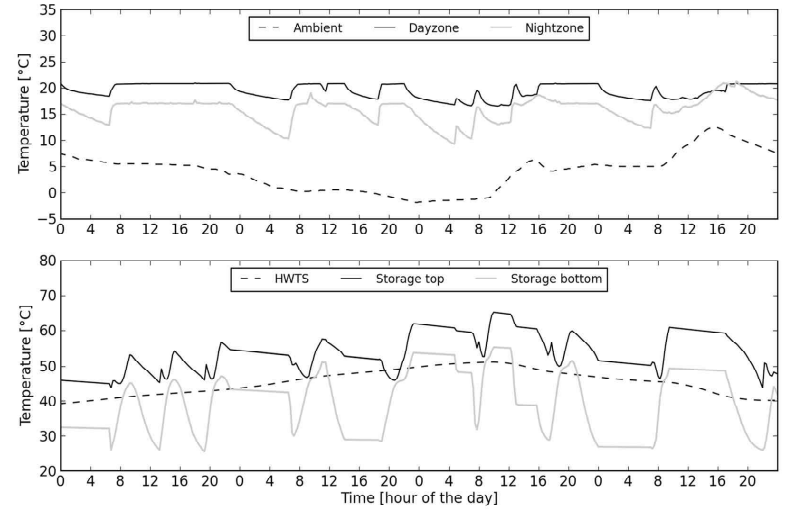

Figure 5 – Time series of ambient temperature and room temperatures (top) and HWTS and storage tank temperatures (bottom) for four typical days

3.3 Heating curve control strategy

In a first series of simulations, the effect of increasing the storage tank size is analysed without changing the control strategy. Figure 6 shows the evolution of heat pump and heating system SPF with the storage size. It is clear that the total system efficiency is always lower than the reference case, due to the additional thermal losses of the storage tank, even for higher heat pump efficiencies (in some cases). The average distribution of the heat pump power as a function of the hour of the day is shown in Figure 7 for different storage volumes.

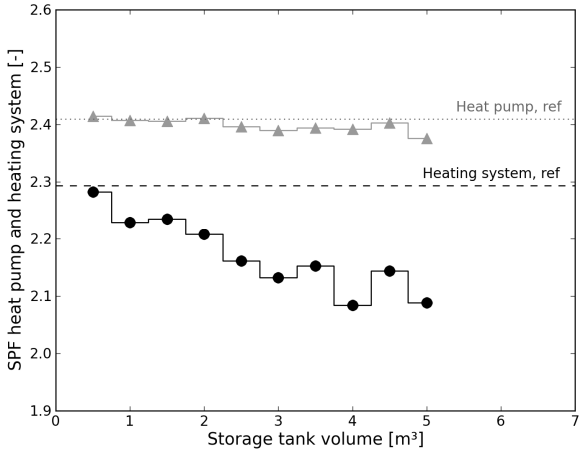

Figure 6 –SPF of heat pump (grey triangles) and total heating system (black dots) for the heating curve control strategy as a function of storage size, compared to the reference case (= 300 l storage tank)

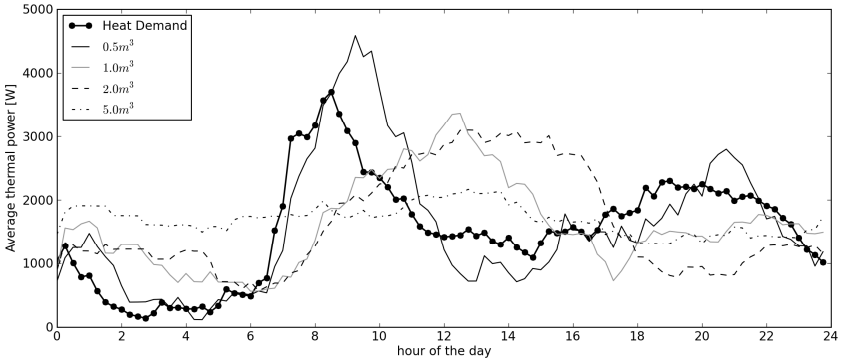

Figure 7 – Average distribution of heat demand and heat pump power as a function of the hour of the day for the heating curve control strategy

It is clear that the matching between the average heat demand and the average heat pump power reduces with increasing storage volume. For a single dwelling this is not very important, but when different buildings with heat pumps are clustered, flattening out of the heat pump operation times will have a large impact on the cluster's peak power and capacity factor.

3.4 Daytime control strategy

The second control strategy aims at increasing the heat pump's SPF by shifting its average operation time. As seen in Figure 4, operating the heat pump in the afternoon would lead to higher SPF's thanks to the higher ambient temperature (on average).

There are different solutions to implement such a control strategy. One option, Model Predictive Control (MPC), tries to optimize the control by using a simulation based forecast of the boundary conditions and state variables (Bianchi, 2006). This approach is for instance applied by Degrauwe et al. (2010) for similar air-to-water heat pumps as used in the current study.

In the current research, we have deliberately chosen for a simple control strategy based on very few real-time measurements. The aim is to study the impact of some variations rather than optimizing the control strategy.

As in the heating curve control, the daytime control will always satisfy equation (8). Based on Figure 4, the daytime period (DTP) is fixed from 12 AM till 7 PM. During this period, the storage tank is charged until it is completely full (equation (9)), outside this period, charging stops when the tank top temperature is again at HWTS + 3K. However, a minimum on-time of 20 minutes for the heat pump is implemented.

In order to increase the probability of charging during DTP, the controller will not wait until equation (8) is met. Therefore, a tank state of charge (SOC) is defined that enables to assess the charge status at any time. When the SOC is below a pre-defined threshold during DTP, charging will start. Even though the tank has 10 nodes, with regard to practical implementation, the SOC is defined based on two temperature measurements only, in the top and 8th layer of the tank (see Figure 2).

The definition is based on the principle that two partial SOC values are determined, one for each temperature sensor, and the tank SOC is computed as the average of those two partial values.

$$SOC_{Tank} = \frac{SOC_{Top} + SOC_{Bot}}{2} \tag{10}$$

The values for the partial states of charge are determined by linear interpolation between a value for SOC=0 and SOC=1, as illustrated in Figure 8.

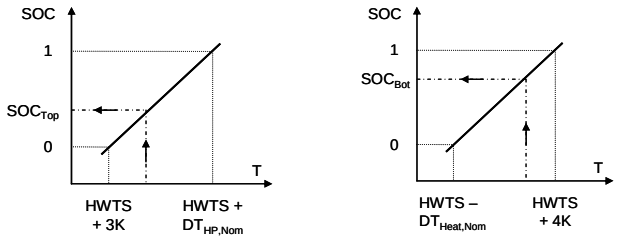

Figure 8 – Principle used to determine the partial SOC_{Top} (left) and SOC_{Bot} (right)

In order to determine the required four boundary conditions for SOC_{Top} and SOC_{Bot} the following reasoning is applied. The tank is completely empty (SOC_{Tank}=0) when equation (8) is met. This defines the TTop for condition SOC_{Top}=0. At that time, it is assumed that TBot

is at the heating system's return temperature, HWTS-$DT_{Heating,\ nom}$, with $DT_{Heating,\ nom}$ the nominal temperature difference between heating supply and return. This results in the condition for SOC_{Bot}=0.

On the other hand, the tank is completely full (SOC_{Tank}=1) when equation (9) is met. This defines the TBot for condition SOC_{Bot}=1. In order to determine the condition for SOC_{Top}=1, it is assumed that when equation (9) is met, the real bottom temperature in the tank (10th node) is equal to HWTS. The assumed TTop at that time is then HWTS + $DT_{HP,\ nom}$, with $DT_{HP,\ nom}$ the nominal temperature difference between condenser in- and outlet.

This definition of SOC is used in both the daytime and grid load control strategies with $DT_{Heating,\ nom}$ = 15 K and $DT_{HP,\ nom}$ = 14 K. It can be noted that SOC_{Tank} is completely depending on HWTS, and therefore it is a unit-free indicator of the energy content of the storage tank with respect to the current heating needs, not compared to the surroundings.

The averaged thermal heat pump power as a function of the hour of the day is presented in Figure 9 for different storage sizes when the daytime control strategy is applied. The DTP can be clearly identified on this graph, and it can be seen that for all storage sizes, the heat pump operates most often during DTP. However, in the case of small tanks, the heat pump has to shut down much before the end of the DTP because the tank is full. As a consequence, for these small tank volumes, the heat pump has to run more often beyond the DTP, especially in the morning when the heat demand is large. From 1 m³ tank volume upwards, it is possible to produce most of the heat during DTP.

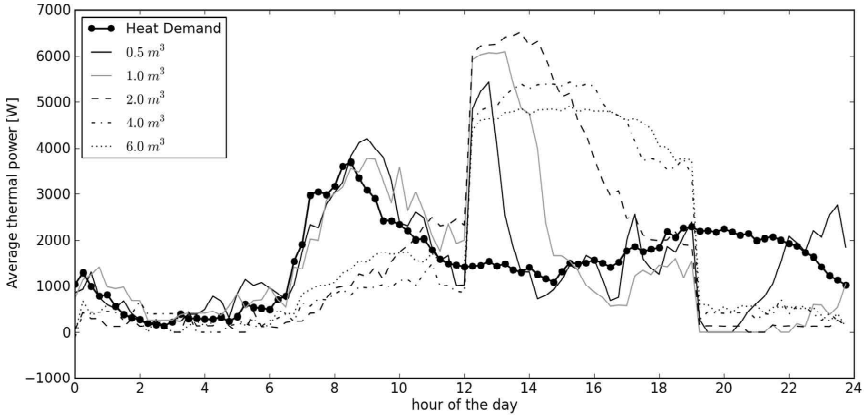

Figure 9 - Average distribution of heat demand and heat pump power as a function of the hour of the day for different storage sizes, using the daytime control strategy

Figure 10 shows that the daytime control strategy is able to raise both the heat pump and system SPF, but only for a small storage tank of 0.5 m³. Due to increasing storage losses, the system SPF drops quickly with increasing tank volume.. Additional simulations have been performed with a better insulation of the tank (5 and 10 m²K/W respectively). The resulting system SPF's are shown in Figure 11. These results show clearly that insulation of the storage tank is a crucial parameter. This conclusion is not new in the context of air-to-water heat pumps, it agrees with measurements performed by Verhelst et al. (2008). With well insulated tanks, it is possible to increase the system SPF with up to 4% compared to the reference situation.

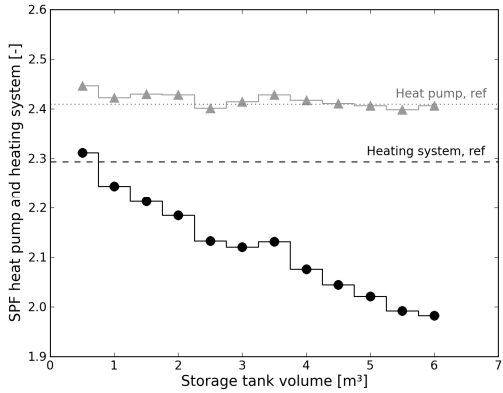

Figure 10 –SPF of heat pump (grey triangles) and total heating system (black dots) for the daytime control strategy as a function of storage size, compared to the reference case

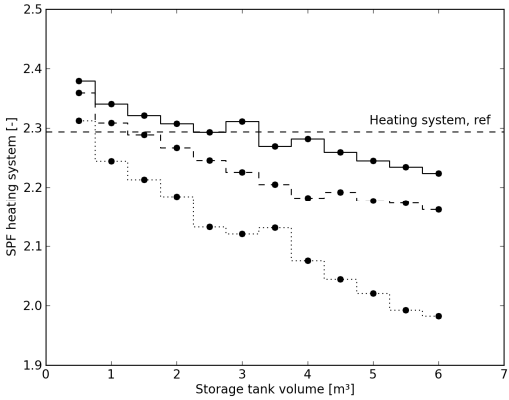

Figure 11 –SPF of total heating system, daytime control strategy, as a function of storage size, compared to the reference case. Three different insulation levels, from lower to higher: 2.5, 5 and 10 m²K/W

3.5 Grid load control strategy

When different buildings with identical or similar energy concepts are connected to the same electricity grid, the simultaneity of the electricity demand and injection peaks can cause the grid to collapse. Therefore, a third control strategy is implemented that tries to reduce peaks, both positive (consumption) and negative (injection).

The principle of the grid load control strategy is to try to keep the storage tank at an intermediate SOC at all times in order to be able to switch off or on the heat pump when the power consumption respective injection surpasses a predefined threshold, identified as B_{Cons} and B_{Inj}.

When the net power exchange P_g reaches the threshold (either B_{Cons} or B_{Inj}), switching on or off the heat pump (on when $P_g<B_{Inj}$, off when $P_g>B_{Cons}$) will always lower the net power exchange (if the total threshold band, B_{Cons} - B_{Inj} is larger than the heat pump power P_{HP}

which is always the case in this study). Defining the switching on condition when there is no immediate emergency is more difficult because the electric power consumption of the heat pump is variable and thus the resulting net power exchange after switching on can not be known in advance.

To cope with this issue, the electricity consumption of the heat pump immediately after switching on ($P_{Hp,last}$) is stored in the internal memory of the controller and the resulting conditions for switching on the heat pump are given by equation (11).

$$\begin{aligned} HP_{on}\ when\ & (TTop < HWTS + 3K) \\ & OR\ (SOC_{Tank} < SOC_{Start}\ \ AND\ P_g < (B_{Cons} - P_{HP,last})) \\ & OR\ (TBot < HWTS + 4K\ \ AND\ P_g > B_{Inj}) \end{aligned} \tag{11}$$

The conditions for switching off the heat pump are given by equation (12):

$$\begin{aligned} HP_{off}\ when\ & \left(t_{HP\,on} > 20\,\text{min}\ AND\ not\,(TTop < HWTS + 3K)\right)\ AND \\ & [\ (SOC_{Tank} > SOC_{Stop}\ \ AND\ P_g > (B_{Inj} + P_{HP}))\ ) \\ & OR\ (P_g > B_{Cons}) \\ & OR\ (TBot > HWTS + 4K)\ \ ] \end{aligned} \tag{12}$$

These equations contain different parameters; in the following simulations SOC_{Start} is always 0.5, SOC_{Stop} is 0.7 and the absolute value of B_{Inj} and B_{Cons} is either 3500 or 4500W.

Figure 12 shows a time series (over two days) with the electricity consumptions and grid load in the top graph and the status of the storage tank in the bottom graph. The horizontal lines on the top graph indicate the quarter hourly peak power. It can be noted that these are often higher or lower than the plotted P_g. This is due to the fact that the quarter hourly peaks contain the maximum values occurring during the considered quarter, whereas all other values are instantaneous values with time steps of fifteen minutes in between.

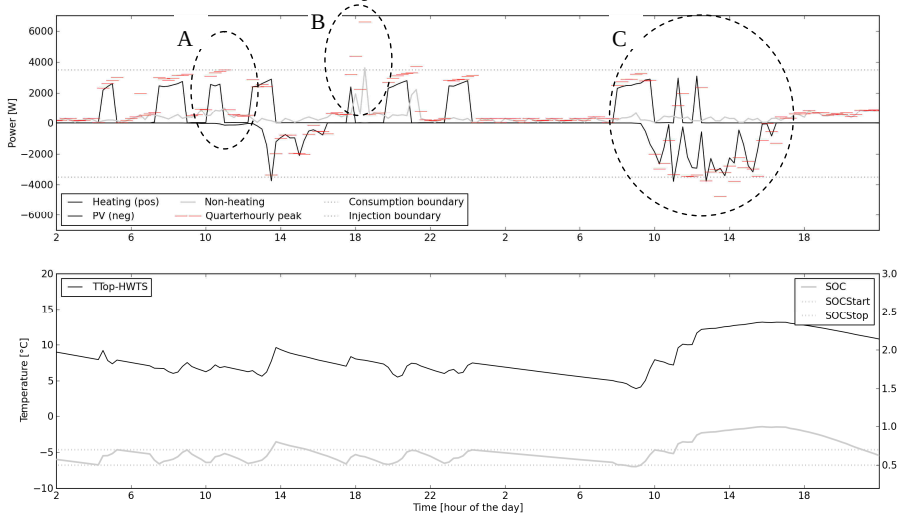

Figure 12 – Time series of electrical powers (top) and storage tank status (bottom) for 2 typical days. The bottom plot also shows the difference between TTop and HWTS. The grid load control strategy has B_{Cons} and B_{Inj} on 3500/-3500W and has a 1m³ storage tank

Figure 12 illustrates some interesting phenomena:

A. the heat pump is shut down, otherwise P_g would become larger than B_{Cons} ;

B. the heat pump is shut down, but this is not enough to limit P_g and 2 (quarter hourly) peaks appear. The first one is occurring during operation of the heat pump, since the heat pump cannot immediately shut down because of the requirement to operate minimum 20 minutes. The second peak is due to the non-heating electricity consumption only;

C. in order to limit power injection to 3500 W, the heat pump starts to charge the storage tank above a SOC of 0.7, but has to stop when TBot reaches HWTS+4K. With a larger tank (or a lower initial SOC), the following peaks could probably have been avoided.

3.6 Grid impact

To assess the degree of success of the studied control strategies, objective indicators need to be defined. In the discipline of electrical engineering, the capacity factor (CF, defined as the peak power/rated connection (kW/kVA)) and full load equivalent hours (FLEHO, defined as yearly consumption/peak power, in h) are often used. These indicators contain no information, however, on the amount of peaks that occur. Moreover, the FLEHO will improve when the consumption increases for a given peak power, making it even less suited to compare control strategies.

In the current study the indicators that have been chosen are the one percent peak (OPP) and the percentage of time with a net grid exchange above 5000 W (both injection and consumption). The OPP is defined as the mean power of the one percent highest quarter hourly peaks. The 5000 W barrier has been chosen since this is a point at which some grid connections might change, i.e. PV systems of more than 5000 W_p should have a three phase connection. The combination of these indicators gives an idea of the value of the highest peaks and the amount of peaks.

A histogram of the quarter hourly peaks is shown in Figure 13 for the reference and the two alternative control strategies. The histogram shows that the majority of quarter hourly peaks is situated between 0 - 1000 W, with a second group of peaks situated between 2000 - 4000 W.

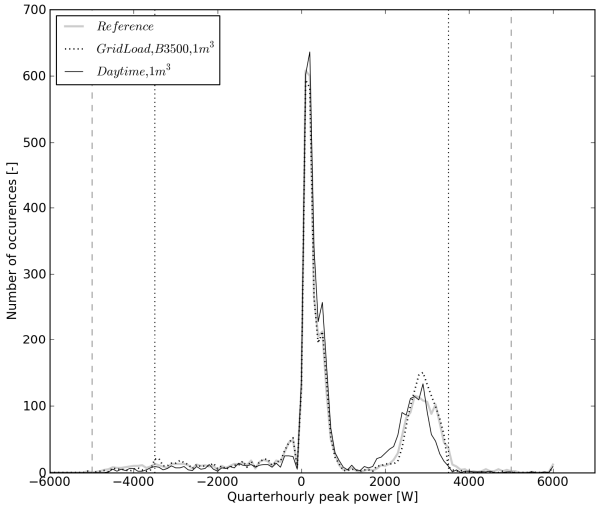

Figure 13 – Histogram of quarter hourly peaks. Ordinate corresponding to the x value shows the amount of peaks during the considered 6 week period for which the peak lies between x +/- 50 W. Consumption is positive. 3 cases are shown: reference, grid load control strategy with both boundaries at -3500 W and 3500 W and 1 m³ storage and daytime control strategy with 1 m³ storage tank. The boundaries are visualised, as is the 5000 W boundary used as indicator

In the current study the indicators that have been chosen are the one percent peak (OPP) and the percentage of time with a net grid exchange above 5000 W (both injection and consumption). The OPP is defined as the mean power of the one percent highest quarter hourly peaks. The 5000 W barrier has been chosen since this is a point at which some grid connections might change, i.e. PV systems of more than 5000 W_p should have a three phase connection. The combination of these indicators gives an idea of the value of the highest peaks and the amount of peaks.

The impact of the grid load strategy on the two defined indicators is presented in Figure 14. The results show that already with a relatively small storage tank of 0.5 m³ or 1 m³, both the OPP and the number of peaks > 5 kW can be significantly reduced. The number of peaks can be reduced by almost 50% in the best cases, the OPP by around 20%. However, the highest peaks could not be eliminated, they are not caused by the heat pump nor the PV system.

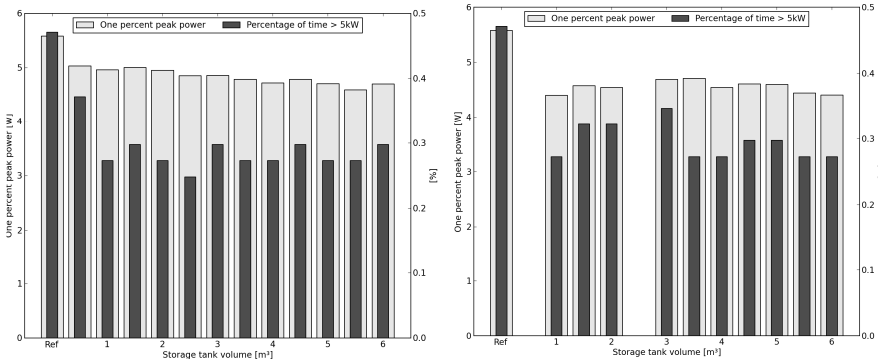

Figure 14 – Impact of grid load control on OPP and percentage of time > 5 kW for different storage tank volumes. Left plot is with boundaries at 4500 and -4500 W, right plot has boundaries at 3500 and -3500 W.

The impact of the daytime control strategy on the grid indicators is presented in Figure 15. It is clear that the results are very positive for 1 m³ and 1.5 m³ storage tanks. The reason for this low grid impact can be understood by analyzing Figure 16, which shows the average electricity production and consumption (heating and non-heating) as a function of the hour of the day. The graph shows that the heat pump works most often during periods characterized by large PV production, thereby reducing both positive and negative power peaks.

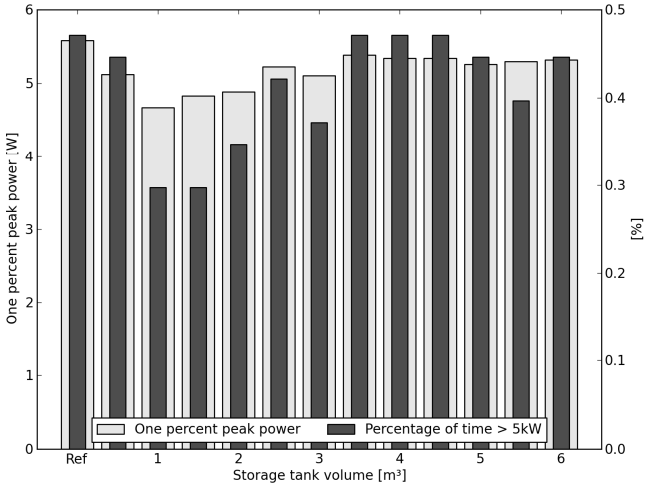

Figure 15 – Impact of daytime control strategy on OPP and percentage of time > 5 kW for different storage tank volumes

The overall results for a selection of cases are shown in Figure 17. From these results, it can be observed that different control strategies and different settings of those control strategies are able to reduce the grid impact. However, all cases have lower system SPF values than the

reference. When the results of Figure 11 are kept in mind, one can conclude that with better insulated storage tanks, the daytime strategy is able to save energy compared to the reference case.

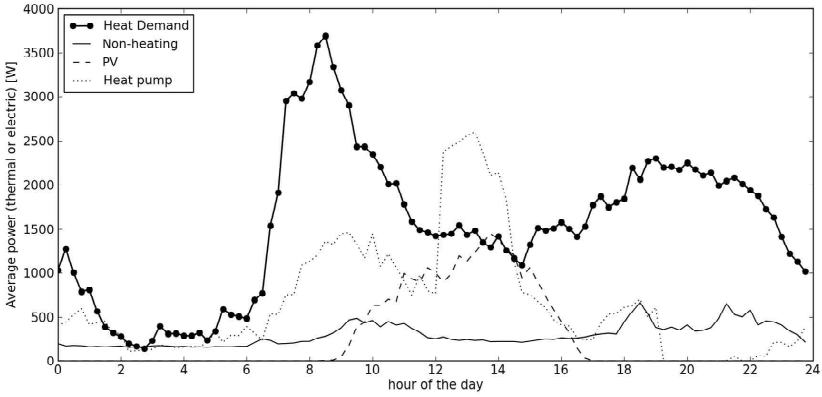

Figure 16 - Average distribution of heat demand (thermal) and electric power for heat pump (daytime control strategy, 1m³ tank), non-heating consumption and PV production as a function of the hour of the day

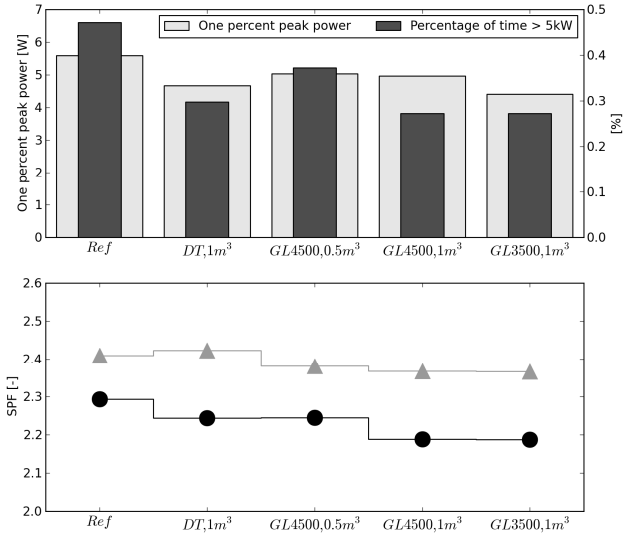

Figure 17 – Comparison of different control strategies. OPP and percentage of time > 5 kW (top), SPF (bottom) of heating system (black dots) and heat pump (grey triangles). DT stands for daytime, GLxxxx for grid load with boundaries xxxx.

4. CONCLUSION

In this study, a dwelling equipped with PV and a heating system based on an air-to-water heat pump has been modeled in Modelica, an open source and object oriented equation based modeling language. The study aimed at investigating the effect of 3 different control strategies (heating curve only, daytime priority and grid load based) on the total efficiency and grid impact of the system.

In order to control the stratified storage tank, a state of charge has been defined based on two temperature measurements in the tank and the current heating water temperature setpoint.

The study has shown that increasing the storage volume will automatically increase the overall energy consumption (and thus decrease the system performance factor) unless an adapted control strategy is applied. With a daytime priority control strategy and a well insulated tank, energy savings are possible, although they are relatively small (4%). This result emphasizes the importance of careful insulation of storage tanks.

In order to reduce the impact on the grid, the grid load control strategy was implemented. The strategy works well and is able to reduce the amount of peaks by almost 50%. The remaining peaks are mainly caused by the non-heating electricity profile. Therefore, the combination of a storage tank of only 1 m^3 and an adapted control strategy is able to eliminate almost completely the consumption peaks caused by users and the heating system. The effectiveness of reducing injection peaks largely depends on the size of the storage tank.

It is noteworthy that the daytime strategy, which is clearly less complicated and does not require power meters, can reach the same effect on the grid impact if the heat pump operation time is prioritized during periods when the PV system is likely to reach high power outputs.

If the capacity factor is to be reduced, which means lowering the highest peak, a more global DSM strategy will be required because the highest peaks in the current model are not caused by the heating or PV system.

This study clearly has its limits, one of the major being the fact that simulations were only carried out over a 6 weeks winter period. The next steps consist of extending the simulations to a whole year, improving the building design in order to reach lower energy demands, and studying the potential impact of storage on the nominal power of the heat pump.

5. ACKNOWLEDGEMENTS

The authors gratefully acknowledge the K.U.Leuven Energy Institute (EI) for funding this research through granting the project entitled *Optimized energy networks for buildings.*

6. REFERENCES

Åkesson, J., Årzén, K., Gäfvert, M., Bergdahl, T., & Tummescheit, H. (2009). Modeling and optimization with Optimica and JModelica.org—Languages and tools for solving large-scale dynamic optimization problems. Computers & Chemical Engineering. doi: 10.1016/j.compchemeng.2009.11.011.

Baetens, R., De Coninck, R., Helsen, L., Saelens, D. (2010). The impact of domestic load profiles on the grid-interaction of building integrated photovoltaic (BIPV) systems in extremely low-energy dwellings, Presented at 'The renewable energy research conference (RERC)', June 06, 2010, Trondheim, Norway

Bianchi, M. A. (2006): Adaptive Modellbasierte Prädiktive Regelung einer Kleinwärmepumpenanlage, PhD Thesis, ETH Zürich.

Clarke, J.A. (2001). Energy simulation in building design (2nd ed.). Oxford: Butterworth-Heinemann.

Davies, M.G. (1993). Definitions of room temperature. Building and Environment 28, 3838-398.

de Almeida, A., Fonseca, P., Bandairinha, R., Fernandes, T., Araújo, R., Nunes, U., Dupret, M., Zimmermann, J.P., Schlomann, B., Gruber, E., Kofod, C., Feildberg, N., Grinden, B., Simeonov, K., Vorizek, T., Markogianis, G., Giakoymi, A., Lazar, I., Ticuta, C., Lima, P., Angioletti, R., Larsonneur, P., Dukhan, S., de Groote, S., de Smet, J., Vorsatz, D., Kiss, B., Loftus, A.-C., Pagliano, L., Roscetti, A. & Valery, D. (2008). REMODECE - Residential monitoring to decrease energy use and carbon emissions in Europe. Final report, p.96.

De Soto, W., Klein, S. A., & Beckman, W. A. (2006). Improvement and validation of a model for photovoltaic array performance. Solar Energy, 80, 78-88. doi: 10.1016/j.solener.2005.06.010.

Degrauwe, D., Verhelst, C., Logist, F., Van Impe, J. & Helsen, L. (2010). Multi-objective optimal control of an air-to-water heat pump for residential heating. In SSB2010 (pp. 1-14).

Edwards, D.K. (1977). Solar absorption by each element in an absorber-coverglass array. Solar Energy 19, 401-402.

Edwards, D.K. (1982). Finite element embedding with optical interference. International Journal of Heat and Mass Transfer 25, 815-821.

EurObserv'ER (2009). Baromètre photovoltaïque / Photovoltaic barometer : 9 533,3 MWc dansl'UE / in the EU. Systèmes solaires - Le journal du photovoltaïque 1, 72-103.

European Heat Pump Association. (2010). Outlook 2010 European Heat Pump Statistics - Summary. Brussels. Retrieved from www.ehpa.org (last consulted on July 16, 2010).

Firth, S., Lomas, K., Wright, A. & Wall, R. (2008). Identifying trends in the use of domestic appliances from household electricity consumption measurements. Energy and Buildings 40, 926-936.

Glorieux, I. & Vandeweyer, J. (2002). Statistische studie nr110 - 24 uur ... Belgische tijd, een onderzoek naar de tijdsbesteding van de Belgen.

Houseman, D. (2009). True Integration Challenges For Distributed Resources In The Distribution Grid. In 20 th International Conference on Electricity Distribution 20 th International Conference on Electricity Distribution Prague , 8-11 June 2009 (p. Paper 0012). CIRED.

Incropera, F.P., and DeWitt, D.P., 2002. Fundamentals of Heat and Mass Transfer. 5th ed. John Wiley & Sons, Hoboken, NJ.

Incropera, F.P., DeWitt, D.P., Bergman, T.L. & Lavine, A.S. (2007). Introduction to Heat Transfer (5th ed.). John Wiley & Sons.

Liesen, R.J. & Pedersen, C.O. (1997). An evaluation of inside surface heat balance models for cooling load calculations. ASHRAE Transactions 103, 485-502.

Liu, D., Chang, W.R. & Lin, J.Y. (2004). Performance comparison with effect of door opening on variable and fixed frequency refrigerators/freezers. Applied Thermal Engineering 24, 2281-2292.

Meteotest, 2008. METEONORM Version 6.1 - Edition 2009.

Pepermans, G., Driesen, J., Haeseldonckx, D., Belmans, R., & D, W. (2005). Distributed generation : definition , benefits and issues $. Energy Policy, 33, 787-798. doi: 10.1016/j.enpol.2003.10.004.

Richardson, I., Thomson, M. & Infield, D. (2008). A high-resolution domestic building occupancy model for energy demand simulations. Energy and Buildings 40, 1560-1566.

Richardson, I., Thomson, M., Infield, D. & Delahunty, A. (2009). Domestic lighting: A high-resolution energy demand model. Energy and Buildings 41, 781-789.

Sera, D., Teodorescu, R., & Rodriguez, P. (2007). PV panel model based on datasheet values. IEEE, (4), 2392-2396.

The European Parliament. (2009). P6_TA(2009)0278 - Energy performance of buildings (recast) - (COM(2008)0780). Energy. Retrieved from http://www.europarl.europa.eu/sides/getDoc.do?pubRef=-//EP//NONSGML+TA+P6-TA-2009-0278+0+DOC+PDF+V0//EN (last consulted on May 28, 2010).

The Modelica Association. (1997). Modelica — A unified object-oriented language for physical systems modeling. Simulation Practice and Theory, 5(6), p32. doi: 10.1016/S0928-4869(97)84257-7.

Torcellini, P., Pless, S., Deru, M., & Crawley, D. (2006). Zero Energy Buildings: A Critical Look at the Definition; Preprint. Retrieved from http://www.osti.gov/bridge/servlets/purl/883663-3U8fQe/ (last consulted on June 02, 2010).

TPDCB, 2010. The power consumption database. Available at: www.tpcdb.com (last consulted on June 25, 2010).

Underwood, C.P. & Yik, F.W.H. (2004). Modelling methods for energy in buildings. Oxford, Blackwell Publishing Ltd.

Verhelst, C., , H. Nolens, K. Schoovaerts, and L. Helsen, "Performance of an air-to-water heat pump system in a low energy residential building: modelling and experimental results", 2008. Presented at the "9th IEA Heat Pump Conference", May. 20-22, 2008, Zürich, Switzerland.

Viessmann. (2006). Vitocal 350, Technical description (p. 11). Zaventem.

Vu Van, T., Woyte, A., Soens, J., Driesen, J., & Belmans, R. (2003). Impacts Of Distributed Generation On Distribution System Power Quality. In 7th International Conference Electrical Power Quality And Utilisation September 17-19, 2003, Cracow, Poland (pp. 585-592).

Wetter, M. (2009). Modelica Library for Building Heating, Ventilation and Air-Conditioning Systems. In The 7th International Modelica Conference (pp. 393-402). The Modelica Association. doi: 10.3384/ecp09430042.

3.3 Assessing electrical bottlenecks at feeder level for residential net zero-energy buildings by integrated system simulation

Applied Energy 96 (2012) 74–83

Contents lists available at SciVerse ScienceDirect

Applied Energy

journal homepage: www.elsevier.com/locate/apenergy

Assessing electrical bottlenecks at feeder level for residential net zero-energy buildings by integrated system simulation

R. Baetens [a,*], R. De Coninck [b,d], J. Van Roy [c], B. Verbruggen [c], J. Driesen [c], L. Helsen [b], D. Saelens [a]

[a] Building Physics Section, Department of Civil Engineering, KU Leuven - Leuven University, Belgium
[b] Applied Mechanics and Energy Conversion Section, Department of Mechanical Engineering, KU Leuven - Leuven University, Belgium
[c] Electrical Energy and Computer Architectures, Department of Electrical Engineering, KU Leuven - Leuven University, Belgium
[d] 3E, Brussels, Belgium

ARTICLE INFO

Article history:
Received 15 July 2011
Received in revised form 14 December 2011
Accepted 31 December 2011
Available online 8 February 2012

Keywords:
Zero energy building
Residential
Thermal demand
Electricity demand
Dynamic simulation
District

ABSTRACT

Recent European communications focus on the enforcement that by 2020 all new buildings are nearly Zero-Energy Buildings (ZEBs) and on the deployment of a European Smart Grid. The presented work focuses on assessing the electrical challenges at neighborhood level of an building stock evolving towards ZEBs, and identifying the resulting challenge in multidisciplinary dynamic simulation models required to perform this assessment.

A tool for Integrated District Energy Assessment by Simulation (IDEAS) is developed. This IDEAS tool allows simultaneous transient simulation of thermal and electrical systems at both building and feeder level.

Residential ZEBs show a self-consumption of locally generated photovoltaic (PV) electricity of 26 ± 4% at building level. Resulting feeder voltage fluctuations and possible transformer overload are quantified as bottlenecks. When all dwellings are intended to achieve a ZEB status, (i) a fraction of 14–47% of local PV supply is wasted by inverter curtailing depending on the feeder strength, while (ii) the peak transformer load is found to be 3.3 kVA per dwelling which may affect power security in existing feeder designs.

1. Introduction

World-wide 38% of the total energy use is used for operating the building stock [1]. To reduce its environmental impact and economical consequences, the European directive 2002/91/EC [2] on energy performance of buildings has been introduced stating energy benchmarks and goals at the level of individual buildings. A recent European recast 2010/31/EU [3] obliges all member regions to enforce that by 2020 'all new buildings are nearly Zero-Energy Buildings' (ZEBs). Although the definition of a nearly-ZEB is not elaborated within this recast, it aims to achieve a combination of energy efficiency and integration of local renewable energy sources. The non-simultaneity between local energy demand and supply may strongly affect the power quality at feeder level – i.e. neighborhood level – of an electricity distribution network. As such, large scale integration of ZEBs in particular and renewable electricity generation in general will require well developed solutions in the form of energy storage, demand side management or both: As such, with the recent communications of the European Commission on the deployment of a European Smart Grid [4] two crucial domains, i.e. climate change and security of power supply, become strongly linked.

Within this framework, the presented paper has a dual focus: (i) assessing the electrical challenges and impact at feeder level of an building stock evolving towards nearly-ZEBs and (ii) identifying the associated challenge in the development of dynamic simulation models at this level which are required to perform this multidisciplinary assessment.

2. Methodology

A tool for Integrated District Energy Assessment by Simulation (IDEAS) is developed and allows integrated transient simulation of thermal and electrical processes at neighborhood level. Related models have been developed in the last decade and two approaches can be distinguished in their development, i.e. (i) models using thermal Building Physics and Systems (BPSs) as starting point, or (ii) models using Electrical Energy Systems (EESs) as starting point.

BPS-based models at neighborhood level combine a dynamic simulation of the heating and cooling demand with a stochastic approach on occupant behavior. The main existing BPS-based models are *LT Urban* [5,6], *SUNtool* [7,8], *TUD-PS* [9] and the methodology

* Corresponding author.
E-mail address: ruben.baetens@bwk.kuleuven.be (R. Baetens).

0306-2619/$ - see front matter © 2012 Elsevier Ltd. All rights reserved.
doi:10.1016/j.apenergy.2011.12.098

by Yamaguchi et al. [10,11]. Each of these models have their specificities which can be attributed to their background: (i) the thermal load calculation for space heating and cooling generally relies on highly simplified building models, e.g. the *LT method* [12], a Radiant Time Series (RTS) or Weighting Factor (WF) method [13,14] or ISO 13790 [15] based models, while (ii) also system modeling is mainly simplified by performance curves. Furthermore, the main focus lies on (iii) the behavior of accommodated occupants [16,17] in offices and their interactions with lighting [18,19], shading [18,20,19], opening of windows [21], comfort [22] and appliances [8,23]. Also (iv) the urban microclimate and shade views for radiant exchanges [24,25] are a point of attention, while (v) the assessment of energy measures at aggregated level is mainly limited to the summation of energy loads [8,9,11].

EES-based models at feeder level combine a physical calculation of the electricity generation and distribution with a stochastic approach on power loads. The main existing EES-based are the models of *IEA-PVPS Task 10* [26], *PV-UPSCALE* [27], and the models of Conti et al. [28], Paatero and Lund [29], Thomson and Infield [30] and Widén et al. [31]. Each of these models have their specificities which can be attributed to their background: the main focus (i) lies on the appliance use of accommodated occupants in dwellings [32–34], and (ii) analysis shows the importance of a fine time resolution of simulation boundary conditions [35,31].

The IDEAS tool differs from existing BPS-based and EES-based models by (i) integrating the dynamics of the hydronic, thermal as well as electrical energy networks at (ii) both the building and aggregated level within a single model and solver as illustrated in Fig. 1. The transient thermal processes are expressed in detail based on the control volume method (CVM), whereas the electric models are expressed with static nodal and line models. The IDEAS tool integrates the (iii) the occupancy, appliance and lighting use of accommodated occupants in dwellings and (iv) includes a fine 1-min time resolution for the boundary conditions. Some aspects of pure BPS-based models will be added in the next stage of the IDEAS tool development, i.e. (v) the behavior of accommodated occupants concerning shading, opening of windows, and (vi) the urban microclimate and radiant exchange shade views. The tool is implemented in Modelica [36] which allows explicit symbolic declaration of each energy flow and system based on differential algebraic equations (DAEs). This DAE system is solved using Petzolds' Differential Algebraic System Solver (DASSL) [37]. Furthermore, Modelica is a pure object-oriented modeling language for component-based development allowing continuous development with limited implementation effort.

3. Model description

A model for a residential zero-energy neighborhood is developed in the IDEAS tool based on a representative set of architectural types, a feasible technology choices and stochastic residential occupant behavior. Their ZEB target is expected to be achievable by combining energy efficiency, heat pumps and building integrated photovoltaic (BIPV) systems covering the electricity consumption on an annual basis. It can be expected from the current strong increase in heat pump and BIPV systems on the domestic market [38,39] that new buildings with these technologies will become standard practice on the short to medium term. As such, this has been considered as a starting point for modeling ZEBs with feasible technology choices.

All simulations are performed for the typical moderate climate of Uccle (Belgium) and daylight saving time (DST) is taken into account [40]. Irradiance data with a time resolution of 1 min are obtained by Meteonorm v6.1 for the moderate climate of Uccle (Belgium) [41] based on the period 1981–2000.

3.1. Neighborhood description

The implemented residential zero-energy neighborhood consists of 33 detached residential buildings based on four different architectural types of detached dwellings, which are schematically shown in Fig. 2 and for which the main characteristics are listed in Table 1. The number of dwellings is determined in agreement with the topology of a radial IEEE 34 Node Test Feeder [42,43]. The architectural types were determined earlier as representative for the Belgian building stock [44] based on main building typologies in different periods and are implemented based on their national statistical spread [45]. All dwellings are modeled as a 2-zone model with the day zone (e.g. living area, kitchen) and night zone (e.g.

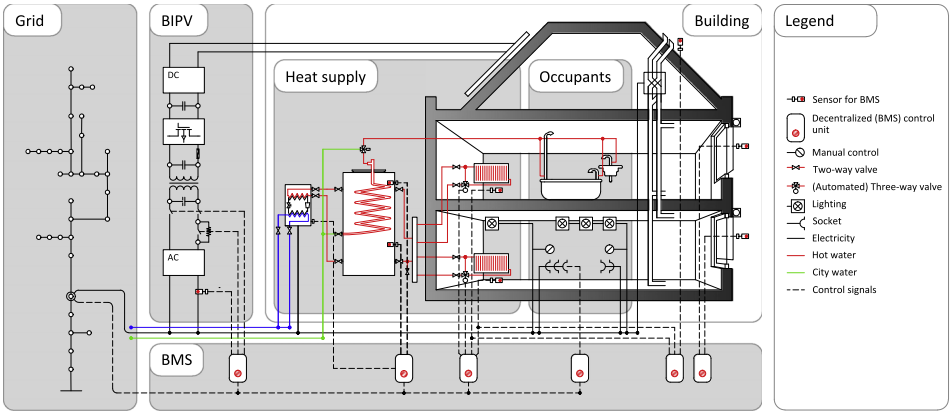

Fig. 1. Representation of the elaborated model in the IDEAS tool. At the level of an individual building, local electricity generation by means of building integrated photovoltaic (BIPV) systems, stochastic behavior of building occupants, the detailed thermal building response, the transient behavior of the heating, ventilation and air conditioning system, and the building management system (BMS). At feeder level, the transient response of the low-voltage electrical distribution grid is included for a residential neighborhood of 33 dwellings.

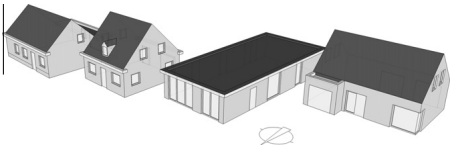

Fig. 2. Representation of the four architectural types of the implemented dwellings.

Table 1
Summary on the properties of the implemented dwellings based on the four representative architectural types, where U_{av} denotes the average overall heat transfer coefficient and HRV the heat recovery ventilation.

	Typ.1	Typ.2	Typ.3	Typ.4
Heated area, m^2	127	98	149	123
Window-floor ratio	0.12	0.19	0.16	0.13
Compactness, m	1.23	1.10	0.87	1.18
Infiltration rate n, h^{-1}	0.03	0.03	0.03	0.03
U_{av}, W/m^2 K	0.145	0.174	0.159	0.158
HRV efficiency	0.84	0.84	0.84	0.84
Design heat load, W/m^2	20.5	28.0	21.6	25.9

bedrooms) of the dwelling respectively. The distribution of internal gains by occupant behavior is based on the allocated location of appliances in these zones. Although only four different architectural types are implemented, all 33 dwellings show different results during simulation because of the stochastic user behavior.

All dwellings are designed as summarized in Table 1 and resulting in a low-energy standard. Heat losses by conduction are reduced to a minimum by applying thermal insulation to obtain an overall mean heat transfer coefficient of 0.11 W/m^2 K, 0.13 W/m^2 K, 0.10 W/m^2 K and 0.8 W/m^2 K for the cavity walls, concrete foundation floors, timber roof constructions and windows respectively. These insulation levels are in line with earlier found economic optima for the residential sector [46] in the Belgian climate. Also ventilation losses are reduced to a minimum: all dwellings are as airtight as possible with a natural infiltration rate of 0.03 ACH. All dwellings are equipped with mechanically balanced, air-to-air heat-recovery ventilation (HRV) with an air change rate of 0.5 h^{-1} and a recovery efficiency of 0.84. Depending on the architectural types these measures result in a design heat load [47] of 20–28 W/m^2 for the moderate climate of Uccle, Belgium.

Furthermore, all dwellings are equipped with exterior solar screens with a total solar transmittance of 0.24 and the windows can be opened for natural ventilation. As a result no active cooling needs to be installed in the dwellings.

3.2. Thermal building model

The transient response of buildings is modeled based on the finite volume method (FVM) and reduced to the response of exterior walls, windows and slab-on-ground components, and a zone component.

The transient zone heat balance is governed by

$$\rho VC\frac{\partial T_c(t)}{\partial t} = \sum_i Q_{cs,i}(t) + Q_{c,o}(t) + Q_{c,a}(t) + Q_v(t) + Q_{inf}(t) \qquad (1)$$

where $\rho V\,C$ (J) is the thermal capacitance of the air volume, $T_c(t)$ (K) is the zone air temperature, $Q_{cs,i}(t)$ (W) is the convective heat transfer of adjacent surface i, $Q_{c,o}(t)$ (W) is the convective heat load of accommodated occupants, $Q_{c,a}(t)$ (W) is the convective heat gain of allocated appliances, $Q_v(t)$ (W) is the heat load by ventilation and $Q_{inf}(t)$ (W) is the heat load by infiltration. Longwave radiation exchange between surfaces in a single zone is treated based on definition of a radiant star node, while shortwave radiation entering the zone through windows and longwave radiative internal gains area distributed based on a emissivity and area weighted fraction.

The resulting transient interior surface heat balance of building envelope components is determined as

$$Q_{net}(t) = Q_c(t) + \sum_i Q_{SW,i}(t) + \sum_i Q_{LW,i}(t) \qquad (2)$$

where $Q_{net}(t)$ (W) denotes the heat flow into the wall, $Q_c(t)$ (W) the temperature dependent heat transfer by convection based on Khalifa [48] and the energy balance of the zone air capacity, $Q_{SW,i}(t)$ (W) shortwave absorption of solar light entering the interior zone and $Q_{LW,i}(t)$ (W) longwave radiant exchange with surrounding interior surfaces by definition of a radiant star node.

The exterior surface heat balance of building envelope components is determined as

$$Q_{net}(t) = Q_c(t) + Q_{SW}(t) + Q_{LW,env}(t) \qquad (3)$$

where $Q_{net}(t)$ denotes the heat flow into the wall, $Q_c(t)$ (W) convective heat transfer determined by the undisturbed wind speed [49], Q_{SW} (W) shortwave absorption of solar light determined by the shortwave surface absorptance and $Q_{LW,env}(t)$ (W) longwave heat exchange with the surroundings based on the radiant-interchange configuration factor between the surface and sky [50]. For slab-on-ground constructions, the exterior heat balance is determined based on ISO 13370 [51]. The calculation of the solar irradiation is based on the sky dome model of Perez et al. [52,53].

Solid FVM heat conduction between the interior and exterior surfaces of building envelope components is governed by

$$\rho VC\frac{\partial T_{FV}(t)}{\partial t} = \sum_i Q_{FV,i}(t) + Q_s(t) \qquad (4)$$

where ρVC (J) is the thermal capacitance of the control volume, $Q_{FV}(t)$ (W) is an energy flux between different control volumes and Q_s (W) is an energy source. For windows, the thermal FVM model is extended for solar absorption by the different glass panes, the presence of gas cavities and transmission of solar irradiation. The heat transfer through these thin gas cavities is described by the surface emissivities and the Nusselt number, while the shortwave absorptance and transmitance through the glazing depending on the angle of incidence of solar irradiation by using the output of the WINDOW 4.0 software [54].

Extended validation and verification by the BESTEST methodology [55] of the IDEAS building model is ongoing and shows encouraging results.

3.3. Thermal building system model

Each of the 33 dwellings has a space heating (SH) and domestic hot water (DHW) system with an identical layout for each dwelling but different capacity, consisting of a modulating air-to-water heat pump (HP), thermal storage by means of a water buffer, a DHW temperature mixing valve and radiators in each building zone as visualized in Fig. 1. The nominal power of the heat production and emission system components are based on the design heat demand [47] of the dwelling.

The HP heats water in a storage tank of 0.25 m^3 which provides hot water for both SH and DHW. The model of this storage tank assumes five stratification layers and contains two temperature sensors for control purposes, i.e. T_{top} and T_{bot} in the upper and 4th layer respectively. Heat losses of the insulated tank to the surroundings are taken into account by a heat transfer coefficient of 0.4 W/m^2 K and a static reference temperature of 15 °C. The water in the storage tank is used for space heating by feeding low-tem-

perature radiators, i.e. a design inlet and outlet temperature of 55 °C and 45 °C respectively at a design outdoor temperature of −8 °C. The DHW is supplied by a heat exchanger in the hot water in the storage tank. A controlled mixing valve sets the output temperature to the set temperature of 45 °C while the heat exchanger effectiveness is assumed to be unity.

The HP model is based on interpolation in a performance map retrieved from manufacturer data [56]. The interpolation defines the heating power Q_{net} and electricity use P_{net} as a function of condenser outlet temperature, the ambient temperature and can modulate to 30%. The coefficient of performance based on manufacturer data [56] is 3.17 at 2/35 °C test conditions (i.e. air/water temperature) and 2.44 at 2/45 °C test conditions for full load operation. The HP is controlled based on the measured and setpoint values for the storage tank temperatures T_{top} and T_{bot}. The HP control setpoints are based on a heating curve for SH (i.e. 55 °C at an outdoor temperature of −8 °C and 20 °C at an outdoor temperature of 15 °C) and the required temperature for DHW of 45 °C which is almost always higher than this heating curve value. The HP will be started when T_{top} is 3 °C below setpoint and shut down when T_{bot} is 3 °C above setpoint. In order to be able to reach the switch off condition on T_{bot}, the condenser water set temperature is always 5 °C higher than the setpoint.

Similar to the thermal building model, also the transient response of the thermal building system is modeled based on FVM. All thermal system components having a fluid flow are governed by the equation

$$H_{f,in}(t) - H_{f,out}(t) + Q_{net}(t) = m_f c_f \frac{\partial T_f(t)}{\partial t} \quad (5)$$

where $H_{f,in}(t)$ and $H_{f,out}(t)$ (J) are the enthalpy of the incoming and outgoing fluid respectively, $Q_{net}(t)$ (W) is the net heat exchange with the surroundings, m_f (kg/s) is the discretized fluid mass in the control volume, c_f (J/kg) is the specific heat capacity of the fluid and T_f (K) is the fluid temperature. In heat emission components, Q_{net} is determined based on EN 1537 [57] and Koschenz and Lehman [58] for embedded systems, and based on EN 442-2 [59] for hydronic radiators. In heat generation components like boilers and heat pumps Q_{net} is determined based on multi-parameter performance curves of commercial appliances.

3.4. Building occupancy model

The stochastic behavior of accommodated occupants for the use of appliances and lighting by the occupants has been implemented as embedded discrete time Markov chains.

The implemented stochastics are consistent with Richardson et al. [60]. The resulting outputs are (i) presence [34] and (ii) activity of the building occupants, (iii) the use of appliances [60] and (iv) the use of lighting [61,62], and depend (only) on (i) the household size, (ii) the present appliances and fixtures, (iii) whether it is a weekday or weekend day and (iv) global irradiances as shown in Fig. 3. Here, occupancy and the use of appliances is used at a 10 min resolution, while the use of lighting has a 1 min resolution. To generate 33 statistically relevant profiles, bottom-up data concerning household size and installed appliances are used based on Belgian [63] and European [60] statistics on household sizes and appliance ownership rates respectively. As such, the main electrical appliances taken into account are domestic lighting, freezer and refrigerator, a music installation, the iron and vacuum cleaner, a personal computer, a television, cooking appliances such as a hob, oven, microwave and kettle, a dishwasher, a tumble dryer and a washing machine. The library of activities can be extended with additional data from time-consumption surveys [45].

For domestic hot water (DHW) consumption, the Becker profile [64] resulting from large scale measurements is chosen based on a comparative literature study [65]. The profile is a statistical profile averaging the behavior of different users to a single profile, whereas profiles for individual dwellings may be found more peaked.

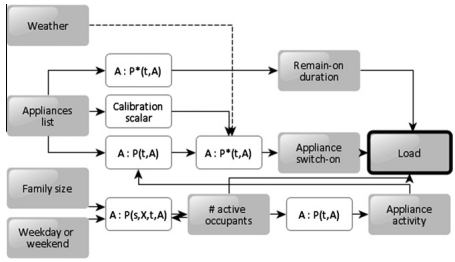

Fig. 3. Decision flowchart at building level on occupancy and the use of domestic appliances. The weather only interferes for determination of the use of lighting.

The knowledge on further stochastic behavior in residential dwellings for opening of windows, manual heating control and solar screen control is still limited or based on a limited data set and therefore not implemented yet.

3.5. Building management system

On/off controllers are implemented for control of the space heating system based on the difference between the room operative temperature and the room set-point temperature given by the user occupancy, i.e. 21 °C when occupants are present and 16 °C otherwise.

Also control of solar shading devices and opening of windows, together with possible bypassing of the HRV unit are managed by the BMS. The HRV unit is bypassed when the temperature of the day-zone surpasses 24 °C and is used again when the temperature drops below 19 °C. The windows are opened when the indoor temperature rises above 24 °C resulting in a natural ventilation rate between 3 and 5 ACH depending on the available window sizes. Windows are closed again when the indoor temperature drops below 21 °C. The automated exterior solar screen is lowered at an irradiance level of 250 W/m^2 and raised again at an irradiance level below 150 W/m^2.

3.6. Domestic electricity model

The nodal voltage U_n of all appliances is set equal to the U_n of the building-to-feeder connection.

All electrical loads of the used appliances in the dwellings are seen as active loads P. In successive work, possible reactive power Q of the heat pumps or electric motors can be taken into account.

All required energy is locally delivered by means of a building integrated photovoltaic (BIPV) system. Recast 2010/31/EU [3] only applies climatisation of the building, where also the domestic electricity consumption is taken into account in order to achieve the on-site net ZEB status. All systems are assumed to be oriented directly South with an inclination of 34° resulting in the highest annual electricity production [66]. Sizing of the BIPV system is performed after a first simulation of the neighborhood to know the exact (simulated) annual energy use to account for.

Local generation by means of a photovoltaic system is modeled with the 5-parameter model of De Soto et al. [67] based on a temperature-dependent diode equivalent circuit [68]. Calculations are based on manufacturer characteristics, i.e. a maximum power

point (mpp) current I_{mpp} of 6.71 A and mpp voltage V_{mpp} of 34.3 V, a short-circuit current I_{sc} of 7.22 A and an open-circuit voltage V_{oc} of 42.3 V at standard testing conditions. The temperature dependence is rather low with temperature coefficients k_i and k_v of 0.00217 and −0.106 respectively. The direct current power output of the BIPV system is converted to an AC power by means of an inverter characterized by a constant inverter efficiency of 0.95.

To avoid excessive feeder voltages, the BIPV system inverter is curtailed when the voltage at the dwellings feeder interface reaches a predefined voltage limit. Curtailing is applied as the distribution system operator currently does not allow the distributed sources to provide voltage control of the distribution feeder, e.g. by reactive power control. This limit is set at an increase of 6% of the nominal feeder voltage or 243.8 V according to national regulations on AREI Art.§235, the Belgian General Regulations for Electrical Installations (and Labor Protection). The inverter control is given a minimal off-time of 5 min before trying to switch on again after voltage disturbances.

The relation at all nodes between the nodal voltage and nodal current in the feeder is determined as

$$P(t) + \jmath Q(t) = U_n(t)\bar{I}_n(t) \tag{6}$$

with $(P(t) + \jmath Q(t))$ the complex power wherefore $P(t)$ (W) is the active power and $Q(t)$ (VA) is the reactive power, $U_n(t)$ (V) is the node voltage and $\bar{I}_n(t)$ (A) the complex conjugate of the node current. Here, U_n can be simulated with an internal feeder structure or set equal to the U_n of the building-to-feeder connection.

3.7. Electric feeder model

A residential district is typically a radial feeder with a rated nominal voltage of 230/400 V wye connection. The considered electricity feeder in the residential district has the same layout as the IEEE radial distribution 34 Node Test Feeder [42,43] as shown in Fig. 1.

The feeder is modeled with cross sections for Aluminum cables of (150,95,50), (95,50,35) and (50,35,25) mm^2 respectively with cable lengths of 16 up to 48 m between the dwellings as typical for a residential district with detached houses. These feeder designs will be referred to as the *strong*, *moderate* and *weak* feeder respectively. Simulations are performed using a single-phase representation of the electricity distribution feeder whereby the line impedances are adjusted to represent a 3 phase feeder with symmetrical load and generation. This simplification might not hold for a large asymmetrical load but since the BIPV capacities are in the 5 kWp range they should have a 3-phase connection [69]. This would imply that most households have a 3-phase connection to the distribution feeder limiting large asymmetrical loads.

A feeder transformer capacity of 160 kVA is taken into account with a core loss of 0.26 kW and an impedance of 0.04 Ω for calculation of the coil losses determined for a short-circuit voltage of 4% of the nominal voltage.

The Belgian low-voltage electricity grid has a nominal voltage of 230 V. For traditional power flows without distributed generation, the voltage at the feeder has a higher value to ensure that the voltage in the entire feeder remains within preset boundaries. The feeder voltage is raised by 2% to 234.6 V as currently common in feeder designs for unidirectional power distribution.

The electric feeder is simulated with a power flow analysis determining nodal voltages and line currents as

$$\Delta U_l(t) = (R + \jmath X) I_l(t) \tag{7}$$

with $(R + \jmath X)$ the line impedance wherefore R (A/V) is the line resistance and X (A/V) is the line reactance, $\Delta U_l(t)$ (V) is the line voltage drop and $I_l(t)$ (A) the current.

4. Results

First, the set of net ZEBs is evaluated at building level. Second, the same evaluation is performed after all dwellings are integrated at feeder level representing a small residential neighborhood. Here, the main focus lies on the resulting differences by taking into account the electricity feeder compared to a study at building level.

Fig. 4 clearly shows the integrated bottom-up approach of modeling in the simulation output results, where indoor operative temperatures and required comfort determine the stratified temperatures in the available storage tank which in turn define the electric power demand of the heat pump which finally (together with occupant behavior and the installed BIPV capacities) determine the voltage perturbations in the electricity feeder.

4.1. Building level

The main focus at building level lies on the achieved ZEB status with acceptable comfort and feasible technology choices and the quantification of non-simultaneity between local energy supply and demand.

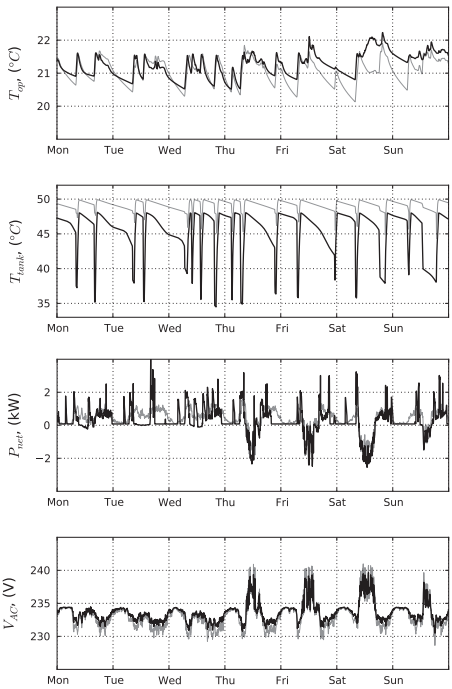

Fig. 4. Example week profile for a random dwelling from the modeled set of (from top to bottom) the indoor operative zone temperatures T_{op} for the day zone and night zone (in black and gray respectively), the bottom and top temperatures T_{bot} and T_{top} of the storage tank (in black and gray respectively) for space heating and domestic hot water, the net electrical power exchange P_{net} (i.e. positive values denote a net demand and negative values denote a net supply to the feeder) and the feeder connection voltage V_{AC}. The gray lines for P_{net} and V_{AC} indicate the averaged for all 33 dwellings within the neighborhood.

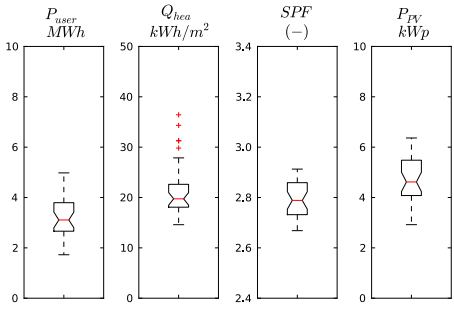

Fig. 5. Quartile boxplot deviations of the annual domestic electricity consumption P_{user}, heat demand Q_{hea} for space heating and domestic hot water, the seasonal performance factors (SPF) of the heat pump and the required photovoltaic capacity P_{PV} to reach a level of net zero-energy for all 33 dwellings. The notches depict the median value.

4.1.1. Net zero-energy dwellings

For all dwellings, the annual household electricity consumption for electric appliances and lighting has a lower and upper quartile of 3.3 ± 0.5 MWh, with extrema of 1.8 and 5.2 MWh which is consistent with Belgian statistics [70]. The annual heat demand for SH and DHW is derived from dynamic simulation and is found to be 18.6 ± 2.5 kWh/m^2, with extrema of 14.2 and 36.4 kWh/m^2 as shown in Fig. 5. The seasonal performance factor (SPF) of the hydronic installations, as defined in prEN 15316-4-2 [71] is found to lie between 2.7 and 2.9 resulting in an annual electricity consumption of 1.0 ± 0.2 MWh, with extrema of 0.7 and 1.5 MWh for SH and DHW. As all thermal energy is provided by the storage tank for both SH and DHW, no distinction can be made between the effective electricity consumption for SH and DHW separately.

Based on the resulting electricity consumptions on annual basis, the resulting BIPV capacities to reach a net ZEB status for each dwelling individually can be determined. Within the moderate climate of Uccle (Belgium), the resulting BIPV capacities are 4.9 ± 0.6 kWp, with extrema of 2.2 and 7.1 kWp for the modeled dwellings as shown in Fig. 5. It must be stated that these values are determined after simulation of the total domestic energy use in order to achieve exactly a net ZEB status on annual basis within the study at building level. In reality, this is not possible as the exact demand for heating can not be calculated and depends on weather conditions whereas also the domestic electricity consumption for appliances is unknown in advance and will change frequently throughout the lifespan of the dwelling. The BIPV sizing will therefore be taken as variable further on and results will be expressed as a function of the design level of net ZEB. Here, a depicted design of net ZEB of 1.0 denotes the exact sizing of the BIPV capacities as described, whereas a design level of net ZEB of e.g. 0.8 represents an under-sizing by 20% at annual basis of the provided local supply of renewable energy.

4.1.2. Non-simultaneity of demand and supply

The effectiveness of the building integrated photovoltaic system for reducing the electricity demand from the main distribution feeder is expressed by quantifying the cover factor $\gamma^{[t_1,t_2]}$ (–) within a time frame $[t_1, t_2]$.

A cover factor indicates to which extent a set of threads is covered by another set of threads. Within this context, the supply cover factor γ_S (–) is defined as 'the ratio to which the local supply is covered by the energy demand' and indicates 'the self-consumption'. Similarly, the demand cover factor γ_D (–) is defined as 'the ratio to which the energy demand is covered by the local supply' and indicates the 'self-generation'. The cover factors γ_S and γ_D are calculated as

$$\gamma_S = \int \min\{P_D, P_S\} dt \left[\int P_S dt\right]^{-1} \tag{8}$$

$$\gamma_D = \int \min\{P_D, P_S\} dt \left[\int P_D dt\right]^{-1} \tag{9}$$

where P_S is the local power supply and P_D the local PV power demand. The term $\min\{P_D, P_S\}$ represents the part of the power demand instantaneously covered by the local PV power supply or the part of the power supply covered by the power demand.

Eqs. (8) and (9), defining the cover factors, indicate that a level of net ZEB is achieved when $\gamma_S = \gamma_D$ for a 1-year period as this implicates that $\int P_S dt = \int P_D dt$. The definition of the cover factors γ (–) focuses on energy levels and is based on the assumption that net supply energy from the building to the feeder is valued equally as net energy demand. The definition could be extended and used

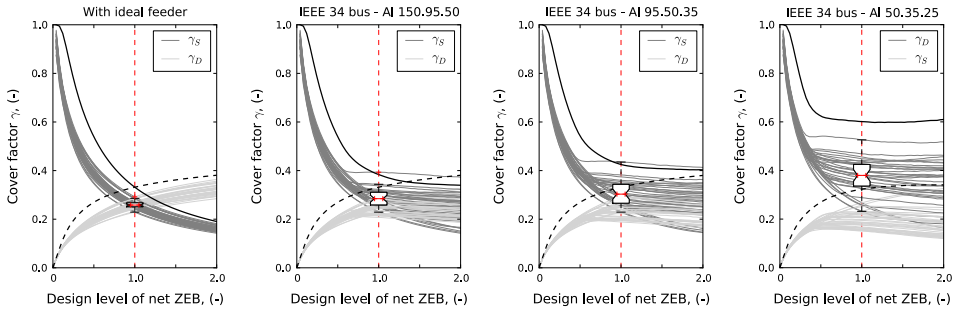

Fig. 6. Annual cover factors γ_D and γ_S plotted against the design level of net zero-energy at building (gray) and aggregated (black) level determined ideally at building level and after integrated district energy system simulation including feeder consequences for the considered feeder designs. Here, a design level of net zero-energy of 1.0 denotes the exact sizing of the photovoltaic capacities as described whereas a design level of net zero-energy of e.g. 0.8 represents an under-sizing by 20% at annual basis of the provided local supply of renewable energies.

for non-power related assessment by scaling P_S and P_D during the integration, e.g. with economic values and thus for assessment of other types of ZEB definitions such as the cost-ZEB [72].

Simulation of all dwellings shows low cover factors for the residential sector in a Belgian (i.e. heating-dominated) climate. The annual self-consumption γ_S^a at building level drops from 0.92 ± 0.05 for a minimal BIPV sizing (i.e. a design level of net ZEB equal to 0.04) down to 0.26 ± 0.03 when a net ZEB is aimed at building level as shown in Fig. 6a. At this aimed level of net ZEB, equal values are found for the annual self-generation γ_D^a at building scale which raises to values 0.32 ± 0.04 when the local BIPV system is strongly over-sized.

Both cover factors γ_S and γ_D show a seasonal pattern for all dwellings. Two reasons can be brought up. First, the solar paradox leads to the contradiction of a higher energy demand during winter caused by increased electricity demand of the domestic heat pumps for SH and the increased demand for lighting, whereas a lower energy supply will be noticed due to shorter daylight periods and lower solar zenith angles. Second, the daily pattern mismatch reflects the mismatch at building level concerning the peaked occupant behavior compared to the solar cycle. A first demand peak can be found in the morning as the demand for SH and DHW rises after waking up. This morning peak is typically sharp and high in low energy dwellings as it is dominated by the heat pump. A second peak can be noticed during noon mainly caused by cooking if not all occupants have a full time job, whereas a final longer period of energy demand is found during the evening is caused by a combination of domestic electricity consumption for use of appliances and heat demand for SH and DHW. In winter, the morning peak and a large part of the consumption in the evening fall beyond the daylight period which enforces the seasonal solar paradox.

This combination of seasonal as well as daily mismatch results in the low momentarily coincidence of local energy supply and demand. The mismatch at building level is rarely seen as a problem in building energy studies as the electricity distribution feeder is seen as a virtual storage. However, correct assessment of this mismatch and its implications implies a study at feeder level.

4.2. Feeder level

Two main differences can be noted at feeder level compared to a study at building level. First, diversification of occupant behavior and BIPV supply allows interchange of electrical energy between dwellings. Second, electrical energy has to be consumed instantaneously when produced which argues not to see the feeder as virtual storage. The integration of all system dynamics and requirements at feeder level shows the electrical bottlenecks at feeder level of the imposed assumptions at building level to reach a net ZEB status for each dwelling.

4.2.1. Demand diversification

When all 33 modeled dwellings are aggregated, slightly higher cover factors can be noted as shown in Fig. 6a by the black curves. The annual self-consumption γ_S^a at aggregated scale drops from 0.99 for a minimal BIPV sizing at each dwelling (i.e. a design level of net ZEB equal to 0.04) down to 0.33 when a net ZEB is aimed at building level for each dwelling. At this aimed level of net ZEB, equal values are found for the annual self-generation γ_D^a at aggregated level which raises to values of 0.38 when all local BIPV systems are strongly over-sized.

The retrieved higher cover factors when net zero-energy dwellings are looked at aggregated level compared to individual dwellings are caused by the diversification of occupant behavior. The electrical energy demand profile of a single dwelling is strongly peaked due to short-time use of electrical appliances and peaks caused by the heat pump. When all 33 modeled dwellings are looked at aggregated level, the peaked profiles are flattened out to a smoother profile as all occupants have a different day rhythm and the earlier mentioned morning and evening peak in demand are much more spread and lower. For a case study where the feeder restrictions are not taken into account as shown in Fig. 6a, the main gain in self-consumption by aggregating all dwellings is found in under-sized BIPV capacities. The reason may be found in the mismatch in both the seasonal and daily patterns. Aggregating electrical energy demand profiles eliminates the daily pattern mismatch to a certain extent, while the seasonal mismatch will take the upper hand once the advantage of the daily pattern is exploited.

In building energy studies considering renewable energy integration, the higher levels of self-consumption and the diversification in electrical energy demand profiles on an aggregated level are often seen as the solution for the non-simultaneity between demand and supply. The remaining low cover factor of 0.33, however, still denotes that a significant share of the electrical energy provision is transferred to the local feeder and that the backbone electricity grid is seen as virtual storage. Here, the integration of all system dynamics and requirements at feeder level has to reveal the electrical bottlenecks at feeder level.

4.2.2. Feeder restrictions

The integration of all system dynamics and requirements at feeder level shows three main bottlenecks which are not taken into account in a study at building level. First, increased resistive feeder losses can be noted. Second, the implied voltage limits for safety and power security reasons limit the possible electrical energy generation and its supply to the feeder. Third, possible overload of the transformer at the connection with the backbone grid can occur. The results will again be analyzed as a function of design level of net ZEB. However, distinction must be made between the design level of net ZEB as determined by the study at building level and the effective level of net ZEB which is determined after integration at feeder level.

First, electrical currents in the feeder and transformer result in resistive losses. For a reference case without BIPV systems, these losses are 1.1%, 1.3% and 2.4% of the total annual demand for the strong, moderate and weak feeder respectively. For all feeder designs, a minimum is found in the losses at a design level of net ZEB around 0.3 showing losses 0.2% pt lower than the reference case whereas the resistive losses rise again to 2.1%, 1.9% and 2.1% of the total annual demand for the strong, moderate and weak feeder respectively for larger BIPV capacities. Overall, the depicted transmission losses remain low which leads to the conclusion that they are of little importance for the assessment of net ZEBs at feeder level.

Second, lost BIPV generation due to curtailing at elevated voltage levels shows much more importance compared to the transmission losses. Moreover, the difference between the different feeder strengths is more profound. For the considered strong feeder, the curtailed generation for an $f_{zeb,des}$ of 1 is 14% of the annual demand at feeder level and rises up to 41% at the level of an individual dwelling depending on its location in the feeder as shown in Fig. 7b. Only 16 of the proposed 33 net ZEBs are effectively ZEBs. An effective level of net ZEB is possible at feeder level when the capacities of the BIPV systems are over-sized 1.36 times for the individual dwellings in the strong feeder. Still only 16 of the proposed 33 net ZEBs are effectively ZEBs but their local over-production at annual basis compensates for the curtailed BIPV generation at feeder level. In contrast to this strong feeder, an effective level of net ZEB at feeder level is not achievable for the moderate and weak feeders. For the considered moderate feeder, the curtailed generation for an $f_{zeb,des}$ of unity is 22% of the annual demand at feeder level and increases up to 52%

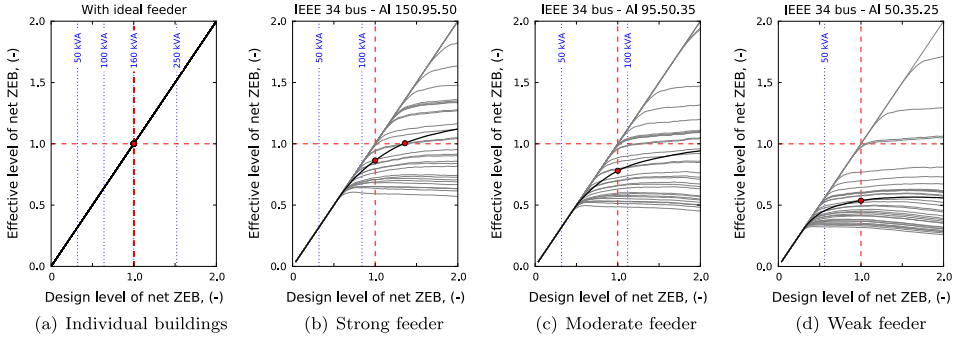

Fig. 7. Effective levels of net zero-energy plotted against the design level of net zero-energy at building (gray) and aggregated (black) level determined ideally at building level and after integrated district energy system simulation including feeder consequences for the considered feeder designs. Here, a depicted design level of net zero-energy of 1.0 denotes the exact dimensioning of the photovoltaic capacities as described whereas a design level of net zero-energy of e.g. 0.8 depicts an under-sizing by a fraction of 20% at annual basis of the provided local supply of renewable energies. The dotted lines indicate the required transformer capacity.

at the level of an individual dwelling depending on its location in the feeder, as shown in Fig. 7c. Only 11 of the proposed 33 net ZEBs are effectively ZEBs. For the considered weak feeder, the curtailed generation for an $f_{zeb,des}$ of unity is 47% of the annual demand at feeder level and rises up to 68% at the level of an individual dwelling depending on its location in the feeder, as shown in Fig. 7d. Only 3 of the proposed 33 net ZEBs are effectively ZEBs.

The overall high generation losses in all feeders show that BIPV curtailing under current limitations and for current feeder designs is a major bottleneck for building energy standards.

The curtailed BIPV generation also influences the effective supply and demand cover factors. As shown in Fig. 6b–d, the resulting effective levels of self-consumption are higher than determined in the study at building level. The effective total BIPV generation stated in the denominator of γ_S does not increase proportionally with the installed BIPV capacities, whereas the total covered electrical energy in the numerator is not affected by curtailing as curtailing is caused by uncovered over-generation. This causes the level of self-consumption γ_S to remain nearly equal independent of the installed BIPV capacities once curtailing occurs, while the level of self-generation γ_D remains approximately unaffected compared to the values determined in the study at building level. The larger spread of γ_S is caused by the dependence of curtailing on the location of the dwelling in the feeder, as locations at the end of a feeder line will show stronger voltage increases.

Third, increased transmission losses and occurring generation losses by curtailing, possible transformer overloads at the connection of the local feeder to the backbone grid have to be considered. Overload of the transformer possibly compromises power supply security to the feeder, differently from BIPV curtailing which only results in drops of expected efficiencies. Based on the study at building level, a peak load of 4.8 kVA per dwelling is found after aggregation results in a total peak load 158 kVA as shown in Fig. 7a. However, the transformer load is affected by curtailing of the BIPV systems. Curtailing occurs at the peaks of total net supply at feeder level and as such reduces the transformer load. For the considered strong feeder, a peak load of 109 kVA is found as shown in Fig. 7b. For the considered moderate feeder, a peak load of 96 kVA is found as shown in Fig. 7c whereas a load of only 66 kVA is found for the considered weak feeder as shown in Fig. 7d. Current common feeder transformers in Belgium have a capacity of 50, 100, 160, 250, 400 and 630 kVA from which may be concluded that transformer problems may occur depending on the combination of the feeder strength and the installed transformer capacity. For strong feeders, the transformer is likely to be overloaded if a transformer of 250 kVA or lower is installed for the depicted set of 33 dwellings. In weaker feeders, curtailing at the BIPV installations results in protection of the feeder load.

5. Discussion

From the mentioned three possible problems at feeder level, two are found to be bottlenecks which are not taken into account in a study at building level: the implied voltage limits for safety and power security result in significant generation losses whereas possible overload of the transformer at the connection with the backbone electricity grid may bring power supply security into danger.

Since the predominant share of net ZEBs is to be achieved by renovation of existing dwellings in the existing building stock and feeders, such substantial required changes in the distribution grid at feeder level may not always be possible and especially not in short term. Important gains at feeder level not only lie in the optimization of the feeder itself but also in taking into account the feeder properties in building energy optimization. This can only be investigated by integrated design and simulation of different energy flows and energy systems as proposed within this work.

5.1. Building optimization for feeder stability

Each component of the overall model at building level, as illustrated in Fig. 1, could be optimized or adapted to cope with restrictions at feeder level and increase the level of self-consumption, i.e. the building design and insulation level, the heat (and cold) supply, the building integrated photovoltaic system, the control strategies of the building management system as well as the occupant behavior.

The physical building design has always been the first point of interest for energy savings at building level. From a feeder point of view, a change of the building design may affect both the daily pattern and seasonal pattern of the total energy use. On the one hand, the design, glazing properties and insulation level define the overall need for thermal energy. An increased ratio of passive thermal gains to thermal losses can shift the focus from a heating-dominated design to a cooling-dominated design of the building reducing the seasonal mismatch between demand and supply. On the other hand,

focusing on heavy-weight buildings may allow the building management system to shift the daily pattern of heat and cold demand. For a given building design, the design of the entire energy system for both space heating and cooling, domestic hot water and local generation by means of renewable energy can be optimized from a feeder point of view. As shown in Figs. 6 and 7, the implemented BIPV capacities play an important role. Part of the required BIPV capacity can be replaced by thermal solar collectors providing direct thermal energy for space heating and domestic hot water, which can be stored in a buffer tank. Consequently, the produced heat no longer has to be provided by the heat pump reducing the chance of strong voltage drops at feeder level cause by simultaneous electricity consumption by heat pumps.

Changing user behavior itself seems difficult but is part of research in several studies which focus on demand side management (DSM) of electrical appliances. Here, domestic appliances are seen as shiftable loads for peak shaving. Also the availability of thermal or electrical energy storage can only be efficiently employed by using proper DSM control strategies. Appropriate assessment of DSM strategies by thermal storage in buildings can only be investigated by integrated design and simulation of different energy vectors and energy systems as proposed within this work. DSM not necessarily requires knowledge on the feeder status and can be rule-based, but rule-based methods should be derived from an integrated approach.

5.2. Feeder optimization for zero-energy building

Besides building optimization towards feeder requirements, the mentioned obvious improvements of a stronger feeder based on larger feeder cable sections to reduce voltage fluctuations and the installation of a stronger transformer remain a good solution for allowing the wide-spread application of net ZEBs. Another physical solution to reduce voltage fluctuations is changing the topology of the feeder layout avoiding long dead-ends.

In current feeders designed for unidirectional power flows, the feeder voltage is slightly higher compared to the nominal feeder voltage. Allowing a variable feeder voltage during the day allows to reduce voltage fluctuations due to changing electrical energy flows. Moreover, power quality benefits from providing electrical energy storage which allows peak shaving but this has to be weighted economically against thermal energy storage in buildings used for peak shaving.

In order to take fully advantage of possible integration of building technology for energy savings, a 'smart' grid combining electrical energy distribution with distribution of data regarding the complete energy chain allows the building management system to interact properly.

6. Future work

Future work will focus on the same duality denoted in this work: (i) the further development, verification and validation of the IDEAS platform, where-after (ii) each of the subdivisions – i.e. the thermal building design, the thermal building system design and its control, the electric building design and its control and the feeder design – will be subject of optimization towards energetic and economic efficiency.

As the IDEAS tool integrates all transient energy flows at feeder level, the tool is suitable for assessment of detailed DSM strategies.

7. Conclusions

A tool for Integrated District Energy Assessment by Simulation (IDEAS) is developed and presented, and used for assessing the electrical challenges at feeder level of a building stock evolving towards ZEBs.

This IDEAS tool allows simultaneous simulation of thermal and electrical processes at both building and feeder level. The tool combines detailed bottom-up statistical and engineering modeling, allowing to encompass occupant behavior, the inclusion of new technologies, and quantification of end-use energy efficiencies based on dynamic simulation.

A set of residential net ZEBs is implemented in the IDEAS tool. The model at feeder level is used to assess electrical bottlenecks not taken into account in common building energy studies at the level of an individual building. Their annual household electrical energy consumption is found between 1.8 and 5.2 MWh, whereas the resulting total annual energy use for SH and DHW is found between 0.7 and 1.5 MWh. The total annual energy use is compensated by a BIPV system with a capacity of 2.2–7.1 kWp. The modeled dwellings show a self-consumption of locally generated PV electrical energy of 26 ± 4% at building level and 33% at neighborhood level.

Resulting feeder voltage fluctuations and possible transformer overload are identified and quantified as bottlenecks in existing feeder designs. First, a fraction of 14–47% of expected local PV supply at feeder level is wasted by inverter curtailing when all dwellings are intended to achieve a level of net ZEB. At building level, these values rise up to a fraction of 41–68%. Second, the feeder peak load is found to be 3.3 kVA per dwelling when inverter curtailing is limited, which may affect power security in existing feeder designs.

Acknowledgements

The authors gratefully acknowledge the Research Foundation – Flanders (FWO) and the KU Leuven Energy Institute (EI) for funding this research.

References

[1] IEA International Energy Agency. Energy technology perspectives 2010, 2010.
[2] The European Parliament. Directive 2002/91/EC of the European Parliament and of the Council of 16 December 2002 on the energy performance of buildings, 2003.
[3] The European Parliament. Directive 2010/31/EU of the European Parliament and of the Council of 19 May 2010 on the energy performance of buildings (recast), 2010.
[4] European Commission. SEC(2011) 463 final – smart grids: from innovation to deployment, COM(2011)202 final, 2010.
[5] Ratti C, Baker N, Steemers K. Energy consumption and urban texture. Energy Build 2005;37:762–76.
[6] Yun G, Steemers K. Implications of urban settings for the design of photovoltaic and conventional façades. Solar Energy 2009;83:69–80.
[7] Kampf J, Robinson D. A simplified thermal model to support analysis of urban resource flows. Energy Build 2007;39:445–53.
[8] Robinson D, Campbell N, Gaiser W, Kabel K, Lemouel A, Morel N, et al. SUNtool: a new modelling paradigm for simulating and optimising urban sustainability. Solar Energy 2007;81:1196–211.
[9] Tanimoto J, Hagishima A, Sagara H. Validation of methodology for utility demand prediction considering actual variations in inhabitant behaviour schedules. J Build Perform Simulat 2008;1(1):31–42.
[10] Yamaguchi Y, Shimoda Y, Mizuno M. Proposal of a modeling approach considering urban form for evaluation of city level energy management. Energy Build 2007;39:580–92.
[11] Yamaguchi Y, Shimoda Y. District-scale simulation for multi-purpose evaluation of urban energy systems. J Build Perform Simulat 2010;3:289–305.
[12] Baker N, Steemers K. The LT method. In: Energy in architecture: the European passive solar handbook. London: Batsford for the Commission of the European Communities; 1992. p. 339.
[13] Spitler JD, Fisher DE, Pedersen CO. The radiant time series cooling load calculation procedure. ASHRAE Trans 1997;103(2).
[14] Kerrisk FF, Schnurr JE, Moore JE, Hunn Bd. The custom weighting-factor method for thermal load calculations in the DOE-2 computer program. ASHRAE Trans 1981;87(2):569–84.
[15] ISO/FDIS 13790. Energy performance of buildings – calculation of energy use for space heating and cooling, vol. 2007, 2008.
[16] Page J, Robinson D, Morel N, Scartezzini J. A generalised stochastic model for the simulation of occupant presence. Energy Build 2008;40(2):83–98.

[17] Wang D, Federspiel CC, Rubinstein F. Modeling occupancy in single person offices. Energy Build 2005;37:121–6.
[18] Reinhart CF. Lightswitch-2002: a model for manual and automated control of electric lighting and blinds. Solar Energy 2004;77:15–28.
[19] Mahdavi A, Mohammadi A, Kabir E, Lambeva L. Occupants' operation of lighting and shading systems in office buildings. J Build Perform Simulat 2008;1:57–65.
[20] Haldi F, Robinson D. On the behaviour and adaptation of office occupants. Build Environ 2008;43:2163–77.
[21] Haldi F, Robinson D. Interactions with window openings by office occupants. Build Environ 2009;44:2378–95.
[22] Fanger PO. Thermal comfort: analysis and application in environmental engineering. New York: McGraw-Hill Book Company; 1970.
[23] Tanimoto J, Hagishima A. Total utility demand prediction system for dwellings based on stochastic processes of actual inhabitants. J Build Perform Simulat 2010;3:155–67.
[24] Robinson D, Stone A. Solar radiation modelling in the urban context. Solar Energy 2004;3(77):295–309.
[25] Robinson D, Stone a. Internal illumination prediction based on a simplified radiosity algorithm. Solar Energy 2006;80:260–7.
[26] IEA International Energy Agency, IEA PVPS task 10: urban-scale phtovoltaic applications, 2006.
[27] Intelligent Energy Europe, PV upscale – urban scale photovoltaic systems, 2006.
[28] Conti S, Raiti S, Tina G, Vagliasindi U. Integration of multiple PV units in urban power distribution systems. Solar Energy 2003;75:87–94.
[29] Paatero J, Lund P. Effects of large-scale photovoltaic power integration on electricity distribution networks. Renew Energy 2007;32:216–34.
[30] Thomson M, Infield D. Impact of widespread photovoltaics generation on distribution systems. IET Renew Power Generat 2007;1(1):33–40.
[31] Widén J, Wäckelgård E, Paatero J, Lund P. Impacts of different data averaging times on statistical analysis of distributed domestic photovoltaic systems. Solar Energy 2010;84(3):492–500.
[32] Widén J, Nilsson AM, Wäckelgård E. A combined Markov-chain and bottom-up approach to modelling of domestic lighting demand. Energy Build 2009;41:1001–12.
[33] Paatero JV, Lund PD. A model for generating household electricity load profiles. Int J Energy Res 2006;30:273–90.
[34] Richardson I, Thomson M, Infield D. A high-resolution domestic building occupancy model for energy demand simulations. Energy Build 2008;40(8):1560–6.
[35] Wright a, Firth S. The nature of domestic electricity-loads and effects of time averaging on statistics and on-site generation calculations. Appl Energy 2007;84:389–403.
[36] Elmqvist H. Modelica – a unified object-oriented language for physical systems modeling. Simulat Practice Theory 1997;5(6):32.
[37] Petzold LR. DASSL: differential algebraic system solver. Tech. rep., Sandia National Laboratories, Livermore, 1982.
[38] European heat pump association, outlook 2010 – European heat pump statistics. Tech. rep., 2009.
[39] EurObserv'ER, "Baromètre photovoltaïque/ Photovoltaic barometer: 9 533.3 MWc dans l'EU/ in the EU.," Systèmes solaires – Le journal de photovoltaïque, vol. 1, 2009. p. 72–103.
[40] van Gent RH. On the history of astronomy, 2011.
[41] Meteotest. METEONORM Version 6.1 – Edition 2009, 2008.
[42] The Institute of Electrical and Electronics Engineers, IEEE 34 Node Test Feeder. Tech. rep., 2010.
[43] Kersting W. Radial distribution test feeders. In: IEEE power engineering society winter meeting, 2001. p. 908–12.
[44] Allacker K. Sustainable building – the development of an evaluation method. Phd, K.U.Leuven, 2010.
[45] Vanneste D, De Decker P, Laureyssen I. Sociaal-Economische Enquête 2001. Monografie. Woning en woonomgeving in België. Tech. rep., 2001.
[46] Verbeeck G. Optimisation of extremely low energy residential buildings. PhD thesis, K.U.Leuven, 2007.
[47] EN 12831. Heating systems in buildings – method for calculation of the design heat load, 2003.
[48] Khalifa AJN. Ntural convective heat transfer coefficient – a review: surfaces in two- and three-dimensional enclosures. Energy Convers Manage 2001;42(4):505–17.
[49] Jürges W. Der Wärmeübergang an einer ebenen Wand. Beihefte zum Gesundheits-Ingenieur 1924;1(19).
[50] Hamilton DC, Morgan WR. Radiant-interchange configuration factors. Tech. rep., National Advisory Committee for Aeronautics, Washington, 1952.
[51] ISO/CD 13370. Thermal performance of buildings heat transfer via the ground calculation methods. Revision of ISO 13370:1998. No. September, 2004.
[52] Perez R, Stewart R, Arbogast C, Seals R, Scott J. An isotropic hourly diffuse radiation model for sloping surfaces: description, performance validation, site dependency evaluation. Solar Energy 1986;36(6):481–97.
[53] Perez R, Seals R, Ineichen P, Stewart R, Meniucci D. A new simplified version of the Perez diffuse irradiance model for tilted surfaces. Solar Energy 1987;39(3):221–31.
[54] Finlayson EU, Arasteh DK, Huizenga C, Rubin MD, Reilly MS. WINDOW 4.0: documentation of calculation procedures. Tech. rep., 1993.
[55] Judkoff R, Neymark J. International energy agency building energy simulation test (BESTEST) and diagnostic method. Tech. rep., National Renewable Energy Laboratory, US Department of Energy, Colorado, 1995.
[56] Daikin Europe N.V., Technical data Altherma ERYQ007A, EKHB007A/ EXHBX007A, EKSWW150-300. Tech. rep., 2006.
[57] prEN 15377-1. Heating systems in buildings – design of embedded water based surface heating and cooling systems. Part 1: Determination of the design heating and cooling capacity; 2005.
[58] Koschenz M, Lehman B. Thermoaktive Bauteilsysteme tabs. Dübendorf: EMPA-Akademie, 2000.
[59] EN 442-2. Radiators and convectors. Part 2: Test methods and rating; 1996.
[60] Richardson I, Thomson M, Infield D, Clifford C. Domestic electricity use: a high-resolution energy demand model. Energy Build 2010;42:1878–87.
[61] Stokes M, Rylatt M, Lomas K. A simple model of domestic lighting demand. Energy Build 2004;36(2):103–16.
[62] Richardson I, Thomson M, Infield D, Delahunty A. Domestic lighting: a high-resolution energy demand model. Energy Build 2009;41(7):781–9.
[63] FOD Economie, Bevolking - Private, grootte en collectieve huishoudens. Tech. rep., 2008.
[64] BR Becker, Stogsdill KE. Development of hot water use data base. In: ASHRAE transactions, vol. 96, (Atlanta, GA). American society of heating, refrigerating and air conditioning engineers; 1990. p. 422–7.
[65] Fairey P, Parker D. A review of hot water draw profiles used in performance analysis of residential domestic hot water systems. Tech. rep., Florida Solar Energy Center, Florida, 2004.
[66] Huld T, Suri M. PVGIS, PV estimation utility, 2010.
[67] De Soto W, Klein SA, Beckman WA. Improvement and validation of a model for photovoltaic array performance. Solar Energy 2006;80:78–88.
[68] Sera D, Teodoresco R, Rodriguez P. PV panel model based on datasheet values. In: IEEE international symposium on industrial electronics; 2007. p. 2392–6.
[69] Synergrid, Specifieke technische voorschriften voor decentrale productie-installaties die in parallel werken met het distirbutienet C10/11, tech. rep., 2009.
[70] Maes D. <http://wwwa.vito.be/edisontest/qs/index.asp>, 2005.
[71] prEN 15316-4-2. Heating systems in buildings – method for calculation of system energy requirements and system efficiencies. Parts 4–2: Space heating generation systems. Heat Pump Syst.
[72] Torcellini P, Pless S, Deru M, Crawley D. Zero-energy buildings: a critical look at the definition. In: ACEEE summer study, Pacific Grove, California, August 14–18, 2006, p. 15.

3.4 Rule-based demand side management of domestic hot water production with heat pumps in zero energy neighbourhoods

Journal of Building Performance Simulation
Vol. 4, No. 7, 2014, 271–288

Article

Rule-based demand side management of domestic hot water production with heat pumps in zero energy neighbourhoods

R. De Coninck[a,b] *, R. Baetens[c], D. Saelens[c], A. Woyte[b] and L. Helsen[a]

[a] *Applied Mechanics and Energy Conversion, Department of Mechanical Engineering, KU Leuven, Belgium*; [b] *3E, Brussels, Belgium*; [c] *Building Physics Section, Department of Civil Engineering, KU Leuven, Belgium*;

(*Accepted version*)

Grid saturation has been reported in electricity distribution systems with a high penetration of photovoltaic (PV) systems. This saturation is often caused by overvoltage and results in curtailing or shutting-down of the PV inverters, leading to a loss of renewable electricity generation.

The presented work assesses the potential of rule-based demand side management (DSM) applied to domestic hot water (DHW) production with heat pumps in dwellings for reducing the non-renewable energy use of the neighbourhood.

The studied case consists of 33 single-family dwellings connected to the IEEE 34 node test feeder in a moderate European climate. Each dwelling is designed as a net zero energy building (NZEB) by adequate design of a heat pump and PV system.

A detailed dynamic simulation model is implemented by use of a cross domain Modelica library for integrated district energy assessment. The user behaviour is obtained from a stochastic model based on Markov chains and survival analysis. Different rule-based DSM control strategies are applied to the individual dwelling's DHW systems.

The results show that for balancing the PV production, active thermal energy storage in the DHW storage tanks is very promising. Even with very basic control algorithms and small storage tanks of 0.3 m^3, curtailing losses can be reduced by 74 %. This represents a net energy saving on neighbourhood level of 3.4 %.

Keywords: demand side management (DSM), rule-based control, photovoltaics (PV), Modelica, thermal energy storage (TES), integrated neighbourhood simulation

Acknowledgment (Author Accepted Manuscript)

This is an Accepted Manuscript of an article published by Taylor & Francis in the Journal of Building Performance Simulation on 14 June 2013 (online version), available: http://www.tandfonline.com/10.1080/19401493.2013.801518.

1. Introduction

1.1 Grid saturation due to overvoltage

Distributed electricity generation (DG) affects the operating conditions of distribution grids in different ways (Dugan and McDermott, 2001; Ackermann and Knyazkin, 2002). One specific issue consists of steady-state voltage rises, which are of particular interest in distribution grids

*Corresponding author. Email: roel.deconinck@3e.eu

ISSN: 1940-1493 print/ISSN 1940-1507 online

DOI: 10.1080/19401493.2013.801518
http://www.informaworld.com

with a large amount of PV systems (Woyte et al., 2006; Caamaño Martin et al., 2008). At times of high solar radiation, these voltage rises may result in a shut down of some of the PV inverters, or a curtailing of the output power by droop control (De Brabandere et al., 2004). These problems will happen more frequently as the cumulative installed PV capacity is expected to keep on rising in existing distribution grids (EPIA, 2012).

As a result of the European policy regarding building energy performance, low energy neighbourhoods will have to become the standard for new construction from 2020 onwards (European Parliament, 2010). In these low energy buildings and neighbourhoods, PV and heat pump technology are often combined in order to reach a yearly 'net zero' energy balance. However, this may lead to inverter shut down or droop control at certain times, causing a loss of renewable electricity generation. For example, Baetens et al. (2012) computed a loss of 14 % to 47 % of the expected local PV electricity generation in a low energy neighbourhood, depending on feeder sizing and parameter settings for the overvoltage shut-down.

Possible solutions to reduce the amount of curtailed power in distribution grids with a large amount of PV systems consist of:

- Feeder reinforcements
- Changing the transformer tap positions to obtain an adapted voltage at the point of common coupling
- Active voltage control with modern inverters (Bletterie et al., 2010)
- Demand side management (DSM)

This paper assesses the potential of rule based DSM applied to the domestic hot water (DHW) production in dwellings with heat pumps. The aim of load shifting is not the voltage control on itself, but a reduction of the non-renewable energy use of the neighbourhood.

1.2 Demand side management

The idea of DSM for this case is straightforward: by shifting electrical loads to time periods of excessive voltage in the grid, curtailing of the inverters can be avoided. There are different options for the shiftable loads. This paper will neither consider load shifting with household appliances like dishwashers, cloth washers and dryers, nor by use of an electrical battery.

The shiftable load is the compression heat pump that produces heat for space heating and DHW. This paper only considers the DHW production as a shiftable load. The required flexibility to enable the decoupling of heat generation and consumption is the thermal energy storage (TES) tank for storage of the domestic hot water. We only consider DHW and exclude space heating from this paper because the latter requires a more detailed analysis in order to cover the different emission systems and control strategies which lies beyond the scope of this paper. As will be shown, the potential of load shifting on DHW is substantial and justifies the current scope. The application of the elaborated methodology on space heating is a topic for future work.

In a previous study, different control strategies had been applied to a heat pump for space heating in a single dwelling (De Coninck et al., 2010). Although it was shown that peak loads can be reduced at the level of an individual building, the impact of these control strategies on the distribution grid and consequently the inverter behaviour could not be assessed. This paper takes the next step by modelling the entire neighbourhood.

1.3 Modelling of neighbourhoods

Simulations or optimizations on a single building level cannot be used to study the operation of the distribution grid. DSM studies on single buildings can be used to study the energy or cost savings in that building, up to the power exchange with the grid. It is however incorrect to use these studies for drawing conclusions about the ability of DSM to compensate for stochastic electricity generation or distribution grid loads. For this purpose, a neighbourhood model is

Table 1. Overview of building model parameters

Element	A (m^2)	U ($W/(m^2\,K)$)	g (-)
Outer facade [a]	135.0	0.22	-
Floor [b]	98.0	0.19	-
Roof [c]	118.0	0.11	-
Windows	33.5	1.10	0.59

[a] 15 cm of PUR between an 8 cm outer and 14 cm inner brick wall.

[b] 10 cm of PUR below a 8 cm screed layer and on a 20 cm concrete slab.

[c] 30 cm of mineral wool between multiplex plates in a timber frame construction.

required, composed of the distribution grid, different buildings and stochastic user behaviour.

On the other hand, neighbourhood (or district) level simulations are not new. Manfren et al. (2011) discuss different aspects of district level simulations whereas Baetens et al. (2012) give a good overview of existing approaches and tools.

DSM applied to heat pumps has to be studied with detailed dynamic models. These models need to include the building, heating, ventilation and air-conditioning (HVAC) and user behaviour. This is required for capturing the interaction between the heating system and the building, the effects of ambient, inside and TES tank temperatures on the heat pump efficiency, the consequences of on/off cycling, etc. Most district simulation tools cannot cope with the desired level of detail in the building model. On the other hand, typical building simulation tools do not allow to model multiple buildings connected to a distribution grid. In order to combine the best of two worlds, we use Modelica.

The present paper shows how thermal energy management can be applied in order to relieve grid saturation on neighbourhood level. Special attention is paid to the modelling of the DHW system because both the hot water demand and the TES tank model largely influence the potential of DSM. Modelica has proven well suited for this purpose.

2. Model

2.1 Overview

The model consists of 33 single-family dwellings connected to the 34-node test feeder of the Institue of Electrical and Electronics Engineers (IEEE) (Kersting, 2001) in the moderate European climate of Uccle, Belgium. It is assumed that all dwellings are identical, built according to a low-energy standard, heated with a modulating air-to-water heat pump and equipped with a PV system covering their complete yearly energy needs. The following paragraphs elaborate on the modelling principles and details, whereas Tables 1 and 2 give an overview of the building and general model parameters respectively.

2.2 Dwelling

A single dwelling typology is used which was identified in the European TABULA project (Loga et al., 2009) as representative for semi-detached single-family houses constructed after the year 2005. This means that all dwellings are identical and that the variation in temperature and load is caused entirely by the stochastic user behaviour. The dwelling has a total heated floor area of 196 m^2, a total volume of 643 m^3, a compactness of 1.58 m and is modelled as a single thermal zone. The dwelling is designed according to a low-energy standard and has massive walls and floors. The composition of the different envelope elements and resulting U-values are given in Table 1.

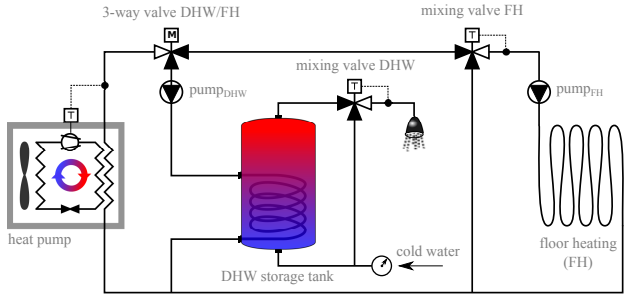

Figure 1. Hydraulic scheme of the heating and DHW system

We suppose an air-tightness corresponding to the low energy standard with a natural infiltration rate of 0.03 air changes per hour (ACH). All dwellings are equipped with mechanically balanced, air-to-air heat-recovery ventilation with an air change rate of 0.5 ACH and a recovery efficiency of 0.84.

All dwellings have exterior solar screens with a solar transmittance of 0.24. As a result no active cooling needs to be installed in the dwellings. The automated exterior solar screen is lowered at a global horizontal irradiation level of 250 W/m^2 and raised again at an irradiation level below 150 W/m^2.

2.3 HVAC system

Each of the 33 dwellings has an identical space heating and DHW system, visualized in Figure 1. Heat is produced by means of a modulating air-to-water heat pump (HP), connected to a floor heating and a DHW storage tank.

2.3.1 Heating

The heat pump model is based on linear interpolation in a performance map retrieved from manufacturer data (Daikin Europe N.V., 2006). The performance map does not take into account (de)frosting of the evaporator as shown in Figure 2 (although it does extend to negative ambient temperatures). The nominal coefficient of performance (COP) is 3.17 at 2/35 °C and 2.44 at 2/45 °C test conditions (i.e. air/water temperature) for full load operation. The thermal power of the heat pump is 3459 W at 2/35 °C.

The interpolation in the performance map defines the heating power $\dot{Q}_{net}$ (W) and electricity use $\dot{P}_{net}$ (W) as a function of condenser outlet temperature, the ambient temperature and modulation level (between 25 % and 100 %). The heat pump can modulate thanks to an inverter at the compressor. In the model, the modulation level mod_{final} (%) is obtained in two steps. First, the initial modulation mod_{init} (%) is computed according to Equation (1), and then limited according to Equation (2). To avoid on/off cycling, a hysteresis is added to the starting condition: the heat pump will only start when $mod_{init} \geq 50\%$.

$$mod_{init} = \frac{\dot{Q}_{demand}}{\dot{Q}_{max}} = \frac{\dot{m} c_p (T_{set} - T_i)}{f(T_{evap}, T_c)} \quad (1)$$

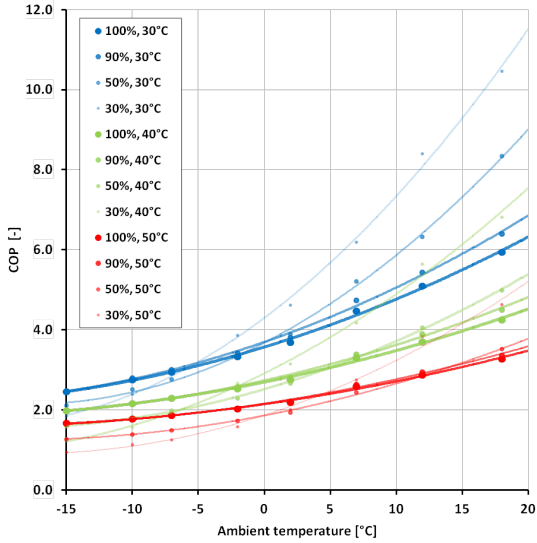

Figure 2. Performance map of the heat pump, showing the COP as a function of ambient temperature for different modulation levels (30 %, 50 %, 90 % and 100 %) and different condenser outlet temperatures (30 °C, 40 °C and 50 °C).

$$mod_{final} = \begin{cases} 0\%(=\text{off}) & \text{if } mod_{init} < 25\%, \\ 100\% & \text{if } mod_{init} \geq 100\%, \\ mod_{init} & \text{else.} \end{cases} \tag{2}$$

In these equations, $\dot{m}$ (kg/s) is the mass flow rate in the condenser, c_p (J/(kg s)) the specific heat capacity of water, T_{set} (K) is the condenser set temperature, T_i (K) is the condenser inlet temperature, $\dot{Q}_{demand}$ (W) is the demanded thermal power and $\dot{Q}_{max}$ (W) is the maximum thermal power at the current evaporator temperature T_{evap} (K) and condenser temperature T_c (K), obtained from the performance map.

The model takes into account the water content of the condenser m_c (kg) and dry capacity c_{dry} (J/K), both connected to the environmental temperature T_e (K) through a thermal conductance UA_{loss} (W/K) in order to obtain a dynamic model with heat losses according to Equation (3).

$$(m_c c_p + c_{dry})\frac{dT_c}{dt} = \dot{m} c_p (T_i - T_c) + \dot{Q} - UA_{loss}(T_c - T_e) \tag{3}$$

In this equation, $\dot{Q}$ (W) is the condensation heat $\dot{Q}_{net}$ augmented with the environmental heat losses $UA_{loss}(T_c - T_e)$. This ensures that the steady state efficiency of the heat pump is identical to the performance data, while adding environmental losses and dynamics to the model. The produced heat is used for charging the floor heating, designed to work at a 35/30 °C regime at design conditions and for charging the domestic hot water storage tank. As mentioned above, the investigated DSM controls only concern the charging of the DHW tank.

2.3.2 Domestic hot water and storage tank

The stratified water energy storage tank is only used for DHW production. It is connected to the heat pump through an internal heat exchanger, and the hot water is withdrawn via a thermostatic mixing valve in order to obtain water at 45 °C. A one-dimensional multinode storage tank model is used. For each node i (numbering starts at the top), the energy balance and mass balance equations are given in respectively Equations (4) and (5) and presented schematically in Figure 3.

$$m_i c_p \frac{dT_i}{dt} = \sum_j c_p \dot{m}_j T_j + \dot{Q}_{cond,i-1} + \dot{Q}_{cond,i} + \dot{Q}_{buo,i} + \dot{Q}_{buo,i-1} + \dot{Q}_{env,i} + \dot{Q}_{HX,i} \quad (4)$$

$$\sum_j \dot{m}_j = 0 \quad (5)$$

In these equations, m_i (kg) is the water mass of the node i with temperature T_i (K) and c_p is the specific heat of water, assumed to be constant and equal to $4177\,\mathrm{J\,kg^{-1}\,K^{-1}}$. The in- and outgoing water flows in node i due to forced circulation are represented by $\dot{m}_j$ (kg/s), their corresponding temperatures by T_j (K) (for outgoing flows, $T_j = T_i$). Heat transfer to neighbouring nodes via conduction is given by $\dot{Q}_{cond}$ (W). Transmission losses to the environment are given by $\dot{Q}_{env,i}$ (W). When the node i contains a section of the internal heat exchanger, the heat transfer from this section into the node is given by $\dot{Q}_{HX,i}$ (W). $\dot{Q}_{buo}$ (W) is the equivalent heat transfer to neighbouring nodes due to buoyancy effects and this term will be elaborated in the following paragraphs. Mass flow rates and heat fluxes entering the node i have a positive sign.

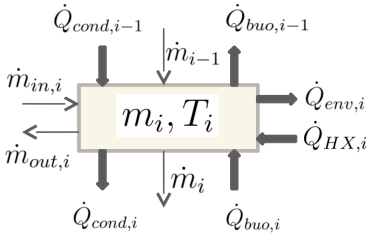

Figure 3. Schematic overview of the nodal energy balance in the TES tank

The storage tank plays a key role in the DSM strategies, therefore specific attention was paid to verification and calibration of the model to manufacturer data. The goal of this calibration is to obtain a robust model formulation, that can be used for different storage volumes. This requires that the model parameters are independent of the size and geometry of the nodes.

Technical information and measurements from the commercial DHW tank Vitocell 100-V, type CVW of 390 l are used to tune the parameters of the model (Viessmann, 2011).

Firstly, geometrical details like tank diameter and height, surface and water content of the internal heat exchanger are set. The heat transfer coefficients of the internal heat exchanger (internal convection, conduction and external convection) are calculated based on heat transfer correlations.

Secondly, the parameters for the transmission losses $\dot{Q}_{\mathrm{env},i}$ are set. In order to obtain a parametric model that allows scaling, a fixed $UA_{fix}(\mathrm{W\,K^{-1}})$ and a surface dependent heat loss coefficient $U_{Ins}(\mathrm{W\,m^{-2}\,K^{-1}})$ are defined. U_{Ins} depends on thickness and thermal conductivity

of the insulation. UA_{fix} accounts for cold bridges and increased heat losses at the connections and is fixed to match the given 24 hour heat losses according to DIN V 18599.

Finally, the remaining parameters to be set are the number of layers and the buoyancy model, which are linked. The aim of this calibration exercise is to find a model with a relatively low number of layers that is robust to changes in storage volume. Therefore, the number of layers and the buoyancy formulation should not influence the yearly performance of the storage tank (or only to a limited extend). Thermal stratification and buoyancy are complex processes depending on tank geometry and operation conditions. Haller et al. (2009) review different methods that have been proposed to characterize thermal stratification in TES tanks. All attempts to include these phenomena in one-dimensional stratified storage tank models are strong simplifications of the 3-D flow patterns that occur (Han et al., 2009). Most one-dimensional stratified storage tank models approximate buoyancy effects as mixing between the layers in case of temperature inversion (Zurigat et al., 1989). In case of a fixed time step simulation, the mixing rate depends on the node volume and simulation time step (Newton, 1995; Mather et al., 2002). In case of continuous time solvers, a parameter is required for the time constant of mixing (Wetter, 2009). Specific buoyancy formulations exist for modelling plume entrainment, caused by the inflow of cold water at the top of the tank (Kleinbach et al., 1993). Kleinbach et al. (1993) and Mather et al. (2002) demonstrate the importance of the number of nodes with regard to accuracy of the model and more specifically the rate of stratification. This stratification plays an important role in the efficiency of the tank and as a consequence the total system (Rosen et al., 2004).

The technical sheet specifies four performance characteristics to tune the model: two discharging and two charging experiments. The discharging experiments show that the number of layers should be as high as 20 or even 40 in order to correctly model the sharp thermocline in discharging situations. However, we will show later that with the correct buoyancy model, a lower number of layers (down to 10 layers) does not have a significant impact on the yearly energy use and DHW comfort. The DHW comfort is defined as the ratio of DHW use at temperatures of at least 40 °C to the total DHW use.

As we model a tank with internal heat exchanger, the buoyancy model can be validated from the two charging experiments (a and b). In a first step, a buoyancy model is chosen, with unknown parameters. For each number of layers, a numeric optimization is carried out to find the optimal model parameters that minimize the sum of the residuals for both experiments a and b. The residual is the difference between the simulated and the specified tank outlet temperature at the final charging time.

We want to find a stable buoyancy formulation, meaning that the model parameters are independent of the number of nodes (between 5 and 40). However, for most buoyancy models, including time constant based node mixing, this is not the case and parameter variations of more than 100 % occur when the number of nodes is divided by two. A buoyancy model that leads to a parameter variability of less than 20 % is presented by Equation 6.

$$Q_{buo,i} = k_{buo}(N)\Delta T_i N^{1.5} \tag{6}$$

In this equation $Q_{buo,i}$ is the heat flow from layer $i+1$ to layer i, ($i = 1$ is top layer), $k_{buo}(N)$ is the model parameter to be identified which depends on N, the number of layers in the model and ΔT_i is the temperature difference between layer $i+1$ and layer i, i.e. zero if no temperature inversion. The resulting optimized $k_{buo}(N)$ as a function of N is shown in Figure 4. Two conclusions can be drawn from this figure: (i) for each number of layers between 5 and 40, a $k_{buo}(N)$ can be found for which the model closely matches the measurements, and (ii) the identified $k_{buo}(N)$ lie all in the interval of $20.8 \pm 20\,\%$.

With the optimal $k_{buo}(N)$ the impact of the number of nodes on the yearly performance of the tank can be analysed. Three different DHW tap profiles are defined (see 2.5.3). Figure 5 shows that for each of these profiles, reducing the number of layers from 40 to 10 will result

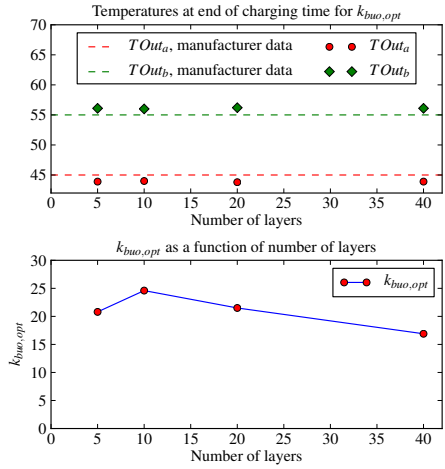

Figure 4. Top: model deviation from the validation data as a function of number of layers. Bottom: optimal $k_{buo}(N)$ according to Equation 6 as a function of number of layers.

in deviations on yearly energy use and DHW discomfort of less than 5 % and 2 % respectively. This is an important result, because neighbourhood simulations with 40 layers in each TES tank require significantly longer computation times.

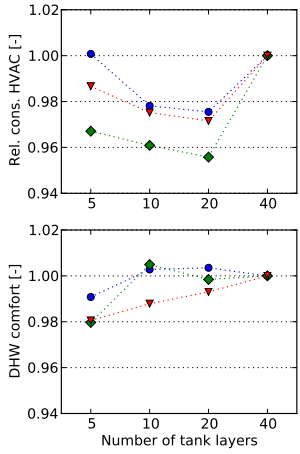

Figure 5. Sensitivity of the yearly energy use and DHW comfort to the number of layers if the optimal $k_{buo}(N)$ is taken according to Figure 4.

Finally, the robustness of the buoyancy model with parameter $k_{buo}(N)$ is checked around $k_{buo,10}$. For each of the three DHW profiles used in Figure 5 and for a constant tank volume,

the tank height and the number of layers is varied to check the sensitivity of $k_{buo,10}$ for small deviations in layer size and height. The results, given in Figure 6, show that small variations in geometry and discretization lead to deviations on yearly energy use and DHW discomfort of less than 2 % and 1 % respectively. These results confirm the robustness of the buoyancy formulation and the stratified storage tank model in general. No additional model enhancements to avoid numerical dissipation have been implemented.

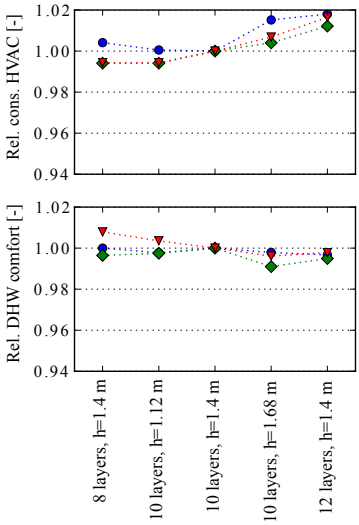

Figure 6. Sensitivity of the yearly energy use and DHW comfort to number of layers and TES tank height for $k_{buo,10}$

This parameter calibration was only done for a 390 l tank and corresponding internal heat exchanger. In this study, it is assumed that the heat exchanger and insulation thickness remain the same for changes in tank volume between 300 l and 500 l. All resulting parameters are found in Table 2 (on page 13).

2.3.3 Control

There are two loops in the HVAC control. The first loop controls the flow rate through the heat pump by sending on/off control signals to $pump_{FH}$ and $pump_{DHW}$. The signal for $pump_{FH}$ is sent by the room thermostat based on the operative temperature, set point and a hysteresis of 1 K (above set point). All dwellings have a constant temperature set point of 20 °C. This approach is chosen for reasons of simplicity given the fully stochastic user presence in combination with floor heating. Moreover, night set back is difficult to implement and has a limited impact in heavy-construction well-insulated and air-tight buildings (Olesen, 2001; Hastings, 2004). The signal for $pump_{DHW}$ is based on the measured and set point values for the storage tank top temperature T_{Top}, measured in the second layer. A hysteresis of 2 K is applied (above set point).

The second loop controls the condenser set temperature. This control is only active when the heat pump condenser receives a flow rate, and distinction is made based on which pump is running. When $pump_{FH}$ is activated, the set point follows a heating curve for space heating, but with an offset of 2 K in order to compensate for distribution losses. When $pump_{DHW}$ is activated, the set point is 5 K higher than the DHW tank set point in order to be able to reach the switch off condition on T_{Top}. Both pumps can be activated simultaneously. When this

happens, the condensor of the heat pump receives the sum of both flow rates and the highest temperature set point precedes.

For the reference case, the DHW tank set point $TSet_{DHW}$ results from a small sensitivity study. The tank set point has a large impact on the operation of the heat pump. If $TSet_{DHW}$ is low, the COP will be higher, but the heat pump will cycle more since after each DHW draw, the tank top temperature will be below the set point. This cycling behaviour will decrease the overall seasonal performance factor (SPF). A low set point will also decrease the DHW comfort (see Section 3.1). A few simulations with different DHW tap profiles led to the conclusion that for the reference case, a fixed DHW tank set point of 53 °C gives a satisfactory trade-off between thermal comfort and energy use.

2.4 Electricity generation

Each dwelling has a building integrated PV system which is sized to cover, on a yearly basis, the total electricity consumption of the dwelling. As the user behaviour influences this consumption, each dwelling will have a different installed PV capacity. Azimuth and inclination of the modules are identical for all dwellings.

The PV system is modelled with the 5-parameter model of De Soto et al. (2006) based on a temperature-dependent diode equivalent circuit (Sera et al., 2007). The efficiency parameters of a PV module are taken from manufacturer characteristics (Sanyo, 2008). The direct current power output of the modules is converted to AC power by means of an inverter with constant efficiency of 95 %.

To avoid excessive feeder voltages, the inverter is switched off when the voltage at the dwelling-feeder interface reaches a predefined limit. This switching-off is applied as the distribution system operator currently does not allow the distributed sources to provide voltage control of the distribution feeder, e.g. by reactive power control. This limit is set at an increase of 10 % of the nominal feeder voltage or 253 V according to national regulations on AREI Art.§235, the Belgian General Regulations for Electrical Installations (and Labour Protection). The inverter control is given a minimal off-time of roughly 300 s before trying to switch on again. To obtain a stable model, each of the 33 inverters has a slightly different off-time between 275 s and 318 s.

2.5 Occupant behaviour

The stochastic behaviour of accommodated occupants concerning presence, the use of appliances and lighting, and domestic hot water withdrawal is implemented as a combination of survival analyses for occupancy and embedded discrete-time Markov chains for the remainder.

2.5.1 Presence

Differently from earlier work (Baetens et al., 2012), occupancy is no longer described based on discrete-time Markov chains. The required differentiation based on household typologies results in a more comprehensive representation of occupancy behaviour at household level and a more realistic representation of the simultaneity of the resulting power demand for space heating and DHW.

Four different family types have been defined based on the work of Cheng and Steemers (2011), ie. (1) a young couple both working full time during weekdays and partly present in the weekend, (2) a family of 4 persons of which one parent works part time, (3) an unemployed couple and (4) a retired couple. For each family type, the average number of persons at home are defined for a typical weekday and a typical weekend. In order to obtain fully stochastic profiles, an uncertainty is applied to the average arrival and departure times for each household and an uncertainty to the average arrival and departure times for each day of the week for the survival analysis. Both uncertainties are defined by a standard deviation σ of 1 hour compared to the family type average and household average respectively. This results in all different occupancy

profiles, while the aggregated profiles by family type still reflect the typical days. To illustrate the result, a weekly aggregated occupancy profile for a single family of type (1) is given in Figure 7 and for a single family of type (4) in Figure 8.

2.5.2 Household electricity load

The implemented stochastics are consistent with Richardson et al. (2010) and are based on discrete-time Markov chains as described by Baetens et al. (2012). The resulting outputs are activity of the building occupants, the use of appliances (Richardson et al., 2010) and the use of lighting (Stokes et al., 2004; Richardson et al., 2009), and (only) depend on the household size, the present appliances and fixtures, whether it is a weekday or weekend day and global irradiances. Here, the use of appliances and lighting has a 1 minute resolution. To generate 33 statistically relevant profiles, bottom-up data concerning household size and installed appliances are used based on Belgian (FOD Economie, 2008) and European (Richardson et al., 2010) statistics on household sizes and appliance ownership rates respectively. As such, the main electrical appliances taken into account are domestic lighting, freezer and refrigerator, a music installation, the iron and vacuum cleaner, a personal computer, a television, cooking appliances such as a hob, oven, microwave and kettle, a dishwasher, a tumble dryer and a washing machine. Figure 7 shows a profile with resulting electricity use and internal gains aggregated to a week for a single family. Internal gains can be lower or higher than the electricity consumption, depending on which appliance is consuming and the occurrence of internal gains from persons.

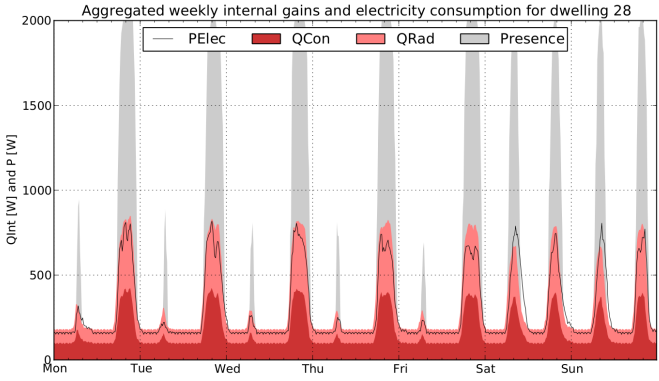

Figure 7. Aggregated weekly presence, internal gains and electricity consumption for a young couple both working full time during weekdays and partly present in the weekend (type (1)). $PElec$ = total electricity consumption without HVAC, $QCon$, $QRad$ = convective respective radiative heat gains. Presence is visualised as the proportion of maximum occupancy, presence during nights when the inhabitants are sleeping is not shown.

2.5.3 Domestic hot water

Special attention has been paid to a solid DHW model because of the increased fraction of the final energy demand for domestic hot water in low energy buildings. There are two important aspects in modelling DHW consumption in building simulation research: the tap profile and the total hot water consumption. Both aspects are discussed below.

The tap profile is strongly related to the activity of the building users, and therefore a stochastic model is needed for which each simulated dwelling shows a different consumption profile that is in accordance with the occupancy and activity of the users. Different stochastic models for the DHW tap profile can be found in the literature (Becker and Stogsdill, 1990; Fairey and Parker, 2004; Jordan and Vajen, 2001; Hendron and Burch, 2007; Widén et al., 2009). The approach within this work is based on the models of Jordan and Vajen (2001) and Widén et al. (2009).

Four different withdrawal categories have been defined, i.e. a short and medium withdrawal, a shower and a bath. For each category, the flow rate, total DHW volume and the average number of occurrences per day is fixed equal to Jordan and Vajen (2001). Ten-minute proclivities are determined based on the occupancy and activity proclivities from Richardson et al. (2010) for each category. The resulting stochastic profile for the DHW tap profile is achieved by discrete-time Markov chains based on a calibration scalar to end up with the desired average equivalent consumption per capita.

The total DHW consumption per capita depends on many parameters. Measurements and estimates made in several studies show a large variance in the results. In the following overview, all consumptions are converted to equivalent volumes at 60 °C, with cold water at 10 °C. A European SAVE study by Lechner (1998) reports an average consumption of 30 l/day per person with a range between 10 l/day and 80 l/day. Marsh (1996) computed a daily consumption for washing of only 14 l/day per person, but if (hot fill) dish and cloth washing are included, this number rises to 41 l/day per person. Widén et al. (2009) used two Swedish measurement campaigns with the following consumptions: about 40 l/day per person for detached houses and between 51 l/day and 154 l/day per person for appartments. Several measurement campaigns followed up by 3E in Belgium have resulted in an average of 30 l/day per person for multi-family houses.

Due to the detailed stochastic model, the average daily DHW consumption is rather an output than an input. For the whole neighbourhood, with 82 residents, the average amounts to 33.1 l/day per person at 60 °C. This consumption is imposed at the flange of the storage tank. Consequently, distribution losses are neglected in this study. An aggregated weekly tap profile for a family of type (4) is shown in Figure 8.

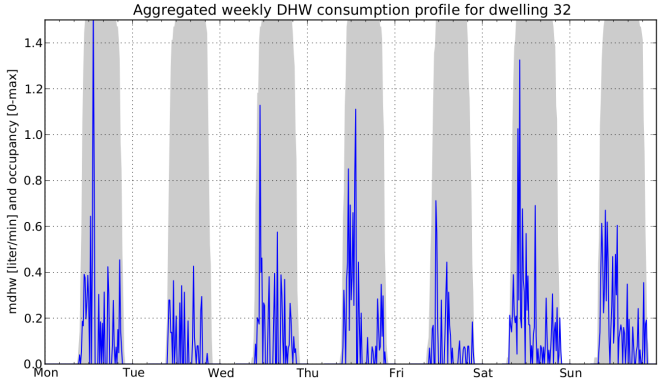

Figure 8. Aggregated weekly presence and DHW consumption for a retired couple (type (4)). Presence is visualised as the proportion of maximum occupancy, presence during nights when the inhabitants are sleeping is not shown.

2.6 Neighbourhood

The dwellings are connected to a low voltage distribution grid, shown in Figure 11 (b) (on page 15). The same IEEE 34 node grid topology is used as in Baetens et al. (2012), and sizing is according to the *medium feeder strength*, which stands for aluminium cables with sections of 95 mm^2, 50 mm^2 and 35 mm^2 for the different lines. The different household types are distributed randomly over the neighbourhood.

Table 2. Overview of model parameters

Symbol	Parameter	Value
Dwelling		
A_{heat} / V_{heat}	Heated floor surface and volume	196 m^2 / 643 m^3
$\dot{V}_{inf}$	Infiltration flow rate	0.03 ACH
$\dot{V}_{ven}$	Ventilation flow rate	0.5 ACH
η_{hr}	Ventilation heat recovery efficiency	0.84
UA_{tot}	Overall heat loss coefficient (incl. infiltration and ventilation with heat recovery)	106 W/K
Φ_{design}	Specific building design heat load (Ukkel, Belgium)	15.8 W/m^2
g_s	Solar transmittance of the solar shading	0.24
$ctrl_s$	Irradiance thresholds for automatic control of solar shading (down - up)	250 - 150 W/m^2
Heating		
$Q_{hp,nom}$	Nominal power of the HP at 2/35 and 2/45 °C	3459 / 3169 W
COP_{hp}	COP of the HP at 2/35 and 2/45 °C	3.17 / 2.45
m_{hp}	Water content of heat pump condenser	10.0 l
UA_{hp}	Transmission losses of heat pump	12.9 W/K
m_{hydr} [a]	Total water content of hydronic heating system (excl. HP, FH and DHW tank)	4.0 l
UA_{hydr} [a]	Total transmission losses of hydronic system (excl. HP, FH and DHW tank)	8.0 W/K
$T_{fh,design}$	Temperature regime floor heating at −8 °C outside	35/30 °C
$TSet_{DHW}$ [b]	Set temperature in DHW storage tank	53 °C
DHW storage tank		
V	Volume	0.3 / 0.5 m^3
H	Height	1.4 m
N_{nodes}	Number of nodes (node 1 is top node)	10
U_{ins}	Transmission losses through insulation	0.4 W/(m^2 K)
UA_{fix}	Additional transmission losses (independent of tank volume)	1.61 W/K
A_{hx}	Surface of internal heat exchanger (coil)	4.1 m^2
Pos_{hx}	Position of the coil (upper tank node - lower tank node)	4 − 10
h_{in}	Convective heat transfer coefficient at inside of coil	4000 W/(m^2 K)
h_{con}	Conduction heat transfer coefficient through coil	3300 W/(m^2 K)
h_{out}	Convective heat transfer coefficient at outside of coil	867 W/(m^2 K)

[a] Combination of different pipes and pumps which can be at different temperatures.

[b] According to a temperature sensor in the second tank node. This set temperature is increased at periods of load shifting in the different DSM strategies in order to start charging the DHW tank. $TSet_{DHW}$ is *never* lower than 53 °C.

2.7 Parameter overview

An overview of the parameters used for the different submodels is given in Table 2.

3. Reference case

3.1 Thermal comfort

With identical buildings and control, the thermal comfort and heat demand depend only on the user behaviour (presence and appliance use). Figure 9 shows that both winter and summer comfort are satisfied for the dwellings with lowest and highest internal gains.

The DHW comfort is calculated as the mass flow rate that is withdrawn at temperatures above 40 °C divided by the total DHW consumption. The mixing valve has a set point of 45 °C. Due to the way the stochastic DHW draw profiles are calculated, every dwelling has a limited number of days during which the total DHW load is very high. Therefore, the DHW comfort varies between 96.4 % and 99.8 % as shown in Figure 10.

3.2 Energy use

Figure 10 gives an overview of the energy use, SPF of the heat pump, primary energy efficiency of the total heating and DHW system and DHW comfort. Despite the low energy standard, the heat demand is predominantly caused by space heating. This is due to the relatively low DHW

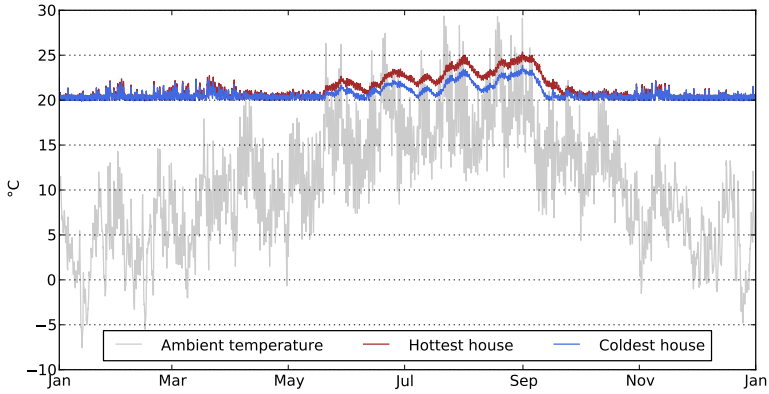

Figure 9. Ambient temperature and operative temperature in the hottest and coldest dwelling

demand profiles and the conservative settings of the automatic solar shading devices. The SPF of the heat pump and the total primary energy efficiency are within acceptable ranges. Taking into account a primary energy factor of 2.5 for electricity, we see that the primary energy efficiency is lower than the SPF of the heat pump. This is due to thermal losses in the storage tank and hydronic circuit. The required nominal power of the PV arrays in order to reach a yearly zero energy balance lies between 5.0 kW and 7.5 kW peak power.

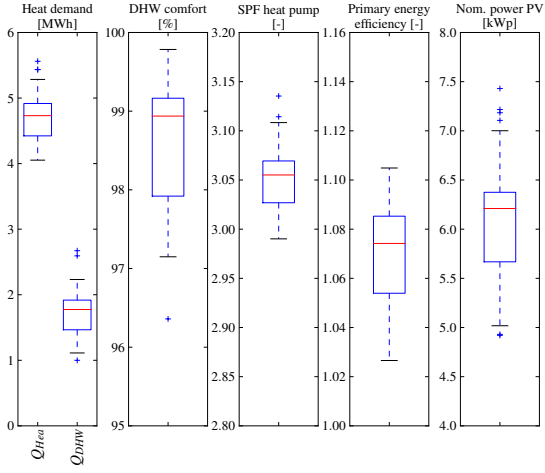

Figure 10. Box plots showing the median and quartile range of indicated variables for the 33 dwellings in the reference case. Outliers (values outside of 1.5 × quartile value) are presented by '+'

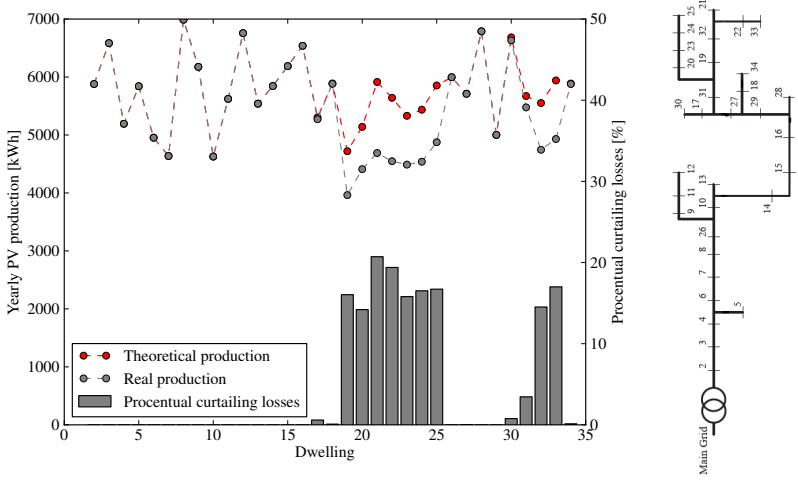

Figure 11. a) Yearly inverter shut-down losses for dwellings according to numbering in grid topology b) .

3.3 Energy balance

Figure 11 shows that inverter shut-down is only affecting 10 out of the 33 dwellings. The shut-down losses can reach up to 20 % of annual PV production of these systems. The losses depend on the position of the dwelling in the grid and the figure shows that the weak branches are those who are furthest away from the transformer.

The net yearly electricity consumption of the neighbourhood E_{NBH} would be $-1.8\,\mathrm{MWh/a}$ in case of an ideal feeder. This means that the neighbourhood would be a net electricity producer on a yearly basis due to slight oversizing of the PV systems. However, due to ohmic grid losses and inverter shut-down, the small yearly overproduction becomes a net consumption of 12.4 MWh/a. Compared to the electricity use of the dwellings, the ohmic losses amount to 3.0 % and the inverter shut-down losses are 4.6 % of the yearly demand. This may seem relatively low, specifically when compared to results of Baetens et al. (2012). For a similar case, Baetens *et al.* found curtailing losses of 22 % and ohmic losses of 1.9 %. The difference in curtailing losses is entirely due to changed regulations: in the model of Baetens *et al.*, the inverters were configured to shut-down at a voltage deviation of 6 %, i.e. 243.8 V, but in the mean time this legislation has been harmonized with EN 50438:2007 and since medio 2012 the limit is fixed at 10 % voltage increase, i.e. 253.0 V (SynerGrid, 2012). The increase in ohmic losses is due to the higher total consumption and installed PV power in the considered neighbourhood.

3.4 Aggregated power profiles

In order to get a better understanding of the phasing between average PV production and the electricity consumption we have aggregated the different power profiles in Figure 12 (upper left). This figure shows the aggregated daily power for user electricity consumption, PV production and HP operation for dwelling 19 which has about 17 % of curtailing losses. The aggregation is done for the whole year, including days without curtailing.

As Figure 12 (upper left) shows, in dwelling 19, the electricity consumption of appliances and lighting has a morning and evening peak. The heat pump also operates most in the morning

and evening, with a time shift of about two hours (later) compared to the user electricity consumption. This can be explained by the morning and evening peaks in water consumption and the presence of a DHW storage tank causing the HP to reheat the tank after most DHW withdrawals. As a result, the electricity consumption is not well in line with the electricity generation profile of the PV system. Curtailing typically takes place between 10h-16h.

4. Demand side management

4.1 Rule-based control strategies

The challenge tackled in this paper is to adapt the control of the DHW production in order to reduce the net yearly electricity consumption of the neighbourhood E_{NBH}. Given the ohmic grid losses, E_{NBH} will never become zero without increasing the PV capacity compared to the reference case, even though most control strategies can reduce the ohmic losses to a small extent.

As mentioned before, reducing curtailing losses is straightforward: if the local consumption is increased sufficiently at periods of high grid voltage, the PV inverters will not shut down. This could however increase E_{NBH} instead of decreasing it. Therefore, the aim is not to reduce curtailing losses but E_{NBH}.

The control strategies are divided in three different categories based on the trigger used to initiate the load shifting. These triggers can be a clock, the power exchange with the grid or the voltage. When the trigger is activated, the temperature set point in the DHW storage tank $TSet_{DHW}$ is increased. The amount of the temperature increase is a parameter of the control and will be varied in the analysis. Some additional variants have been defined as shown in Table 3. Only rule-based control strategies are considered in this paper. Comparing rule-based DSM with full neighbourhood optimal control could be the topic of future research.

For reference: the simulations were executed on desktop computers with two different cpu's (Intel Xeon(R) at 2.53 GHz and at 3.07 GHz) and depending on the cpu and (primarily) the control strategy the simulation time was between 1.2 and 4.3 days for simulating one year.

4.2 Load shifting

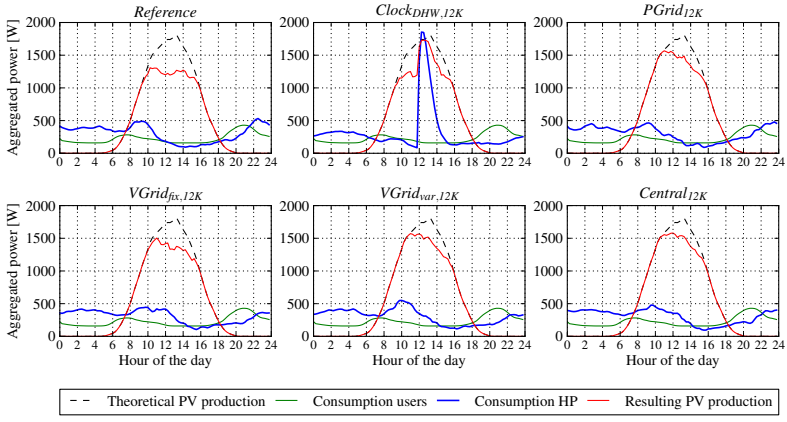

Figure 12. Aggregated power density profiles for dwelling 19 with a DHW storage tank of 0.3 m^3.

Table 3. Overview of DSM control strategies

Name	Trigger for DSM	Details	Implementation effort
$Clock_{DHW}$	Clock	Between 12h00 and 16h00, $TSet_{DHW}$ is increased.	Very low, no sensors required.
PGrid	Power exchange of the dwelling with the grid	When the power injection in the grid surpasses P_{lim}, $TSet_{DHW}$ is increased. P_{lim} is the same regardless PV sizing.	Moderate. Requires power measurement, preferentially based on inverter output before curtailing and without HP consumption to avoid unstable control or the need for large hysteresis.
$VGrid_{fix}$	Voltage at dwelling's grid connection	When the voltage surpasses V_{lim}, $TSet_{DHW}$ is increased. V_{lim} is the same for all dwellings and is typically a few Volt lower than 253 V [a].	Low, only requires a single voltage measurement.
$VGrid_{var}$	Voltage at dwelling's grid connection	When the voltage surpasses V_{lim}, $TSet_{DHW}$ is increased. V_{lim} depends on the position of the dwelling in the grid.	Low on building side, only requires a single voltage measurement. Power flow calculation required once in order to determine V_{lim} for each dwelling.
Central	Voltage at dwelling's grid connection and temperature of DHW tank.	A central intelligence is present with access to the voltage and temperature of the DHW tank in each dwelling. When somewhere in the grid V_{lim} is exceeded, $TSet_{DHW}$ of the DHW tank with lowest temperature is increased, regardless of the position of that dwelling in the grid.	High. Requires centralised monitoring and control and can conflict with privacy of the occupants.

[a] In all simulations with $VGrid_{fix}$, V_{lim} has been set to 251 V, 2 V lower than the shut-down limit to create a safety margin.

[b] The power flow calculation imposes an equal load to all dwellings for which the maximum voltage in the grid reaches 251 V. The corresponding voltage at each connection point is V_{lim}.

A first strategy for shifting the HP operation is a clock-based increase of $TSet_{DHW}$. To keep this DSM control very simple, the temperature is increased at the same time (12h-16h) in *every* house on *all* days of the year, even when there is no curtailing risk at that moment or position in the grid. The aggregated power profiles for $Clock_{DHW,12K}$, with a daily temperature increase of 12 K is shown in Figure 12 (upper middle). We can see a clear shift in the operation of the heat pump with a very sharp peak at 12h. As a consequence, the morning and evening peaks are largely flattened. The result is a strong reduction of inverter shut-down between 12h and 14h. The effect does not last till 16h as the heat pumps in the neighbourhood switch off one by one when the temperature in their respective storage tank reaches the increased $TSet_{DHW}$.

The voltage increase in the grid is caused by simultaneous injection of surplus electricity by all dwellings. When we try to increase the self-consumption γ_S at times of high injection power we expect the curtailing losses to decrease. Figure 12 (upper right) shows the effect of $PGrid_{12K}$. The shift of HP operation is much less pronounced as for $Clock_{DHW,12K}$. This is because this DSM control is only active on sunny days and the aggregated profile is computed based on all days of the year. Nevertheless, the impact on curtailing losses is high, specifically in the morning. In the afternoon, when the storage tanks in the neighbourhood start reaching the increased $TSet_{DHW}$, the effect is lower. It has to be noted that in this control strategy, *all* dwellings participate, even if they do not suffer from inverter shut-down. As the trigger for DSM is a fixed and identical P_{lim} for all dwellings, this control will be activated more often for large PV systems.

The reason for inverter shut-down being excessive voltage, it seems more logic to base the DSM strategy on a measurement of the voltage at the dwelling's grid connection. There are two options for setting the voltage limit V_{lim} at which $TSet_{DHW}$ is increased. In the $VGrid_{fix}$ strategy, P_{lim} is the same for all dwellings (251 V). In $VGrid_{var}$, P_{lim} depends on the position of the dwelling and the characteristics of the feeder. The idea is to activate the control in the

dwellings when based on their own voltage measurement there is a good reason to suspect that curtailing is about to happen somewhere else. The effect on the aggregated power for both controls with a $\Delta TSet_{DHW}$ of 12 K is shown in Figure 12 (lower left and middle). The impact of sharing the burden among all dwellings can clearly be seen: $VGrid_{var,12K}$ reduces the curtailing losses more than $VGrid_{fix,12K}$.

A more advanced DSM control based on V_{lim} requires a central management system that has access to all voltages in the grid and the temperatures in the DHW tanks and that can increase $TSet_{DHW}$. This way, the controller can select which HP is to start to avoid curtailing. Ideally, the controller would take into account the grid topology and select the dwelling(s) that will have most effect on the anticipated problem. However, the *Central* control investigated in this paper only selects based on storage tank temperature. With a maximum $\Delta TSet_{DHW}$ of 12 K, the resulting aggregated power is shown in Figure 12 (lower right). The *Central* strategy is clearly more complicated and expensive than all other studied controls as it requires a central system for monitoring and control. However, it is still much easier (and cheaper) than model predictive control (MPC) as it does not require weather and user behaviour forecasts, system models and an optimisation framework.

4.3 Resulting net yearly electricity consumption

So far, we have only discussed the load shifting behaviour of the DSM control strategies and the resulting reduction in curtailing for a single case (dwelling 19). In this section we also consider the effects of the higher average storage tank temperature and shifted heat pump operation on the total net electricity consumption of the neighbourhood, E_{NBH}. We define the net electricity savings as $\Delta E_{\mathrm{NBH}} = E_{\mathrm{NBH,\ DSM}} - E_{\mathrm{NBH,\ ref}}$. Figure 13 shows the *loss-benefit space* for the neighbourhood. In this graph, every marker is the final result of a control strategy on neighbourhood level. The number in the marker is the increase in $TSet_{DHW}$ when the control is activated. The horizontal axis represents the relative electricity demand compared to the reference case. The vertical axis shows the relative curtailing and ohmic losses compared to the reference. Therefore, the reference lies in the origin, and a case for which gains and savings are equal would lie on the *status quo line*, the diagonal through the origin. The resulting net savings for every case ΔE_{NBH}, is the difference between relative savings and relative consumption and is represented by the vertical distance of the marker to the status quo line.

A first remarkable result is the good performance of the most simple control strategy, $Clock_{DHW,4K}$. It is the only control for which the electricity demand is substantially lower than the reference case −3.4 MWh, and at the same time it is able to reduce curtailing losses by 2.3 MWh. These effects add together and result in ΔE_{NBH} of 5.6 MWh. As a matter of fact, no single other control strategy can do better. Variants of $Clock_{DHWK}$ with $\Delta TSet_{DHW}$ equal to 8 K or 12 K are much less interesting. They can reduce the curtailing losses a little bit further, but the savings on electricity demand completely vanish. The reason why $Clock_{DHW,4K}$ outperforms all other strategies is the fact that besides reducing curtailing losses on sunny days, it also has a benefit during almost all other days. As pointed out earlier by De Coninck et al. (2010), the timed increase of $TSet_{DHW}$ shifts the operation of the air-to-water HP to the afternoon, when the ambient temperature is often a few degrees higher than in the morning or evening. As long as $\Delta TSet_{DHW}$ is low, this effect outweighs the performance loss due to the increased condenser temperature and the additional thermal losses in the TES tank and hydronic circuit. This is confirmed by the median of the HP's SPF for all dwellings: it rises from 3.06 in the reference case to 3.17 for $Clock_{DHW,4K}$.

Furthermore, when the tank temperature is temporarily increased, the top of the tank will still be warm enough after the next DHW withdrawal and the tank does not have to be reheated as soon as in the reference case. This will improve the stratification in the tank and lead to the following benefits:

- less heat pump cycles, resulting in lower thermal losses of the heat pump and hydronic

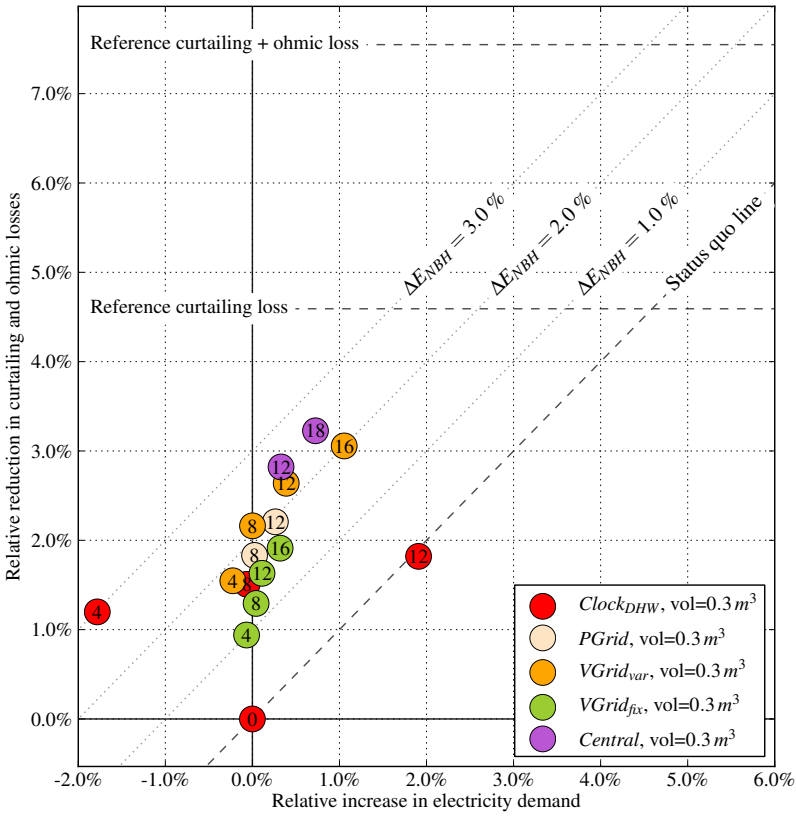

Figure 13. Loss-benefit space for rule-based DSM with 0.3 m^3 DHW storage tank.

circuit

- lower condenser temperatures at the start of the next tank heating cycle, resulting in a higher SPF
- lower average temperatures at the bottom and middle of the tank, resulting in lower thermal losses for these layers.

The cumulative result of these effects is a reduction of total thermal losses for the entire neighbourhood of 4.2 MWh (= 8.5 %). Of course, the other strategies benefit from similar effects, but only during the sunny periods when their DSM strategy is activated. This means that all other strategies can be combined with $Clock_{DHW,4K}$ in order to try to combine the benefits from both strategies. Some results of combined strategies are discussed in section 4.5.

Figure 13 also shows the results for the other strategies for different values of $\Delta TSet_{DHW}$. We see that for all strategies, both electricity demand and reduction of curtailing losses increase

with rising values of $\Delta TSet_{DHW}$. Therefore, the net neighbourhood savings, ΔE_{NBH} tend to show a maximum as a function of $\Delta TSet_{DHW}$. Sometimes the maximum does not seem to be reached because simulations with temperature increases of more than 18 K are not performed to stay within the validity range of the heat pump model.

There is a clear rank in the performance of the control strategies. We put them in order of decreasing effectiveness (based on ΔE_{NBH}) , and indicate which $\Delta TSet_{DHW}$ gives the best result:

(1) $Clock_{DHW}$, optimal $\Delta TSet_{DHW} = 4\,\mathrm{K}$
(2) *Central*, optimal $\Delta TSet_{DHW} = 12\,\mathrm{K}$ and $18\,\mathrm{K}$
(3) $VGrid_{var}$, optimal $\Delta TSet_{DHW} = 12\,\mathrm{K}$
(4) *PGrid*, optimal $\Delta TSet_{DHW} = 12\,\mathrm{K}$
(5) $VGrid_{fix}$, optimal $\Delta TSet_{DHW} = 16\,\mathrm{K}$.

Overall, we can conclude that for a $0.3\,\mathrm{m}^3$ storage tank and with the proper $\Delta TSet_{DHW}$, these rule-based control strategies are able to reduce E_{NBH} by 3.0 MWh to 5.6 MWh. This corresponds to a reduction of curtailing losses by 35 % to 65 %. Compared to the total electricity demand of the neighbourhood (without taking into account PV production), these savings represent 1.6 % to 3.0 %.

4.4 Effect of increased storage tank size

All results discussed so far were based on a DHW storage tank of $0.3\,\mathrm{m}^3$. It is clear that by increasing the volume of this tank, the system will be able to reduce the curtailing losses even more. However, the thermal losses will also be higher, and may overcompensate the benefits of additional load shifting. Figure 14 shows the results with a storage tank size of $0.5\,\mathrm{m}^3$. In this figure, also the reference case has this larger DHW tank. This does barely influence the reference curtailing losses, but increases the E_{NBH} of the reference case by 1.6 MWh.

As expected, all strategies are able to reduce the curtailing losses further than with a $0.3\,\mathrm{m}^3$ storage tank. The most notable change is a reduced performance of the $Clock_{DHW}$. Whereas for all other strategies, the position of the markers is very similar to the previous results, the markers of $Clock_{DHW}$ are clearly shifted to the right. This specifically means that the increased system performance of $Clock_{DHW,4K}$ is less pronounced with a larger storage tank. As a result, this strategy is outperformed by the more complicated control strategies $VGrid_{var}$ and *Central*.

The real merit of a larger storage tank has to be evaluated by comparison with the original reference case which has the smaller tank. This is done in Figure 15, where the reference case with DHW tank of $0.3\,\mathrm{m}^3$ is placed in the origin. In a first instance, we do not discuss the three markers at the end of the arrows (they will be discussed in the next section). From this figure we can clearly see the shift of all cases with a DHW tank of $0.5\,\mathrm{m}^3$ to the right and upwards (except for the reference). However, none of the cases with a larger storage tank is able to compensate the additional electricity demand by stronger reduction of curtailing losses. This brings us to an important conclusion of this study: with the simulated control strategies it does *not* make sense to install additional thermal energy storage to increase the DSM capabilities of the systems.

4.5 Combinations with $Clock_{DHW,4K}$

Finally, we want to combine the merits of the most simple strategy on the days *without* curtailing with the performance of the advanced strategies on the days *with* curtailing. This has been simulated for three cases and visualised with arrows in Figure 15.

The combinations are indeed an improvement of the original strategies. The improvement in energy efficiency is a little bit smaller than anticipated, but on the other hand there is even an additional reduction of curtailing losses. However, our previous conclusion holds: the systems with the smaller storage tank show a better energy performance.

The best results are obtained with the combination of $Clock_{DHW,4K}$ and $VGrid_{var,16K}$. This

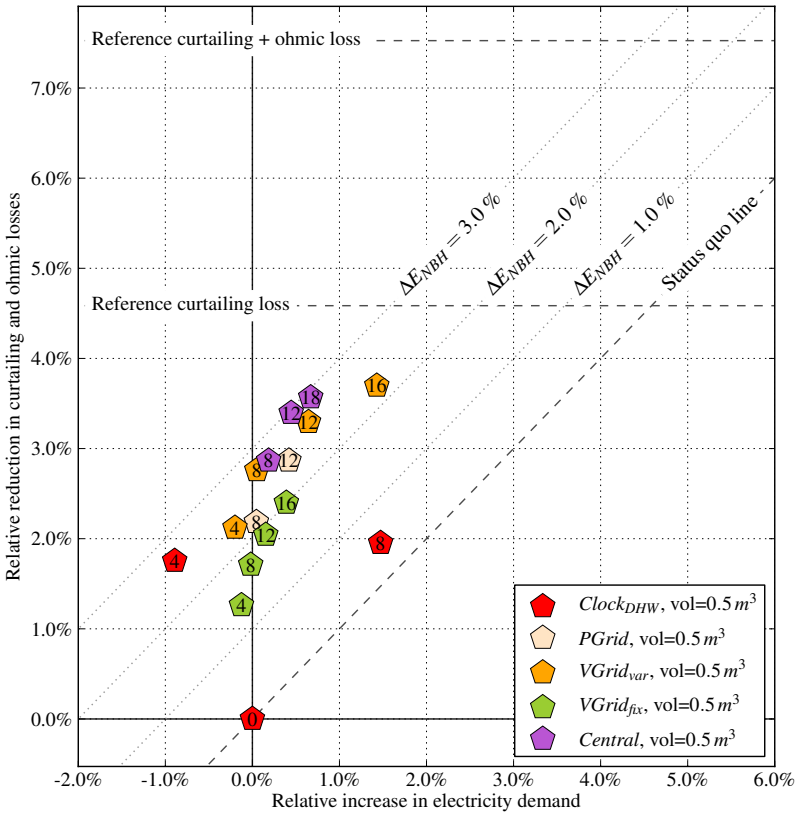

Figure 14. Loss-benefit space for rule-based DSM with 0.5 m^3 DHW storage tank.

simulation realised a ΔE_{NBH} of 6.4 MWh which corresponds to a reduction of curtailing losses by 74 % or a reduction of E_{NBH} by 3.4 %. We could have simulated more combinations and other values for $\Delta TSet_{DHW}$. For instance, from Figure 15 it can be anticipated that a combination of $Clock_{DHW,4K}$ with $VGrid_{var,12K}$ or $Central_{18K}$ will bring ΔE_{NBH} even higher. There are probably also other control strategies worth investigating. However, with the current results, we already show that simple rule-based controls are able to strongly reduce curtailing losses in low energy dwellings with a high PV penetration while decreasing the net electricity demand.

4.6 Load matching and grid interaction indicators

The aim of this study is to decrease the net electricity consumption of the neighbourhood E_{NBH} as a whole by avoiding PV inverter shut-down. Therefore, a neighbourhood model has been

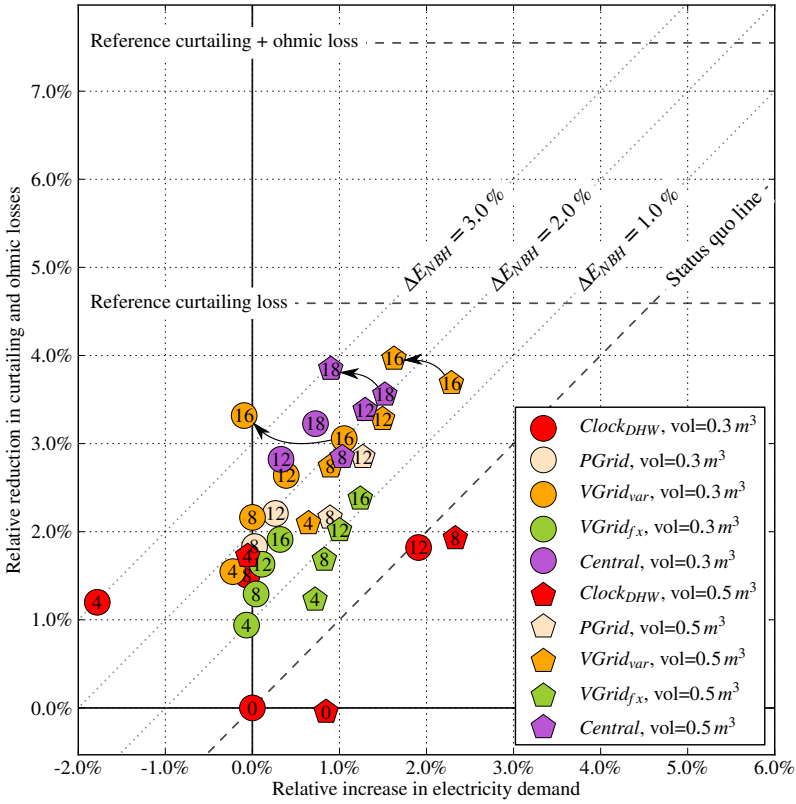

Figure 15. Loss-benefit space for rule-based DSM with 300 l and 500 l DHW storage tank. The three markers at the end of arrows are combinations of that control strategy with $Clock_{DHW,4K}$

developed in Modelica. When such a model is not available and the only tool at hand is a stand-alone building simulation program, the interaction of the building with the electricity grid can be characterized by load matching and grid impact (LMGI) indicators. LMGI indicators are defined by different authors (Salom et al., 2011; Verbruggen et al., 2011; Baetens et al., 2012) in order to quantify the balance between local electricity generation and consumption and the consequences of distributed generation on the electricity grid. In this section we will consider more specifically the self-consumption γ_S and self-generation γ_D, calculated as

$$\gamma_S = \frac{\int \min\{P_D, P_S\} dt}{\int P_S dt} \tag{7}$$

$$\gamma_D = \frac{\int \min\{P_D, P_S\} dt}{\int P_D dt} \tag{8}$$

where P_S is the local power supply (ie. PV production) and P_D the local power demand. The term $\min\{P_D, P_S\}$ represents the part of the power demand instantaneously covered by the local PV power supply or the part of the power supply covered by the demand (Baetens et al., 2012).

These indicators have to be used with caution because they are biased by bad control and inefficiency. For example, the operation of a heat pump at very high temperatures in order to store thermal energy during times of local overproduction of electricity will clearly increase the self-consumption. However, there is no guaranteed energy saving on total system level and/or reduction in greenhouse gas emissions. The very contrary can be true, as will be shown here.

A scatter plot of the average self-consumption and self-generation for all dwellings in the neighbourhood and for all investigated control strategies is shown in Figure 16. In this figure, both indicators are plotted as a function of the relative energy savings of the neighbourhood ΔE_{NBH}. This figure shows how biased these LMGI indicators can be. Although it is true that all efficient strategies have high indicators, the opposite is *not* true: a high indicator does not imply a high energy efficiency. As an example, we can consider the points in the left upper corner of the figure: these cases have a higher self-consumption and self-generation than the reference case, but result in an increased electricity consumption of the neighbourhood. In order to save energy, it should therefore *never* be the aim to increase the self-consumption of individual buildings as such.

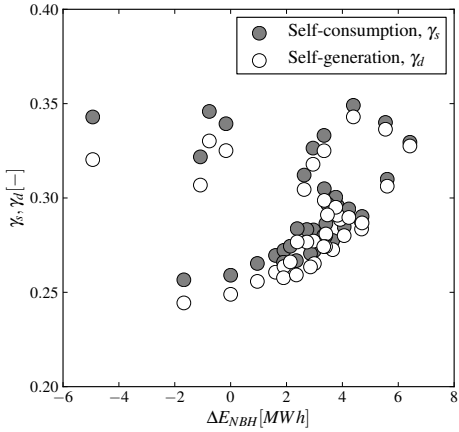

Figure 16. Scatter plot of average self-consumption and self-generation for all control strategies versus ΔE_{NBH}

This reasoning can be extended to neighbourhoods, districts, countries. As long as the studied system is interfaced with other consumers and production units which are not included in the model, side-effects on the global scale occur and conclusions on global system level have to be drawn with care. Sometimes such conclusions are simply not valid. It is therefore *not* the aim to increase the self-consumption of the neighbourhood as a whole.

5. Summary and conclusions

We have presented an integrated bottom-up approach to model and simulate neighbourhoods with Modelica. The model includes multiple single-family dwellings and the low voltage grid to which they are connected. For each of the dwellings, the model incorporates a thermal building model, HVAC system with DHW storage tank, air-to-water heat pump and floor heating, and a fully stochastic user behaviour model for presence, appliances, lighting and DHW use.

The model is used to study inverter curtailing losses in a low energy neighbourhood with 33 dwellings with a high total installed PV power. In the reference case, inverter shut-down causes an electricity generation loss of 8.6 MWh or 4.6 % of the initial electricity demand of the neighbourhood. A first conclusion is that these losses are much lower than previously reported results under similar circumstances. The reason can be found in changed regulations, allowing voltage deviations in the distribution grid of up to 10 % instead of 6 % previously.

In order to reduce this loss, different rule-based DSM strategies applied to the DHW production are proposed and simulated, both for a 0.3 m^3 and 0.5 m^3 DHW tank. Different conclusions are drawn from the results.

- The curtailing losses can be reduced to a large extent by different rule-based control strategies. However, the net energy saving is generally smaller than the reduction in curtailing losses because of increased thermal losses.
- The simulated controls realise *net* savings of up to 74 % of the original curtailing losses. This corresponds to a reduction of the electricity demand of the total neighbourhood (without taking PV generation into account) by 3.4 %.
- Rule-based control strategies can be very straightforward. The most simple one, $Clock_{DHW,4K}$, is just a timed increase of the set temperature in the storage tank and is difficult to beat. The most advanced control under investigation, *Central* brings only limited additional energy savings compared to $VGrid_{var}$.
- The best results are obtained when the whole neighbourhood participates in the load shifting, including dwellings that never experience curtailing. This can be accomplished when the trigger for DSM is a (fixed) injection power or a dwelling-dependent voltage limit (which leads to better results).
- Load matching and grid interaction indicators must be used with care. Both the very effective and ineffective control strategies can have a high self-consumption γ_s and self-generation γ_d. This result can be generalized: it is often not possible to draw valid conclusions on a global scale from a model of a local system.
- Increasing the DHW storage size from 0.3 m^3 to 0.5 m^3 always results in a higher electricity consumption, regardless of the control strategy used.

This study shows that even with small TES tanks and very simple controls, PV inverter shut-down can strongly be reduced. Model predictive control strategies are *expected* to lead to better results. However, they require significantly higher investments which may not be compensated by additional savings. Future research has to concentrate on the window of improvement by MPC over the already successful rule-based controls.

6. Acknowledgement

The authors gratefully acknowledge the KU Leuven Energy Institute (EI) for funding this research through granting the project entitled *Optimized energy networks for buildings* and the European Commission for granting the *Performance Plus* project in the 7^{th} Framework Programme.

References

Ackermann, T. and V. Knyazkin (2002). Interaction between distributed generation and the distribution network: operation aspects. In *IEEE/PES Transmission and Distribution Conference and Exhibition*, Volume 2, pp. 1357–1362.

Baetens, R., R. De Coninck, J. Van Roy, B. Verbruggen, J. Driesen, L. Helsen, and D. Saelens (2012). Assessing electrical bottlenecks at feeder level for residential net zero-energy buildings by integrated system simulation. *Applied Energy 96*(Special issue on Smart Grids, Renewable Energy Integration, and Climate Change Mitigation - Future Electric Energy Systems), 74–83.

Becker, B. and K. Stogsdill (1990). Development of Hot Water Use Data Base. In *ASHRAE Transactions*, Volume 96, Atlanta, GA, pp. 422–427. American Society of Heating, Refrigerating and Air Conditioning Engineers.

Bletterie, B., A. Gorsek, B. Uljanic, A. Woyte, T. Vu Van, F. Truyens, and J. Jahn (2010). Enhancement of the Network Hosting CapacityClearing Space for/with PV. In *European Photovoltaic Solar Energy Conference*.

Caamaño Martin, E., H. Laukamp, M. Jantsch, T. Erge, J. Thornycroft, H. De Moor, S. Cobben, D. Suna, and B. Gaiddon (2008). Interaction Between Photovoltaic Distributed Generation and Electricity Networks. *Progress in photovoltaics: research and applications 16*(7), 629–643.

Cheng, V. and K. Steemers (2011). Modelling domestic energy consumption at district scale: A tool to support national and local energy policies. *Environmental Modelling & Software 26*, 1186–1198.

Daikin Europe N.V. (2006). *Technical data Altherma ERYQ007A, EKHB007A / EKHBX007A, EKSWW150-300*. Oostende.

De Brabandere, K., A. Woyte, R. Belmans, and J. Nijs (2004). Prevention of inverter voltage tripping in high density PV grids. In *19th EU-PVSEC, Paris*, Number June, pp. 4–7.

De Coninck, R., R. Baetens, B. Verbruggen, J. Driesen, D. Saelens, and L. Helsen (2010). Modelling and simulation of a grid connected photovoltaic heat pump system with thermal energy storage using Modelica. In P. Andre, S. Bertagnolio, and V. Lemort (Eds.), *8th International Conference on System Simulation in Buildings (SSB2010)*, Number June, Liège, pp. P177.

De Soto, W., S. A. Klein, and W. A. Beckman (2006, January). Improvement and validation of a model for photovoltaic array performance. *Solar Energy 80*(1), 78–88.

Dugan, R. and T. McDermott (2001). Operating conflicts for distributed generation on distribution systems. In *Proceedings of the 45th Rural Electric Power Conference*, Little Rock, AR, USA, pp. A3/1–A3/6. IEEE.

EPIA (2012). Global market outlook for photovoltaics until 2016. (EPIA).

European Parliament (2010). Directive 2010/31/EU on the energy performance of buildings (recast). pp. 13–35.

Fairey, P. and D. Parker (2004). *A Review of Hot Water Draw Profiles Used in Performance Analysis of Residential Domestic Hot Water Systems*. Florida Solar Energy Center.

FOD Economie (2008). Bevolking - Private, grootte en collectieve huishoudens. Technical Report http://tinyurl.com/y8o662r (accessed on 22 January 2013).

Haller, M. Y., C. a. Cruickshank, W. Streicher, S. J. Harrison, E. Andersen, and S. Furbo (2009, October). Methods to determine stratification efficiency of thermal energy storage processes Review and theoretical comparison. *Solar Energy 83*(10), 1847–1860.

Han, Y., R. Wang, and Y. Dai (2009, June). Thermal stratification within the water tank. *Renewable and Sustainable Energy Reviews 13*(5), 1014–1026.

Hastings, S. (2004, April). Breaking the heating barrier. *Energy and Buildings 36*(4), 373–380.

Hendron, R. and J. Burch (2007). Development of standardized domestic hot water event schedules for residential buildings. In *Energy Sustainability 2007*, Number August.

Jordan, U. and K. Vajen (2001). *Realistic Domestic Hot-Water Profiles in Different Time Scales*. Marburg.

Kersting, W. (2001). Radial distribution test feeders. *IEEE Power Engineering Society Winter Meeting, 2001* (C), 908–912.

Kleinbach, E., W. Beckman, and S. Klein (1993, February). Performance study of one-dimensional models for stratified thermal storage tanks. *Solar Energy 50*(2), 155–166.

Lechner, H. (1998). *Analysis of Energy Efficiency of Domestic Electric Storage Water Heaters*. Study for the Directorate General for Energy (DGXVII) of the Commission of the European Communities Contract No. SAVE-4.1031/E/95-013.

Loga, T., N. Diefenbach, C. Balaras, E. Dascalaki, M. S. Zavrl, A. Rakuscek, V. Corrado, S. Corgnati, H. Despretz, C. Roarty, M. Hanratty, B. Sheldrik, W. Cyx, M. Popiolek, J. Kwiatowski, M. GroB, C. Spitzbart, Z. Georgiev, S. Lakimova, T. Vimmr, K. B. Wittchen, and J. Kragh (2009). Use of building typologies for energy performance assessment of national building stocks. Existent experiences in European countries and common approach. Technical Report June 2009, First TABULA Synthesis report.

Manfren, M., P. Caputo, and G. Costa (2011). Paradigm shift in urban energy systems through distributed generation : Methods and models. *Applied Energy 88*(4), 1032–1048.

Marsh, R. (1996). *Sustainable housing design : an integrated approach*. Ph. D. thesis, University of Cambridge.

Mather, D., K. Hollands, and J. Wright (2002, July). Single- and multi-tank energy storage for solar heating systems: fundamentals. *Solar Energy 73*(1), 3–13.

Newton, B. (1995). *Modeling of Solar Storage Tanks*. Ph. D. thesis, University of Wisconsin-Madison.

Olesen, B. (2001). Control of floor heating and cooling systems. In *CLIMA-2000*, Number September, pp. 15–18.

Richardson, I., M. Thomson, D. Infield, and C. Clifford (2010, October). Domestic electricity use: A high-resolution energy demand model. *Energy and Buildings 42*(10), 1878–1887.

Richardson, I., M. Thomson, D. Infield, and A. Delahunty (2009). Domestic lighting: A high-resolution energy demand model. *Energy and Buildings 41*(7), 781–789.

Rosen, M. a., R. Tang, and I. Dincer (2004, February). Effect of stratification on energy and exergy capacities in thermal storage systems. *International Journal of Energy Research 28*(2), 177–193.

Salom, J., J. Widén, J. Candanedo, I. Sartori, K. Voss, and A. J. Marszal (2011). Understanding Net Zero Energy Buildings: Evaluation of load matching and grid interaction indicators. In *Proceedings of Building Simulation 2011*, Volume 6, Sydney, Australia, pp. 2514–2521.

Sanyo (2008). *HIP-230HDE1 photovoltaic module*. http://www.technosun.com/eu/downloads/search-documentation.php (accessed on 22 January 2013).

Sera, D., R. Teodorescu, and P. Rodriguez (2007). PV panel model based on datasheet values. *IEEE* (4), 2392–2396.

Stokes, M., M. Rylatt, and K. Lomas (2004). A simple model of domestic lighting demand. *Energy and Buildings 36*(2), 103–116.

SynerGrid (2012). *Specifieke technische voorschriften voor decentrale productie-installaties die in parallel werken met het distributienet*. (C10/11 - revisie 4 juni 2012).

Verbruggen, B., R. De Coninck, R. Baetens, D. Saelens, L. Helsen, and J. Driesen (2011). Grid impact indicators for active building simulation. In *Innovative Smart Grid Technologies (ISGT), 2011 IEEE PES*, Number 2, pp. 1–6. IEEE.

Viessmann (2011). *Vitocell- 100-V, 390 liter, Datenblatt*. http://tinyurl.com/cdpv8rr (accessed on 21 April 2013).

Wetter, M. (2009). Modelica Library for Building Heating, Ventilation and Air-Conditioning Systems. In *The 7th International Modelica Conference*, pp. 393–402. The Modelica Association.

Widén, J., M. Lundh, I. Vassileva, E. Dahlquist, K. Ellegå rd, and E. Wäckelgå rd (2009,

July). Constructing load profiles for household electricity and hot water from time-use dataModelling approach and validation. *Energy and Buildings 41*(7), 753–768.

Woyte, A., V. V. Thong, R. Belmans, and J. Nijs (2006). Voltage fluctuations on distribution level introduced by photovoltaic systems. *IEEE Transactions on Energy Conversion 21*(1), 202–209.

Zurigat, Y. H., K. J. Maloney, and A. J. Ghajar (1989). A comparison study of one-dimensional models for stratified thermal storage tanks. *Journal of Solar Energy Engineering;(USA) 111*(3).

3.5 Conclusion

Starting from a single building simulation and ending with detailed neighbourhood simulations, this chapter showed how the interaction between buildings and the electricity distribution grid can be studied. The IDEAS library has proven to be useful to simulate integrated effects of several buildings on the local distribution grid.

The results show that it is possible to reduce the grid impact with simple rule-based controls. However, increasing the size of thermal energy storage will almost automatically increase the energy use while the impact on the distribution grid is often marginal. The controls have different degrees of complexity and need of monitoring data, but most of them are easy to implement. Nevertheless, rule-based control is expected to be outperformed by model-predictive control (MPC). The development of the required control model for MPC is the topic of the next chapter.

Chapter 4

Grey-box building models

This chapter is accepted for publication as:
R. De Coninck, F. Magnusson, J. Åkesson, and L. Helsen, "Toolbox for development and validation of grey-box building models for forecasting and control", *Journal of Building Performance Simulation*, 2015, Accepted on 28/04/2015.
Personal contribution: 75 %

4.1 Introduction

This chapter describes the development of a toolbox for identifying grey-box models based on building monitoring data. The model development is considered as a bottleneck for the roll-out of MPC in buildings. Thus, the toolbox is developed with automation in mind. To validate the methodology, the toolbox is applied to the monitoring data of a dwelling in Germany as part of the IEA EBC Annex 58 project[1].

The aim of the toolbox is to obtain a control model for the MPC. Besides its use for MPC, the model can be used for forecasting building loads or to assess the available building flexibility as elaborated in Chapter 5. It is *not*

[1]Reliable Building Energy Performance Characterisation Based on Full Scale Dynamic Measurements. Operating agent: Prof Staf Roels, K.U.Leuven, Department of Civil Engineering, Building Physics Section, Kasteelpark Arenberg 40, B-3001 Leuven, Belgium, Project duration 2011-2015, website: http://www.kuleuven.be/bwf/projects/annex58/index.htm

the intention to estimate building properties. Although the obtained grey-box models are physically meaningful, for most buildings the resulting model will be too much reduced to deduce physical building properties from the estimated model parameters.

4.2 Toolbox for development and validation of grey-box building models for forecasting and control

Toolbox for development and validation of grey-box building models for forecasting and control

Roel De Coninck[a,b,c], Fredrik Magnusson[d], Johan Åkesson[e], Lieve Helsen[b,c]
[a]3E nv, 1000 Brussels, Belgium,
[b]KU Leuven, Department of Mechanical Engineering, 3001 Heverlee, Belgium,
[c]EnergyVille, 3600 Waterschei, Belgium,
[d]Department of Automatic Control, Lund University, SE-221 00 Lund, Sweden,
[e]Modelon AB, Ideon Science Park, SE-223 70 Lund, Sweden

Abstract

As automatic sensing and Information and Communication Technology (ICT) get cheaper, building monitoring data becomes easier to obtain. The availability of data leads to new opportunities in the context of energy efficiency in buildings.

This paper describes the development and validation of a data-driven grey-box modelling toolbox for buildings. The Python toolbox is based on a Modelica library with thermal building and Heating, Ventilation and Air-Conditioning (HVAC) models and the optimisation framework in JModelica.org. The toolchain facilitates and automates the different steps in the system identification procedure, like data handling, model selection, parameter estimation and validation.

To validate the methodology, different grey-box models are identified for a single-family dwelling with detailed monitoring data from two experiments. Validated models for forecasting and control can be identified. However, in one experiment the model performance is reduced, likely due to a poor information content in the identification dataset.

Keywords: grey-box models, parameter estimation, collocation method, validation, Modelica

Acknowledgment (Author Accepted Manuscript)

This is an Accepted Manuscript of an article published by Taylor & Francis in the Journal of Building Performance Simulation. The article was accepted on 28th of April 2015 and will be available at http://www.tandfonline.com/10.1080/19401493.2015.1046933.

Introduction

The continuous progress in ICT has led to the availability of small and low-cost sensors, low-power wireless data transfer protocols, cheap and accessible data storage and powerful servers. Applied to the building sector, these technologies can be used to collect large amounts of building monitoring data at relatively low costs. The abundance of data gives rise to new opportunities and applications in existing buildings like fault detection, energy efficiency analysis and model-based building operation. A first step in many of these applications is the creation of a building energy system model.

Models can be classified according to the white-box, grey-box and black-box paradigm. (Bohlin, 1995; Madsen and Holst, 1995; Kristensen et al., 2004; Henze and Neumann, 2011). Although the boundaries between these categories are blurry and often overlapping, this paradigm is useful for understanding the modelling procedure. White-box modelling bases the model solely on prior physical knowledge of the building. Most building simulation software falls under this category, like TRNSYS, EnergyPlus and many others (Crawley et al., 2008). Black-box modelling bases the model solely on response data (monitoring of the building) and a universal model set, including e.g. AR and ARMAX. Although physical insight is not required for making a black-box model, a model structure has to be chosen and this often involves making assumptions about the system, for example with regard to linearity. Grey-box identification methods and tools cater for the situation where prior knowledge of the object is not comprehensive enough for satisfactory white-box modelling and, in addition, purely empirical black-box methods do not suffice because the

involved physical processes are too complex. Grey- and black-box models are also called inverse models.

The difference between white- and grey-box modelling is not in the complexity of the model. A single-state model can be a white-box model if all parameters can be fixed based on physical knowledge only. However, when one or more parameters in a white-box model are estimated based on a fitting of the model to measurement data, the model becomes grey, no matter its complexity. Therefore, the distinction between white and grey cannot be made by only looking at the model structure: one has to know how the model parameters have been identified.

All three model types can be either deterministic or stochastic. A deterministic model cannot explain the differences between the model output and the true variations of the states (observations). Madsen and Holst (1995) therefore introduced a Wiener process in the system equations to cope with the simplifications of the model and uncertainties in inputs and monitoring. The obtained model is a stochastic state-space model.

For existing buildings with available monitoring data, the grey-box approach is considered to combine the best of two worlds: physical insight and model structure from the white-box paradigm and parameter estimation and statistical framework from the black-box paradigm. This paper describes an approach to grey-box modelling for buildings and the development of a toolbox combining Modelica and Python. The resulting framework will be referred to as *the toolbox* in the remainder of this paper and will be validated on a single-family dwelling. The toolbox is not publicly available, but can be obtained with an open-source license for research purposes by contacting the authors of this paper.

The toolbox has been developed with two purposes in mind. A first application is model predictive control (MPC). In this context, the grey-box model serves as the control model in a feed-back loop with the building. According to Henze (2013), the process of model identification accounts for 70 % of the effort for implementing an MPC controller. Automating this process can therefore reduce the total cost of MPC in buildings. To validate such a control model, the k-step prediction performance is used. A second application is load forecasting for real buildings. The forecast horizon is typically one day or one week. In this case, a different metric to validate the model is required: the simulation performance. This is the model deviation from a measured output in an open-loop simulation when measured disturbances are applied.

It is clear that a model showing a good simulation performance will also have a good k-step prediction performance. The opposite is not true. Therefore, we will use the simulation performance as quality criterion for the model validation.

This paper is split in two parts. The first describes the methodology and development of the toolbox. The second describes the validation results for a well monitored experimental single-family dwelling near Munich, Germany. The validation is carried out for two different experiments on the same building.

Part I
Methodology

Overview

A high-level overview of the toolbox is shown in Figure 1. The toolbox is composed of four major components:

1. the Modelica library *FastBuildings* with thermal zone models, HVAC components and building models;
2. different *.mop files* specifying the model components and which parameters to estimate;
3. *JModelica.org* as a middle layer for compilation of the *.mop files* as well as formulation and solution of the optimisation problem;
4. Python module *greybox.py* delivering the user interface and top-level functionality.

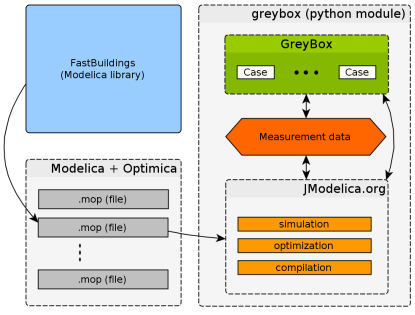

Figure 1: Overview of the grey-box buildings toolbox.

Modelica library *FastBuildings*

Modelica is an equation-based modelling language for cyber-physical systems (Elmqvist, 1997). The object-oriented philosophy stimulates model reuse, resulting in many available libraries, often open-source and free. Modelica is gaining importance in the building simulation community (Wetter, 2011; Wetter and Van Treeck, 2013). The choice for Modelica for the construction of the models is based on three major arguments (Wetter, 2009). Firstly, Modelica allows for linear, non-linear and hybrid model formulations and therefore it does not limit the model structure as such. Secondly, Modelica is equation-based, thus allowing efficient Newton-type solvers to be used as an alternative to for example genetic algorithms. Thirdly, Modelica has a *connector* concept to support component-based modelling.

The *FastBuildings* library targets low-order building modelling. The library has sub-packages for thermal zone models (including windows), HVAC, user behaviour, inputs, buildings and examples. Single and multi-zone building models can be created easily by instantiating one of the predefined templates in the `Building` sub-package and redeclaring the desired submodels, like the thermal zone, HVAC or window model. The following design principles are applied throughout the library.

- The thermal connectors are `HeatPorts` from the `Modelica.Thermal` package, which is part of the *Modelica Standard Library* (MSL).
- Thermal resistors and capacitances are not used from the MSL. Simplified versions with less auxiliary variables are implemented. They have exactly the same interface and connectors to ensure compatibility with the MSL.
- A strict naming convention is used for consistency and to enable the *greybox.py* toolbox to automate certain tasks.
- The library heavily relies on the `extends` construct in order to avoid code duplication. This is specifically useful for the thermal zone models that have increasing complexity as a function of their order.
- An `inner/outer` component `simFasBui` passes all inputs like weather data, occupancy etc. from the top level to all sublevels.
- The models for thermal zones, HVAC and user behaviour have exactly the same interface as their equivalents in the *IDEAS* library. *IDEAS*, developed by KU Leuven and 3E, is an open-source library for modelling and simulation of buildings and integrated districts (Baetens et al., 2012). Therefore, it is very easy to replace one or more detailed components from an *IDEAS*-based model by a low-order equivalent from the *FastBuildings* library.

Currently, the thermal zone models available in the *FastBuildings* library are based on a resistor-capacitance (RC) network analogy which is often used for the modelling of thermal processes. This is however not required: any model that specifies a relationship between the heat flows and temperatures at the interface of a thermal zone can be implemented. Different examples of models in the library are schematically presented in Figure 5 in Part II.

The *FastBuildings* library largely contains the domain specific knowledge that is fundamental in grey-box modelling. Different thermal zone models often encountered in literature are present in the library and it is very easy to add more models (Davies, 2004; Bacher and Madsen, 2011; Sourbron et al., 2013; Reynders et al., 2014). The *FastBuildings* library is very dynamic in the sense that it is being extended with extra building models the more it is applied to different cases. How these models are chosen in a forward selection approach is explained in Section *Toolbox functionality and work flow*. The *FastBuildings* library is distributed with the *Modelica license 2* and can be found in the *openIDEAS* source code repository on Github (KU Leuven and 3E, 2014).

The JModelica.org platform

The toolbox relies heavily on the JModelica.org platform, which is an open-source tool for simulation and optimisation of dynamic systems described by Modelica code (Åkesson et al., 2010). For simulation purposes, JModelica.org uses the Functional Mockup Interface (Blochwitz et al., 2011). For optimisation purposes, JModelica.org offers various algorithms and also supports the Modelica language extension Optimica (Åkesson, 2008). Optimica allows for high-level formulation of dynamic optimisation problems of the type presented in Section I.

Every model structure for which the parameters have to be estimated is characterised by a different

.mop file. These files are very similar to ordinary Modelica (*.mo*) files, but they can also contain Optimica code. Each *.mop* file has the same structure and has to define two models: one model for simulation, called `Sim`, and one for parameter estimation, called `Parest`. By default, the models are based on the *FastBuildings* Modelica library, which has been developed in conjunction with this toolbox. However, this is not required for the toolbox to work, as long as some naming conventions are followed. Any parameter present in the model can be estimated, including initial values of the states.

The toolbox estimates the unknown model parameters using JModelica.org's algorithm based on direct collocation. Collocation is used to discretise time, which reduces the optimisation problem to a nonlinear program (NLP), as presented in Section *Solution method* and described in more detail in Magnusson and Åkesson (2012), where in particular optimal control is also treated. JModelica.org utilises third-party NLP solvers, which require first- and second-order derivatives of all expressions in the NLP with respect to all decision variables. CasADi is used to obtain these by algorithmic differentiation (Andersson et al., 2012). In this paper we use the NLP solver IPOPT with the sparse linear solver MA27 from HSL (Wächter and Biegler, 2006; HSL, 2013).

Problem formulation

Identification of the unknown model parameters is formulated as a dynamic optimisation problem of the general form

$$\begin{aligned}
&\text{minimise} && \int_{t_0}^{t_f} e(t)^T Q e(t)\,\mathrm{d}t, && \text{(1a)}\\
&\text{with respect to} && x(t), w(t), u(t), p,\\
&\text{subject to} && F(t, \dot{x}(t), x(t), w(t), u(t), p) = 0, && \text{(1b)}\\
& && x(t_0) = x_0, && \text{(1c)}\\
& && \forall t \in [t_0, t_f].
\end{aligned}$$

The system dynamics are modelled by a differential-algebraic equation (DAE) system (1b), where t is the time, $x(t)$ is the state, $w(t)$ is the vector-valued algebraic variable, $u(t)$ is the vector-valued system input, which includes both control variables and disturbances, and p is the vector of parameters to be estimated.

Algebraic variables often occur in Modelica models. A typical example is the conversion of measured electricity consumption in a radiative and a convective fraction. The resulting radiative and convective heat fluxes are contained in $w(t)$.

The DAE system may be implicit, non-linear, time-variant, and high-index. It is the result of the compilation of the *FastBuildings* model. In the case of high-index systems, index reduction is automatically performed by the JModelica.org compiler.

Since a gradient-based method is applied to solve the dynamic optimisation problem, F needs to be twice continuously differentiable with respect to all of its arguments (except the first one). This disables the use of hybrid models. Initial conditions are given by specifying the initial state, as given by (1c), where t_0 is the start time. The initial state is usually unknown, in which case some, or all, elements of x_0 can also be introduced as elements of the vector p.

The objective (1a) of the optimisation is to minimise the integrated quadratic deviation e of the model output from the corresponding measurement data. The model output y is typically some of the states, but could also be some of the algebraic variables (and also inputs, as discussed below). The matrix Q, which typically is diagonal, is used to weigh the different outputs. The measurement data is assumed to be a function of time, denoted by y_M. Since measurements are typically discrete in time, they are simply interpolated linearly to form y_M. The output deviation e is then given by

$$e(t) := y(t) - y_M(t). \tag{2}$$

The inputs can be treated in two different ways. The first is to assume that the inputs are known exactly by their measurement data and treat them as fixed values instead of decision variables. The second way is to have an error-in-variables approach where the inputs are kept as decision variables and treat them as model output, that is, include them in the vector y and penalise their deviation from the corresponding measurement data. The second way is useful for coping with uncertainties in measurement data.

Solution method

The approach taken to solve the optimisation problem (1) is based on low-order direct collocation as presented by Biegler (2010). The idea is to divide the time horizon into a number of elements, n_e, of fixed (but possibly distinct) lengths h_i and approximate the time-variant system variables $\dot{x}, x, w$ and u by a polynomial of time within each element, called a colloca-

tion polynomial. These polynomials are determined by enforcing the dynamic constraints at a certain number of points, n_c, within each element. These points are called collocation points and $t_{i,k}$ is used to denote collocation point number $k \in [1..n_c]$, where $[1..n_c]$ denotes the integer interval between 1 and n_c, in element number $i \in [1..n_e]$.

The system variables' values at these points, denoted by

$$(\dot{x}_{i,k}, x_{i,k}, w_{i,k}, u_{i,k}, e_{i,k}) := \\ (\dot{x}(t_{i,k}), x(t_{i,k}), w(t_{i,k}), u(t_{i,k}), e(t_{i,k})),$$

are then interpolated based on Lagrange interpolation polynomials to form the collocation polynomials. There are different schemes for choosing the placement of collocation points with different numerical properties. In this paper we only consider Radau collocation.

All collocation methods correspond to special cases of implicit Runge-Kutta methods and thus inherit desirable stability properties making them suitable for stiff systems.

This approximation reduces (1), which is of infinite dimension, into a finite-dimensional nonlinear program (NLP) of the form

$$\begin{aligned}
\text{min.} \quad & \sum_{i=1}^{n_e} \left(h_i \sum_{k=1}^{n_c} \omega_k e_{i,k}^T Q e_{i,k} \right), && \text{(3a)} \\
\text{w.r.t.} \quad & \dot{x}_{i,k}, x_{i,l}, w_{i,k}, u_{i,k}, p, \\
\text{s.t.} \quad & F(t_{i,k}, \dot{x}_{i,k}, x_{i,k}, w_{i,k}, u_{i,k}, p) = 0, && \text{(3b)} \\
& x_{1,0} = x_0, && \text{(3c)} \\
& x_{n,n_c} = x_{n+1,0}, \quad \forall n \in [1..n_e - 1], && \text{(3d)} \\
& \dot{x}_{i,k} = \frac{1}{h_i} \sum_{j=0}^{n_c} \alpha_{j,k} \cdot x_{i,j}, && \text{(3e)} \\
& \forall i \in [1..n_e], \quad \forall k \in [1..n_c], \quad \forall l \in [0..n_c].
\end{aligned}$$

The NLP objective (3a) is an approximation of the original objective (1a) based on Gauss-Radau quadrature, where the measurement error $e_{i,k}$ in each collocation point is summed and weighted by the corresponding element length h_i and quadrature weight ω_k, which depends on the choice of collocation points. Note that the decision variables are not only the unknown parameters p, but also the discretised system variables $\dot{x}_{i,k}, x_{i,l}, w_{i,k}$, and $u_{i,k}$ (unless it has been eliminated). The constraint (1b) from the continuous-time model dynamics is transformed into the discrete-time constraint (3b) by enforcing it only in each of the collocation points.

Since the states need to be continuous (but not differentiable) with respect to time, the new continuity constraint (3d) needs to be introduced. Because we use Radau collocation, where no collocation point exists at the start of each element, this also requires the introduction of the new variables $x_{i,0}$, which represent the value of the state at the start of element i. With the introduction of $x_{1,0}$, the initial condition (1c) is transcribed into (3c).

Finally, we introduce the constraints (3e) to capture the dependency between x and $\dot{x}$, which is implicit in (1). The state derivative $\dot{x}_{i,k}$ in a collocation point is approximated by a finite difference of the collocation point values of the state in that element. The finite difference weights $\alpha_{l,k}$ are related to the butcher tableau of the Runge-Kutta method that corresponds to the collocation method.

All that remains is to solve the NLP (3) in order to obtain an approximate solution to the original problem (1). We do this numerically using IPOPT, as described in Section *The JModelica.org platform*.

Toolbox functionality and work flow

The user interacts with the toolbox through the *grey-box.py* Python module. This module defines two classes `GreyBox` and `Case`, as shown in Figure 1. The idea is to instantiate the `GreyBox` class once for the system identification of a given building. The `GreyBox` object will contain many different instances of the `Case` class. Every `Case` is an attempt (successful or not) to obtain a model for the given building. The `Case` therefore keeps track of the model structure, identification data, initial guess, solver settings and results of a single parameter estimation attempt. The functionality of the toolbox is packed in methods of the `GreyBox` class and can be grouped into different domains, according to the foreseen workflow. This is shown in Figure 2. This workflow is discussed in the following paragraphs.

The methods under **data handling** are used to load the data files, resample the data if desired, create data slices of given lengths (for example one week, but can be any period) and show a plot of any data slice. Typically, one data slice is the training set, and the other slices can be used for cross-validation. Resampling the data is an important step because the toolbox automatically chooses the collocation points to coincide with the measurements. Thus, the (size of) the numerical problem (3) is strongly dependent on the chosen sam-

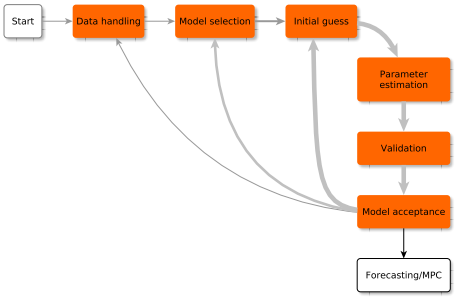

Figure 2: Workflow and high-level functionality in the toolbox.

pling time, and it is often a good strategy to start with a large sampling time and refine it in a later stage.

When the data has been pre-processed, a model structure has to be specified in the **model selection** step. This is accomplished by specifying the path to a *.mop* file. There are two models in the *.mop* file: a Modelica model for simulation, called `Sim`, and a Modelica + Optimica model for parameter estimation, called `Parest`. The main difference is that in the model `Parest`, the value of the Optimica attribute `free` is set to `true` for each parameter to be estimated. The compilation of both models happens automatically by invoking the corresponding JModelica.org functionality. Model information (state vector, parameter vector and required inputs) and solver settings are also obtained in this step.

Before the parameter estimation can be attempted, an **initial guess** has to be specified for each element in the parameter vector. These can be set by default, by inheritance, by Latin hypercube sampling or manually.

When the default initial guesses are used, an appropriate value is chosen for each parameter, based on its name. For example, the naming convention in *FastBuildings* forces all parameter names for thermal resistances to start with 'R' (like R_{Wal}), for thermal capacities with 'C' (like C_{Zon}), for fractions with 'fra' (like fra_{Rad}), etc. Based on the first letter(s) of a parameter to be estimated, a default initial value will be set.

An alternative for obtaining the initial guess is to start from the optimised parameter vector of a previous case, the *parent* case. This is especially useful when a new *.mop* file is selected that has similarities with a previously processed *.mop* file. Due to the naming conventions in *FastBuildings*, the corresponding parameters will have the same name. Therefore, the best initial guess for a similar parameter in the new model will be the optimal value from the parent. For new parameters, the default initial guess method described above is used.

The last automated option to obtain initial guesses is based on Latin hypercube sampling. Due to the non-convexity of the problem, there can potentially exist many local minima. To investigate the parameter search space more systematically and increase the chances of finding a global minimum, a Latin hypercube sampling method has been implemented. This method will take a single initial guess as well as lower and upper bounds for each parameter and derive a univariate beta distribution from these three values. The distribution can be symmetric or asymmetric, as shown in Figure 3.

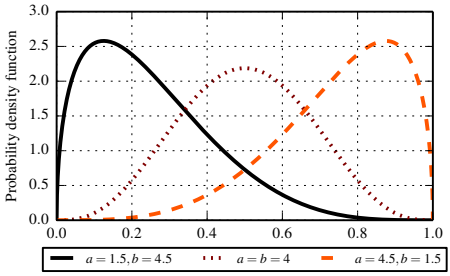

Figure 3: Symmetric and asymmetric beta distributions. The parameters a and b characterise the probability density function.

The Latin hypercube sampling will then derive n stratified samples from each distribution and combine them randomly to obtain n different initial guesses. Each of these guesses will be copied to a new `case` to keep track of the results.

When a `case` has an initial guess for the parameter vector, the **parameter estimation** can be started. However, the NLP (3) requires good initial guesses for each of the decision variables (including all collocated states and algebraic variables). This is handled by simulating first with the `Sim` model and the initial guess of the parameter vector. The resulting simulation trajectories are used as initial guesses for the decision variables in (3). Numerical scaling factors for each system variable are also computed as the infinity norm of the corresponding trajectory.

The solution time and the number of iterations can vary a lot depending on the initial guess and the abil-

ity of the model to represent the measurement data. Through the IPOPT interface, the toolbox allows the specification of a maximum solution time and/or a maximum number of iterations after which it will interrupt the optimisation.

The estimation adds the optimised parameter vector to the `case`, as well as the IPOPT solver statistics.

The **validation** of the results is always based on a post-simulation with the `Sim` model and the optimised values of the parameter vector. This can be done on the training data (auto-validation) or on any other dataset (cross-validation). There are both visual and quantitative validation methods. The visual methods contain, for example, time series plots of the resulting trajectories and corresponding residuals, scatter plots of the residuals with monitoring data and a plot of the autocorrelation function of the residuals. This also implies a check on the weights of the matrix Q from (1a) in case the error-in-variables method is used. When a full Latin hypercube sample has been estimated, a visual check of the different local optima is implemented. This can be used to judge whether the sample was large enough to suppose that the global optimum has been found. The quantitative methods are based on a computation of the root-mean-square error (RMSE) for each trajectory in the vector e from (2). As the RMSE is computed based on post-simulation with adaptive step length, discretisation errors in the collocation method are accounted for in the model validation process.

A computation of the confidence interval for each of the estimated parameters is implemented. This gives an indication of the accuracy of the estimation and the parameter's influence on the model's input-output behaviour. The standard deviation of the estimated parameters $\hat{p}$ is computed according to Englezos and Kalogerakis (2000). The standard deviation for parameter i is the square root of the diagonal element on (i,i) in the covariance matrix $\mathrm{cov}(\hat{p})$ of the estimated parameters, which is given by

$$\mathrm{cov}(\hat{p}) = \hat{\sigma}^2 (J^T J)^{-1},$$

where $\hat{\sigma}^2$ is the estimated variance of the output deviation e. J is composed based on the results of a simulation with the estimated parameters and sensitivities computations activated. J contains the sensitivities of the model outputs with respect to the estimated parameters as shown in Eq. (4).

$$J = \begin{bmatrix} \frac{\partial y_1(t)}{\partial p_1} & \frac{\partial y_1(t)}{\partial p_2} & \cdots & \frac{\partial y_1(t)}{\partial p_{n_p}} \\ \frac{\partial y_2(t)}{\partial p_1} & \frac{\partial y_2(t)}{\partial p_2} & \cdots & \frac{\partial y_2(t)}{\partial p_{n_p}} \\ \vdots & \vdots & \ddots & \vdots \\ \frac{\partial y_{n_y}(t)}{\partial p_1} & \frac{\partial y_{n_y}(t)}{\partial p_2} & \cdots & \frac{\partial y_{n_y}(t)}{\partial p_{n_p}} \end{bmatrix} \tag{4}$$

In this equation, $y_1 \ldots y_{n_y}$ are the n_y model outputs and $p_1 \ldots p_{n_p}$ are the n_p free parameters. This method can only be applied when the model output is equal to one or more states.

The final step in the system identification is **model acceptance**. Model acceptance is needed on two levels: for a single model, and between different models. For a single model, generally a Latin hypercube sampling is executed and the resulting global optimum is accepted if it is a *valid* solution. Valid means that:

- the parameters do not lie on the specified minimum or maximum bounds;
- the parameter values are physically reasonable;
- the confidence intervals are within reasonable bounds.

These criteria are not totally objective and often require an expert's check on the model. If the global optimum is not valid, the local optima are analysed and may contain a valid model. If no valid model is found within the sample, there are different options. A new Latin hypercube sample can be generated with different distributions and/or a larger sample size. Sometimes it can also help to change numerical settings for the solver or to resample the data differently. If none of these solutions leads to a valid model, the selected model structure cannot be matched to the considered identification dataset and a different model structure has to be chosen.

A *forward selection* approach is preferred for inter-model acceptance. This approach starts with a very simple model, generally a first order single zone model with a low number of free parameters. Then, model order and complexity are increased until (i) the models cannot be validated or (ii) the RMSE in cross-validation cannot be improved anymore. The selection of the candidate models in this procedure is not systematic. The procedure can be carried out manually or automatically. The manual solution is a trial and error procedure, often accompanied by tailor-made models based on the results of previous identification attempts. For the automatic solution, the modeller makes a selection of models that is passed to the toolbox. The

toolbox will then sort the models according to the number of parameters and start with the identification of the least complex one. Validation tests are specified by the user and the toolbox will automatically select the best valid model. Which models are passed to the toolbox is again a user-specified choice based on expertise and available meta-information. It is of course possible to pass every model of the *FastBuildings* library, but this will often result in an unacceptable CPU-time. Even if the forward selection procedure is not as strict as the one presented by Bacher and Madsen (Bacher and Madsen, 2011), it has several practical advantages. Firstly, the initial guesses and distributions for the parameters can be inferred from previously identified models. This is enabled by a strict naming convention in the *FastBuildings* library and by the fact that similar model components like walls, infiltration, solar gains etc. are repeated in more complex models. Secondly, starting from the first identified model, there is always a reference performance (RMSE) with which the new results can be compared. This approach avoids overfitting of the model, as will be demonstrated in Part II.

Data requirements

The developed grey-box modelling approach is intended for existing buildings. The aim is not to develop a detailed emulator model, but to develop a simplified low-order model that works well in an MPC context or for predicting loads in buildings. For practical use in existing buildings, we can not count on the existence of detailed emulator models, hence model order reduction approaches are excluded. Therefore, the aim is to develop a methodology that can cope with very little meta-information and a limited amount of measurement data.

With regard to the meta-information, the requirements depend on the complexity of the model. For very simple models, typically single-zone and without HVAC components, there is no need for any a-priori knowledge of the building. Only the location of the building has to be known if weather data is to be obtained from a generic weather service. Other building properties, like building size, orientation, window area, envelope properties etc. are not required. Nevertheless, this information can be beneficial for fixing initial guesses and for validation of estimated parameters.

The more meta-information we want to use, the more manual interventions are needed in the identification procedure. Therefore, this information is optional. By default, initial guesses are hard coded based on naming conventions. This means for example that all resistances in a model are attributed the same initial value, unless a resistance with the same name has been estimated in the parent `case` of the current model. In this situation, the initial guess is the optimised value from the parent `case`. Experience shows that the combination of these initial guesses with the Latin hypercube sampling is sufficient to find good parameter estimates also without using a-priori knowledge. Also for the very first model in the forward selection approach, which is supposed to be very simple, this works reliably.

The toolbox uses upper and lower bounds for the parameter estimation. The main reason for these bounds is to reduce the feasible region and thus the search space. Most bounds reflect basic physical laws, for example by imposing that resistances, capacities, gA values and fractions have to be positive. For fractions, an upper bound of one can be imposed, but it can also be relaxed. This can be used for example to obtain internal gains as a fraction of measured electricity consumption. Thanks to body heat gains, this estimated fraction is allowed to be larger than one. Most parameters do not have an upper bound because it is impossible to specify them without using meta-information. If a parameter estimation would result in unrealistic high values, this is to be detected by either too high confidence intervals, an expert check on the values or bad cross-validation. The use of bounds for the starting temperatures of the states is illustrated in Part II.

Sometimes, meta-information can be replaced by an analysis of the available data. For example, a large window area on a specific orientation can be discovered automatically by a correlation analysis on zone temperatures with incident radiation on different orientations. This information is then used to select which solar radiation components are used as disturbances in the model.

For more complex models however, more meta-information is needed. When a multi-zone model is created, information about the position of available zone measurements (temperature, humidity, electricity consumption etc.) is very useful to decide on the zoning strategy. If the model has to contain the HVAC system, some information is necessary, in particular about the presence of specific equipment. This information is used to adapt the model structure to the installed HVAC system.

The first requirement for the monitoring dataset is

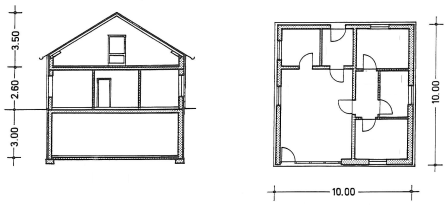

Figure 4: Front view and ground floor of the experimental house (north is up). For experiment 2, Zone 2 *refers to the 3 small rooms in the north.*

Setup	Exp. 1	Exp. 2
Period	Summer	Winter
Blinds	Closed	Open
Zoning	Single zone	Two zones (doors closed and sealed)
Heating	Sequence	Different sequence

Table 1: Overview of the differences between both experiments.

that the meaning of all variables is clear. The dataset has to contain at least the indoor and ambient temperature and heating/cooling loads at hourly interval. The ambient temperature (and other weather variables) can also be obtained from a weather service if the location of the building is known. The availability of more variables is beneficial and will improve the model. Electricity consumption monitoring (with sub-metering for plug power) is strongly recommended. More submeters for electricity always improve the information content and usability, for example for creating equipment scheduling profiles. When the HVAC system is to be modelled, a measurement of the energy use of different components is required.

Occupancy measurements are often not available. Mostly, the model does not need the occupancy itself, but the internal gains from body heat transfer. In offices, these are correlated with plug power. Alternatively, occupancy can be modelled based on measurements of relative humidity or CO_2. This is not yet implemented in the current version of the toolbox.

Part II
Validation

Methodology

Experimental setup

A detailed experiment was set up by Fraunhofer IBP (Holzkirchen, Germany) in order to collect monitoring data from well-known buildings near Munich, the *twin houses* (Kersken et al., 2014). We use monitoring data from one of these houses. A schematic overview of the building is given in Figure 4.

Two experiments are performed, resulting in two datasets of about 40 days each. Each experiment consists of consecutive periods of free floating operation, a randomly ordered logarithmically distributed binary sequence (ROLBS) for heat inputs and a temperature controlled operation. The differences between the experiments are detailed in Table 1.

There are no users in the experimental house. The heating consists of electrical heaters in each of the spaces. By consequence, the models presented in this paper focus on the building only and do not include components for users or HVAC.

Control versus forecasting

The presented grey-box approach aims at identifying models for forecasting and control. We have argued that the simulation performance is the correct criterion to validate the models, and it is sufficient to validate models for forecasting. However, a model with a good simulation performance is not necessarily suited for optimal control. Some additional criteria are:

- observability: models that are not observable cannot be initiated in the right state with an adapted state estimation procedure;
- complexity: the model has to fit in an optimal control framework. In particular, non-linear models are difficult to optimise;
- solver time: even if the requirements above are fulfilled, solving the OCP may require more time than is available between subsequent control steps.

However, we are confident that the models presented in this paper are suited for MPC. Firstly, state estimation has been implemented on identical and very similar models as those presented in this paper (Vande Cavey et al., 2014). Secondly, the presented models are all linear (even if the *FastBuildings* library and our our optimal control framework *JModelica.org* both allow non-linear models). Thirdly, we have tested

those models in MPC and the computation times for solving the OCP are around one minute or much less depending on the initialisation and forecasting horizon.

The ultimate validation of a control model is by assessing its control performance, but this is subject to future work. We therefore assume that the models considered here are suitable for control if they have a good simulation performance.

Simulation performance

The simulation performance is quantified by the simulation error SE. It is a weighted average of the root mean square error (RMSE) for a set of n model outputs:

$$SE = \sum_{j=1}^{n} q_j(RMSE_j), \tag{5}$$

where

$$RMSE_j = \sqrt{\frac{\sum_{i=1}^{m} (y_j(t_i) - M_j(t_i))^2}{m}}.$$

The weighting factors q_j are the diagonal elements of matrix Q of (1a). For each selected output variable, $y_j(t_i)$ is the model output at time instant t_i and $M_j(t_i)$ is the corresponding measurement. The model outputs are taken at m time instants, corresponding to the data points. These m data points may be the raw measurement data or the result after a downsampling operation. The measurement data M is used to form y_M in (2) by interpolation. However, as the toolbox sets the collocation points so that they coincide with the time instants t_i defined by the (resampled) measurement data, no interpolation is actually needed.

It is important to implement the validation as cross-validation (as opposed to auto-validation). This means computing the simulation performance on a section of the dataset that was *not* used for identification. For validation of the control performance, a short validation period of about 1 day is sufficient. However, in order to validate the load forecasting application, we need a much longer dataset. As our experiments contain each 40 days of data, we split them in two equal parts: the identification and (cross-)validation subsets. We will refer to the simulation performance in cross-validation as *prediction performance*.

For the validation simulation, an initial state vector is required. This state vector can be identified by filtering techniques from measurement data up to the start time of the validation dataset. In this study, the validation dataset starts where the identification dataset ends. Therefore, the state vector can be determined as the model state at the end of the identification period.

As explained in Part I, the forward selection approach results in a single grey-box model for a given dataset. We will call this model the *accepted* model. It is the model resulting in the lowest SE on the cross-validation dataset that is *valid*.

For the experimental house however, almost all meta-information is available: dimensions, construction, window positions, material properties, ventilation rates etc. In order to validate the grey-box toolbox for its intended use and work flow, none of this meta-information is used in the modelling phase.

Experiment 1

Data handling and zoning

The available dataset is very detailed. There are different temperature sensors (in different rooms and also within a single room to measure stratification), heat flux measurements, humidity sensors etc. The sampling period of the data is 10 minutes. We start the forward selection procedure with a simple single-zone model lumping all heated spaces, and we neglect the interaction with the boundary spaces (attic and cellar). For this thermal zone, an average zone temperature T_{Zon} has to be defined. As we know nothing about the building (we do not use the available meta-information) we just average all temperatures of the heated spaces and sum their heating loads. We also resample the 10 minute data to hourly values. This reduces the size of the numerical problem because the toolbox automatically chooses the collocation points to coincide with the measurements. An overview of all models that are successfully identified *and* validated in the forward selection procedure is shown in Figure 5.

A first model

The first single-zone model is model A of Figure 5. The model has only one state T_{Zon}. The free parameters are the thermal capacity C_{Zon} and start temperature $T_{Zon}(0)$, the total solar transmittance gA of the windows and a total heat loss coefficient R_{Wal} representing all heat losses to the ambient temperature T_{Amb} (see Table 2).

Model inputs are the ambient temperature T_{Amb}, global horizontal radiation $I_{Glo,Hor}$, and summed heating loads Q_{Hea}. The use of the global horizontal radiation instead of the radiation on several vertical surfaces is an approximation that allows us to estimate only one

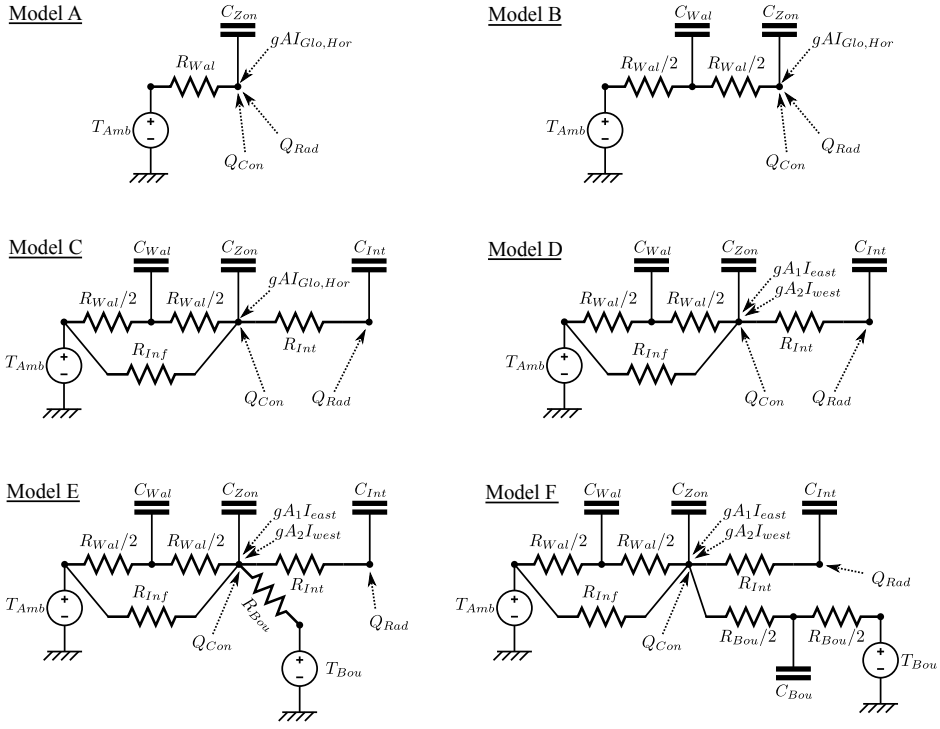

Figure 5: Overview of identified valid models for experiment 1. See the nomenclature at the end of this article for the meaning of the variables.

Parameter	Estimated value	95% conf.
C_{Zon}	5.4e7 J/K	+/- 2.2e6
R_{Wal}	7.0e-3 K/W	+/- 1.2e-4
$T_{Zon}(0)$	30.0 °C	-
gA	2.65 m^2	+/- 0.16 m^2

Table 2: Overview of free parameters and their estimated values for the first order model (model A).

gA value. In subsequent model refinements we will use the radiation components on different orientations and multiple windows. The identification is based on a minimisation of $RMSE(T_{zon})$.

As for all models that will be discussed below, a Latin hypercube sample with initial guesses has been created and the best result of this sample is presented. Table 2 gives the resulting parameter estimates and their estimated 95% confidence interval for the first order model. The $RMSE_{auto}$ is 0.61 K and the $RMSE_{cross}$ is 2.01 K which is not very accurate. Still, this model is a good starting point and it provides useful initial guesses for the parameters in more detailed models.

Model refinements

Different models of increasing complexity have been identified. Without discussing all attempts in detail, we try to give an overview of the model improvements. An overview of the RMSE values for auto and cross-validation of all successfully identified models is shown in Figure 6 and the model schemes are shown in Figure 5. The accepted model is discussed in more detail in the next section.

Model B The single state model cannot capture all dynamics in the measurement data. More states are needed. A variety of additional states can be suggested, such as internal mass T_{Int}, inertia of the building envelope T_{Wal}, inertia of the heat emission system T_{Hea} etc. Different two-state models have been identified, the best model (on cross-validation) has an additional state for the walls (model B). This model has six free parameters (of which two are initial temperatures of the states). The $RMSE_{auto}$ is 0.31 K and $RMSE_{cross}$ is 0.76 K. This is a substantial improvement compared to the single-state model.

Model C We can still improve the model by increasing its order to three states. Many attempts lead indeed to lower RMSE values in auto-validation, but *not* in cross-validation. This means these models are overfitted. We found one model however that slightly improves $RMSE_{cross}$ to 0.74 K. This model is able to reduce $RMSE_{auto}$ by 50% to 0.15 K but this barely results in a better prediction performance. The model has an additional state for the thermal inertia in the zone and an additional resistance r_{Inf} in parallel with the wall. This leads to 10 free parameters.

Model D An analysis of the residuals reveals a correlation between model error and solar radiation. We still use the global horizontal radiation $I_{Glo,Hor}$ to estimate a single gA value. The incorporation of solar gains can be refined by adding windows and connecting each window to a different solar radiation. In our attempts, we obtained the best results with two windows, connected to the vertical global radiation on East and West respectively. This resulted again in a large reduction of $RMSE_{auto}$ to 0.10 K and a small reduction of $RMSE_{cross}$ to 0.71 K.

Model E When analysing the data, we have found a possible cause for the discrepancy between the results in auto and cross-validation. In the identification dataset, the mean attic temperature is higher than in the validation set, leading to overestimation of temperatures on cross-validation. When we add a thermal resistance to the attic and estimate its value we can indeed improve the prediction performance. The obtained model has an $RMSE_{auto}$ of 0.09 K and $RMSE_{cross}$ is 0.56 K. The model has 12 parameters, and none of the estimated values are physically impossible or are positioned at their minimum or maximum boundary. This is an important validation criterion, it requires however an expert check.

All subsequent attempts to improve the model lead to *non-physical* models. This may seem a non-issue since we are dealing with grey-box models in which the parameters are allowed to represent lumped characteristics. However, experience shows that when models have unrealistic values for the physical (lumped) parameters, these are always accompanied by extremely large confidence intervals.

Model F A different situation occurs when all physical parameters have acceptable values, but the estimated initial temperatures for the states are at the imposed boundaries (270 K and 310 K by default). When this happens for a state corresponding to a large time constant (large RC value), the state does not act very dynamically and the energy balance of the model is biased. However, it is often possible to obtain a valid model by limiting the initial state temperatures to a

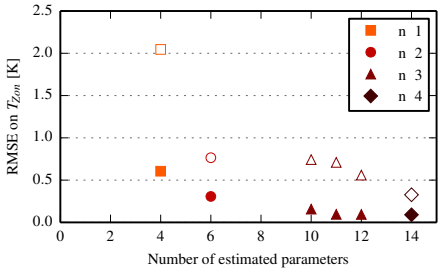

Figure 6: RMSE values for auto-validation (filled markers) and cross-validation (hollow markers) for the different models as a function of the number of estimated parameters and the model order n.

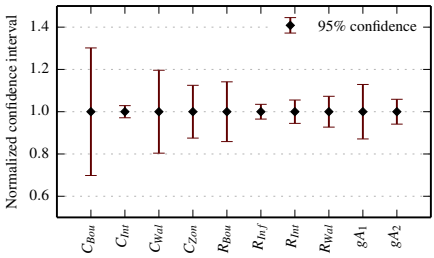

Figure 7: Normalised confidence interval for the parameters in the accepted model for experiment 1.

narrow bound based on physical insight and analysis of the measurement data. This will never lead to a lower RMSE on auto-validation because we exclude the *optimal* solution from the feasible region. However, it may result in a lower RMSE on cross-validation and thus a better prediction performance. What happens is that the numerically (slightly) better solution is shifted to a more physical solution.

This is also observed in experiment 1. We try to improve the model with 12 parameters by adding a state for the boundary with the attic (model F). This adds two parameters to be estimated, the thermal capacity of the boundary C_{Bou} and the initial temperature of this state $T_{Bou}(0)$. The optimisation returns $T_{Bou}(0) = 270$ K (-3.15 °C). Physically, we know this temperature should lie somewhere between the temperatures of the zone and the attic. By increasing the lower bound to 22.9 °C we find a valid model with an $RMSE_{auto}$ of 0.09 K and a strongly improved $RMSE_{cross}$ of 0.33 K. This model, with 14 parameters, is the accepted model. It will be discussed in more detail below. Further attempts led to non-physical models or did not improve the forecasting performance while adding unnecessary model complexity.

Model validation

Table 3 gives the resulting parameter estimates for model F. The normalised confidence intervals are shown in Figure 7. The toolbox does not compute confidence intervals for the initial temperatures of the states. We can see that all confidence intervals are reasonably small. Together with the physically meaningful parameters this is an indication of validity for our model. More specifically, this indicates that the model is not overfitted.

Par.	Meaning	Value
C_{Bou}	State boundary to attic	8.1e+07 J/K
C_{Int}	State internal mass	2.6e+07 J/K
C_{Wal}	State building envelope	2.3e+08 J/K
C_{Zon}	State zone	3.4e+06 J/K
$T_{Bou}(0)$	Initial temperature	22.9 °C
$T_{Int}(0)$	Initial temperature	29.6 °C
$T_{Wal}(0)$	Initial temperature	27.1 °C
$T_{Zon}(0)$	Initial temperature	30.3 °C
R_{Bou}	Resistance to attic	3.4e-2 K/W
R_{Inf}	Resistance to ambient	1.5e-2 K/W
R_{Int}	Resistance $C_{Zon} \leftrightarrow C_{Int}$	1.0e-3 K/W
R_{Wal}	Resistance envelope	1.8e-2 K/W
gA_1	gA windows East	0.46 m^2
gA_2	gA windows West	1.03 m^2

Table 3: Overview of estimated parameters for the accepted model (model F) for experiment 1.

Figures 8 and 9 show the measured and simulated zone temperatures for the identification and validation datasets respectively. The latter represents the simulation performance *SE* as we have only one model output T_{Zon} in (5). We can see that, given perfect predictions of the disturbances, the model is able to predict the measured temperature very well, even in an open-loop simulation over 20 days. However, a disadvantage of the accepted model is that it is dependent on a prediction of the temperature of the attic. Without this information, the simulation performance would be poor. The control performance can still be good if an online estimation and/or state estimation compensates for the slow dynamics caused by the presence of the attic. This will be elaborated in future research.

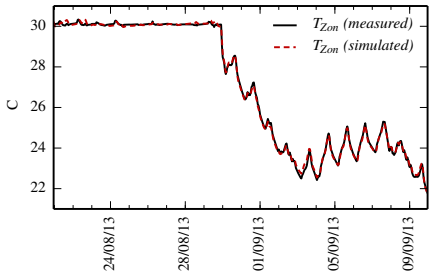

Figure 8: Measured and simulated zone temperature for the identification dataset (auto-validation) in the accepted model for experiment 1.

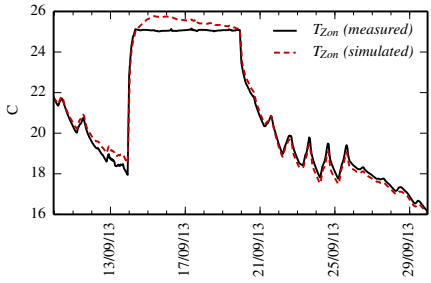

Figure 9: Measured and simulated zone temperature for the validation dataset (cross-validation) in the accepted model for experiment 1.

From these results, we conclude that the grey-box model is validated for both forecasting and control of the dwelling monitored in this experiment.

Experiment 2

Data handling and zoning

One of the fundamental differences compared to experiment 1 is that in this experiment, two different temperature regimes are maintained leading to two distinct thermal zones. Each of these zones is composed of different rooms. The most basic zoning approach consists of modelling only two zones and averaging the measurements in individual rooms accordingly. We will call these zones $Zon1$ and $Zon2$. Models with more than two zones have not been investigated.

Again, we do not use available meta-information but simply average all available measurements and we re-

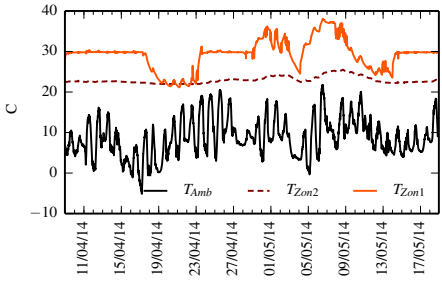

Figure 10: Measured (averaged) temperatures for both zones and ambient temperature for the full experiment 2. The first half of the data is the identification dataset, the second half is the validation set.

sample the data to hourly values. From a plot of the averaged measured zone temperatures (see Figure 10), we can see that T_{Zon2} has a different control and is very stable. Also the heating power for zone 2 is about ten times smaller than for zone 1 (not shown). As we will see later, this will complicate the estimation of the dynamics of zone 2.

Single-zone models

In contrast to experiment 1, we aim for a two-zone model. There will be no boundary condition so we will be able to predict the temperature for both zones simultaneously when only their heating power and the weather conditions are known. However, in order to get a grip on the dynamics and the orders of magnitude for the parameters, we first try to identify two single-zone models with the temperature of the other zone as a boundary condition. This will also provide useful indications regarding the order of magnitude of the *SE* of the two-zone model.

Without describing all steps to create the models we briefly discuss the results for the single-zone models. For both zones we have found a good fit with model B of Figure 5 (with an additional resistance R_{Bou} between T_{Zon} and the boundary temperature of the other zone). It is a second-order model with 8 parameters of which two are initial temperatures. Each zone has a single window connected to the radiation on a vertical, south oriented plane (instead of the global horizontal radiation as indicated in the scheme of model B).

Table 4 gives the resulting parameter estimates for both models. The corresponding RMSE values are given in Table 5. The normalised confidence intervals

Parameter	Zon1	Zon2	Unit
C_{Int}	1.7e7	2.7e7	J/K
C_{Zon}	2.6e6	1.2e7	J/K
$T_{Int}(0)$	26.4	22.7	°C
$T_{Zon}(0)$	29.5	22.5	°C
R_{Bou}	6.2e-3	2.9e-2	K/W
R_{Int}	1.3e-3	6.0e-4	K/W
R_{Wal}	3.9e-2	4.8e-2	K/W
gA	3.1	0.28	m^2

Table 4: Overview of estimated parameters for the accepted single-zone models for experiment 2.

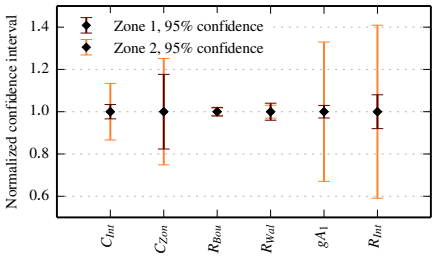

Figure 11: Normalised confidence intervals for the estimated parameters for both single-zone models.

are shown in Figure 11. From these results we can see the following:

- for all parameters, the order of magnitude is roughly the same for both zones;
- the thermal resistance of the boundary is a factor 5 higher when estimated from zone 2;
- zone 2 has a much better $RMSE_{auto}$ than zone 1, but a higher $RMSE_{cross}$;
- the confidence intervals for zone 2 are much larger, except for R_{Bou} and R_{Wal};
- both zones have higher solar aperture areas than for experiment 1. This makes sense considering that in experiment 1 the blinds were closed, and in experiment 2 they are open.

The low $RMSE_{auto}$ for zone 2 is misleading. Both the confidence intervals and cross-validation show that the model for zone 2 is not very good. We can understand this result by analysing the measurement data as shown in Figure 10. The temperature in zone 2 is extremely flat during the identification period. Therefore, the thermal inertia in this zone is not excited and consequently it is very hard or even impossible to estimate the time constants and other parameters of a dynamic model. We can conclude that poor datasets (with little excitation of the states) cause difficulties for the identification of dynamic models. Whenever possible, the building control system should cause sufficient excitation of all building components during the identification period. This conclusion has been formulated previously in literature, amongst others by Sourbron et al. (2013) and Žáčeková et al. (2014).

We now try to identify a two-zone model by combining the two single-zone models.

	$RMSE_{auto}$	$RMSE_{cross}$
Zone 1	0.27 K	0.51 K
Zone 2	0.07 K	0.65 K
SE	0.34 K	1.16 K

Table 5: RMSE of individual zone models and resulting SE.

Two-zone model

The two-zone model has two outputs on which the simulation error SE will be computed according to (5): T_{Zon1} and T_{Zon2}. We take both weight factors $w_j = 1$.

For the model of the boundary between both zones two options are explored: a thermal resistance, or a wall composed of two resistances and a capacity. In principle, the parameter values should not deviate much from the ones in Table 4. We also expect the largest parameter deviations for the parameters with the largest confidence intervals.

Without an additional state in the boundary wall between the zones, the results are not very good: the model has an SE_{auto} of 0.37 K and SE_{cross} of 1.74 K. Moreover, the initial temperature of C_{Int} for zone 2 lies at the boundary of 270 K (-3.1 °C) and rises monotonically during the identification period, thus falsifying the energy balance.

With an additional state C_{Bou} as shown in Figure 12, the simulation performance improves. However, analysis of the estimated parameters reveals again an initial temperature $T_{Int}(0)$ of 270 K. This time however, the capacity C_{Int} is not very large, and an attempt to narrow down the feasible region for the initial temperature leads to a valid model. The SE_{auto} becomes 0.335 K and SE_{cross} drops to 1.65 K. We should not be surprised that SE_{auto} drops slightly below the level of 0.343 K obtained with the two single-zone models: an

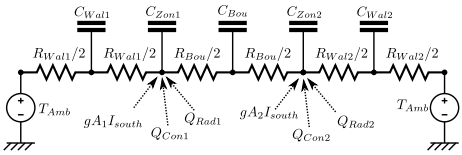

Figure 12: Accepted two-zone model for experiment 2.

Parameter	Zon1	Zon2	Unit
C_{Int}	1.9e7	1.1e8	J/K
C_{Zon}	2.8e6	5.5e8	J/K
$T_{Int}(0)$	26.8	23.9	°C
$T_{Zon}(0)$	29.2	22.5	°C
R_{Int}	1.4e-3	4.0e-5	K/W
R_{Wal}	2.0e-2	5.9e-3	K/W
gA	2.4	18.7	m^2
C_{Bou}	4.0e9		J/K
R_{Bou}	1.7e-2		K/W
$T_{Bou}(0)$	25.3		°C

Table 6: Overview of estimated parameters for the accepted two-zone model for experiment 2.

additional degree of freedom is introduced with C_{Bou}.

Further attempts to improve the model were not successful, the accepted model is discussed in more detail below.

Model validation

Table 6 shows the resulting parameter estimates for the accepted model presented in Figure 12. All parameters have physical values. For zone 1, the parameters barely shift compared to the single-zone model. For zone 2 however, most parameters change with a factor of $\pm$ 10. This again indicates that the identification dataset is worse for zone 2.

When the *SE* is split in the RMSE values for each zone separately, Table 7 is obtained. Zone 1 has a very good performance, also in cross-validation. Zone 2 however has a bad $RMSE_{cross}$. By comparison of Table 5 and Table 7, we see that the single-zone model for Zone 2 has a better prediction performance than the two-zone model. If we were more interested in predicting zone 2 than zone 1, we need to increase the weighting factor w_2 from Eq. (5).

The bad simulation performance of zone 2 also becomes evident when comparing the measured and simulated zone temperatures. These are shown in Figures 13 and 14. For zone 1 however, the prediction performance is very good, despite the deviation on zone 2. Again, we can stress the importance of online identification and state estimation in order to avoid recurring model bias.

	$RMSE_{auto}$	$RMSE_{cross}$
Zone 1	0.23 K	0.51 K
Zone 2	0.10 K	1.14 K
SE	0.33 K	1.65 K

Table 7: RMSE and SE of accepted two-zone model.

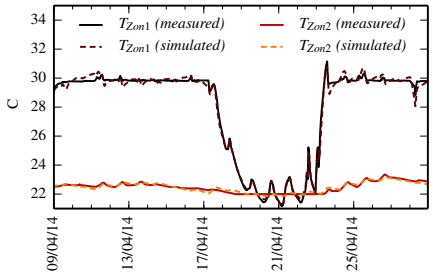

Figure 13: Measured and simulated temperature of both zones for the identification dataset (auto-validation) in the accepted model for experiment 2.

Conclusion

Inverse modelling is gaining attention in the building simulation community. More specifically grey-box modelling is considered as a strong framework for the creation of low-order models for analysis and control

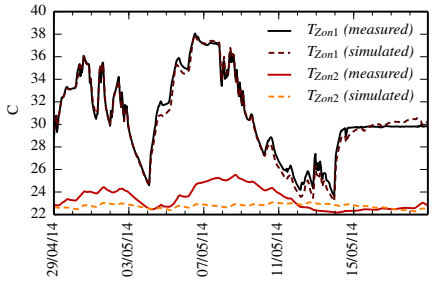

Figure 14: Measured and simulated temperature of both zones for the validation dataset (cross-validation) in the accepted model for experiment 2.

of monitored buildings. The first part of this paper presents an approach to obtain grey-box models in a largely automated way, which are applicable in both MPC and forecasting.

The first step is the creation of a building library with many potential model candidates. The Modelica package *FastBuildings* contains low-order models for thermal zones, HVAC, users, single and multi-zone buildings.

Next, a toolbox is presented that largely automates the parameter estimation of the *FastBuildings* models. It is implemented as a Python module that wraps the functionality of *JModelica.org* and presents the user a high-level interface for all common operations. The use of a gradient-based method allows an efficient numerical solution of the parameter estimation problems. Specific attention is paid to robustness and ease-of-use. A Latin hypercube sampling of the parameter search space overcomes local-minima issues related to the non-convexity of the optimisation problem. The toolbox is not publicly available, but can be obtained with an open-source license for research purposes by contacting the authors.

The toolbox is validated on two datasets generated by the detailed monitoring of a single-family house near Munich, Germany. In experiment 1, a single-zone building is identified that has a very good prediction performance. In an open-loop simulation over 20 days on the cross-validation dataset, the model deviations are very small with an $RMSE_{cross}$ of only 0.33 K.

In experiment 2, a two-zone building is identified with mixed performance. For the first zone, a good prediction performance is achieved with an $RMSE_{cross}$ of 0.51 K. The second zone however has more difficulties. Due to a weak excitation in the identification dataset, an $RMSE_{cross}$ of 1.14 K is obtained. This clearly points out the need of good identification data.

Finally, we want to point out two advantages of the proposed methodology that come from the use of Modelica. Firstly, the grey-box model is equation-based. This means that we have an acausal model relating all variables with equations, as opposed to an input-output model with a predefined information flow direction. Therefore, inputs and outputs can be switched as long as the problem is balanced. For example, given a temperature set point, the grey-box model would predict the heating load. Secondly, Modelica creates a large freedom in the model formulation by allowing also non-linear model components. These are typically encountered in heat transfer coefficients and HVAC equipment. Future developments of the grey-box toolbox and the *FastBuildings* library will explore these options.

Nomenclature

Symbol	Meaning
T	Temperature
C	Thermal capacity
R	Thermal resistance
Q	Thermal flux
gA	Solar admittance
I	Solar radiation

Subscript	Meaning
Zon	Zone (mostly denoting air)
Int	Internal
Wal	Walls / building envelope
Emb	Embedded (heating or cooling) system
Inf	Infiltration
Bou	Boundary
Amb	Ambient (outdoor)
Con	Convective
Rad	Radiative

Acknowledgement

Roel De Coninck wishes to thank Innoviris (Region of Brussels) for supporting this work on the side of 3E via the ITEA2 project *Enerficiency* (contract RBC/11 DS 143a) and the European commission for supporting his work on behalf of KU Leuven by supporting the FP7 project *PerformancePlus* (contract nb. 308991). Fredrik Magnusson acknowledges support from the Swedish Research Council through the LCCC Linnaeus Center and is also a member of the ELLIIT Excellence Center at Lund University.

References

Åkesson, J. (2008). Optimica—an extension of modelica supporting dynamic optimization. In *Proc. 6th International Modelica Conference 2008*.

Åkesson, J., K.-E. Årzén, M. Gäfvert, T. Bergdahl, and H. Tummescheit (2010, November). Modeling and optimization with Optimica and JModelica.org—languages and tools for solving large-scale dynamic optimization problems. *Computers and Chemical Engineering 34*(11), 1737–1749.

Andersson, J., J. Åkesson, and M. Diehl (2012). CasADi – A symbolic package for automatic differentiation and optimal control. In S. Forth, P. Hovland, E. Phipps, J. Utke, and A. Walther (Eds.), *Recent Advances in Algorithmic Differentiation*, Lecture Notes in Computational Science and Engineering, Berlin. Springer.

Bacher, P. and H. Madsen (2011, February). Identifying suitable models for the heat dynamics of buildings. *Energy and Buildings 43*(7), 1511–1522.

Baetens, R., R. De Coninck, J. Van Roy, B. Verbruggen, J. Driesen, L. Helsen, and D. Saelens (2012). Assessing electrical bottlenecks at feeder level for residential net zero-energy buildings by integrated system simulation. *Applied Energy* ((Special issue on Smart Grids, Renewable Energy Integration, and Climate Change Mitigation - Future Electric Energy Systems)).

Biegler, L. T. (2010). *Nonlinear Programming: Concepts, Algorithms, and Applications to Chemical Processes*. MOS-SIAM Series on Optimization. Mathematical Optimization Society and the Society for Industrial and Applied Mathematics.

Blochwitz, T., M. Otter, M. Arnold, C. Bausch, C. Clauß, H. Elmqvist, A. Junghanns, J. Mauss, M. Monteiro, T. Neidhold, et al. (2011, March). The functional mockup interface for tool independent exchange of simulation models. In *"8th International Modelica Conference"*, Dresden, Germany, pp. 20–22.

Bohlin, T. (1995). Editorial - Special issue on grey box modelling. *International Journal of Adaptive Control and Signal Processing 9*, 461–464.

Crawley, D. B., J. W. Hand, M. Kummert, and B. T. Griffith (2008, April). Contrasting the capabilities of building energy performance simulation programs. *Building and Environment 43*(4), 661–673.

Davies, M. G. (2004). Simple Models for Room Response. In *Building Heat Transfer*, Chapter 14, pp. 311–334. Chichester: John Wiley & Sons, Ltd.

Elmqvist, H. (1997). Modelica - A unified object-oriented language for physical systems modeling. *Simulation Practice and Theory 5*(6), 32.

Englezos, P. and N. Kalogerakis (2000, October). *Applied Parameter Estimation for Chemical Engineers*, Volume 81 of *Chemical Industries*. CRC Press.

Henze, G. P. (2013, May). Model predictive control for buildings: a quantum leap? *Journal of Building Performance Simulation 6*(3), 157–158.

Henze, G. P. and C. Neumann (2011). Building simulation in building automation systems. In J. L. M. Hensen and R. Lamberts (Eds.), *Building performance simulation for design and operation*, pp. 401–440.

HSL (2013). A collection of Fortran codes for large scale scientific computation. http://www.hsl.rl.ac.uk.

Kersken, M., I. Heusler, and P. Strachan (2014, September). Erstellung eines neuen, messdatengestützten validierungs-szenarios für gebäude-simulationsprogramme. In *Christoph van Treeck, Dirk Müller (eds.) Proceedings of BauSIM 2014*, Aachen, Germany, pp. 144–151. IBPSA.

Kristensen, N. R., H. Madsen, and S. B. Jorgensen (2004, February). Parameter estimation in stochastic grey-box models. *Automatica 40*(2), 225–237.

KU Leuven and 3E (2014). open-IDEAS source code repository. https://github.com/open-ideas.

Madsen, H. and J. Holst (1995). Estimation of continuous-time models for the heat dynamics of a building. *Energy and Buildings 22*, 67–79.

Magnusson, F. and J. Åkesson (2012, September). Collocation methods for optimization in a Modelica environment. In *9th International Modelica Conference*, Munich, Germany.

Reynders, G., J. Diriken, and D. Saelens (2014, October). Quality of grey-box models and identified parameters as function of the accuracy of input and observation signals. *Energy and Buildings 82*, 263–274.

Sourbron, M., C. Verhelst, and L. Helsen (2013, May). Building models for model predictive control of office buildings with concrete core activation. *Journal of Building Performance Simulation 6*(3), 175–198.

Vande Cavey, M., R. De Coninck, and L. Helsen (2014). Setting up a framework for model predictive control with moving horizon state estimation using JModelica. In *10th International Modelica Conference*, Lund, Sweden, pp. 1295–1303.

Wetter, M. (2009, June). Modelica-based modelling and simulation to support research and development in building energy and control systems. *Journal of Building Performance Simulation 2*(2), 143–161.

Wetter, M. (2011). A view on future building system modeling and simulation. In J. L. M. Hensen and R. Lamberts (Eds.), *Building performance simulation for design and operation*, pp. 28.

Wetter, M. and C. Van Treeck (2013). IEA EBC Annex 60 - New generation computational tools for building and community energy systems based on the Modelica and Functional Mockup Interface standards. http://iea-annex60.org/about.html.

Wächter, A. and L. T. Biegler (2006). On the implementation of a primal-dual interior point filter line search algorithm for large-scale nonlinear programming. *Mathematical Programming 106*(1), 25–57.

Žáčeková, E., Z. Váňa, and J. Cigler (2014, December). Towards the real-life implementation of MPC for an office building: Identification issues. *Applied Energy 135*, 53–62.

4.3 Conclusion

This chapter reported on the development and validation of a grey-box toolbox for reduced order modelling of buildings and HVAC systems. The toolbox makes use of grey-box models and this results in physically meaningful control models.

The physical interpretation of the models is however not straightforward. Even though the parameter estimates come with (often relatively narrow) confidence intervals, the corresponding physical property may lay outside of the found interval. This is explained by the very low-order of the models. As the resulting parameters will lump different physical phenomena, it is not possible to link the estimated parameter values to detailed building properties.

The physical structure of the models is still useful though. This difference with black-box models leads to four advantages in favour of grey-box models. Firstly, it allows to specify models with a structure that is expected to fit well to the data. For example, based on physical expertise, one may include an additional resistance for infiltration as a bypass over a wall component. Secondly, the parameters may still contain useful information and can help to diagnostic the model or to validate it. Most parameters can only have values with a specific sign or order of magnitude, and this knowledge can be used to reduce the feasible region for the parameter estimation problem as well as for model validation. Thirdly, the models will be more robust to extrapolation. This is an important property of grey-box models and it is specifically interesting in an MPC because the optimiser will often operate the model at the boundaries of the feasible region. These operating conditions are often not encountered in the identification dataset. Finally, under certain circumstances, it is possible to modify the model even without estimation of newly added parameters. An example is given in the next chapter where an additional hypothetical thermal energy storage is added to a grey-box model to study the potential of thermal energy storage for increasing the flexibility of a building.

Chapter 5

Flexibility in buildings

This chapter is submitted for publication as:
R. De Coninck and L. Helsen, "Quantification of flexibility in buildings by cost curves - methodology and application", *Applied Energy*, 2015, Submitted on 17/03/2015.

5.1 Introduction

In this chapter, a methodology will be presented that makes use of the grey-box models developed in Chapter 4 to quantify the potential for demand response with thermal systems in buildings. A general approach, applicable to a wide variety of buildings and distributed generation systems is presented. The methodology is applied to the KK building and the resulting flexibility costs are compared with the imbalance price in the Belgian power system.

5.2 Quantification of Flexibility in Buildings by Cost Curves - Methodology and Application

Quantification of Flexibility in Buildings by Cost Curves - Methodology and Application

Roel De Coninck[a,b,c,*], Lieve Helsen[a,c]

[a] *KU Leuven, Department of Mechanical Engineering, Celestijnenlaan 300 box 2421, 3001 Heverlee, Belgium*
[b] *3E nv, Kalkkaai 6, 1000 Brussels, Belgium*
[c] *EnergyVille, 3600 Waterschei, Belgium*

Abstract

The smart grid paradigm implies flexible demand and energy storage in order to cope with the variability of renewable energy sources. Buildings are often put forward as a potential supplier of flexibility services through demand side management (DSM) and distributed energy storage, partly as thermal energy. This paper presents a bottom-up approach for the quantification of this flexibility service. Cost curves are computed from the solution of optimal control problems with low-order models. These curves show the amount of flexibility and their associated cost. The method is generic and can be applied to heating, ventilation and air-conditioning (HVAC) services, thermal energy storage (TES) and local electricity production. A case study is performed on a monitored office building in Brussels, Belgium. The results reveal a large variation in both flexibility and cost depending on time, weather, utility rates, building use and comfort requirements. The study shows that for the studied day, flexibility is not for free. The mean flexibility cost has the same order of magnitude as the imbalance price in the Belgian power system.

Keywords: Buildings, Flexibility, Demand Response, Optimal Control, Case Study

1. Introduction

Due to the increased deployment of renewable energy systems with variable generation profiles, the need for flexible generation, flexible demand and energy storage increases. Simultaneously the electricity system evolves from a centralized to a distributed architecture with small-scale distributed generation (DG), distributed storage (DS) and controllable loads, often referred to as distributed energy resources (DER) [1]. This evolution, in combination with advanced ICT and control systems, leads to *smart grids* in which highly distributed loads are involved in power system control actions [2]. The benefits of increased responsiveness of the loads are described by Kirschen [3] and Strbac [4]. Buildings have a high energy demand and therefore they play a key role in the roll-out of these smart grids.

Buildings can offer frequency regulation or voltage control services to the energy and ancillary service markets through demand side management (DSM) [5, 6, 7, 8]. Gellings [9] defines DSM from a utility perspective as *"the planning and implementation of those electric utility activities designed to influence customer uses of electricity in ways that will produce desired changes in the utility's load shape"*. By simplifying the categories of DSM proposed by Palensky and Dietrich [10] we can say that DSM is composed of energy efficiency (EE) and demand response (DR). Flexibility is closely related to DR. In the context of this article we define the flexibility of a building as *the ability to deviate from its reference electric load profile*. We will quantify this ability and express flexibility in kWh over a specified time span. Simultaneously we will compute the costs associated with the corresponding DR action and express it in € or €/kWh.

The aim of this work is to enable a quantitative comparison of the flexibility and corresponding costs between different buildings and groups of buildings. The developed metric can be used in the design process or when selecting a set of buildings to include in a DR scheme. It is not the intention to develop a methodology for operational decision making or real-time operation.

The first section in this paper gives an overview of how the flexibility concept has been treated in the literature. We show that there is no common metric or

*Corresponding author
Email address: roel.deconinck@3e.eu ()

indicator to quantify flexibility. In the second section, a methodology is developed to quantify flexibility and the cost of the associated DR actions. This information is presented in a *cost curve*. The third section describes the application of the methodology on an office building in Brussels. The building and its HVAC system are presented and a low-order model is identified based on available monitoring data. In the last section we compute cost curves for different time spans, comfort requirements and system configurations and discuss the results.

2. Literature review

Flexibility is easy to define, but difficult to quantify. Petersen et al. [11] specify that *"The flexibility of a given system is a unique, innate, state-and time dependent quality. In conversation it is therefore sometimes said that flexibility is the ability to deviate from the plan. That characterization of flexibility is very insightful, but it still leaves us with the problem of defining both the ability to deviate and the plan"*. However, this is not sufficient: we also have the problem of defining the *cost to deviate from the plan*. Based on these costs, we could choose the most cost-effective ones to deliver the required flexibility for a given power system. Cochran et al. present a comprehensive overview of different techno-economic interventions to increase flexibility [12]. The authors mention that the relative costs are illustrative, confirming the need to quantify them in a reliable way.

There are different approaches to quantify energy use and costs. For a single building, generally a detailed model of the specific system or building is developed. The model typically takes electricity price profiles as input, and cannot take into account the different feedback mechanisms between load and centralized production. Many authors have studied load shifting control strategies in single building simulation or optimisation [13, 14, 15, 16]. The reason for load shifting is a reduction of peak power, consumption, emissions or costs. Sreedharan et al. present a case study computing the cost-effectiveness of load-shifting for five buildings in California [17]. They conclude that the cost-effectiveness depends on site-specific characteristics, thus affirming the need for a more elaborated approach. These studies rarely define flexibility nor present a general methodology to assess the potential for different buildings. Six et al. simply define the flexibility of an appliance as the number of hours the operation can be delayed [18]. Flexibility is a key concept in the recently finished *LINEAR* project [19, 20]. In *LINEAR*, flexibility is defined as "*the maximum time a certain power draw can be delayed or additionally called upon at a certain moment during the day*" This definition expresses flexibility in units of time and does not clearly quantify plan, deviation nor cost. In the EU FP7 project *ADDRESS* [21], an hourly flexibility index is calculated proportionally to the hourly load. The hourly load is computed according to the probability of use of the considered appliance during the day.

To quantify energy use and costs for multiple buildings, a top-down or a bottom-up approach can be chosen. The top-down approach mostly starts from the electricity generation park and models the demand by load curves. In these studies, the flexibility of the buildings is defined as the elasticity of the demand as a function of the electricity price [22, 23]. In this approach, the detailed (thermal) dynamics of the buildings are neglected, and very general assumptions about the demand elasticity have to be made. It is therefore an input to the model, and not a result. A bottom-up approach starts from very simple and generalized models of the buildings and solves a unit commitment or (distributed) optimal control problem in order to optimise the operation of the full system [24]. This approach can be agent-based to allow operational optimization in the context of energy markets and smart grids [25, 26, 27, 28]. These methods assess the impact of load shifting on the total system, but do not quantify the amount nor cost of the flexibility of real buildings. Finally, the analogy between multiple buildings and virtual power plants (VPPs) can be made. The flexibility service that a VPP can offer is described by different authors [29, 30, 31]. Cochran et al. give an overview of methods to quantify flexibility [12] in power systems, but it is not applicable to individual buildings.

A calculation method to quantify the flexibility of buildings and its costs was not found in the scientific literature. This paper elaborates a generic method that results in cost curves. The cost curves allow to aggregate the flexibility of different buildings or DER systems in general. Moreover, the methodology is illustrated by application to a case of space heating with heat pumps in an office building.

The methodology developed in this paper was presented in a first version in De Coninck et al. [32]. A few months after this publication, Oldewurtel et al. published a similar idea [33]. This paper further develops on the methodology of the original work, integrates some of the ideas of Oldewurtel et al. and presents a case study on a real occupied building.

3. Quantification of system flexibility

3.1. Definitions

We use the following terms and conventions in this article.

- *Reference*: control that minimizes operational cost while ensuring good thermal comfort (if applicable). This is the standard use case for a system operator.
- *Flexibility interval* $[t_i - t_e]$: the time span during which the flexibility is computed, typically one up to three hours for intra-day load shifting.
- *Positive flexibility*: ability to *increase* power consumption during the flexibility interval.
- *Negative flexibility*: ability to *decrease* power consumption during the flexibility interval.
- *System*: the set of components that can be controlled to influence the *electricity* load profile. This can be a single on-off controlled component (like a chiller) or an entire DER system with multiple degrees of freedom.
- *Optimal control problem (OCP)*: numerical optimization problem of the following form (in continuous time):

$$\begin{aligned} \underset{u}{\text{minimize}} \quad & J(t, \dot{x}, x, w, y, u) && \text{(1a)} \\ \text{subject to} \quad & F(t, \dot{x}, x, w, y, u) = 0, && \text{(1b)} \\ & g(t, \dot{x}, x, y, u) = 0, && \text{(1c)} \\ & h(t, \dot{x}, x, y, u) \geq 0, && \text{(1d)} \\ & x(0) = x_0. && \text{(1e)} \end{aligned}$$

In this formulation, $t \in [0, t_h]$ is time with t_h the prediction horizon, $u \in \mathbb{R}^n$ is the control signal, J the objective, t_h is the prediction horizon, $F(\cdot)$ is the system model with states x, algebraic variables y and disturbances w. $g(\cdot)$ and $h(\cdot)$ are additional equality and inequality constraints. $x, \dot{x}, w, y$ and u are all time-dependent but for readability we have omitted the time dependency notation. The objective J can have different forms as elaborated below.

3.2. Overview

The method is based on the solution of at least three OCPs with an appropriate system model. The first OCP solves the reference operation of the building. This OCP typically has the objective to minimise the operational costs with constraints on thermal comfort and a prediction horizon of one or more days. This solution is *the plan* according to Petersen et al. [11]. The *deviation from the plan* can be obtained by modifying the objective function of the OCP. By specifying a target consumption (zero or very high) during the flexibility interval, we can force the solution to minimise respectively maximise the consumption during that specific time span while still aiming for minimal costs over the total prediction horizon. The shifted energy use during that interval is the flexibility (negative respectively positive). By definition, the energy cost of this new OCP will be higher than for the reference, and the difference is the *cost of deviating from the plan*. These three optimizations are used to build up a cost curve as illustrated in Figure 1. Optionally, intermediate points on the cost curve can be obtained by solving additional OCPs that force the solution to intermediate power levels. The following paragraphs elaborate the approach in more detail.

3.3. System model

The first step is the creation of an appropriate system model $F(\cdot)$. The main requirement for the model is that is has to be suitable for solving the OCP according to Eq. (1) (or its equivalent discrete-time formulation). The model should have a good simulation performance over the required prediction horizon. The one-step prediction performance which is typically used to assess control models is therefore not the correct metric to select the system model. Finally, the model has to be reliable in the entire feasible region because the solution of the different OCPs will push the system to non-common operating conditions, often on the boundaries specified by Eq. (1d). The case study in Section 4 is based on a data-driven grey-box model.

3.4. Reference scenario

The aim of the reference scenario is to optimise the system operation with respect to the operational cost. For simplicity, we only consider energy costs in the remainder of this paper, but other costs like water consumption of cooling towers, maintenance and lifetime impact of the operation can be considered as well. If we consider a constant gas tariff c_g and a time dependent

electricity tariff c_e, we can write the energy costs over the total prediction horizon as

$$J_c = \int_0^{t_h} (c_g P_g + c_e P_e) \mathrm{d}t \tag{2}$$

with P_g the gas consumption and P_e the electricity consumption.

If the system is a building, thermal comfort has to be guaranteed. There are generally two solutions to handle thermal comfort in optimal control. A first solution consists of adding an allowed comfort band as *hard constraints* in Eq. (1d). The second solution consists of adding a discomfort cost J_d to the objective J

$$J = J_c + \gamma J_d \tag{3}$$

where γ is a weighting variable. In the case of so-called *soft constraints*, an allowed comfort band is specified and J_d increases quadratically as a function of deviations outside this band [34]. A special situation called *temperature reference tracking* occurs when the comfort band is reduced to a single target temperature T_{Set}. In this situation, J_d can be written as

$$J_d = \int_0^{t_h} \theta_{occ} (T_{Zon} - T_{Set})^2 \mathrm{d}t \tag{4}$$

where T_{Zon} is the actual zone temperature and $\theta_{occ} = 1$ during occupation and $\theta_{occ} = 0$ elsewhere. In the case study, both hard constraints and temperature reference tracking are implemented.

The prediction horizon t_h and flexibility interval $[t_i - t_e]$ have to be set. It is important to set t_h large enough to take into account all effects of the control on the system, also for processes with large time constants. Typical values for t_h are 4 to 15 days. The flexibility interval is chosen somewhere in the beginning of the interval $[0 - t_h]$.

From the solution of this optimisation problem we obtain on the one hand the total operational cost over the prediction horizon $J_{c,ref}$ and on the other hand the electricity consumption *during the flexibility interval*, E_{ref} from Eq. (5).

$$E = \int_{t_i}^{t_e} P_e \mathrm{d}t \tag{5}$$

3.5. Flexibility range

Starting from the reference scenario, we now compute the minimum and maximum possible power use during the flexibility interval. We can do so by modifying the objective from Eq. (3) to

$$J = J_c + \gamma J_d + \varphi J_f \tag{6}$$

where φ is a weighting factor and J_f is the flexibility objective formulated as

$$J_f = \left(\int_{t_i}^{t_e} P_e \mathrm{d}t - E_{target} \right)^2 = (E - E_{target})^2 \tag{7}$$

In this equation, E_{target} is the target electricity consumption during the flexibility interval. With the new formulation of J, the solver will try to obtain a predefined electricity use E_{target} during the flexibility interval while maintaining the aims to guarantee thermal comfort and to minimize the electricity cost during the whole prediction horizon.

The maximal and minimal consumption are obtained by setting E_{target} to zero or a high value respectively. The high value is the maximal reachable load, obtained as the sum of the nominal power of all controllable loads. Equation (5) is used to compute the modified electricity consumption E_{max} and E_{min} and then we obtain the maximal positive and negative flexibility $\Phi_\uparrow$ and $\Phi_\downarrow$ with

$$\Phi_\uparrow = E_{max} - E_{ref} \geq 0 \tag{8a}$$
$$\Phi_\downarrow = E_{min} - E_{ref} \leq 0 \tag{8b}$$

Similarly, the modified total cost J_c is obtained from Eq. (2) which leads to the relative costs $\Gamma_\uparrow$ and $\Gamma_\downarrow$ with

$$\Gamma_\uparrow = J_{c,max} - J_{c,ref} \geq 0 \tag{9a}$$
$$\Gamma_\downarrow = J_{c,min} - J_{c,ref} \geq 0 \tag{9b}$$

It can be seen that the relative costs will always be positive.

3.6. Cost curves

The flexibility range can be graphically represented in a cost curve, shown in Figure 1. The costs curve shows the flexibility Φ on the horizontal axis and the corresponding cost Γ on the vertical axis. The point associated with the reference control strategy is located in the origin. The two points $(\Phi_\uparrow, \Gamma_\uparrow)$ and $(\Phi_\downarrow, \Gamma_\downarrow)$ show how much the load can maximally increase respectively decrease in the flexibility interval compared to the reference, and at which absolute cost.

It can be anticipated that intermediate deviations from the reference scenario will not lie on a straight line between the origin and the extremes. Moreover, it is possible that some intermediate consumption deviations cannot be reached due to discrete power levels in the control

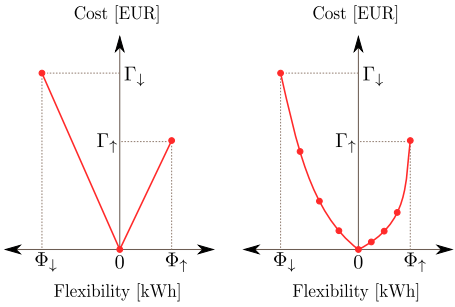

Figure 1: Principle of cost curves without (left) and with intermediate points (right).

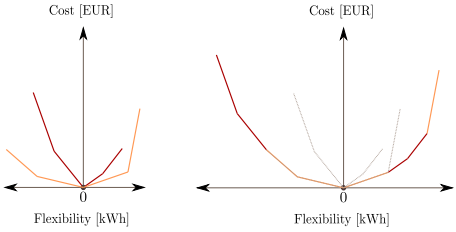

Figure 2: Aggregation of two separate cost curves (left) into a total cost curve for the combination of both systems (right).

(like on/off instead of modulation). Therefore, it may be useful to investigate intermediate flexibility points inside the range $[\Phi_\downarrow, \Phi_\uparrow]$. They are obtained by solving the OCP with E_{target} in Eq. (7) set to the desired intermediate flexibility.

Most often, delivering less flexibility than $\Phi_\downarrow$ or $\Phi_\uparrow$ will be possible at lower specific costs. As the specific cost, in €/ kWh, corresponds to the gradient of the cost curve, a convex curve indicates an increase of the specific costs with increased delivery of flexibility. This is illustrated in Figure 1 on the right hand side.

3.7. Aggregation

An interesting feature of cost curves is that they can easily be aggregated to represent the flexibility of a system that is composed of different subsystems, like a VPP. As an example, the aggregation of two different cost curves is shown in Figure 2.

The aggregation is based on a piecewise sum of line segments, sorted according to their slope. This methodology can easily be scaled up to aggregation of multiple

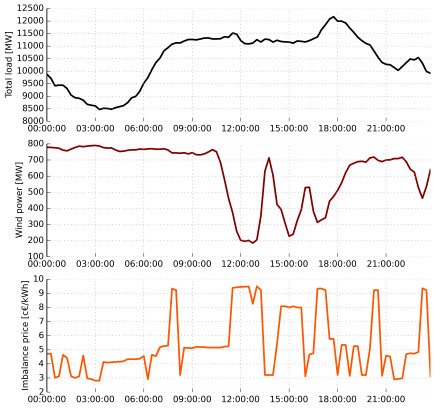

Figure 3: Belgian grid data for 8^{th} of January 2015 showing total load (top), wind electricity generation (center) and imbalance price (bottom). The imbalance price is the average value of positive and negative imbalance prices. Source: Elia [35].

cost curves, and in different levels. It is clear that an aggregated system can provide more flexibility than a single system. Also, by aggregating systems it is often possible to offer flexibility at a lower cost.

4. Case study

4.1. Objective

The methodology presented in Section 3 is applied to an existing office building in Brussels, Belgium, called the Kalkkaai building. To maintain the interactions between weather data, time and user behaviour, the case study is based on monitoring data of Thursday 8^{th} of January 2015 and the results are linked to the grid situation of this day as obtained from the Belgian electricity transmission system operator Elia [35].

Figure 3 shows the total load for Belgium, the electricity generation from wind power and the mean value of the positive and negative imbalance prices. The figure shows that the peak power consumption occurs between 17h and 19h local time. The figure also illustrates the variability of the wind power production and of the imbalance prices. The latter seem partly correlated to the wind power production, but this relation has not been investigated further.

This case study aims at identifying the flexibility of the building throughout this day and in particular during

Figure 4: View of the Kalkkaai building, west façade.

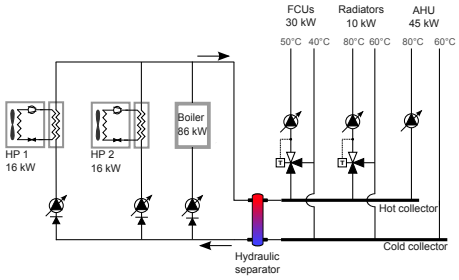

Figure 5: Hydraulic scheme of the heating system with indications of nominal thermal power. HP1 and HP2 are the heat pumps, FCU stands for fan coil unit and AHU for air handling unit.

the evening power peak. The flexibility costs can be compared to the imbalance prices and other measures to mitigate the peak.

4.2. Kalkkaai building

The Kalkkaai building is the headquarter of 3E, located in Brussels, Belgium. It is composed of two floors of about 480 m^2 each and hosts 40-70 people. The building's HVAC and internal zoning has been refurbished in 2013.

Figure 4 shows the west façade of the building. The large windows together with the open space in front makes this façade sensitive for solar gains and conductive heat losses. The other façades oriented east and south are closer to the neighbouring buildings and have relatively more shadow and less windows.

An overview of the heat production, distribution and emission systems is given in Figure 5.

The heat production is covered by a condensing gas boiler (nominal power of 87 kW) and two identical air-to-water heat pumps of 16 kW_{th} each. These three production units are operated in a cascade system.

The heat distribution consists of 3 circuits:

1. fan coil units (FCU) in all office spaces,
2. radiators (in toilets and entrance),
3. air handling unit (AHU).

The building is occupied on weekdays during typical office hours, but large occupancy variation is not unusual. The occupants have manual control over the lighting and temperature setting in each of the rooms.

The building is used as a field test for model predictive control (MPC). The control variables in the current setup are the thermal power produced by each of

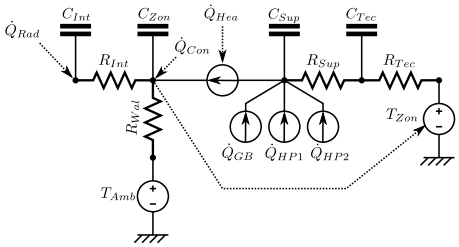

Figure 6: Overview of the control model for MPC and flexibility assessment.

the three heat production units. The MPC cannot control the heat consumption of the building directly because the FCUs are manually controlled by the occupants. This case study makes use of the control model derived for MPC to compute the flexibility. More details about this model are presented below.

4.3. Control model

A grey-box control model has been identified with the *Grey-Box Buildings* toolbox of De Coninck et al. [36]. It is impossible to create a multi-zone model with the available monitoring data because the heat consumption is only measured at building level. To obtain a single-zone model, all room temperature measurements are averaged into T_{Zon}. As described in [36], a forward selection method is applied that starts from a first order model and gradually increases complexity until no further improvements in simulation performance can be obtained on the cross-validation dataset. A schematic presentation of the resulting model is given in Figure 6.

The model has four states: two in the building (C_{Zon} for zone air and C_{Int} for internal mass) and two in the heating system (C_{Sup} for supply water and C_{Tec} for the technical room). The radiative part of internal gains is represented by $\dot{Q}_{Rad}$ and the convective gains/losses of internal gains and the AHU are represented by $\dot{Q}_{Con}$. The heat consumption of the building is $\dot{Q}_{Hea}$ and the produced heat of the boiler and both heat pumps is $\dot{Q}_{GB}$, $\dot{Q}_{HP1}$ and $\dot{Q}_{HP2}$. There are four thermal resistances, R_{Int}, R_{Wal}, R_{Sup} and R_{Tec}. T_{Amb} is the ambient temperature, obtained from a local measurement.

The on/off schedule for the AHU is obtained from the electricity consumption measurement of the AHU and the mass flow rate has been estimated in the parameter estimation process.

The model does not take into account solar gains. The reason is that during the system identification process, the solar radiation input was not retained as a significant disturbance. This result is explained by the relatively low glazing fraction (except for the west façade), the shading due to neighbouring buildings, and the use of an identification data set with monitoring data of December 2014 and January 2015.

Internal gains are generated by the use of electrical appliances and body heat gains. A separate measurement of plug power and lighting power is available. This measurement is used for internal gains from appliances. Unfortunately, there is no direct measurement of occupancy. However, as plug power is correlated to occupancy (more than lighting because of the large lighting circuits in landscape offices), we derive an occupancy profile from the plug power measurement. The standby power consumption is subtracted by supposing an occupancy of zero persons every night at 00h00.

Figure 6 only represents the dynamic heat transfer processes. The gas consumption $\dot{P}_g$ of the condensing boiler and electricity consumption of both heat pumps $\dot{P}_{HP1}$ and $\dot{P}_{HP2}$ are computed from equations for the boiler efficiency η and the coefficient of performance (COP) of the heat pumps, COP_{HP1} and COP_{HP2}. These efficiency models are obtained by linear regression on the monitoring data based on the following predictors: T_{Sup}, T_{Amb} and the produced thermal power [37]. A forward selection is applied to avoid overfitted models. The resulting performance curves are

$$\eta = 0.813 - 1.60e^{-6}\dot{Q}^*_{GB} \tag{10a}$$

$$COP_{HP1} = 2.86 + 0.10T^*_{Amb} - 3.61e^{-2}T^*_{Sup} - 3.87e^{-3}T^*_{Amb}T^*_{Sup} \tag{10b}$$

$$COP_{HP2} = 2.57 + 3.27e^{-2}T^*_{Amb} - 2.30e^{-2}T^*_{Sup} \tag{10c}$$

In these equations, the predictor variables are relative values in order to obtain physically meaningful results for the intercept:

$$\begin{aligned}\dot{Q}^*_{GB} &= \dot{Q}_{GB} - 86000\\ T^*_{Amb} &= T_{Amb} - (7 + 273.15)\\ T^*_{Sup} &= T_{Sup} - (35 + 273.15)\end{aligned}$$

It is noteworthy that both heat pumps, though identical, have a different performance model. The OCP will exploit these differences.

4.4. Optimal control

This subsection details the implementation of the OCP presented by Eq. (1). The control variable u is composed of $\dot{Q}_{GB}$, $\dot{Q}_{HP1}$, $\dot{Q}_{HP2}$ and $\dot{Q}_{Hea}$. Although it is impossible to control the heat consumption of the building $\dot{Q}_{Hea}$ due to the manual operation of the heat emission systems, this input is required for the model to control the thermal comfort in the building. Constraints are put on the positive derivatives of $\dot{Q}_{GB}$, $\dot{Q}_{HP1}$ and $\dot{Q}_{HP2}$ to stabilise the control signals and take into account inertia in the heat production. The maximum thermal power of the boiler and electrical power of the heat pumps is limited. Finally, a constraint of 80 °C is put on T_{Sup}.

The objective function takes the form of Eq. (6) with $T_{Set} = 21.8\,°C$ (reference tracking). This comfort set point is obtained by trial and error on the real building in order to obtain good thermal comfort in each of the zones.

The following tariffs apply to the Kalkkaai building: $c_g = 4.3458\,c€/kWh$, $c_e = 7.323\,c€/kWh$ or $9.431\,c€/kWh$ for low respectively high tariff hours. The high tariff applies every work day between 8h and 23h. The prediction horizon t_h is 4 days.

The numerical solution of the OCP is obtained with JModelica.org [38]. Direct collocation is used to discretise time, which reduces the optimisation problem to a nonlinear program (NLP)[39]. JModelica.org utilises third-party NLP solvers, which require first- and second-order derivatives of all expressions in the NLP with respect to all decision variables. CasADi is used to obtain these by algorithmic differentiation [40]. We used the NLP solver IPOPT with the sparse linear solver MA27 from HSL [41, 42]. The collocation elements are placed on a regular grid with 15 minutes interval and two collocation points per element.

Before we compute the flexibility, it is interesting to visualise the reference operation for the Kalkkaai building on the 8th of January 2015. Figure 7 shows the most

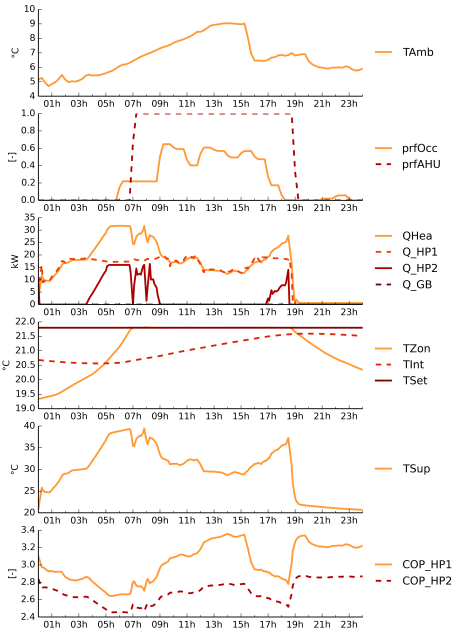

Figure 7: Overview of the reference scenario for 8^{th} of January 2015. $prfOcc$ and $prfAHU$ are profiles for the occupancy and AHU (base 1).

important trajectories obtained by solving the OCP for the reference scenario.

We can see that HP1 is operating at full load during this entire period while HP2 works at part load. In the next section we will investigate the flexibility during the evening peak between 17h and 19h.

5. Results and discussion

We first present the cost curve with temperature reference tracking and then with a comfort band with hard constraints. Next we analyse how the flexibility is influenced by adding a thermal energy storage. We then analyse the evolution of $\Phi_{\downarrow}, \Phi_{\uparrow}, \Gamma_{\downarrow}$ and $\Gamma_{\uparrow}$ over the entire day. This section is ended with a comparison between the flexibility costs and the imbalance price in the Belgian power system.

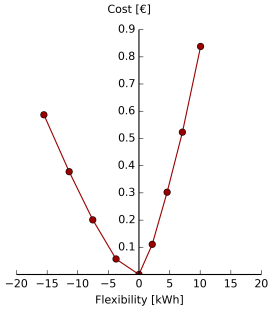

Figure 8: Cost curve for flexibility interval between 17h and 19h on the 8^{th} of January 2015 with reference temperature tracking.

5.1. Reference temperature tracking

The cost curve for the flexibility between 17h and 19h on the 8^{th} of January 2015 is shown in Figure 8. The building has both positive and negative flexibility.

How the system is controlled for delivering the maximum positive flexibility is shown in Figure 9. Due to the reference tracking, the controller is not allowed to increase the temperature in the building. The flexibility is obtained by activating both heat pumps at maximal power and using the capacity of the supply water as temporary buffer. It is clear that this strongly decreases the COP of both heat pumps.

To deliver negative flexibility during this load peak, the system stops both heat pumps and starts the gas boiler instead. This is visualised in Figure 10. In this hybrid system, this is always possible when the reference control chooses to use the heat pumps.

5.2. Comfort band

To assess the effect of temperature reference tracking, a flexibility cost curve with comfort band limiting T_{Zon} between 21.8 °C and 23.5 °C is shown in Figure 11. By choosing the lower comfort boundary to be identical to T_{Set} of the reference tracking, we enforce the same thermal comfort. Figure 11 shows that also the flexibility is identical, but the cost of the positive flexibility is about 20 % lower compared to reference tracking.

As shown in Figure 12 this is achieved by increasing T_{Zon}, or in other words, by using passive thermal energy storage in the thermal mass of the building. T_{Sup} also has to increase in order to be able to deliver this higher thermal power to the building, but the increase is less pronounced and thus the COP of the heat pumps is less

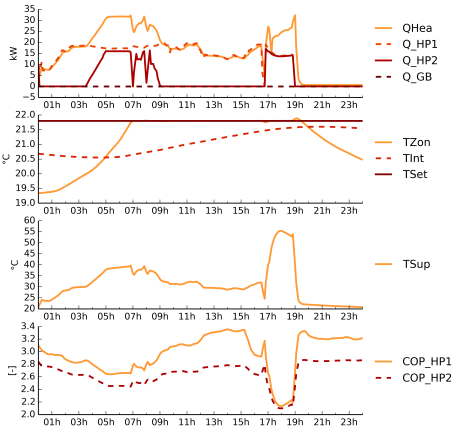

Figure 9: Control for offering maximum positive flexibility with reference temperature tracking.

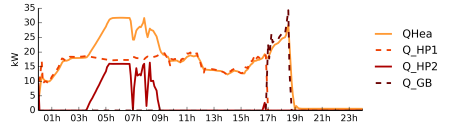

Figure 10: Control for offering maximum negative flexibility with reference temperature tracking.

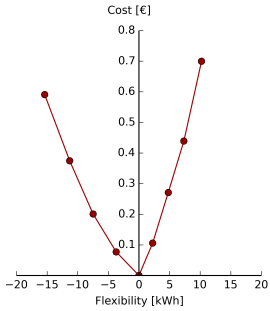

Figure 11: Cost curve for flexibility interval between 17h and 19h on the 8^{th} of January 2015 with comfort band instead of reference tracking.

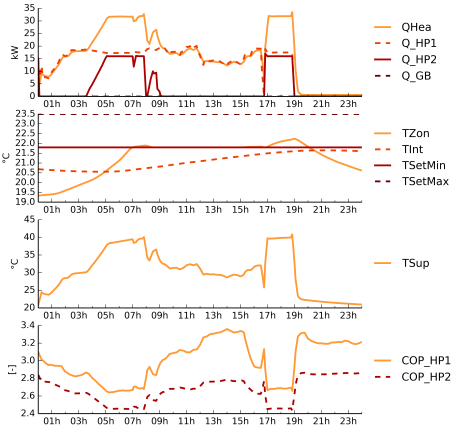

Figure 12: Control for offering maximum positive flexibility with a comfort band.

reduced. Additionally, this increase of T_{Zon} will slightly reduce the heat requirements for the next day thanks to the slow time constant of C_{Int}. This illustrates the importance of taking sufficiently long prediction horizons in order to correctly assess the total costs of the DR actions.

5.3. Active thermal energy storage

The flexibility of buildings is often attributed to active thermal energy storage (TES), for instance in hot water tanks [43]. In the technical room of the Kalkkaai building, two tanks of 1000 L each are installed. These tanks have not been used up to now. We use this case study to assess the impact of these buffers on the flexibility of the Kalkkaai building.

The model of Figure 6 is extended with a single capacity that lumps the storage capacity of both tanks. The thermal losses of the tanks are connected to the technical room. An additional control variable $\dot{Q}_{Tes}$ is required to represent charging (positive) and discharging (negative) of the water buffer.

The resulting cost curve is plotted in Figure 13 (curve C). We can clearly see that TES reduces the cost of flexibility. The flexibility range also shifts towards positive flexibility. This is explained by a different reference scenario when using the TES tanks: the system has buffered a small quantity of heat during the day for use between 17h and 19h. By consequence, the reference electricity consumption in the flexibility interval is

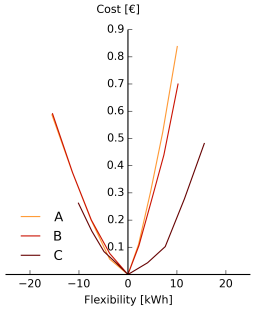

Figure 13: Cost curve comparison for Kalkkaai building with flexibility interval between 17h and 19h on the 8^{th} of January 2015. (A) reference tracking, (B) comfort band, (C) reference tracking with TES.

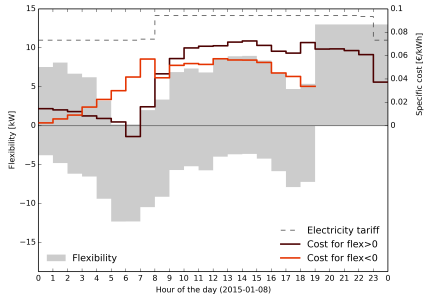

Figure 14: Daily flexibility availability for the 8^{th} of January 2015 with flexibility interval of 1h for the scenario with reference temperature tracking. The negative value for $\Gamma_{\uparrow}$ at 06h00 is a numeric artefact caused by small relative differences.

smaller, leading to less negative and more positive flexibility.

5.4. Temporary evolution of flexibility

The cost curves are snapshots: they represent flexibility at a very specific moment with specific boundary conditions like building use and weather. We can get an overview of the evolution of flexibility through time by plotting the minimum and maximum flexibility indicators ($\Phi_{\downarrow}, \Phi_{\uparrow}, \Gamma_{\downarrow}, \Gamma_{\uparrow}$) in a single graph.

An example is shown in Figure 14. This graph shows the evolution of the flexibility and *specific* costs (in c€/kWh). The electricity tariff is added as a reference.

Both flexibility and costs vary widely throughout the day. The specific costs lie between zero and 7.5 c€/kWh with negative flexibility being slightly cheaper. Beside the wide spread, an important conclusion from this graph is that the average cost of flexibility is not negligible. Nevertheless, depending on the convexity of the cost curve, intermediate levels of flexibility may be considerably cheaper than the extreme ones presented here.

By analysis of the results, we have identified several influencing factors for the given heating system. The ambient temperature has a significant effect on the results. Firstly via its dominant impact on the heat demand of the building and secondly via its effect on the heat pump COP. As the method is cost-based, the electricity tariff has an important impact on both the flexibility and the costs. The time of the day and occupancy profile of the building influence how useful a load shift or increase of internal energy is. Finally, the results are

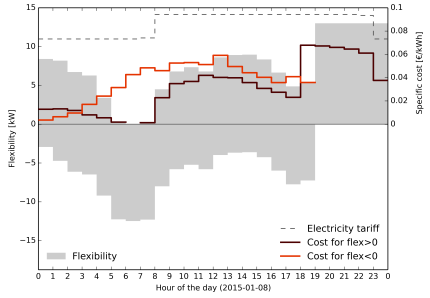

Figure 15: Daily flexibility availability for the 8^{th} of January 2015 with flexibility interval of 1h for the scenario with comfort band.

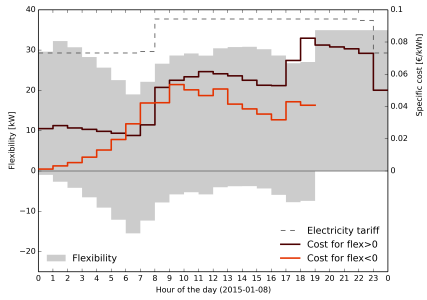

Figure 16: Daily flexibility availability for the 8^{th} of January 2015 with flexibility interval of 1h for a scenario with a comfort band, without gas boiler.

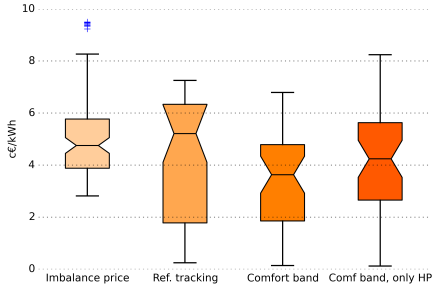

Figure 17: Comparison of imbalance price and flexibility costs $\Gamma_{\downarrow}$ and $\Gamma_{\uparrow}$ for the Kalkkaai building on the 8^{th} of January 2015 with flexibility interval of 1h for different scenarios.

affected by the control freedom to change thermal comfort in the building.

Figure 15 shows the equivalent graph for the scenario with a comfort band. We observe that allowing the activation of building thermal mass reduces the costs for positive flexibility by almost 50 % during the occupied hours.

Figure 16 shows the results for a new scenario in which the hybrid heating system of the Kalkkaai is replaced by a monovalent heat pump system. For simplicity, we have used the COP model of HP1 as presented in Eq. (10b) and upscaled the power of the heat pump to 86 kW. A thermal comfort band with hard constraints is implemented. As expected, the main difference is the increase of positive flexibility that can be delivered. Simultaneously, we observe an increase in the maximum cost.

Even when activating building thermal mass is possible, flexibility is not for free: each thermal load shift has an associated cost. If that would not be the case, the reference scenario is not optimal and there is a potential for reducing the energy costs in the reference control of the system.

5.5. Benchmarking the cost of flexibility in buildings

We have shown that the cost of flexibility in buildings depends on many factors and varies widely through the day and year. We would need to apply the methodology to a large set of buildings in order to get a better understanding of the mean and variance of the flexibility costs.

Nevertheless, this case study allows comparing the flexibility costs of the Kalkkaai building with the known imbalance price on the 8^{th} of January 2015. Figure 17 shows this comparison by means of boxplots of $\Gamma_{\downarrow}$ and $\Gamma_{\uparrow}$ for different scenarios and for the imbalance price.

The figure shows that the mean of the imbalance price and flexibility costs $\Gamma_{\downarrow}$ and $\Gamma_{\uparrow}$ have the same order of magnitude, but with lower quantiles for the flexibility costs. This means that there are several hours during which the Kalkkaai building could offer its flexibility at a significantly lower cost than the imbalance price. The graph also clearly shows the impact of a moderate activation of thermal mass in the building: the mean flexibility cost for the scenario with comfort band is lower than with reference tracking.

As mentioned before, Figure 17 is based on $\Gamma_{\downarrow}$ and $\Gamma_{\uparrow}$, the costs for delivering the minimum and maximum flexibility $\Phi_{\downarrow}$ and $\Phi_{\uparrow}$. If the cost curves are convex, the costs for delivering intermediate levels of flexibility can be considerably lower.

6. Conclusion

We have developed a methodology to quantify flexibility in buildings. The methodology returns on the one hand the amount of energy that can be shifted to or from a specified flexibility interval and on the other hand the costs associated with this load shifting. This information is presented in a cost curve, allowing easy comparison between buildings and aggregation of flexibility.

The methodology is based on the solution of multiple optimal control problems with a suitable building model. The reference scenario is an optimally con-

trolled building with regard to thermal comfort and operational costs. Therefore, load shifting will always result in a higher cost for the building operator.

A case study on an office building in Brussels reveals that these costs are not negligible. If the studied building would have shifted its load on the 8^{th} of January 2015, the costs would have been slightly lower than the recorded imbalance price for the Belgian power system. However, it is shown that replacing the temperature tracking strategy by an allowed comfort band, the flexibility costs decrease. Adding a moderately sized thermal energy storage tank would further decrease these costs. Finally, offering less flexibility than the maximum potential $\Phi_{\uparrow}$ and $\Phi_{\downarrow}$ is often possible at lower specific costs due to the convexity of the cost curve.

The two main findings of the case study are firstly the large spread in both flexibility and costs and secondly the confirmation that flexibility in buildings is not for free. Load shifting may come at zero costs for household appliances, but for thermal systems in buildings the costs of flexibility are computable and should be taken into account.

Acknowledgment

The authors gratefully acknowledge the following projects and institutes for supporting this work:

- the FP7 project *PerformancePlus* funded by the European Commission (KU Leuven, contract nb. 308991),
- the project *Optimal energy networks for buildings* funded by the KU Leuven Energy Institute (KU Leuven),
- *Flexipac* funded by the Région Wallonne, DGO4 (3E, contract nb. 1250570).

Bibliography

[1] G. Chicco, P. Mancarella, Distributed multi-generation: A comprehensive view, Renewable and Sustainable Energy Reviews 13 (3) (2009) 535–551.

[2] D. S. Callaway, I. a. Hiskens, Achieving Controllability of Electric Loads, Proceedings of the IEEE 99 (1) (2011) 184–199. doi:10.1109/JPROC.2010.2081652.

[3] D. S. Kirschen, Demand-side view of electricity markets, IEEE Transactions on Power Systems 18 (2) (2003) 520–527. doi:10.1109/TPWRS.2003.810692.

[4] G. Strbac, Demand side management: Benefits and challenges, Energy Policy 36 (12) (2008) 4419–4426. doi:10.1016/j.enpol.2008.09.030.

[5] G. S. Pavlak, G. P. Henze, V. J. Cushing, Optimizing commercial building participation in energy and ancillary service markets, Energy and Buildings 81 (2014) 115–126. doi:10.1016/j.enbuild.2014.05.048.

[6] P. Zhao, G. P. Henze, S. Plamp, V. J. Cushing, Evaluation of commercial building HVAC systems as frequency regulation providers, Energy and Buildings 67 (2013) 225–235. doi:10.1016/j.enbuild.2013.08.031.

[7] D. Wang, S. Parkinson, W. Miao, H. Jia, C. Crawford, N. Djilali, Hierarchical market integration of responsive loads as spinning reserve, Applied Energy 104 (2013) 229–238. doi:10.1016/j.apenergy.2012.10.054.

[8] D. Wang, S. Parkinson, W. Miao, H. Jia, C. Crawford, N. Djilali, Online voltage security assessment considering comfort-constrained demand response control of distributed heat pump systems, Applied Energy 96 (2012) 104–114. doi:10.1016/j.apenergy.2011.12.005.

[9] C. Gellings, The concept of demand-side management for electric utilities, Proceedings of the IEEE 73 (10) (1985) 1468–1470.

[10] P. Palensky, D. Dietrich, Demand Side Management: Demand Response, Intelligent Energy Systems, and Smart Loads, Industrial Informatics, IEEE Transactions on 7 (3) (2011) 381–388. doi:10.1109/TII.2011.2158841.

[11] M. Petersen, K. Edlund, L. Hansen, J. Bendtsen, J. Stoustrup, A taxonomy for modeling flexibility and a computationally efficient algorithm for dispatch in smart grids, in: American Control Conference (ACC), 2013, IEEE, Washington, DC, 2013, pp. 1150–1156.

[12] J. Cochran, M. Miller, O. Zinaman, M. Milligan, D. Arent, B. Palmintier, M. O'Malley, S. Mueller, E. Lannoye, A. Tuohy, Others, Flexibility in 21st Century Power Systems, Tech. rep., National Renewable Energy Laboratory (NREL), Golden, CO. (2014).

[13] A. I. Cohen, C. C. Wang, An optimization method for load management scheduling, IEEE Transactions on Power Systems 3 (2) (1988) 612–618.

[14] A. Rabl, L. Norford, Peak load reduction by preconditioning buildings at night, International Journal of Energy Research 15 (9) (1991) 781–798.

[15] R. Halvgaard, N. K. Poulsen, H. Madsen, J. B. Jorgensen, Economic model predictive control for building climate control in a smart grid, in: Innovative Smart Grid Technologies (ISGT), 2012 IEEE PES, 2012, pp. 1–6. doi:10.1109/ISGT.2012.6175631.

[16] G. Reynders, T. Nuytten, D. Saelens, Potential of structural thermal mass for demand-side management in dwellings, Building and Environment 64 (2013) 187–199. doi:10.1016/j.buildenv.2013.03.010.

[17] P. Sreedharan, D. Miller, S. Price, C. Woo, Avoided cost estimation and cost-effectiveness of permanent load shifting in California, Applied Energy 96 (2012) 115–121. doi:10.1016/j.apenergy.2011.08.029.

[18] D. Six, J. Desmedt, D. Vanhoudt, J. Van Bael, Exploring the flexibility potential of residential heat pumps combined with thermal energy storage for smart grids, in: 21st International Conference on Electricity Distribution, no. 0442, Frankfurt, 2011, pp. 6–9.

[19] W. Cardinaels, I. Borremans (Eds.), Demand Response for Families - Linear Final Report, EnergyVille, Genk, 2014.

[20] T. Nuytten, B. Claessens, K. Paredis, J. V. Bael, D. Six, Flexibility of a combined heat and power system with thermal energy storage for district heating, Applied Energy 104 (2013) 583–591. doi:10.1016/j.apenergy.2012.11.029.

[21] R. Belhomme, E. al., ADDRESS technical and commercial con-

ceptual architectures, in: Deliverable 1.1, 2009, Ch. 3.5.3, p. 85.
[22] C. De Jonghe, Short-term demand response in electricity generation planning and scheduling - Facilitating wind power integration, Ph.D. thesis, KU Leuven (2011).
[23] N. Venkatesan, J. Solanki, S. K. Solanki, Residential Demand Response model and impact on voltage profile and losses of an electric distribution network, Applied Energy 96 (2012) 84–91. doi:10.1016/j.apenergy.2011.12.076.
[24] K. Bruninx, D. Patteeuw, E. Delarue, L. Helsen, W. D'haeseleer, Short-Term Demand Response Of Flexible Electric Heating Systems: The Need For Integrated Simulations, in: 10th International Conference on the European Energy Market (EEM), Stockholm, Sweden, 2013, pp. 1–10. doi:10.1109/EEM.2013.6607333.
[25] S. D. J. McArthur, E. M. Davidson, V. M. Catterson, A. L. Dimeas, N. D. Hatziargyriou, F. Ponci, T. Funabashi, Multi-agent systems for power engineering applications - part 1 : Concepts, approaches and technical challenges, IEEE Transactions on Power Systems 22 (4) (2007) 1743–1752.
[26] K. Kok, Z. Derzsi, J. Gordijn, M. Hommelberg, C. Warmer, R. Kamphuis, H. Akkermans, Agent-Based Electricity Balancing with Distributed Energy Resources - A Multiperspective Case Study, Proceedings of the 41st Annual Hawaii International Conference on System Sciences (HICSS 2008) (2008) 173–173doi:10.1109/HICSS.2008.46.
[27] Z. Zhou, W. K. V. Chan, J. H. Chow, Agent-based simulation of electricity markets: a survey of tools, Artificial Intelligence Review 28 (4) (2009) 305–342. doi:10.1007/s10462-009-9105-x.
[28] T. Rajeev, S. Ashok, Dynamic load-shifting program based on a cloud computing framework to support the integration of renewable energy sources, Applied Energy 146 (2015) 141–149. doi:10.1016/j.apenergy.2015.02.014.
[29] M. Braun, P. Strauss, A review on aggregation approaches of controllable distributed energy units in electrical power systems, International Journal of Distributed Energy Resources 4 (4) (2008) 297–319.
[30] D. Pudjianto, C. Ramsay, G. Strbac, Virtual power plant and system integration of distributed energy resources, Renewable Power Generation 1 (1) (2007) 10–16. doi:10.1049/iet-rpg.
[31] I. Bel, A. Valenti, J. Maire, J. Corera, P. Lang, Innovative operation with aggregated distributed generation, in: Proceedings of the 19th Conference on Electricity Distribution (CIRED), no. 0461, Vienna, 2007, pp. 21–24.
[32] R. De Coninck, L. Helsen, Bottom-up quantification of the flexibility potential of buildings, in: Building Simulation, 13th International Conference of the International Building Performance Simulation Association, IBPSA, Aix-les-Bains, France, 2013.
[33] F. Oldewurtel, D. Sturzenegger, G. Andersson, M. Morari, R. S. Smith, Towards a standardized building assessment for demand response, in: Proceedings of the IEEE Conference on Decision and Control, IEEE, Firenze, Italy, 2013, pp. 7083–7088. doi:10.1109/CDC.2013.6761012.
[34] C. Verhelst, Model Predictive Control of Ground Coupled Heat Pump Systems for Office Buildings, Ph.D. thesis, KU Leuven (2012).
[35] Elia, Elia grid load, `http://www.elia.be/en/grid-data/data-download`, accessed: 2015-02-12.
[36] R. De Coninck, F. Magnusson, J. Åkesson, L. Helsen, Development and validation of grey-box building models for forecasting and control, Journal of Building Performance Simulation (Submitted on 24/12/2014).
[37] S. Seabold, J. Perktold, Statsmodels: econometric and statistical modeling with python, in: Proceedings of the 9th Python in Science Conference (Scipy 2010), 2010, pp. 57–61.
[38] J. Åkesson, K.-E. Årzén, M. Gäfvert, T. Bergdahl, H. Tummescheit, Modeling and optimization with Optimica and JModelica.org - Languages and tools for solving large-scale dynamic optimization problems, Computers & Chemical Engineering 34 (11) (2010) 1737–1749. doi:10.1016/j.compchemeng.2009.11.011.
[39] F. Magnusson, J. Åkesson, Collocation Methods for Optimization in a Modelica Environment, in: 9th International Modelica Conference, Munich, Germany, 2012.
[40] J. Andersson, J. Åkesson, M. Diehl, CasADi - A symbolic package for automatic differentiation and optimal control, in: S. Forth, P. Hovland, E. Phipps, J. Utke, A. Walther (Eds.), Recent Advances in Algorithmic Differentiation, Lecture Notes in Computational Science and Engineering, Springer, Berlin, 2012.
[41] A. Wächter, L. T. Biegler, On the Implementation of a Primal-Dual Interior Point Filter Line Search Algorithm for Large-Scale Nonlinear Programming, Mathematical Programming 106 (1) (2006) 25–57.
[42] HSL, A collection of Fortran codes for large scale scientific computation, `http://www.hsl.rl.ac.uk`, accessed: 2015-01-14.
[43] A. Arteconi, N. Hewitt, F. Polonara, State of the art of thermal storage for demand-side management, Applied Energy 93 (2012) 371–389. doi:10.1016/j.apenergy.2011.12.045.

5.3 Conclusion

The approach to quantify flexibility is based on the idea of a reference operation, the plan, and a deviation of the plan. Computing different deviations of the plan results in a potential for demand shifting and an additional cost compared to the plan. This information can be represented on a cost curve. The cost curves offer the advantage of visual comparison between different buildings and an easy aggregation of different buildings.

The case study on the KK building shows that for a given building, the flexibility is largely time dependent. Both the amount and cost of flexibility vary widely during a single day, and more variation is expected on a seasonal scale. However, the flexibility is often cheaper than the imbalance price at that moment. While flexibility may not be used directly in order to restore the imbalance, it may be used through aggregation to bid in any of the reserve markets. This chapter has shown that flexibility can be quantified and that the costs for DR on thermal systems in buildings have to be taken into account when this flexibility is offered to the energy or reserve markets.

Chapter 6

Application and validation of the tool chain to the KK building

This chapter is submitted for publication as:
R. De Coninck and L. Helsen, "Practical implementation and evaluation of model predictive control for an office building in brussels", *Energy and Buildings*, 2015, Submitted on 17/03/2015.

6.1 Introduction

This last chapter applies the tool chain as defined in Figure 2.1 to the pilot project of the KK building. The building and resulting grey-box model are presented, the MPC is detailed and the results are analysed by comparing monitored days with MPC control with monitored days with conventional, rule-based control (RBC).

6.2 Practical implementation and evaluation of model predictive control for an office building in Brussels

Practical implementation and evaluation of model predictive control for an office building in Brussels

Roel De Coninck[a,b,c,*], Lieve Helsen[a,c]

[a] *KU Leuven, Department of Mechanical Engineering, Celestijnenlaan 300 postbox 2421, 3001 Heverlee, Belgium*
[b] *3E nv, Kalkkaai 6, 1000 Brussels, Belgium*
[c] *EnergyVille, 3600 Waterschei, Belgium*

Abstract

A model predictive control (MPC) has been implemented in a medium-sized office building in Brussels, Belgium. This paper presents the implementation of the controller and the measured performance in comparison with the default, rule-based control (RBC). The building has two floors and a total size of 960 m^2. The controllable system is the hybrid heat production consisting of two air/water heat pumps and a condensing gas boiler. The practical situation does not allow controlling end-units in the different zones of the building. The MPC makes use of a Modelica grey-box control model resulting from a system identification with monitoring data. The paper covers the monitoring, model identification, forecasting of disturbances, state estimation, formulation and solving of the optimal control problem (OCP) and transmission of the control signals. The performance is evaluated on a daily basis based on analysis of heating degree days, thermal comfort, energy costs and primary energy consumption. The results show that the model predictive controller is able to provide a similar or better thermal comfort than the reference control while reducing the energy costs by more than 30 %. This is due among others, to a better use of the heat pumps and an adapted hot water supply temperature.

Keywords: model predictive control (MPC), grey-box models, field test, validation, Modelica

1. Introduction

Bad control of energy systems in buildings is responsible for large energy efficiency losses. Even in new and modern buildings, inefficient control and operation often increases the primary energy consumption for heating, cooling and air-conditioning (HVAC) by 20 % or more [1, 2].

Model predictive control (MPC) is one of several solutions to improve building control efficiency [3, 4, 5, 6, 7, 8, 9, 10]. By specifying high-level objectives and using the power of numerical optimization, a model predictive controller can automatically adapt to new operating conditions and take into account expected future building dynamics. The controller can also incorporate the delivery of additional services like reserves [11] or peak load reduction [12].

The core of the MPC concept is the optimal control problem (OCP). This mathematical problem is formulated in continuous time as

$$\underset{u}{\text{minimize}} \quad J \tag{1a}$$
$$\text{subject to} \quad F(t, \dot{x}, x, w, y, u) = 0, \tag{1b}$$
$$g(t, \dot{x}, x, y, u) = 0, \tag{1c}$$
$$h(t, \dot{x}, x, y, u) \geq 0, \tag{1d}$$
$$x(0) = x_0. \tag{1e}$$

In this formulation, $t \in [0, t_h]$ is time with t_h the prediction horizon, $u \in \mathbb{R}^n$ is the control signal, J the objective, $F(\cdot)$ is the system model with states x, algebraic variables y and disturbances w. $g(\cdot)$ and $h(\cdot)$ are additional equality and inequality constraints. $x, \dot{x}, w, y$ and u are all time-dependent but for readability we have omitted the time dependency notation.

MPC is based on the solution of an OCP at every control time step. The OCP is initialised from an estimated state of the system based on measurements (= feedback) and takes into account forecasted disturbances and dynamic system behaviour (= feedforward) [13].

Figure 1 shows a general overview of the MPC framework that will be detailed and implemented in Section 3.

*Corresponding author
Email address: roel.deconinck@3e.eu ()

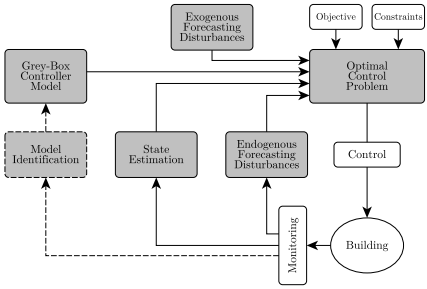

Figure 1: Overview of the MPC framework.

Figure 2: View of the Kalkkaai building, west façade.

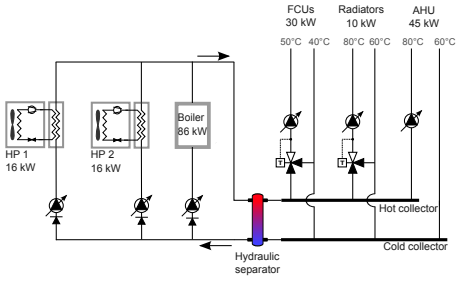

Figure 3: Hydraulic scheme of the heating system.

This paper describes the implementation of MPC in the Kalkkaai building, the headquarters of 3E in Brussels. The implementation with real operating conditions including measurement errors, controllability limitations, communication issues etc. is an important step in the validation of MPC as viable alternative for controlling real-life buildings. The MPC performance is compared to the conventional control algorithm during the winter of 2014-2015.

This paper is structured as follows. Section 2 gives a general overview of the field test, building and HVAC system and the controllable loads. Section 3 describes the implementation of the MPC by elaborating each step of the tool chain of Figure 1. The results are presented in Section 4. We compare operational costs, energy use and thermal comfort of the MPC with the conventional control. These results are discussed in more detail in Section 5 where we try to quantify the benefits of the new control strategy for the Kalkkaai building. Finally, Section 6 summarises the conclusions.

2. Field test Kalkkaai building

2.1. Building

The Kalkkaai building is the headquarter of 3E, situated in Brussels, Belgium. It is composed of two floors of about 480 m^2 each and hosts 40-70 people. The building's HVAC and internal zoning has been refurbished in 2013.

Figure 2 shows the west façade of the building. Despite the large windows, the solar gains are limited in the winter due to the west orientation and the shading of neighbouring buildings. The other façades have much less windows and are even more shaded by other buildings.

An overview of the heat production, distribution and emission systems is given in Figure 3.

The heat production is covered by a condensing gas boiler (nominal power of 86 kW) and two identical air/water heat pumps of 16 kW_{th} each. These three production units are operated in a cascade system.

The heat distribution consists of 3 circuits:

1. fan coil units (FCU) in all office spaces,
2. radiators (in toilets and entrance),
3. air handling unit (AHU).

The building is occupied on weekdays during typical office hours, but large occupancy variation is not unusual. The occupants have manual control over the lighting and temperature setting in each of the rooms.

2.2. Control system

Due to the manual control of the FCUs by the occupants, the building energy control and management system (BECMS) cannot control the heat consumption

of the building directly. The BECMS controls the hot water supply temperature T_{Sup} to influence the heat consumption indirectly. T_{Sup} is controlled according to a heating curve based on the ambient temperature, with indoor temperature compensation. A PI controller tracks this heating curve by controlling the total thermal power to be produced. An example of the resulting hot water supply temperature is given in Section 5, Figure 11. A specific cascade controller distributes this power set point over the three heat production units based on a comprehensive set of rules. This control is called the *rule-based control* (RBC).

Unfortunately, there is no high-level control of the AHU. The AHU is switched on/off according to a weekly schedule. The same schedule is applied to the hot water circulation pump to the heating coil. There is no feedback on the supply air temperature.

The implementation of MPC as high level control makes use of the BECMS for the low level control. By consequence, the limited controllability of heat supply and supply air temperature affects the MPC as much as the conventional control. The supplier of the BECMS allows to get and set any monitored or controlled variable directly by a file transfer protocol (FTP). The MPC uses this protocol to control the thermal power of the boiler and both heat pumps directly. How these control signals are computed is explained in the next section.

3. Implementation of the MPC tool chain

This section elaborates on the practical implementation of the model predictive controller. The different processes of Figure 1 are discussed in detail.

3.1. Monitoring

A Kairos time series database has been set up as central storage for all monitoring data, predictions and control set points. There are different sources for these data.

The BECMS monitors the heat production and distribution at the level of the technical room. There are measurements of several water temperatures, heat fluxes, natural gas consumption and different HVAC related electricity consumptions. The latter include submetering for each of the heat pumps and circulation pumps. All relevant monitoring data is extracted from the BECMS using the FTP every 15 s and stored in the Kairos database.

An independent system (from a different manufacturer) monitors the building. We refer to this as the building monitoring system (BMS). The BMS monitors room temperatures, relative humidities and electricity consumptions at building level. The latter include submetering for lighting (by floor), plug load (by floor), the server room, the chiller and AHU. The measured data is obtained by posting http requests on a webserver and parsing the returned json objects to upload the data to the Kairos database.

Weather data is obtained from a third source. Through collaboration in the EU FP7 project *PerformancePlus*, the university of Oldenburg, Germany provides both past weather data and weather forecasts [14, 15, 16]. These contain ambient temperature, solar radiation, wind speed and relative humidity. This data is posted on a specific FTP-server and processed to time-series that are stored in the Kairos database.

With all these different data sources and systems, the overall monitoring system is vulnerable for failures. Some failures are harmless and only generate extra manual work to recover data and store it in the database, others lead to unrecoverable data loss. Despite the use of different systems, some important variables are not monitored at all, like occupancy, CO_2 concentrations, the supply air temperature and the heat consumption of the individual rooms in the building. Also, the room air temperatures are measured at irregular intervals and obtained with delays of up to half an hour. These shortcomings will affect the options for modelling and control as we will see in the next paragraphs. Nevertheless, this represents the real world and it is important to analyse the MPC performance in real conditions.

3.2. Grey-box model identification

The MPC is based on a grey-box control model which has been identified with the *Grey-Box Buildings* toolbox of De Coninck et al. [17]. It is impossible to create a multi-zone building model with the available monitoring data because the heat consumption is only measured at building level. To obtain a single-zone model, all room temperature measurements are arithmetically averaged into T_{Zon}. A weighted averaging based on room size would physically be more meaningful, but the required meta-information will often not be readily available for many buildings. In order to demonstrate an MPC that is easily applicable to a wide variety of buildings, we try to limit the use of meta-information as much as possible.

A forward selection method is applied that starts from a first order model and gradually increases complexity until no further improvements in simulation performance can be obtained on the cross-validation dataset [17]. A schematic presentation of the resulting model is given in Figure 4.

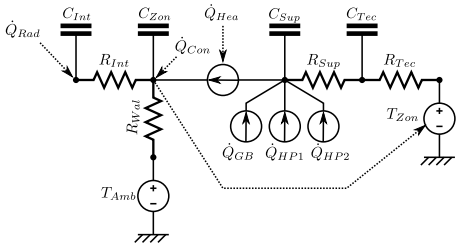

Figure 4: Schematic presentation of the control model for MPC.

The model has four states: two in the building (C_{Zon} for zone air and C_{Int} for internal mass) and two in the heating system (C_{Sup} for supply water and C_{Tec} for the technical room). The radiative part of internal gains is represented by $\dot{Q}_{Rad}$ and the convective gains/losses of internal gains and the AHU are represented by $\dot{Q}_{Con}$. The heat demand of the building is $\dot{Q}_{Hea}$ and the produced heat of the boiler and both heat pumps is $\dot{Q}_{GB}$, $\dot{Q}_{HP1}$ and $\dot{Q}_{HP2}$ respectively. There are four thermal resistances, R_{Int}, R_{Wal}, R_{Sup} and R_{Tec}. T_{Amb} is the ambient temperature, obtained from a local measurement.

The model does not take into account solar gains. The reason is that during the system identification process, the solar radiation input was not retained as a significant disturbance. This result is explained by the relatively low glazing fraction (except for the west façade), the shading due to neighbouring buildings, and the use of an identification data set with monitoring data of December 2014 and January 2015. The control model is therefore only valid for the winter season, but this is sufficient for this case study. Future research will consider the adaptation of the control model over different seasons.

Internal gains are generated by the use of electrical appliances and body heat gains. For the use of electrical appliances we chose a top-down approach. Starting from the total electricity consumption of the building, we subtract all sub-meters we consider not to correspond to internal gains. For the Kalkkaai building these are the sub-meters for the HVAC system and the servers. A bottom-up approach would only take into account the sub-meters we think correlated with internal gains. By consequence, a top-down approach is a maximum estimator of internal gains from equipment and a bottom-up approach a minimum estimator.

There are no direct measurements of internal gains generated by body heat transfer nor of occupancy. However, as plug power is correlated to occupancy, we derive an occupancy profile from the plug power measurement. The standby power consumption is removed by supposing an occupancy of zero persons every night at 00h00 and then the profile is normalised. This is illustrated in Figure 5. The resulting occupancy profile (between 0 and 1) is used as a disturbance and an additional parameter to be estimated n_{occ} is introduced in the model to represent the number of occupants corresponding to a profile value of one. More details about the forecasting of these disturbances are given in subsection 3.3.

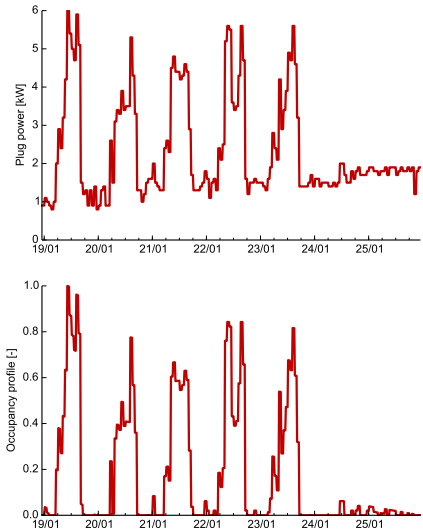

Figure 5: Plug power (top) and derived occupancy profile (bottom) for a typical week.

The RC scheme in Figure 4 only represents the dynamic heat transfer processes. The gas consumption $\dot{P}_g$ of the condensing boiler and electricity consumption of both heat pumps $\dot{P}_{HP1}$ and $\dot{P}_{HP2}$ are computed from equations for the boiler efficiency η and the coefficient of performance (COP) of the heat pumps, COP_{HP1} and COP_{HP2}. These efficiency models are obtained by linear regression on the monitoring data based on the following predictors: T_{Sup}, T_{Amb} and the produced thermal power $\dot{Q}_{GB}$ for the boiler or the electrical power $\dot{P}_{HP}$ for the heat pumps [18]. A forward selection is applied to avoid overfitted models. The resulting performance curves are given in Eq. (2).

Table 1: Overview of endogenous and exogenous disturbances. *Global horizontal radiation was not retained as significant disturbance in the model identification process.

Endogenous	Exogenous
Plug power	Ambient temperature
Occupancy	Global horizontal radiation*
Schedule AHU	

$$\eta = 0.87 - 8.85e^{-7}\dot{Q}^*_{GB} + 4.82e^{-3}T^*_{Amb} \quad (2a)$$

$$COP_{HP1} = 2.61 + 5.45e^{-2}T^*_{Amb} - 1.23e^{-2}T^*_{Sup} - 1.18e^{-4}\dot{P}^*_{HP1} - 1.54e^{-5}T^*_{Amb}\dot{P}^*_{HP1} \quad (2b)$$

$$COP_{HP2} = 2.58 + 3.84e^{-2}T^*_{Amb} - 2.50e^{-2}T^*_{Sup} - 1.42e^{-4}\dot{P}^*_{HP2} - 1.50e^{-5}T^*_{Amb}\dot{P}^*_{HP2} \quad (2c)$$

In these equations, the predictor variables are relative values in order to obtain physically meaningful results for the intercept:

$$\dot{Q}^*_{GB} = \dot{Q}_{GB} - 86000$$
$$\dot{P}^*_{HP} = \dot{P}_{HP} - 6500$$
$$T^*_{Amb} = T_{Amb} - (7 + 273.15)$$
$$T^*_{Sup} = T_{Sup} - (35 + 273.15)$$

It is noteworthy that both heat pumps, though identical, have a slightly different performance model. The OCP will exploit these differences.

3.3. Forecasting of disturbances

In the model identification process we have defined different disturbances and estimated the corresponding parameters. We distinguish between endogenous and exogenous disturbances. Endogenous disturbances are measured locally and forecasted based on algorithms we have developed ourselves. Exogenous disturbances can be measured locally or remotely and their forecasts are obtained from external services, typically weather services. A mixture of both is possible, eg. when an exogenous forecast is corrected based on a local measurement. An overview of both types of disturbances is given in Table 1.

We have implemented the most simple persistence models for the forecasting of all three endogenous disturbances. The forecasted value for $t = t_f$ is the value measured exactly one week before, at $t = t_f - 604800s$. This is illustrated for plug power in Figure 6. On some

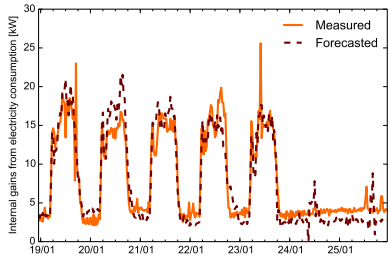

Figure 6: Overview measured and forecasted values for plug power for one week in January 2015.

days, like Tuesday 20/01 and in the weekend, we observe a bias, but in general the forecast captures well the general trends of the plug power profile.

The forecasts of the exogenous disturbances are provided by a weather service. We obtain these forecasts from the University of Oldenburg in the framework of the EU FP7 project *PerformancePlus*. The only exogenous input in the used model is T_{Amb}, the ambient temperature. This temperature is also measured on-site. Differences between the forecasted and measured values of up to 5 K have been observed. In order to take into account local conditions, the forecast is adjusted by the difference between the forecasted value and the measured value for $t = 0$.

3.4. State estimation

Since not all states of the control model can be measured, state estimation is a required step in any model predictive control scheme. The state estimation problem boils down to examining the past monitoring data and reconciling these measurements with the model to determine the most likely value of the state at the current time [19]. There are many different approaches for state estimation depending on the model structure.

We have implemented a very basic and intuitive approach based on the parameter estimation technique of the Grey-Box Buildings toolbox [17]. Instead of estimating the parameters of a model that minimize the measurement residuals, we estimate only the initial states for a model with given parameters. In the present implementation, 24 hours of historical measurements are used, and the decision variables of the parameter estimation problem are the initial values of each of the 4 states presented in Figure 4. The state at the end

of the 24h interval, the current time $t = 0$, is the estimated state. Then, for the measured states T_{Zon} and T_{Sup}, instead of using the estimated state, the current measurement is retained.

Finally, in order to obtain a more stable control, the measurement of T_{Zon} is compared to the reference temperature tracking setpoint T_{Set}. If $| T_{Zon} - T_{Set} | \leq 0.2$ K, T_{Zon} is taken equal to T_{Set}. This correction avoids abrupt changes in the control for small deviations from the set point.

We are aware of the simplicity of the implemented state estimation. It is planned to implement more advanced state estimations in the near future, in particular the approaches described by Vande Cavey et al. and Bonvini et al. [20, 21], and analyse their impact on the performance of the MPC.

3.5. Optimal control

This subsection details the implementation of the OCP presented by Eq. (1). The control variable u is composed of $\dot{Q}_{GB}$, $\dot{Q}_{HP1}$, $\dot{Q}_{HP2}$ and $\dot{Q}_{Hea}$. Although it is impossible to control the heat consumption of the building $\dot{Q}_{Hea}$ due to the (uncontrolled) manual operation of the heat emission systems, $\dot{Q}_{Hea}$ is required for the model to control thermal comfort in the building. Constraints are put on the positive derivatives of $\dot{Q}_{GB}$, $\dot{Q}_{HP1}$ and $\dot{Q}_{HP2}$ to stabilise the control signals and take into account inertia in the heat production systems. The maximum thermal power of the boiler and electrical power of the heat pumps are limited. Finally, a constraint of 80 °C is put on T_{Sup}.

The objective function in Eq. (1) is expanded as a weighted sum of the energy costs J_c and the thermal discomfort cost J_d

$$J = J_c + \gamma J_d \tag{4}$$

where γ is a weighting variable. The energy costs can be written as

$$J_c = \int_0^{t_h} (c_g \dot{P}_g + c_e \dot{P}_e) \mathrm{d}t \tag{5}$$

with t_h the prediction horizon, $\dot{P}_g$ the gas consumption, $\dot{P}_e$ the electricity consumption, the gas tariff $c_g = 4.3458$ c€/kWh and the electricity tariff $c_e = 7.323$ c€/kWh or 9.431 c€/kWh for low respectively high tariff hours. The high tariff applies every work day between 8h and 23h.

The thermal discomfort cost J_d is implemented as a reference temperature tracking:

$$J_d = \int_0^{t_h} \theta_{occ} (T_{Zon} - T_{Set})^2 \mathrm{d}t \tag{6}$$

where T_{Zon} is the actual zone temperature and $\theta_{occ} = 1$ during occupation and $\theta_{occ} = 0$ elsewhere. The occupation hours are from 07h00 till 19h00 on weekdays. The reference temperature T_{Set} equals 21.8 °C before 24/02/2015 and 21.5 °C after 24/02/2015. This comfort set point is obtained by trial and error on the real building in order to obtain good thermal comfort in each of the zones.

The control time step is 5 minutes, the open loop control horizon is 1 hour. This means that every 5 minutes, the controller will compute a new control signal by interpolation in the control trajectories of the last solved OCP and transmit these to the building. If the last control trajectories were computed more than 1 hour ago, a new state estimation is performed and the OCP will be solved again. The prediction horizon t_h in the OCP is 24 hours.

The numerical solution of the OCP is obtained with JModelica.org [22]. Direct collocation is used to discretise time, which reduces the optimisation problem to a nonlinear program (NLP)[23]. JModelica.org utilises third-party NLP solvers, which require first- and second-order derivatives of all expressions in the NLP with respect to all decision variables. CasADi is used to obtain these by algorithmic differentiation [24]. We used the NLP solver IPOPT with the sparse linear solver MA27 from HSL [25, 26]. The collocation elements are placed on a regular grid with 15 minutes interval and two collocation points per element.

4. Results

In this section, we compare the performance of the conventional rule-based control (RBC) with the MPC. The comparison is carried out on a daily basis, for working days only. First, the used metrics for the comparison are introduced and then the results are presented.

4.1. Metrics for comparison of MPC with RBC

We define three key performance indicators (KPI) and one normalisation variable as shown in Table 2.

The first KPI, the energy cost J_c, is computed according to Eq. (5). The second KPI, the primary energy consumption J_e, is obtained from

$$J_e = \int_{t_i}^{t_e} (2.5 \dot{P}_e + \dot{P}_g) \mathrm{d}t. \tag{7}$$

Table 2: Key performance indicators and normalisation variable for building performance analysis.

Symb.	Unit	Meaning
J_c	€	Energy cost
J_e	kWh	Primary energy consumption
J_d^*	minutes	Thermal discomfort
HDD	K d	Heating degree days (normalisation variable)

We use a primary energy factor of 2.5 for electricity and 1.0 for natural gas. The values of t_i and t_e will be given below. As J_c is part of the objective function and J_e is not, it is logic to judge the merits of the MPC on J_c. However, in Section 5 we will discuss also the primary energy consumption of both control strategies.

In order to make fair comparisons between days, a time shift is implemented prior to the computation of all metrics. As will be shown later, the MPC will often start the heat pumps long before comfort is required at 07h00 in the morning. Often, one or both heat pumps start at 23h00 in the evening, at the beginning of the low electricity tariff period. Therefore, we shift time so the days start and end at 19h00, the end of the occupation period. As a result, t_i is 19h00 of the previous day, t_e is 19h00 of the analysed day.

Additionally, to cover accidental or intentional heating in the weekend, we add the energy use and costs of the weekend to the KPIs for Monday.

The third KPI, the thermal discomfort J_d^*, is not calculated as in Eq. (6). To bring the computation in line with international standards, the thermal discomfort is calculated according to EN 15251 [27]. For every working day, we compute the total time during which thermal comfort is outside the boundaries of category I. This category is defined by a PPD higher than 6 %. When taking a clothing factor of 1.0 and a metabolism rate of 1.2, the temperature boundaries corresponding to PPD = 6 % are on 21.0 °C and 23.0 °C. As overheating does not occur in the measured data, the practical computation of J_d^* is the total time during working hours where $T_{Zon} \leq 21.0\,°C$. We express J_d^* in minutes per day. Next, an acceptable comfort violation is fixed at 5 % of the working hours outside of category I. This results in a maximum of 36 minutes per working day. In other words: when the measured T_{Zon} is less then 36 minutes below 21.0 °C, the comfort for that day is good.

To normalise the different days, the heating degree days (HDD) are computed on a daily basis, with a base temperature of 16.5 °C. Also for the computation of the HDD the implemented time shift makes sense. The evolution of the ambient temperature during evening and night impacts the heating needs for the future, not the past.

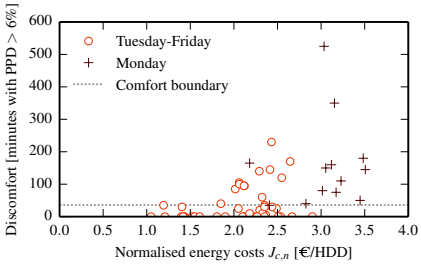

Figure 7: Overview of thermal discomfort and normalised energy costs for all weekdays in the measurement data.

Finally, for some analyses the KPIs are normalised with the HDD for fair comparisons between different days. We denote the normalised KPIs by the subscript n.

4.2. Comparison of MPC with RBC

Figure 7 shows the thermal discomfort and normalised energy costs for all weekdays and makes a distinction between Mondays and the other weekdays. The acceptable thermal comfort boundary, 36 minutes for which PPD > 6%, is also plotted.

The figure shows a large spread in both comfort and costs. On Mondays, the variability is even higher, with on average both a higher discomfort and higher costs than on other weekdays. This is expected because the building is not heated in the weekends. We focus the analysis on Tuesdays-Fridays to increase the similarity between the analysed days.

Figure 8 is obtained by removing the Mondays and plotting the MPC days in a different colour. Both control strategies are able to provide good thermal comfort on most days, but the RBC has many outliers with bad comfort while the MPC does not have any. It is also clear that the mean normalised costs are lower for MPC than for RBC. This means that on average, the MCP is able to provide a better thermal comfort at a significantly lower cost.

To quantify the savings, only days with acceptable comfort are compared in an energy signature plot [28]. Instead of regressing the primary energy consumption J_e on the heating degree-days, the regression is made on

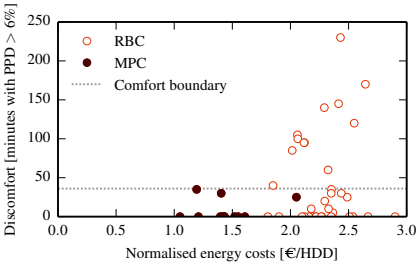

Figure 8: Thermal discomfort and normalised energy costs for Tuesday-Friday, for RBC and MPC.

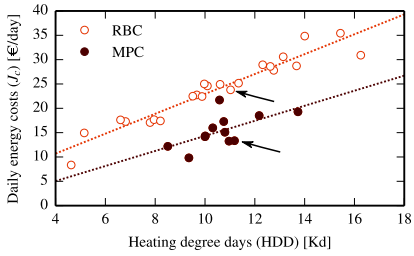

Figure 10: Selection of two similar days for comparing the building operation between RBC and MPC.

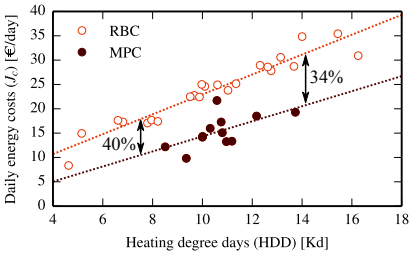

Figure 9: Daily energy costs J_c and savings of MPC versus RBC as a function of heating degree-days (HDD). Only Tuesday-Friday, only days with good thermal comfort.

the costs J_c so it is more correct to speak of a cost signature plot. By making a distinction between the RBC and MPC days, the savings can be visualised. This is shown in Figure 9. The figure shows that despite the use of daily intervals, the regression of daily costs on daily HDD yields a good correlation, in particular for the RBC days. There is more spread on the MPC days, but this is not problematic. Based on both regressions, we have computed the relative daily cost savings: they vary between 30 % and 40 %. These results are discussed in more detail in the next section.

5. Discussion

The MPC is able to provide a similar or better thermal comfort than RBC at a significantly lower energy cost. In this section we try to understand and pinpoint the reasons for the improved performance by analysing the results in more detail.

The mechanism for providing thermal comfort is completely different for both control strategies. The RBC is based on a heating curve with indoor temperature compensation. This means that T_{Sup} is adapted proportionally as a function of $T_{Zon} - T_{Set}$. In the MPC, minimising the deviation from T_{Set} is an explicit objective of the controller. Whenever the building is too cold, the MPC will take abrupt actions to correct T_{Zon}. The effectiveness of this correction will depend on the weighting factor γ from Eq. (4) and on the general quality of the MPC, which is the result of the cumulative effect of model mismatch, quality of disturbance forecasts and accuracy of the state estimation. When γ is sufficiently large and the MPC has no major quality problems, thermal comfort will be guaranteed. The three MPC days with J_d^* close to the boundary of 36 minutes have suffered from either a large model mismatch, wrong forecasts or a bad state estimation.

The cost savings realised by MPC are large. We analyse the operation of the MPC versus the RBC on two similar days to illustrate typical differences in the control of the heating system. The choice of both days is shown in Figure 10. A time series plot of the most relevant control and operation variables for these days is shown in Figure 11. The plot confirms that both days have a similar profile for T_{Amb}.

Figure 11 shows that the control strategy of the MPC is very different from the RBC. A first remarkable difference is the start-up time. The RBC has a weekly schedule, with a start-up at 05h00 in order to reach 21 °C at 07h00 in the morning. The MPC however starts already at midnight and slowly preheats the building. This preheating makes use of the heat pumps at a relatively low supply water temperature T_{Sup}. The heat pump power is gradually increased, and so does T_{Sup}. Around 06h00,

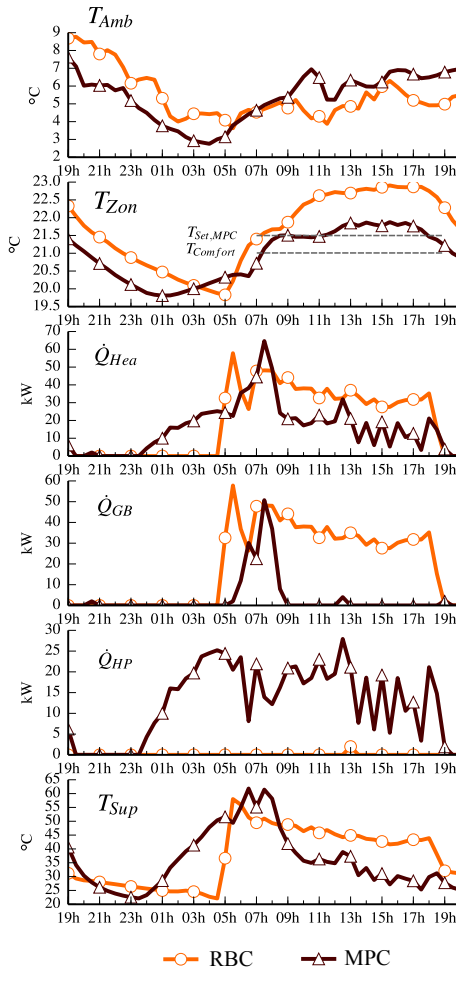

Figure 11: Comparison of operation of two similar days between RBC and MPC. $\dot{Q}_{HP}$ is the sum of $\dot{Q}_{HP1}$ and $\dot{Q}_{HP2}$.

the gas boiler is fired for the purpose of reaching a T_{Zon} of 21.5 °C at 07h00.

A second major difference is the operation of the heat production units. The RBC never uses the heat pumps during this day and this has been confirmed for other days with similar ambient temperatures. The MPC has a model that predicts the performance of each heat production unit. As shown in Eq. (2), these models include the thermal or electrical power, T_{Amb} and T_{Sup}. By consequence, the MPC *knows* how to operate these units in such a way that the overall energy costs are minimised. For the studied day, the MPC mainly uses the heat pumps and only operates the gas boiler when the required power $\dot{Q}_{Hea}$ is high.

A third important difference concerns the supply water temperature T_{Sup}. The RBC follows the heating curve with room temperature compensation. The supply water reaches a maximum temperature of about 55 °C in the morning and slowly decreases from there for the rest of the day. In contrast, the profile of T_{Sup} in case of MPC is totally different. Interestingly, T_{Sup} is not always lower. We observe three time periods with different behaviour: before 05h00, between 06h00 and 09h00 and after 09h00. In the first period, T_{Sup} rises steadily with increased heat pump power. Around 06h00 the MPC strongly increases the produced power in order to increase T_{Sup} and allow $\dot{Q}_{Hea}$ to rise. In this time block, T_{Sup} reaches even 60 °C. When T_{Zon} has reached T_{Set}, the supply water temperature is reduced drastically and stays remarkably low for the rest of the day. The result is a reduction of about 50 % of the heat consumption of the building between 09h00 and 19h00. The analysis of different days reveals the same patterns.

Figure 11 also shows that the MPC does not really meet its target of 21.5 °C at 07h00. This is the consequence of a model mismatch, bad forecasts, a wrong state estimation or a combination of these errors. We can analyse how the MPC expected this specific day to be by comparing the results of the solution of the OCP at 21h00 with the real operation. This is shown in Figure 12.

The figure shows a significant difference between the solution of the OCP at 21h00 and the real measured operation of the building with MPC. One of the causes is a wrong forecast of T_{Amb}. The locally measured T_{Amb} is higher than the forecasted in the early morning and significantly lower in the afternoon. Nevertheless, this difference cannot explain the missed target of 21.5 °C at 07h00. On the contrary, with the higher ambient temperature it should have been easier to reach the set point.

Before 07h00 there is little or no occupancy and electricity consumption. As ambient temperature, occu-

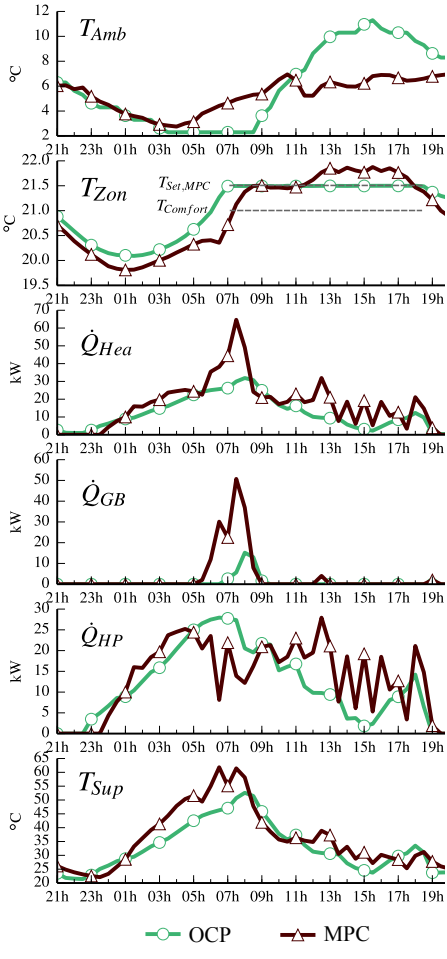

Figure 12: Comparison between expected operation (OCP) and MPC. The OCP was solved at 21h00 with a prediction horizon t_h of 24h. The MPC has an open-loop horizon of 1 h. $\dot{Q}_{HP}$ is the sum of $\dot{Q}_{HP1}$ and $\dot{Q}_{HP2}$.

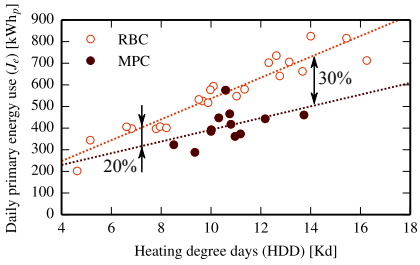

Figure 13: Energy signature showing primary energy use versus heating degree days for both RBC and MPC days. Only Tuesday-Friday, only days with good thermal comfort.

pancy and plug power are the only forecasted disturbances, this specific error is unlikely to be caused by bad forecasts.

By consequence, the error is a manifestation of errors in the model and/or state estimation. As the real state is not measured and the experiment cannot be repeated, we cannot distinguish between these two sources of error. That is why we are currently developing a detailed emulator model of the Kalkkaai building on which we can test different versions of MPC under identical boundary conditions. This will be reported in the near future.

Thanks to the feed-back of the building (every hour), the MPC is able to correct the errors. At 06h00 the controller realises that more power is needed in order to reach T_{Set} and starts the gas boiler. One hour later, at the next update, T_{Set} is still not reached. The power of the gas boiler, which was already being reduced by the controller, is increased again. This time this is sufficient to reach the set point around 08h00. The consequence of these actions is a considerably higher T_{Sup} in the morning.

In the afternoon, the MPC adapts to the lower ambient temperature. The heat delivered to the building, $\dot{Q}_{Hea}$ is higher than foreseen by the OCP at 21h00. Nevertheless, the MPC is able to strongly reduce T_{Sup} and operate both heat pumps at a very high efficiency.

Table 3 summarises the observed differences between the two control strategies on the analysed days. The table distinguishes between three main control concepts: the operation schedule, the supply water temperature and the choice of heat production units.

The objective of the MPC is to minimise energy costs and thermal discomfort. How this translates into pri-

Table 3: Synthesis of observed differences between RBC and MPC for two similar days.

Concept	RBC	MPC
Operating times	Fix schedule.	Free. Very early start observed and slow pre-heating of building with low tariff electricity and high COP.
Hot water supply temperature T_{Sup}	Heating curve with indoor temperature compensation.	Free. Mainly lower values of T_{Sup} but also higher values observed. Resulting T_{Sup} depends on dynamic processes.
Heat production	Mainly condensing gas boiler.	Mainly heat pumps at partial load. Gas boiler for peaks.

mary energy use is visualised in a proper energy signature plot, as shown in Figure 13. The energy savings are clearly less pronounced than the cost savings but still substantial. In the first place, this is due to the objective in the OCP. A second reason is the electricity tariff. Thanks to low night tariff, the potential for cost savings is larger than for energy savings. Nevertheless, the MPC realises a reduction of primary energy use between 20 % and 30 % which is a very important added value of the cost driven operational optimisation. This single example may not be generalised, but it illustrates that if the energy tariffs reflect the primary energy content of the different energy vectors to some extent, economical objectives can lead to ecological benefits.

6. Conclusion

We have presented the step-by-step implementation of MPC in an office building in Brussels. The control variables are the produced thermal power of the condensing gas boiler and of two identical air/water heat pumps. The MPC makes use of a 4^{th} order grey-box model, simple weekly persistence models for the forecasting of endogenous disturbances and a deterministic state estimation. By introducing rather detailed performance maps for the heat pumps and the boiler, the model knows the implications of the operation on equipment efficiency.

The objective function of the controller is a weighted average of a temperature reference tracking and energy costs. The MPC has been operated in real-time in the winter of 2014-2015 and is compared to the conventional RBC control.

The results show an average cost saving between 34 % and 40 % compared to the reference control. Even the primary energy use, which is not directly covered by the objective function, is decreased by more than 20 %.

The main differences between the MPC and RBC strategies are that the MPC uses the heat pumps much more, starts up very early to pre-heat the building and strongly reduces the supply water temperature once the comfort set point has been reached.

On the one hand, the energy savings would have been smaller if the conventional control had used the heat pumps more often. On the other hand, these savings are realised with an MPC containing many simplifications in different steps of the process. There is still room for improving the MPC performance. The results of this single experiment cannot be generalised but they are certainly encouraging towards the use of MPC for controlling thermal systems in buildings.

Acknowledgement

The authors gratefully acknowledge the following projects and institutes for supporting this work:

- the FP7 project *PerformancePlus* funded by the European Commission (KU Leuven, contract nb. 308991),
- the project *Optimal energy networks for buildings* funded by the KU Leuven Energy Institute (KU Leuven),
- *Flexipac* funded by the Région Wallonne, DGO4 (3E, contract nb. 1250570).

Bibliography

[1] M. Ardehali, T. F. Smith, Literature review to identify existing case studies of controls-related energy-inefficiency in buildings for national building controls information program, Tech. rep., University of Iowa, Department of Mechanical Engineering, Iowa City, Iowa (2001).

[2] D. Gyalistras, M. Gwerder, F. Oldewurtel, C. N. Jones, M. Morari, B. Lehmann, K. Wirth, V. Stauch, Analysis of Energy Savings Potentials for Integrated Room Automation, in: 10th RHEVA World Congress CLIMA, REHVA, Antalya, Turkey, 2010.

[3] G. Henze, D. Kalz, S. Liu, C. Felsmann, Experimental Analysis of Model-Based Predictive Optimal Control for Active and Passive Building Thermal Storage Inventory, HVAC&R Research 11 (2) (2005) 189–213. doi:10.1080/10789669.2005.10391134.

[4] S. Prívara, J. Široký, L. Ferkl, J. Cigler, Model predictive control of a building heating system: The first experience, Energy and Buildings 43 (2-3) (2011) 564–572. doi:10.1016/j.enbuild.2010.10.022.

[5] F. Oldewurtel, A. Parisio, C. N. Jones, D. Gyalistras, M. Gwerder, V. Stauch, B. Lehmann, M. Morari, Use of Model Predictive Control and Weather Forecasts for Energy Efficient Building Climate Control, Energy and Buildings 45 (2011) 15–27. doi:10.1016/j.enbuild.2011.09.022.

[6] C. Verhelst, F. Logist, J. Van Impe, L. Helsen, Study of the optimal control problem formulation for modulating air-to-water heat pumps connected to a residential floor heating system, Energy and Buildings 45 (2011) 43–53. doi:10.1016/j.enbuild.2011.10.015.

[7] M. Gruber, A. Trüschel, J.-O. Dalenbäck, Model-based controllers for indoor climate control in office buildings âĂŞ Complexity and performance evaluation, Energy and Buildings 68 (2014) 213–222. doi:10.1016/j.enbuild.2013.09.019.

[8] M. Gwerder, D. Gyalistras, C. Sagerschnig, R. S. Smith, D. Sturzenegger, Final Report : Use of Weather And Occupancy Forecasts For Optimal Building Climate Control âĂŞ Part II : Demonstration (OptiControl-II), Tech. Rep. September, Automatic Control Laboratory, ETH, Zurich, Zwitzerland (2013).

[9] P. Li, D. Li, D. Vrabie, S. Bengea, S. Mijanovic, Experimental Demonstration of Model Predictive Control in a Medium-Sized Commercial Building, in: 3rd International High Performance Buildings Conference, Purdue, 2014.

[10] S. C. Bengea, A. D. Kelman, F. Borrelli, R. Taylor, S. Narayanan, Implementation of model predictive control for an HVAC system in a mid-size commercial building, HVAC&R Research 20 (2014) 121–135. doi:10.1080/10789669.2013.834781.

[11] G. S. Pavlak, G. P. Henze, V. J. Cushing, Optimizing commercial building participation in energy and ancillary service markets, Energy and Buildings 81 (2014) 115–126. doi:10.1016/j.enbuild.2014.05.048.

[12] J. E. Braun, Reducing energy costs and peak electrical demand through optimal control of building thermal storage, ASHRAE transactions 96 (2) (1990) 876–888.

[13] C. Verhelst, Model Predictive Control of Ground Coupled Heat Pump Systems for Office Buildings, Ph.D. thesis, KU Leuven (2012).

[14] E. Lorenz, J. Hurka, D. Heinemann, H. G. Beyer, Irradiance Forecasting for the Power Prediction of Grid-Connected Photovoltaic Systems, IEEE Journal of Selected Topics in Applied Earth Observations and Remote Sensing 2 (1) (2009) 2–10. doi:10.1109/JSTARS.2009.2020300.

[15] E. Lorenz, J. Kühnert, D. Heinemann, Short term forecasting of solar irradiance by combining satellite data and numerical weather predictions, 27th European Photovoltaic Solar Energy Conference and Exhibition 9 (2012) 4401–4405.

[16] P. Undén, L. Rontu, H. Järvinen, P. Lynch, J. Calvo, HIRLAM-5 Scientific Documentation, Tech. rep., SMHI, Norrköping, Sweden (2002).

[17] R. De Coninck, F. Magnusson, J. Åkesson, L. Helsen, Development and validation of grey-box building models for forecasting and control, Journal of Building Performance Simulation (Submitted on 24/12/2014).

[18] S. Seabold, J. Perktold, Statsmodels: econometric and statistical modeling with python, in: Proceedings of the 9th Python in Science Conference (Scipy 2010), 2010, pp. 57–61.

[19] J. Rawlings, D. Mayne, Model Predictive Control - Theory and Design, 2013. doi:10.1002/9781119941446.ch3.

[20] M. Vande Cavey, R. De Coninck, L. Helsen, Setting up a framework for model predictive control with moving horizon state estimation using JModelica, in: 10th International Modelica Conference, Lund, Sweden, 2014, pp. 1295–1303. doi:10.3384/ECP140961295.

[21] M. Bonvini, M. D. Sohn, J. Granderson, M. Wetter, M. A. Piette, Robust on-line fault detection diagnosis for HVAC components based on nonlinear state estimation techniques, Applied Energy 124 (2014) 156–166. doi:10.1016/j.apenergy.2014.03.009.

[22] J. Åkesson, K.-E. Årzén, M. Gäfvert, T. Bergdahl, H. Tummescheit, Modeling and optimization with Optimica and JModelica.org - Languages and tools for solving large-scale dynamic optimization problems, Computers & Chemical Engineering 34 (11) (2010) 1737–1749. doi:10.1016/j.compchemeng.2009.11.011.

[23] F. Magnusson, J. Åkesson, Collocation Methods for Optimization in a Modelica Environment, in: 9th International Modelica Conference, Munich, Germany, 2012.

[24] J. Andersson, J. Åkesson, M. Diehl, CasADi - A symbolic package for automatic differentiation and optimal control, in: S. Forth, P. Hovland, E. Phipps, J. Utke, A. Walther (Eds.), Recent Advances in Algorithmic Differentiation, Lecture Notes in Computational Science and Engineering, Springer, Berlin, 2012.

[25] A. Wächter, L. T. Biegler, On the Implementation of a Primal-Dual Interior Point Filter Line Search Algorithm for Large-Scale Nonlinear Programming, Mathematical Programming 106 (1) (2006) 25–57.

[26] HSL, A collection of Fortran codes for large scale scientific computation, `http://www.hsl.rl.ac.uk`, accessed: 2015-01-14.

[27] CEN, EN 15251:2007. Indoor environmental input parameters for design and assessment of energy performance of buildings addressing indoor air quality, thermal environment, lighting and acoustics (2007).

[28] A. Rabl, A. Rialhe, Energy signature models for commercial buildings : test with measured data and interpretation, Energy and Buildings 19 (1992) 143–154.

6.3 Conclusion

This chapter has illustrated how the MPC tool chain is implemented on a real office building. The grey-box model that was identified based on monitoring data contains detailed performance map components for both heat pumps and the gas boiler and is thus able to decide which heat producer is to be operated at any time in order to minimize the control objective.

The thermal comfort with MPC was equal or better as with RBC. A saving on the heating energy costs of more than 30 % is realised. This saving goes hand in hand with a saving of primary energy use of more than 20 %.

It is important to note that the realised savings depend on the performance of the benchmark, the rule-based control. In the KK building, the conventional control has a zone-compensated heating curve and a set of rules to activate the heat pumps. By comparing the MPC with the RBC, guidelines for improving the RBC were identified. More precisely, by activating the heat pumps more often, the performance of the RBC would increase.

However, the results also reveal that a heating curve is not as flexible as the MPC. Therefore, even with an optimally tuned RBC, savings are expected with MPC. Moreover, it should be noted that while configuration costs are often mentioned as a main barrier to implement MPC, tuning a RBC can also be very time-consuming and costly.

Chapter 7

Conclusion

This chapter presents a summary of the main contributions and findings of this thesis. Based on these results, suggestions for future research are formulated.

7.1 Synthesis

Model predictive control is a promising technology to improve energy efficiency in buildings and unlock building flexibility towards the energy markets. The main bottleneck for the implementation of MPC in buildings is the time-intensive configuration of the controller, a process that has to be repeated for every individual building. The objective of this work is to *develop and demonstrate a tool chain for automated deployment of MPC in buildings based on data-driven, grey-box building models.*

This goal has been reached. I have developed an MPC tool chain and applied it to the KK building in the winter of 2014-2015. This resulted in energy cost savings between 34 % and 40 % and primary energy savings of more than 20 %.

Besides this tool chain, I want to point out two other main contributions of this work. Firstly, this thesis was one of the foundations of the multi-domain Modelica library *IDEAS*, together with simultaneous theses at other KU Leuven departments. IDEAS has proven to be highly valuable for the assessment of relevant research questions in buildings and districts where different disciplines interact. Moreover, the continued active development of IDEAS illustrates its relevance still today.

Secondly, in this work I propose a methodology for assessing in a generic way the amount of flexibility a building can deliver and the associated costs. While demand response and flexibility are concepts long known in the building energy research domain, a universal method to quantify the amount of energy that can be shifted and the cost for the building operator were missing.

More details about all these achievements is structured according to the definition of the four main problems from Figure 1.1.

Integrated system simulation

In a first part of this work, presented in Chapter 3, I have focused on integrated multi-disciplinary simulation with high-order models to quantify energy use and thermal comfort in buildings and neighbourhoods. These simulations have explored the interactions between buildings, their HVAC systems, distributed energy resources and the electricity distribution network. For this purpose, it was necessary to develop a new simulation framework. This resulted in the Modelica library IDEAS, a collaborative and open-source library that is still being actively further developed today at several departments in KU Leuven.

In particular, low-energy dwellings with heat pumps, photovoltaic systems and thermal energy storage have been studied. These technologies are often combined in new dwellings and renovation projects and can have a considerable impact on the operation of the electricity distribution grid. This is confirmed by the simulations. We have quantified the curtailing of PV electricity generation for different neighbourhood configurations.

The grid interaction is influenced by the control of thermal systems in the buildings. I showed that rule-based demand side management is able to reduce these curtailing losses significantly. This is achieved by choosing different periods for the heat pumps to charge the DHW tank. However, increasing the volume of these tanks in order to increase its storage capacity is rarely a good idea. The simulations show repeatedly that a larger tank will almost always result in a larger net energy use when the control is rule-based.

Since a few years, the paradigm of *self-consumption* has risen, in particular in the context of domestic PV systems. Our simulations show self-consumption rates in the range of 25 % to 35 % in net-zero energy dwellings. Increasing this rate is often proposed as a solution to electrical network issues and several battery-based product developments witness this trend. The economic viability of these products, largely determined by legal context, in particular feed-in tariffs, is often decoupled from the energetic benefits at total system scale.

The simulations reveal that increasing self-consumption does not guarantee a reduced energy use at neighbourhood level.

Grey-box building models

While the rule-based control strategies are able to reduce energy use and mitigate grid interaction issues, it is expected that they are outperformed by model predictive control. A major bottleneck for MPC is the control model development. I have developed a grey-box toolbox to support and even automate a data-driven model identification. The choice for grey-box models, as opposed to black-box models, is not inspired by a best-seller but by practical usability. Having a physical model with interpretable parameters is a major advantage with regard to both model development and validation.

The grey-box buildings toolbox is based on *FastBuildings*, an open-source Modelica library developed within this research to represent buildings by low-order models. Application of the toolbox to the monitoring data of a dwelling shows the ability of a low-order model to obtain a good simulation performance. This is an important feature for control models for buildings where time constants, and by consequence the prediction horizon, can span several days.

Flexibility of buildings

As was shown in Chapter 3, the studied grid interaction issues can be mitigated by demand response. DR exploits the *flexibility* of buildings to adapt their load profiles. This concept of flexibility is often used, but rarely quantified. For power systems, quantification metrics and assessment methods are described in the literature, but not for buildings.

In Chapter 5, I have proposed a methodology to quantify the flexibility of buildings. For a specified time interval, the method returns both the amount of electricity that can be shifted and the associated costs for the building operator. This information can be represented graphically in a *cost curve*. The cost curves can be aggregated for multiple buildings and allow comparing the cost of DR in buildings with other technological solutions to balance electricity production and use. The results of the application of the methodology to the KK building are summarised below.

Field test KK building

The office building of 3E, the KK building, serves as a living lab for testing and demonstration of this work. The monitoring data of different sources is collected in a central database and used to identify a grey-box model with the toolbox presented in Chapter 4. The availability of sensors in real buildings sets limits to the available data, which in turn impacts the model structure that can be used. The resulting model is a single zone model with two states for the building and two states for the heating system. By introducing rather detailed performance maps for the heat pumps and the boiler based on ambient temperature, supply water temperature and load, the model can predict the implications of the operation on equipment efficiency. This is an important feature of the control model for a hybrid heating system.

A first application of the grey-box model is an assessment of the flexibility of the KK building. The results show a high variability of the flexibility and the costs over a day. This mainly shows that flexibility of thermal systems in buildings is not free. The DR actions always result in a net cost for the building operator. Nevertheless, during most of the day, the costs are lower than the imbalance price in the power system. This confirms the potential of DR in buildings for the purpose of balancing electricity generation and consumption.

Finally, an MPC has been implemented in the KK building. The MPC controls the thermal power of the gas boiler and both heat pumps. It is not possible to control the heat consumption of the building or the room temperature set points directly. The MPC can predict these and influence them indirectly through the supply water temperature. All necessary components of the MPC as presented in Figure 2.1 are implemented, albeit some in a simplified way. The demonstrated MPC on the KK building is thus a first attempt, there is still room for improvement.

Despite these simplifications, the MPC is able to reduce the energy costs for heating of the KK building by 34 % to 40 %. Even the primary energy use, which is not covered by the objective function, is decreased by more than 20 %. The savings are realised by a combination of: a much earlier start-up (pre-heating of the building), use of the heat pumps instead of the gas boiler and a drastic reduction of the supply water temperature once the building has reached its temperature set point.

This result is beyond expectations as most publications report savings around 20 %. On the one hand, this is explained by the default operation of the gas boiler in the conventional control. The rule to switch on the heat pumps is too pessimistic most of the time. Improving this rule would reduce the savings of the MPC. On the other hand, the behaviour of the MPC cannot

be captured in simple rules, unless they become as complicated as the MPC itself. The capability of MPC to adapt to any situation and to anticipate to future disturbances makes it superior to any rule-based control. Moreover, the implemented MPC is far from perfect. Disturbance predictions and state estimation can still be improved, and it may even be possible to reduce the model mismatch with a better grey-box model.

In conclusion, I am hopeful that MPC is a viable and good alternative to conventional control for thermal systems in buildings. The potential savings strongly depend on the reference situation and on the degrees of freedom of the control. They may both be lower or higher than in the KK building. This is the drawback of single experiments like the field test on the KK building: the results cannot be generalised. More experiments or commercial implementations are needed to obtain representative results for all buildings.

As stated in the introduction, the main issue is the implementation effort. The road to full automatic deployment of MPC controllers is still long and has many turns. The final goal is not MPC on itself, but efficient and flexible buildings integrated in a sustainable energy supply system. I started this PhD with the ambition to make a few steps on that road. The steps may be small, but I hope they were significant and heading in the good direction.

7.2 Future research

There are many opportunities and needs for continued research in the topics covered by this work. Below, I give a personal view on some of the short and long term challenges.

The neighbourhood simulations presented in Chapter 3 are a big step forward starting from single building simulations but they still lack scalability. Running a yearly simulation of a neighbourhood with about 30 two-zone dwellings can take several days. Without reducing the level of detail, upscaling these simulations to districts with hundreds or thousands of buildings is not feasible. A solution could be to use a novel type of solver, a quantised state system (QSS) solver [1, 2]. QSS solvers are able to solve larger models considerably faster. Currently, these solvers are not compatible with the IDEAS model formulation, so either IDEAS, the Modelica compiler or the solver need to be adapted. Another solution consists of parallelising the simulation with a co-simulation framework. While this solution decreases CPU-time, it still relies on a heavy computing infrastructure. In conclusion, upscaling will have to go hand-in-hand with decreasing the model order and complexity by linearisation and model-order

reduction. This is challenging, in particular for thermo-hydraulic simulations. Controlling the simulation accuracy becomes very important.

The development of the grey-box buildings toolbox will continue, both at 3E and KU Leuven. Automation should be brought to a next level with a fully automatic forward selection procedure including validation. First tests have illustrated the potential of this feature. Pre-processing of the data can be improved in order to make a pre-selection of significant variables for the identification. Multi-zone buildings are possible today, but still require more manual work and expert knowledge than desired. It is still an open question if the proposed methodology is applicable to obtain multi-zone models with tens or hundreds of individual rooms, both for the model identification as for solving the OCP. Simultaneously, including humidity and CO_2 in the model looks promising. Monitored time series of their concentration contains information about occupancy, ventilation and infiltration rates. Simple first order models may be sufficient to model their concentration. Specifically humidity is interesting because this is easy and cheap to measure. Another potential development would be to do (surface) temperature measurements of the heat or cold emission systems in individual rooms in order to obtain the necessary information for multi-zone models. Temperature measurements are much easier and cheaper than heat flux measurements. Also, good indicators for (control) model performance are needed. The difference between practical usability of the k-step prediction performance, the simulation performance and the control performance is not clear. Based on a good indicator, on-line identification can be triggered if the model needs to be adapted. Finally, it is not yet clear which measurement data is needed to obtain a good control model. More insight in the minimum requirements for the set of sensors would help to find the good balance between monitoring cost and MPC performance.

On the level of MPC there is also room for improvements. The persistence models used for forecasting disturbances seem very simple but are not easy to improve. Nevertheless, having good forecasts is crucial for MPC, so continuous attention has to be given to using the best possible disturbance models. The implemented state estimation is very simplified. More advanced state estimation frameworks have to be tested and implemented. Finally, an online identification would increase the adaptability of the MPC to seasons (position of the sun, fixed shadings, seasonal user behaviour), changes in material properties (like humidity of insulation, dirty windows) or equipment (maintenance/replacing of HVAC systems). Online identification would allow a quick implementation of MPC in a building with a continuous self-learning control model that improves as the available dataset for identification becomes more rich over time.

A planned next step is to demonstrate MPC on different buildings. This will allow us to generalise the results, refine the saving potential fork and get a grip

on the case-specific potential. It is expected that every new implementation will be a step towards more automation and robustness of the full tool chain.

However, there are several research questions that are hard to answer with real-life implementations because experiments cannot be repeated with the same boundary conditions. At this point, emulator models are needed. These are detailed and calibrated models that can be considered as *virtual buildings*. We started the development of an emulator model for the KK building. With this virtual building, we plan to test different controllers under identical circumstances. This will allow us improving the state estimation, forecasting and model mismatch and assess their impact on the overall MPC performance before implementation on a real case.

The application of MPC for unlocking energy efficiency can be studied at building scale. For unlocking flexibility we have to study the larger system and apply MPC to neighbourhoods or districts. For this purpose, new distributed optimisation frameworks are being developed, also by colleagues at KU Leuven. There are several challenges of different kinds, and the validation of such frameworks to a real-life case is more complicated than it was on the KK building. Nevertheless, this is a necessary and rewarding step if we want to use the flexibility of buildings as a distributed energy resource.

7.3 Bibliography

[1] F. Bergero, X. Floros, J. Fernández, E. Kofman, and F. E. Cellier, "Simulating modelica models with a stand-alone quantized state systems solver", in *Proceedings of the 9th International Modelica Conference*, Munich, Germany, Nov. 2012, pp. 237–246. DOI: 10.3384/ecp12076237.

[2] X. Floros, F. Bergero, N. Ceriani, F. Casella, E. Kofman, and F. Cellier, "Simulation of smart-grid models using quantization-based integration methods", in *Proceedings of the 10th International Modelica Conference*, 2014, pp. 787–797. DOI: 10.3384/ecp14096787.

Appendix A: Concepts of control theory

Since the pioneering work of R. Kalman and others in the middle of the 20^{th} century, control theory has evolved to a vast scientific domain with a solid mathematical basis. Different concepts are clearly defined and widely used, both for linear and non-linear control systems. We will briefly introduce the important concepts of observability, controllability, identifiability and stability and discuss these concepts for linear, time-invariant (LTI) systems. The concepts of observability and controllability were originally introduced by R. Kalman in [1]. The overview below is additionally based on [2–4].

We consider an LTI in state space formulation in continuous time:

$$\dot{x}(t) = Ax(t) + Bu(t) \tag{7.1a}$$

$$y(t) = Cx(t) \tag{7.1b}$$

In this equation, $x(t) \in \Re^n$ is the state vector with initial value $x(t_0) = x_0$, $u(t) \in \Re^m$ is the input vector, $y(t) \in \Re^p$ is the output vector (the measurements). The matrices have dimensions $A \in \Re^{n \times n}$, $B \in \Re^{m \times n}$ and $C \in \Re^{p \times n}$.

Observability

Generally speaking, we say that a system is *observable* if the behaviour of the entire system can be obtained from the system's outputs. More precisely, observability means that measurements of the input and output signals over a

finite time interval can be processed in order to uniquely determine the initial state.

It can be shown that a LTI state-space system is observable if the rank of the *observability matrix* is equal to n:

$$rank \begin{bmatrix} C \\ CA \\ CA^2 \\ \vdots \\ CA^{n-1} \end{bmatrix} = n \tag{7.2}$$

The study of observability is closely related to observer (estimator) design. An observer or estimator produces estimates of the system state variables using information about the system inputs and outputs. We have referred to this functional requirement in the MPC tool chain as the state estimation.

To verify the observability of the used models we would first need to transform the Modelica models into a state space formulation as given in Equation (7.1). This is not implemented in the current tool chain. One solution to obtain a state space formulation consists of using the linearisation option of a Modelica tool like eg. Dymola. The advantage of this approach is that it would also work for the non-linear models in the FastBuildings library. The model will then be linearised in the given working point specified by a state vector and inputs.

Controllability

If the input can be used to steer any state of the system to the zero state within a finite time interval, the system is said to be *controllable*. More formally this is defined as follows.

Definition 1. *A state $x \in \Re^n$ is controllable to the origin if for a given initial time t_0 there exists a finite final time $t_f < t_0$ and a piecewise continuous input signal $u(t)$ defined on $[t_0, t_f]$ such that with initial state $x(t_0) = x$, the final state $x(t_f) = 0$.*

It can be shown that a LTI state-space system is controllable if the rank of the *controllability matrix* is equal to n:

$$rank \begin{bmatrix} B & AB & A^2B & \dots & A^{n-1}B \end{bmatrix} = n \tag{7.3}$$

More generally, it turns out that if a system is controllable to the origin, then it is also possible to steer the state trajectory to any final state in finite time via a suitable input signal.

Controllability is an important concept with regard to the design of feedback-control laws. A fundamental result is that controllability of the open-loop state equation is both necessary and sufficient to achieve arbitrary closed-loop eigenvalue placement via state feedback.

Similar to the discussion of observability, to verify the controllability of the used models we would first need to transform the Modelica models into a state space formulation as given in Equation (7.1). This is not implemented in the current tool chain.

In practice, even if not all states are controllable, this does not mean that the model is useless for control. More specifically, if the model is stable and observable, and the control objective is formulated based on the model outputs $y(t)$, good control performance is possible. In this case, all states that intervene in the control objective are controllable and the other states are stable. As all states are observable, a state estimator can be implemented, also for the uncontrollable states.

Stability

Another important concept in control theory is *stability*. Different forms of stability can be defined and more generally these can be separated in internal stability and bounded-input, bounded-output (BIBO) stability. Without discussing these different definitions in detail, we can intuitively expect that correctly identified thermal building models are BIBO stable. With bounded inputs, all the states will remain bounded and in absence of perturbations (zero-input) the system will return to an equilibrium state. Proving this statement and investigating stability for all the FastBuildings models is outside the scope of this work and can be subject for future research.

Even if a state is not stable, we can still use the concepts introduced above. We have defined observability and controllability of the complete state vector. We have seen that the system is controllable (observable) if all components of the state vector are controllable (observable). The natural question to be asked is: do we really need to control and observe all state variables? In some applications, it is sufficient to take care only of the unstable components of the state vector. This leads to the definition of stabilizability and detectability.

Definition 2. *A linear system (continuous or discrete) is detectable if all unstable modes are observable.*

Definition 3. *A linear system (continuous or discrete) is stabilizable if all unstable modes are controllable.*

For more information we refer to the control literature.

Identifiability

Finally, in model identification the concept of identifiability is used. A distinction can be made between structural and output identifiability. A detailed overview of the state of the art can be found in [5].

The identifiability has not been verified explicitly for the models in the FastBuildings library. It is expected that all models are structural identifiable based on a careful modelling and use of building domain expertise. A typical example of a model that would not be structurally identifiable is a model with two resistances in parallel between two states or between a state and an input. There would be an infinite number of solutions to the parameter estimation problem because both resistances can be combined into a single resistance. The output identifiability is ensured by using rich datasets. If a dataset does not contain enough information for a given model detail, the level of detail is to be reduced. So the non-identifiability of specific model-data combinations is taken care of by the forward selection approach implemented in the toolbox.

Bibliography

[1] R. Kalman, "Contributions to the theory of optimal control", *Boletin de la Sociedad Matematica Mexicana*, vol. 5, pp. 102–119, 1960.

[2] R. L. Williams II and D. A. Lawrence, *Linear state-space control systems*. Hoboken, New Jersey: John Wiley & Sons, Inc., 2007, ISBN: 9780471735557.

[3] M. Verhaegen and V. Verdult, *Filtering and System Identification - A least Squares Approach*. New York: Cambride University Press, 2007, ISBN: 9780521875127.

[4] Z. Gajic and M. Lelic, *Modern Control System Engineering*. Upper Saddle River, NJ: Prentice-Hall, Inc, 1996, ISBN: 0-13-134116-2.

[5] C. Agbi, “Scalable and robust designs of model-based control strategies for energy-efficient buildings”, PhD thesis, Carnegie Mellon University, 2014.

Curriculum

Roel De Coninck
°03/08/1977

Kapelstraat 1
3370 Boutersem, Belgium
roeldeconinck@gmail.com

Experience

2015-current: 3E, Brussels
Senior Expert R&D.
Optimisation, model predictive control, buildings and HVAC.

2010-2015: KU Leuven (50%) and 3E (50%)
PhD, collaboration between 3E and KU Leuven.
Title: Grey-Box Based Optimal Control for Thermal Systems in Buildings - Unlocking Energy Efficiency and Flexibility.

2008-2010: 3E, Brussels
Reference expert HVAC and solar thermal systems.
Responsible for project execution, R&D, (international) acquisitions, quality control and knowledge management of the Buildings and Sites team.

2001-2008: 3E, Brussels
Project engineer and project manager.
Topics: building energy simulation, HVAC design, solar thermal systems and macro-economical studies.

2000-2001: Volvo Cars Ghent
Automation engineer.

Education

2006: Atic course air-conditioning.

2004: Atic course heating systems.

1995-2000: KU Leuven
Burgerlijk Werktuigkundig-Elektrotechnisch ingenieur, optie energie (Master of Mechanical engineering).

1998-1999: TU Graz
Erasmus exchange.

1989-1995: Don Bosco Haacht
Mathematics-Sciences.

List of publications

Articles in international journals

[1] R. De Coninck and L. Helsen, "Practical implementation and evaluation of model predictive control for an office building in brussels", *Energy and Buildings*, 2015, Submitted on 17/03/2015.

[2] R. De Coninck, F. Magnusson, J. Åkesson, and L. Helsen, "Toolbox for development and validation of grey-box building models for forecasting and control", *Journal of Building Performance Simulation*, 2015, Accepted on 28/04/2015.

[3] R. De Coninck and L. Helsen, "Quantification of flexibility in buildings by cost curves - methodology and application", *Applied Energy*, 2015, Submitted on 17/03/2015.

[4] R. De Coninck, R. Baetens, D. Saelens, A. Woyte, and L. Helsen, "Rule-based demand side management of domestic hot water production with heat pumps in zero energy neighbourhoods", *Journal of Building Performance Simulation*, vol. 4, no. 7, pp. 271–288, 2014. DOI: 10.1080/19401493.2013.801518.

[5] R. Baetens, R. De Coninck, J. Van Roy, B. Verbruggen, J. Driesen, L. Helsen, and D. Saelens, "Assessing electrical bottlenecks at feeder level for residential net zero-energy buildings by integrated system simulation", *Applied Energy*, vol. 96, no. Special issue on Smart Grids, Renewable Energy Integration, and Climate Change Mitigation - Future Electric Energy Systems, pp. 74–83, 2012, ISSN: 03062619. DOI: 10.1016/j.apenergy.2011.12.098.

[6] R. Baetens, R. De Coninck, L. Helsen, and D. Saelens, "The impact of load profile on the grid-interaction of building integrated photovoltaic (bipv) systems in low-energy dwellings", *Journal of Green Building*, vol. 5, no. 4, pp. 137–147, 2010.

Articles in international conference proceedings

[1] R. De Coninck, F. Magnusson, J. Åkesson, and L. Helsen, "Grey-box building models for model order reduction and control", in *10th International Modelica Conference*, Lund, Sweden, Mar. 2014, pp. 657–666. DOI: 10.3384/ECP14096657.

[2] M. Vande Cavey, R. De Coninck, and L. Helsen, "Setting up a framework for model predictive control with moving horizon state estimation using jmodelica", in *10th International Modelica Conference*, Lund, Sweden, 2014, pp. 1295–1303. DOI: 10.3384/ECP140961295.

[3] R. De Coninck and L. Helsen, "Bottom-up quantification of the flexibility potential of buildings", in *Building Simulation, 13th International Conference of the International Building Performance Simulation Association*, Aix-les-Bains, France: IBPSA, 2013.

[4] R. Baetens, R. D. Coninck, J. V. Roy, B. Verbruggen, J. Driesen, L. Helsen, and D. Saelens, "Assessing electrical bottlenecks at feeder level for residential net zero-energy buildings by integrated system simulation", no. i, 2011.

[5] R. De Coninck, D. Devriendt, S. Thiesse, B. Huberlant, and A. Woyte, "Online software platform for dedicated product related simulations", in *Proceedings of Building Simulation 2011*, Sydney, Australia, 2011, pp. 2696–2702.

[6] B. Verbruggen, R. De Coninck, R. Baetens, D. Saelens, L. Helsen, and J. Driesen, "Grid impact indicators for active building simulation", in *Innovative Smart Grid Technologies (ISGT), 2011 IEEE PES*, IEEE, 2011, pp. 1–6, ISBN: 9781612842202.

[7] B. Verbruggen, J. Van Roy, R. De Coninck, R. Baetens, L. Helsen, and J. Driesen, "Object-oriented electrical grid and photovoltaic system modelling in modelica", in *8th International Modelica Conference*, Dresden, Germany, 2011, p. 9.

[8] R. Baetens, R. De Coninck, L. Helsen, and D. Saelens, "The impact of the heat emission system on the grid-interaction of building integrated photovoltaics in low-energy dwellings", in *8th International Conference on System Simulation in Buildings (SSB2010)*, vol. 1, 2010, P137.

[9] R. Baetens, R. De Coninck, L. Helsen, and D. Saelens, "The impact of domestic load profiles on the grid-interaction of building integrated photovoltaic (bipv) systems in extremely low-energy dwellings", in *Renewable Energy Research Conference 2010 - Zero Emission Buildings*, M. Haase and A. G. Hestnes, Eds., Trondheim: Tapir Academic Press, 2010, pp. 3–14, ISBN: 978-82-519-2623-2.

[10] R. De Coninck, R. Baetens, B. Verbruggen, J. Driesen, D. Saelens, and L. Helsen, "Modelling and simulation of a grid connected photovoltaic heat pump system with thermal energy storage using modelica", in *8th International Conference on System Simulation in Buildings (SSB2010)*, P. Andre, S. Bertagnolio, and V. Lemort, Eds., Liège, 2010, P177.

[11] K. Achten, R. De Coninck, G. Verbeeck, and J. Van Der Veken, "Analyzing the economic feasibility of permutations of energy saving measures with batch simulations and pareto optimization", in *Building Simulation 2009*, 2009, pp. 660–667.

[12] R. De Coninck, B. Labedan, and F. Lavoye, "350 kw of dual solar cooling for optimal flexibility and economic performance", in *3rd International Conference Solar Air-Conditioning*, Palermo, Italy, 2009, P93.

[13] B. Labedan and R. De Coninck, "Product related dedicated software development based on trnsys and trnsed", in *Building Simulation 2009*, 2009, pp. 1935–1941.

[14] R. De Coninck and J. Berte, "Design of the self-supporting belgian antarctic station: a passive building running on sun and wind energy", in *Proceedings of the Building Physics Symposium in honour of Professor Hugo Hens*, S. Roels, G. Vermeir, and D. Saelens, Eds., Leuven: Laboratory of Building Physics, Catholic University Leuven, Belgium, 2008, pp. 271–275.

[15] R. De Coninck and K. Achten, "Solar absorption cooling in the renewable energy house in brussels: two summers of operation", in *2nd International Conference on Solar Air-Conditioning*, Tarragona, Spain, 2007, P110.

Presentations on international conferences without full proceedings

[1] R. De Coninck, F. Magnusson, J. Åkesson, and L. Helsen, "A tool chain for model predictive control of buildings based on grey-box models", in *Intelligent Building Operations Workshop*, Boulder, CO, 2013.

[2] R. De Coninck, C. Verhelst, A. De Broe, A. Woyte, and L. Helsen, "Needs for optimal control in renewable energy systems", in *AFG'11 - 15th Austrian-French-German Conference on Optimization*, Toulouse, 2011, pp. 1–3.

FACULTY OF ENGINEERING SCIENCE
DEPARTMENT OF MECHANICAL ENGINEERING
APPLIED MECHANICS AND ENERGY CONVERSION
Celestijnenlaan 300b - bus 2420
3001 Heverlee
roeldeconinck@gmail.com
https://www.mech.kuleuven.be/en